



DOCTORAL THESIS

**Novel protein immobilization
approaches for the
development of vaccine
candidates and enzymatic
reactors.**

Tomas Pose Boirazian

INTERNATIONAL PHD SCHOOL OF THE UNIVERSITY OF
SANTIAGO DE COMPOSTELA



DOCTORAL PROGRAMME IN MOLECULAR MEDICINE

SANTIAGO DE COMPOSTELA 2021

D./Dna. **Tomas Pose Boirazian**

Título da tese: **Novel protein immobilization approaches for the development of vaccine candidates and enzymatic reactors.**

Presento a miña tese, seguindo o procedemento axeitado ao Regulamento, e declaro que:

- 1) A tese abarca os resultados da elaboración do meu traballo.
- 2) De ser o caso, na tese faise referencia ás colaboracións que tivo este traballo.
- 3) Confirmo que a tese non incorre en ningún tipo de plaxio doutros autores nin de traballos presentados por min para a obtención doutros títulos.

E comprométome a presentar o Compromiso Documental de Supervisión no caso de que o orixinal non estea na Escola.

En **Santiago de Compostela, 14 de Xullo de 2021.**

Sinatura electrónica

AUTORIZACIÓN DO DIRECTOR / TITOR DA TESE

Novel protein immobilization approaches for the development of vaccine candidates and enzymatic reactors.

D./Dna. José Manuel Martínez Costas

INFORMA:

Que a presente tese, correspóndese co traballo realizado por D/Dna. Tomas Pose Boirazian, baixo a miña dirección, e autorizo a súa presentación, considerando que reúne os requisitos esixidos no Regulamento de Estudos de Doutoramento da USC, e que como director desta non incorre nas causas de abstención establecidas na Lei 40/2015.

De acordo co indicado no Regulamento de Estudos de Doutoramento, declara tamén que a presente tese de doutoramento é idónea para ser defendida en base á modalidade de Monográfica con reprodución de publicacións, nos que a participación do/a doutorando/a foi decisiva para a súa elaboración e as publicacións se axustan ao Plan de Investigación.

En 30 de Xulio de 2021

ACKNOWLEDGMENTS



As it is the case in science, our project was technically challenging. Luckily, challenges were exciting and learning and growing opportunities plentiful. I would like to warmly thank a great number of people for their lessons and help, and above all, for challenge and inspire me, for spending countless hours with me, and for changing my life for good.

First and foremost, I would like to thank my thesis supervisor Prof. José Martínez Costas for bearing with me, even at the darkest of times, with unending patience, constant good advice, and a positive attitude. Thank you for all your multifaceted support, and for challenging my insecurities. I have learned a tremendous amount from you. It was a pleasure working with you. Thank you for being such a wonderful supervisor for which I am lucky to be one of your students. I would like to thank Dr. Gemma Eibes as well, because even though she has not been my "official" co-director, she has always been a great support and reference.

This project was funded by the Ministerio de Ciencia e Innovación and the Center for Research in Biological Chemistry and Molecular Materials (CiQUS), where I was based for the duration of the Ph.D. program and gave me the opportunity to perform a visiting exchange at the University College London (UCL). In addition, I want to thank the ENOVA initiative, a science and technology “Network on Vaccine Adjuvants”, funded by COST through the EU Framework Programme Horizon 2020, for sponsoring me and giving me the opportunity to spend a few months as a visiting researcher at the National Institute for Biological Standards and Control (NIBSC) in the United Kingdom. For that, I would like to thank Dr. Sandra Diebold for giving me the opportunity to join her lab, and for the great experience in the field of cancer immunotherapy. I want to thank my colleagues at NIBSC, Mimmy and Maria, for your advice, friendship and for keeping me in good spirits.

I want to thank my colleagues at CiQUS, most of them at the 3rd floor. Special thanks to Natalia for the ice-cream support and the Harry Potter movies, Uxia for being such an amazing support, Rebeca for inculcating on me the value of keeping my lab bench clean (even against my own will), Irene for your amazing ideas and your continuous help, and Jacobo for your advice and your help when I need it. Thanks to other CiQUS and USC colleagues as well, you are too many to name here. Thanks for being such good company.

I want to thank all my family for all the support received. Especially to my parents and my sister, who even though these years have been tough, has always been supporting me and being that necessary beacon at many times. Thank you for being by my side and for putting up with me (which is not little).

I want to thank Prof. Abdul Basit and Dr. Alvaro Goyanes for letting me be part of their work in such an amazing topic as 3D printing. What started as a summer internship, ended up as a chapter on my thesis which makes me very proud of our work. A big thanks to all the members at the BRG group, thank you Pat, Christine, Francesca, JJ, Moe, Tom, Farhan, Atheer, Fabrizio, Nour, Sarah and Bonnie for being such an excellent example to aspire to, and for your kindness. To be honest I don't even know how Bonnie still put up with me.

Finally, I want to thank my very good friends Brais, David and Johnny for your kindness, warmth and support in the good days as well as in the bad days.

TABLE OF CONTENTS

Abbreviations	15
Introduction	27
1. Protein immobilization	29
2. Immobilization strategies	30
2.1. The IC - tagging technology.....	30
2.1.1. The family Reoviridae	30
2.1.2. Replicative cycle of avian reovirus.	32
2.1.2.1. Entry and decapsidation.	32
2.1.2.2. Gene expression.....	34
2.1.2.3. Morphogenesis and exit.....	34
2.1.3. The muNS protein.....	35
2.1.3.1. Structural features.....	35
2.1.3.2. The IC-Tagging platform	38
2.2. 3D printing.....	43
2.2.1. Binder jetting	45
2.2.2. Powder bed fusion.....	46
2.2.3. Material jetting.....	46
2.2.4. Direct energy deposition.....	47
2.2.5. Sheet lamination.....	47
2.2.6. Material extrusion	48
2.2.7. Vat photopolymerisation	49
Objectives	53
Materials and Methods	56
1. Materials	58
1.1. Biological material.....	58
1.1.1. Eukaryotic cells	58
1.1.2. Prokaryotic cells	58
1.1.3. Plasmids.....	59



1.1.4. Antibodies.....	59
1.1.4.1 Primary antibodies.....	59
1.1.4.2. Secondary antibodies.....	59
1.1.4.3. Capture antibodies.....	60
1.1.4.4. Standars.....	61
1.1.5. Enzymes.....	62
1.2. Non-biological material.....	62
1.2.1. Culture media.....	62
1.2.2. Solutions and buffers.....	62
1.2.3. Pharmaceuticals.....	64
1.2.4. Flow Cytometry Materials:.....	65
1.2.5. Enzyme-linked immunosorbent assay for detection of cytokines.....	65
1.2.6. In vivo imaging Materials.....	66
2. Methods.....	66
2.1. manipulation of cell cultures.....	66
2.1.1. Handling conditions.....	66
2.1.2. Propagation and conservation of cell lines.....	66
2.1.3. Obtaining bone marrow derived Flt3L dendritic cells (Flt3L -BMDCs)...	67
2.1.4. Obtaining GM-CSF - BMDCs.....	67
2.1.5. Preparation of splenocytes for T-cell cytotoxic activity tests.....	68
2.1.6. Ex vivo Preparation and restimulation of splenocytes for flow cytometry	69
2.1.7. In vitro immune activation assay.....	69
2.2. Manipulation of nucleic acids.....	71
2.2.1. Plasmid DNA purification.....	71
2.2.2. Polymerase chain reaction.....	71
2.2.3. Isolation and purification of DNA fragments.....	71
2.2.4. Cutting and joining of DNA fragments.....	72
2.2.5. Recombinant plasmids construction.....	72
2.3. Protein expression and manipulation.....	73
2.3.1. Generation of dual plasmids for expression in bacteria.....	73
2.3.2. Protein expression in bacteria.....	75
2.3.3. Purification of nanospheres from bacteria.....	75
2.3.4. Electrophoretic analysis of angels SDS-PAGE.....	76

2.3.5. Determination of luciferase activity in vitro	76
2.3.6. Determination of Halo-tag activity in vitro	76
2.4. Handling of cell cultures	77
2.4.1. Propagation and preservation of cell lines	77
2.5. Immunological techniques.....	78
2.5.1.ELISA protocol for detection cytokines.....	78
2.6. Limulus amoebocyte lysate (lal) assay.....	79
2.7. B16 HER2 pseudo-metastasis mouse model.....	79
2.7.1 Mice.....	79
2.7.2. Preparation of tumor cells.....	80
2.7.3. Tumor growth profiles.....	80
2.7.4. Treatment with MS and control.....	80
2.7.5. Statistical analysis	82
2.8. In vivo imaging.....	82
2.8.1. Luciferase in vivo imaging.....	82
2.8.2. Halotag in vivo imaging	83
2.9. CotA enzymatic activity	84
2.9.1. Laccase standard activity assays.....	84
2.9.2. Optimum pH.....	84
2.9.3. Optimum temperature and thermostability	85
2.9.4. Decolorization of RB19.....	85
2.9.5. Stability Against Inactivating Agents	85
2.9.6. Storage stability	86
2.9.7. Reusability of the MS	86
2.10. 3D printing procedure	86
2.10.1. 3D object design.....	86
2.10.2. Formulation and 3D printing of Printzyme	86
2.10.3. Printlet mass and dimensions	87
2.10.4. Environmental scanning electron microscopy (ESEM).....	88
2.10.5. 3D printed <i>Trametes versicolor</i> enzyme activity assay	88
2.10.6. Assessment of the enzymatic activity remaining within Printzyme.....	89
2.10.7. Optimal pH and temperature for free <i>Trametes versicolor</i> laccase.....	89
2.10.8. Effect of pH and temperature on free laccase and Printzyme stability ...	90
2.10.9. Reusability studies.....	90

2.10.10. Removal of pharmaceuticals by Printzyme	91
2.10.11. High-performance liquid chromatography (HPLC) analysis	91

Results..... 93

Chapter 1. Enzyme immobilization via the IC - Tagging technology 95

1. Introduction	97
2. Enzyme immobilization	97
3. Immobilization of enzymes through the ic-tagging system.....	101
3.1. Rationale	101
3.2. CotA gene construct tagged with the IC fragment	103
3.3. Enzymatic activity of the encapsulated CotA	105
3.4. Effect of pH on CotA activity and stability	106
3.5. Stability against inactivating agents.....	108
3.6. Optimum temperature and thermostability.....	109
3.7. Reusability of NS-CotA and ability to decolorate organic dyes	112
3.8. Discussion.....	114

Chapter 2. Enzyme immobilization and biocatalysis via 3D printing 118

1. Introduction	120
2. 3D designing of the printzyme	123
3. Formulation and 3D printing of printzyme.....	124
4. Initial enzymatic activity assessment of printzymes	127
5. Optimal ph and temperature for printzyme activity.....	129
6. Effect of ph and temperature on printzyme stability	131
7. Reusability of printzymes.....	134
8. Removal of pharmaceuticals using printzyme	135
9. Discussion	138


Chapter 3. Cancer epitopes immobilization via the IC – Tagging system ..143

1. Introduction	145
1.1. Cancer vaccines.....	145
1.2. Tumor antigen targets.....	147
1.3. Adjuvant substances in cancer immunotherapy	148



1.4. Toll-like receptors (TLRs).....	149
1.5. Endosomal TLR signaling.....	151
1.6. The IC-tagging technology for vaccine production.....	151
2. Possible application of the ic-tagging system in cancer immunotherapy	156
2.1. Rationale	156
2.2. Construction of IC-tagged OVA and TRP2 for bacterial expression.....	157
2.3. Endotoxin levels in the preparations.....	159
2.4. Comparison of the PBMC activation by NS by the in vitro MAT.....	161
2.5. Comparison of the in vitro DCs activation test by the NS formulation	172
2.6. Induction of anti-tumor immunity by NS	180
2.7. Monitoring the bio-distribution of NS by in vivo imaging.....	187
3. Discussion	192
General conclusions.....	195
Summary	199

ABBREVIATIONS

°C	Celsius Degrees
3DP	3D printing
Ab	Antibody
ABTS	2,2'-azino-bis(3 ethylbenzothiazoline-6-sulfonic acid)
AHSV	African Horse Sickness Virus
AM	Additive manufacturing
APC	Antigen Presenting Cell
ARV	Avian Reovirus
ATP	Adenosine triphosphate
B16 OVA cells	Murine tumor cell line used for research as a model for human skin cancers expressing ovalbumin
B cells	Lymphocytes having the presence of a B-cell
BJP	Binder jet printing
BMDCs	Bone Marrow-derived Dendritic Cells
 BTV	Bluetongue Virus
CAD	Computer-aided design

CAM	Computer-aided manufacturing
CD8+ T	Cytotoxic T Lymphocyte
CFSE-labelled	Carboxyfluorescein succinimidyl ester labelled
CI	Co-initiator
CLIP	Continuous liquid interface production
CPG ODN	CpG oligodeoxynucleotides
CTL assay	Cytotoxic T Lymphocyte assay
DAPI	4',6-diamidino-2-phenylindole
DCs	Dendritic Cells
DI	Deionized
DLP	Digital light processing
DNA	Deoxyribonucleic Acid
dNTP	Deoxynucleotide triphosphates
DTT	Dithiothreitol
EDTA	Ethylenediamine tetraacetic acid
ELISA	Enzyme-Linked ImmunoSorbent Assay


EP	European Pharmacopoeia
ER	Endoplasmic Reticulum
ESEM	Environmental scanning electron microscope
FDA	Food and Drug Administration
FDM	Fused deposition modelling
Fig.	Figure
Flt3L	FMS-like tyrosine kinase 3 ligand
FW	Forward G
GFP	Green fluorescent protein
GM-CSF	Granulocyte macrophage colony stimulating factor
HBV	Hepatitis B virus
HIV-AIDS	Human immunodeficiency virus and acquired immunodeficiency syndrome
HPLC	High-performance liquid chromatography
IC	Intercoil domain
IFA	Incomplete Freund's adjuvant



IFN	Interferon
IFNAR -/-	Mice lacking the alfa interferon receptor
IgG	Immunoglobulin G
IL	Interleukin
IL -12 p40	Subunit beta of interleukin 12 or cytotoxic lymphocyte
maturation factor p40	
IP	Intraperitoneal
IPTG	Isopropyl β - d-1-thiogalactopyranoside
IV	Intravenously
kDa	Kilodalton
LAL	Limulus amoebocyte lysate
LAP	Lithium phenyl-2,4,6-trimethylbenzoylphosphinate
LB	Luria Bertani
LPS	Lipopolysaccharide
Luc	Firefly luciferase

MWD	Molecular weight distribution
MAT	Monocyte Activation Test
MFI	Mean fluorescent intensity
MHC class I	Major Histocompatibility Complex type I
MHC class II	Major Histocompatibility Complex Class II
ml	Milliliter
mM	Millimolar
MOI	Multiplicity of infection
MPLA	Monophosphoryl lipid A
mRNA	Messenger ribonucleic acid
MRV	Mammalian Reovirus
MS	Microspheres
MVA	Modified Vaccinia Ankara Virus
ng	Nanogram
NIR	Near-infrared
NK cell	Natural killer cell



NLS	Nuclear Localization Sequence
NS	Nanospheres
O.D.	Optical density
OVA	Ovalbumin
PBJ	Powder bed jetting
PBMC	Peripheral Blood Mononuclear Cell
PBS	Phosphate-buffered saline
PCR	Polymerase chain reaction
PEG	Polyethylene glycol
PEGDA	Polyethylene glycol diacrylate
Pfu	Plaque-forming unit
poly I:C	Polyinosinic-polycytidylic acid
PRR	Pattern Recognition Receptors
QuilA	Saponin, detergent derived from the plant <i>Quillaja Saponaria</i>
	<i>Molina</i>
RNA	Ribonucleic Acid

ROI	Region of interest
RP	Rapid prototyping
rpm	Revolutions per minute
RT	Room temperature
RV	Reverse
RVFV	Rift Valley Fever Virus
SA	Surface area
SD	Standard deviation
SDS	Sodium Dodecyl Sulfate
SDS-PAGE	Dodecyl sulphate and polyacrylamide gel electrophoresis
sec	Entry sequence for the endoplasmic reticulum
SEM	Scanning electron microscopy
Sf9	Clonal isolate of <i>Spodoptera frugiperda</i> Sf21 cells
SLA	Stereolithography
SLS	Selective laser sintering
SOP	Standard Operating Procedure



ssRNA	Single stranded RNA
STL	Stereolithography file
TAA _s	Tumor associated antigens
TAE	Tris-Acetate-EDTA
TC	Tissue culture
T cells	Lymphocytes having the presence of a T-cell receptor (TCR)
TEM	Transmission electron microscopy
Th1 cells	T helper cells
TLR	Toll-like receptor
T _m	Melting temperature
TNF- α	Tumor necrosis factor alpha
TPP	Two-photon polymerization
TRB –	Resuspension buffer without magnesium
TRB +	Resuspension buffer with magnesium
TRIS	Tris(hydroxymethyl)aminomethane
TRP-1	Tyrosinase related protein-1

TRP-2	Tyrosinase-related protein-2
TSA _s	Tumor specific antigens
TSS	Transformation solution
μm	Micrometers
μl	Microliter
U/ml	Units per milliliter
U/l	Units per litre
UV	Ultraviolet
VLP	Virus-like particles
WC	Water content
WHO	World Health Organization
WT	Wild type
λ	Wavelength

INTRODUCTION

1. PROTEIN IMMOBILIZATION

Protein immobilization on solid supports offers a wide range of opportunities in the biotech industry. Its many possible applications in diverse fields reach from enzyme immobilization that promotes an enhancement in the physicochemical properties, to vaccine candidate generation, reducing the associated production costs and improving the immunogenic performance of the candidate. The immobilization process implicates profound science in both substrate surface and proteins. Proteins are composed of amino acids polymerized jointly through the formation of peptide bonds. One or more polypeptide chains fold into a 3-dimensional (3-D) bioactive protein, with many exposed functional groups such as carboxyl, amine, hydroxyl, and sulfhydryl. Regarding the immobilization strategy, the conformation of the immobilized protein needs to be seriously considered. In the enzyme field, the active site is usually a groove or pocket where the target or substrate molecules bind and experience a chemical reaction. In order to function properly, this active site needs to be in specific and appropriate conformation and accessible to the target. This is why protein immobilization in random orientation on a solid support can result in unexpected denaturation and blocking of the active site followed by the natural loss of activity. On the other field discussed in this thesis, protein-based vaccine generation strategies, immobilization strategies have been also demonstrated to deliver quality results. This is because immune responses to a particular antigen are considerably improved if the antigen is presented and coupled to some sort of virus-sized particle in an ordered, repetitive array (1). In this field, the correct protein folding is also critical for the generation of the optimal immune response against the chosen epitope/protein. The rationale behind this fact is that the generation of antibodies or the triggering of a cellular response is very dependent of the protein conformation, and therefore, the conformation of antigens in the chosen support is of critical importance for optimal stimulation of protective as well as durable immune responses (2).

In traditional strategies, proteins are often adhered to a substrate surface via physical adsorption through hydrophobic forces and/or electrostatic interactions (3, 4). Although this is the most direct strategy, adsorption is relatively unstable and difficult to control, causing high background signals, reducing the sensitivity and causing false positive outcomes. Another prevalent path for protein attachment is covalent bonding between the feasible functional groups homogeneously positioned on the surface of proteins and properly modified substrates, producing adequate and irreversible connections (5, 6). More accessible protein immobilization strategies have attracted attention from various fields. With proper design, the protein immobilization approach can result in a homogenous protein attachment in a preferable orientation, which overcomes protein misfolding and the insufficient exposure of functional domains/epitopes. Currently, two different strategies are available at the research group for the generation of immobilized proteins with different applications that will be discussed during this thesis. These can be classified into bio/chemical *in vivo* affinity-mediated immobilization via the IC-tagging system, and molecular imprinting technique immobilization via the use of 3D printing. This thesis addresses the application of these two techniques for the immobilization of active and properly folded proteins for their use as vaccines and enzymatic reactors. Advantages and challenges of each strategy as well as techniques for characterization of oriented protein attachment are also included.

2. IMMOBILIZATION STRATEGIES

2.1. THE IC-TAGGING TECHNOLOGY

This technology has been developed from studies on the morphogenesis of avian reoviruses.

2.1.1. The family Reoviridae

The Reoviridae family includes viruses widely distributed in nature through a variety of hosts, from fish and mammals to insects and plants, with different pathological manifestations. Viruses in this family share several common

characteristics, including: i) replicate in the cytoplasm of infected cells using similar strategies for both replication and expression of viral proteins; ii) possess a fragmented genome composed of 10 to 12 double-stranded RNA fragments (dsRNA); and iii) contain two or three concentrically arranged protein shells with an external diameter between 70-80 nm.

Based on the structural characteristics of the virions, on the number of genomic segments and the strategies of the replicative cycle, the members of this family have been grouped into fifteen different genera (Figure 1). Only the *Orthoreovirus*, *Orbivirus*, *Rotavirus*, and *Coltivirus* are capable of infecting humans and other vertebrates, while the other genera are infecting the rest of the aforementioned hosts.

The Reoviridae family

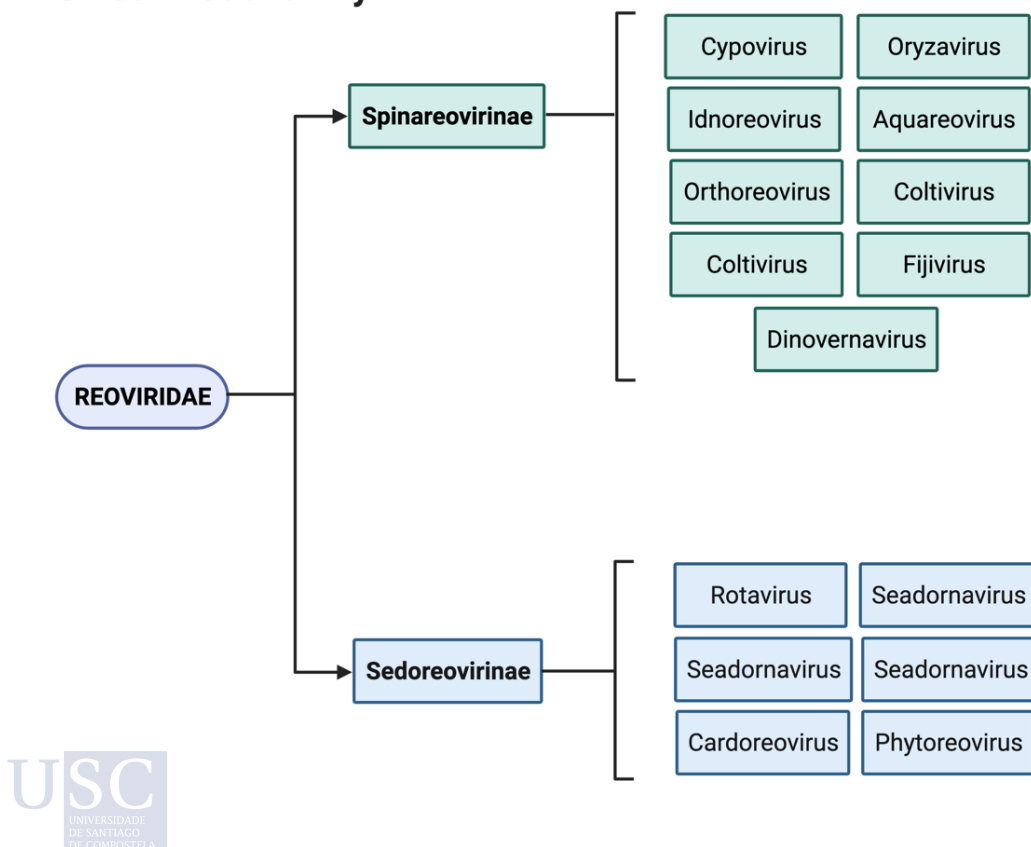


Figure 1. The *Reoviridae* family. (Source: adapted from: Mertens, P. P. C., et al. "Family reoviridae." 2000).

Members of the *Orthoreovirus* genus possess ten genomic dsRNA segments confined within a double protein coat, between 70-90 nm in external diameter (7). The most important groups of this genus are the non-fusogenic mammalian reovirus (MRVs) and the fusogenic avian reovirus (ARVs). Both share many morphological, physicochemical as well as structural characteristics (8). Even so, they differ in aspects such as host, pathogenicity and biological properties, highlighting that ARVs are fusogenic and only MRVs have hemagglutinating activity (9).

The avian reoviruses are very widespread pathogens in birds, generally causing asymptomatic infections, although certain strains produce high mortality rates among infected birds (10). Virulent strains are responsible for multiple infectious syndromes, among which viral tenosynovitis or infectious arthritis, which consists of joint inflammation with injuries to the gastrocnemius tendons, is the first condition with which these viruses were related. They have also been associated with multiple other enteric and respiratory conditions, slowing down their growth and causing bone changes that directly affect the productivity of the farms. Furthermore, evidence suggests that susceptibility to ARV infections is related to age, with older birds being more resistant to infections. The main route of transmission is oral-fecal, although respiratory and egg infections have also been reported.

2.1.2. Replicative cycle of avian reovirus.

2.1.2.1. Entry and decapsidation.

The binding of the virus to the cells is mediated by specific interactions between the σC protein and cell surface receptors (11, 12). The cellular receptor for ARVs has not been identified yet, but appears to be a ubiquitous protein, since ARVs are also capable of adhering and replicating in mammalian cell lines. ARV-infected chicken embryonic fibroblasts have been observed under electron microscopy, where it can be seen that the entry of the virus is through receptor-mediated endocytosis (Figure 2)

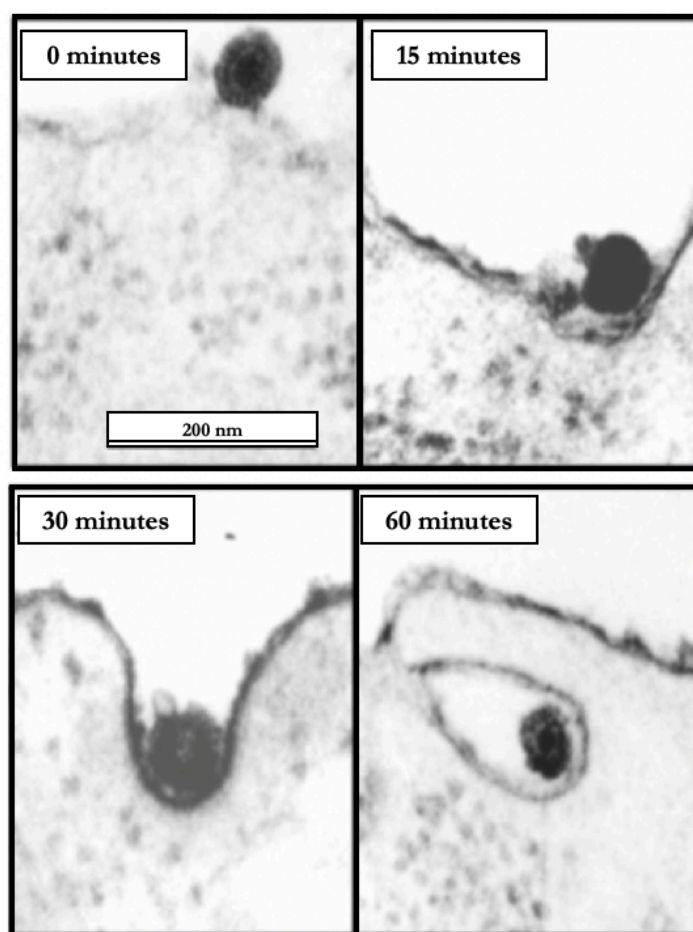


Figure 2. Electron microscope view of the avian reovirus entry at different time points. (Source: adapted from: Benavente, J., and J. Martinez-Costas. "Early steps in avian reovirus morphogenesis." *Reoviruses: Entry, Assembly and Morphogenesis* (2006)).

Decapsidation of the virus takes place in the interior of endosomes (Figure 3) and in order to happen, an acidification of the environment is required and consequently the proteolytic processing of the μ BC protein occurs, generating the δ and δ' peptides (13, 14). The mechanism that allows the cores to cross the endosomal membrane to reach the cytoplasm is still unknown.

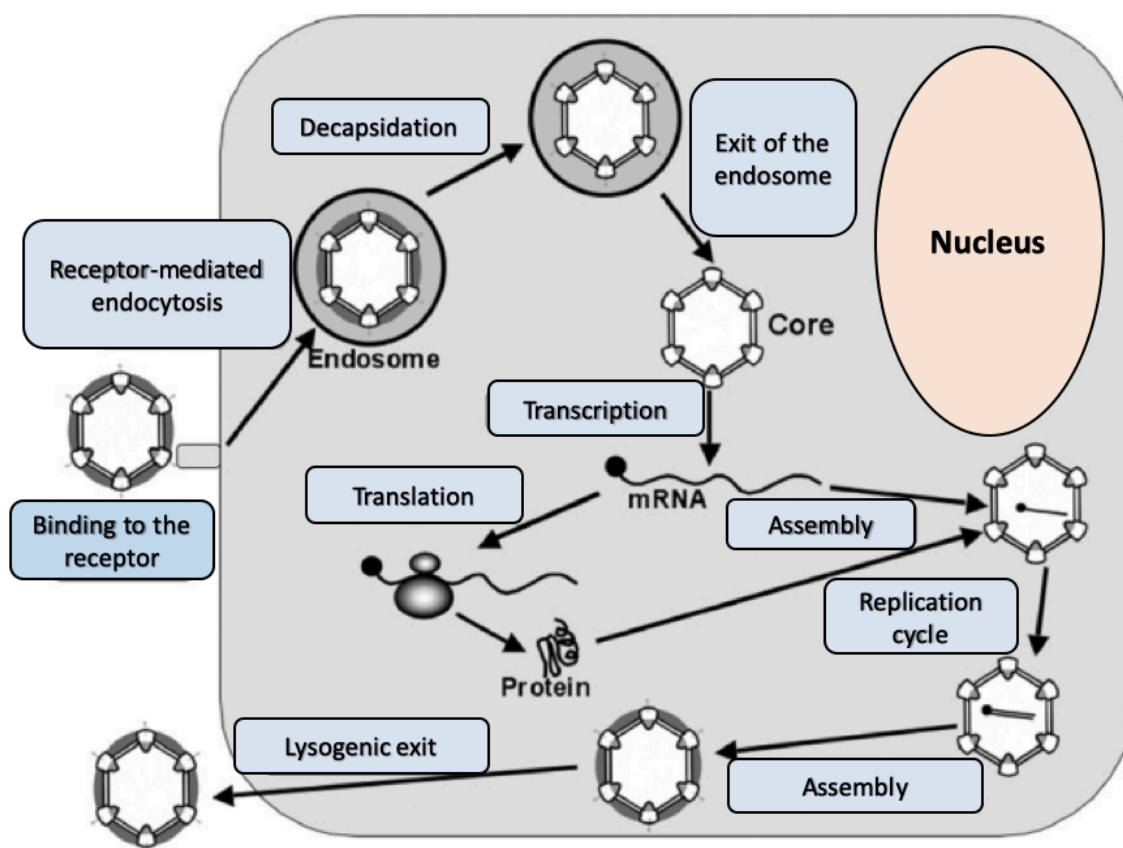


Figure 3. Proposed model for the replicative cycle of avian reovirus. (Source: adapted from Javier Benavente and Jose Martínez-Costas. "Avian reovirus: structure and biology." *Virus research* 123.2 (2007)).

2.1.2.2. Gene expression

The λ B protein with its RNA polymerase activity is responsible for catalyzing the synthesis of the 10 mRNAs using the negative strand of the genomic segments as a template. Viral mRNAs are synthesized in the core and exit through the turrets formed by λ C acquiring a type 1 cap at the 5' end (15).

2.1.2.3. Morphogenesis and exit

Members of the *Reoviridae* family assemble into dense cytoplasmic inclusions called viroplasm, viral inclusions, or viral factories. These structures are not

associated with organelles, membranes, or microtubules, and present both structural and non-structural proteins as well as partially or fully assembled viral particles (7, 16). It is within these structures that the assembly of the new virions takes place, with the incorporation of viral proteins being a totally controlled and selective process (17). MuNS is responsible for forming the framework on which viroplasms are built, specifically and directly recruiting the σ NS, λ A and λ C proteins to these inclusions. Although little is known about the exit of viral particles from infected cells, two forms of spread are expected: cell lysis, or cell fusion induced by the p10 protein, which would allow the spread of the virus between adjacent cells without being exposed to the immune system of the host (13, 18). Apoptosis triggered by avian reovirus also enhances viral spread (19).

2.1.3. The muNS protein

2.1.3.1. Structural features

Protein muNS is encoded by the avian reovirus M3 gene, with 1996 bp and a single open reading frame. It is a 635 amino acid non-structural viral protein with a molecular weight of 70.8 kDa (17, 20). This sequence differs to a great extent with the muNS of MRV, as only 28.3% similarity between sequences (20).

It is the only viral protein capable of forming inclusions when expressed individually in transfected cells and, as mentioned, is thought to be the main organizer of ARV viroplasms (21).

A bioinformatic analysis of its aminoacid sequence predicted the existence of two regions with a possible “coiled-coil” structure, lying between positions 451-472 (Coil1 or C1) and 540-599 (Coil2 or C2) (21).

Our laboratory performed an extensive deletion mutant analysis to determine the regions of muNS that are essential for viroplasm formation. First, it was found that the C-terminal region of the sequence is essential for the formation of inclusions. Deletions from the amino terminal end were performed reaching the following conclusions. No change is observed in the inclusions formed with the elimination of the first 140 amino acids. However, elimination of the first 380 amino acids resulted

in the formation of smaller, regular and spherical inclusions (Figure 4), and such phenotype was maintained upon the deletion reached residue 448. Deletions from amino acid 448 onwards, resulted in a total loss of the ability to form inclusions. It is for this reason that the fragment of muNS from 448 to 635 was named muNS-Mi (21), to denote the minimal portion of muNS that is still able to form inclusions efficiently. As their size is in the micrometer range, the spherical inclusions formed by muNS-Mi were named microspheres (MS).

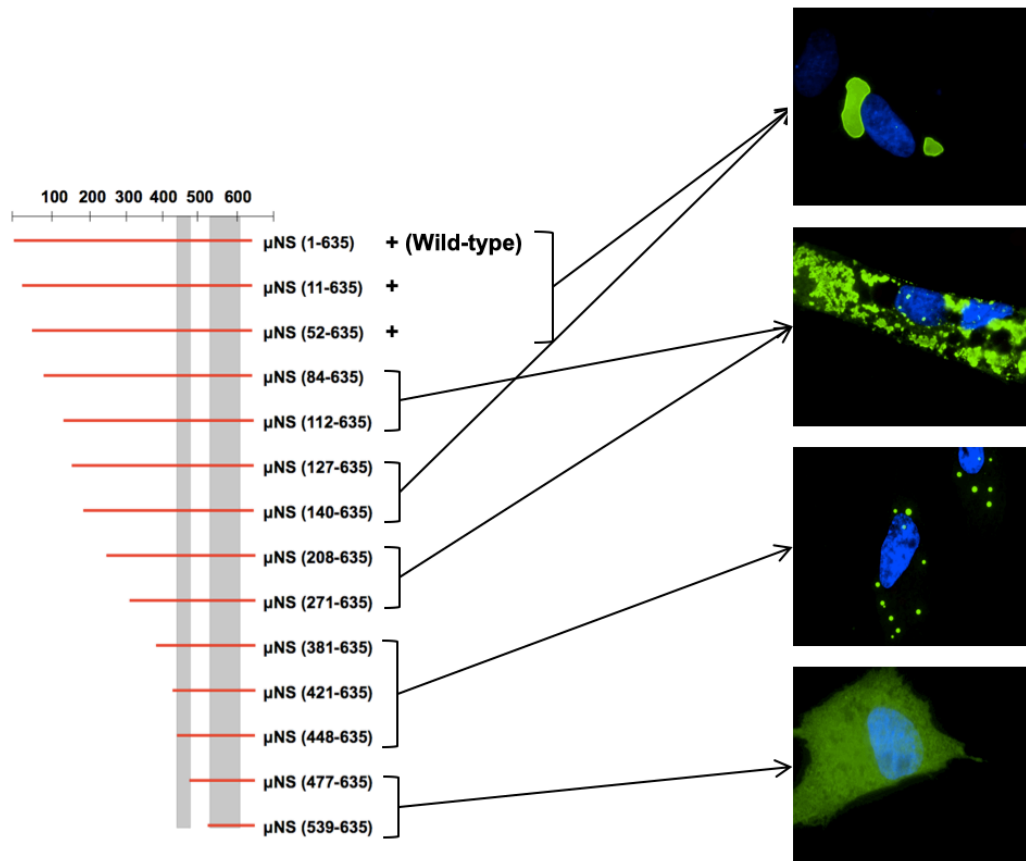


Figure 4. N-terminal deletion mutants of the muNS protein. Full-length muNS is schematically indicated by a horizontal red bar containing residues 1 to 635 (the locations are marked numerically on the top and right). A similar red bar indicates each single truncation, spanning the approximate region corresponding to the construct. The positions of two already mentioned coiled-coil components predicted in the sequence of muNS are signaled by two vertical gray bars. On the right of the figure, immunofluorescence images of representative phenotypes. The muNS protein is seen in green and the nuclei were stained with DAPI (blue). (Source: adapted from: Brandariz-Nuñez, Alberto, et al. "Avian reovirus μ NS protein forms homo-oligomeric inclusions in a microtubule-independent fashion, which involves specific regions of its C-terminal domain." *Journal of virology* 84.9 (2010)).



In the same study it was also found that some of the mutants (muNS 84-635, muNS 112-635, muNS 208-635 and muNS 271-635) formed amorphous aggregates that are polyubiquitinated and degraded by the cell, something that does not happen

for the original protein or for the spherical inclusions formed by the muNS-Mi, again indicating that the latter are ordered structures.

MuNS-Mi can be divided into four different domains, two of them are the previously mentioned regions Coil 1 and Coil 2. These two domains are separated by a region of 61 residues called Intercoil domain or IC (between residues 477 and 539). The fourth and last region is at the C-terminus of the Coil 2 region and lies between residues 605 and 635, called the C-tail or CT domain (21).

Our laboratory has carried out various studies to characterize the role played by the different muNS domains in the formation of the inclusions. In first place, the C1 domain participates in the generation of the oligomers and consequently the MS through a process of self-association, as it can be substituted by dimerization domains such as GFP or CA-C (dimerization domain of the HIV virus capsid protein). Similar substitution studies were also performed for the CT domain. In this case, the resulting phenotype was directly dependent on the substitute domain indicating that CT is involved in the orientation of interactions between muNS monomers. Finally, for the IC domain, point mutations in highly conserved residues such as Cys 489 and His 487, lead to a total loss of the ability to form inclusions.

2.1.3.2. The IC-Tagging platform

Through this characterization process, the research group also discovered the enormous affinity that the IC domain has for muNS inclusions of muNS-Mi MS, which opened the door to its use as a molecular “tag”, basis of the so-called “IC-Tagging” methodology (21). This system is made up of two components: on one hand, protein muNS-Mi and its ability to form microspheres when it is expressed in both prokaryotic and eukaryotic cells. On the other hand, the IC domain, which can be fused to any protein of interest at either the amino or carboxyl terminus and does not alter the characteristics or cellular location of the protein. However, when both components are co-expressed simultaneously, a relocation of the labeled protein to MS occurs due to the aforementioned high affinity of IC for the MS.

What is more, it has also been shown that this relocation process does not deprive the protein of interest to undergo post-translational modifications, allowing

practically any type of protein to be relocated to the MS regardless of its nature and of its natural cellular location (Figure 5), which opens up a wide range of possibilities of use.

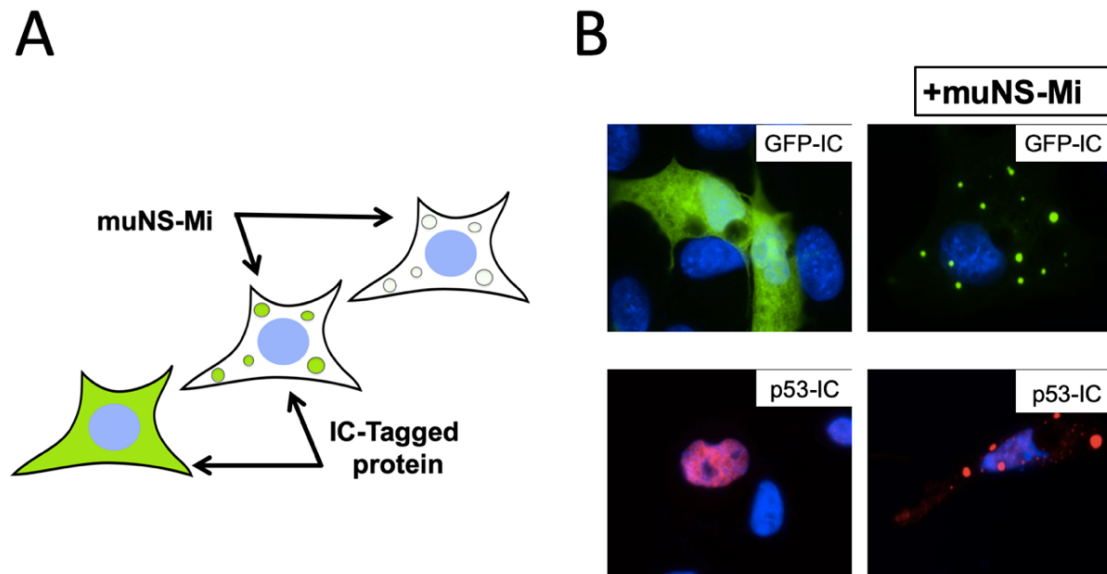


Figure 5. Basics of IC-Tagging. **A.** Expressing a protein tagged with the IC the distribution in the cell doesn't suffer any change. Expressing muNS-Mi produces the formation of the MS in the cytoplasm. Finally, co-expressing both in the same cell induces the relocation of the tagged protein into the MS. **B.** DF-1 monolayers transfected with plasmids expressing the GFP-IC and p53-IC proteins in the presence (Right column) or absence (Left column) of the muNS-Mi expressing plasmid. In the case of GFP, we observed the proteins by autofluorescence of GFP (green), while IC-tagged p53 (red) was observed by indirect immunofluorescence. The nuclei were stained with DAPI (blue).

Some of these modifications and interactions have been previously demonstrated, as is the case of the tetrameric DsRed protein. This protein requires the interaction of four monomers to evolve its fluorophore, and this interaction occurs through the C-terminus (22). Thus, if the protein is labeled with the IC tag at the C-terminus, is not capable of evolving the fluorophore and does not fluoresce. Still, if this tagged protein is co-expressed with muNS-Mi, the Ds-red protein is relocated to the MS and recovers fluorescence, demonstrating that within the MS,

proteins have the ability to interact, undergo post translational modifications and carry out complex reactions (23).

As mentioned, this platform works both in bacteria, where the diameter of the spheres is around 400 nanometers (NS, nanospheres), and in eukaryotic cells such as insect cells, where they have a larger size, in between 1 and 4 microns (Figure 6, compare B and A). In addition to its ease of use and simplicity in purification, enzymes retain their activity inside the MS. This was demonstrated for different enzymes, as is the case of luciferase (21).

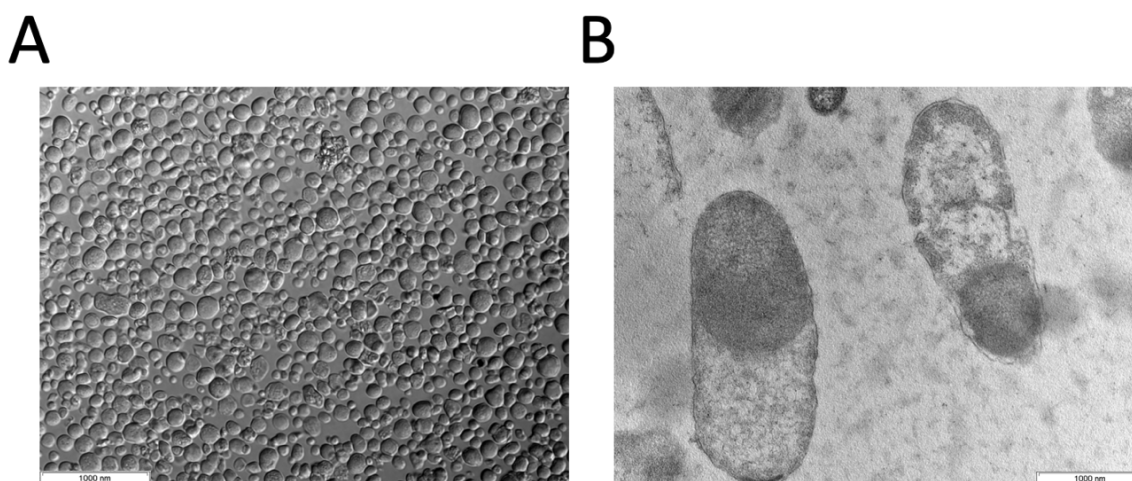


Figure 6. Images of the MS and NS produced in Sf9 cells and in bacteria. A. Bright field image of MS produced using the baculovirus system in Sf9 cells. **B.** Electron microscopy image of the NS produced in BL21 bacteria showing one NS per bacteria.

MS can also be loaded with glycoproteins, as a variant that is capable of entering the endoplasmic reticulum (ER) was developed (24). The adaptation of the system to this route opened the possibility of generating subunit vaccines against enveloped viruses, whose structure poses a challenge for their development (Figure 7).

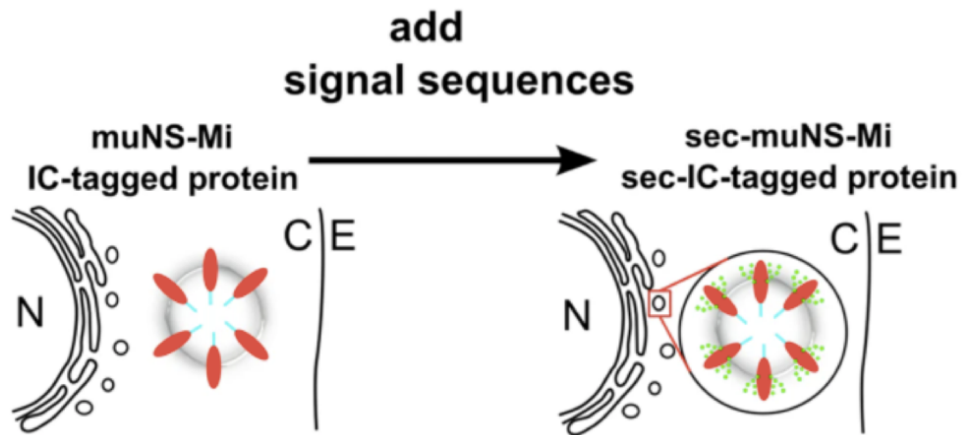


Figure 7. Formation of muNS-Mi MS inside the ER. Our hypothesis: adding a signal peptide on the sequence of muNS-Mi will create a version of that protein (sec-muNS-Mi) that will form MS inside the ER (on the right: the green spots represent sugar modifications). N-nucleus, C-cytosol, E-extracellular medium. (Source: adapted from Barreiro-Piñeiro, Natalia, et al. "IC-Tagging methodology applied to the expression of viral glycoproteins and the difficult-to-express membrane-bound IGRP autoantigen." (2018)).

As proof of concept glycoproteins, Gn from Rift Valley Fever Virus (RVFV) and the Vesicular Stomatitis Virus glycoprotein (VSV-G) were successfully loaded in glycosylated state in ER-located MS (24) (Figure 8). In addition, the bacteria-adapted version of IC-tagging works very well for difficult-to-express proteins such as the membrane-bound IGRP autoantigen (24).

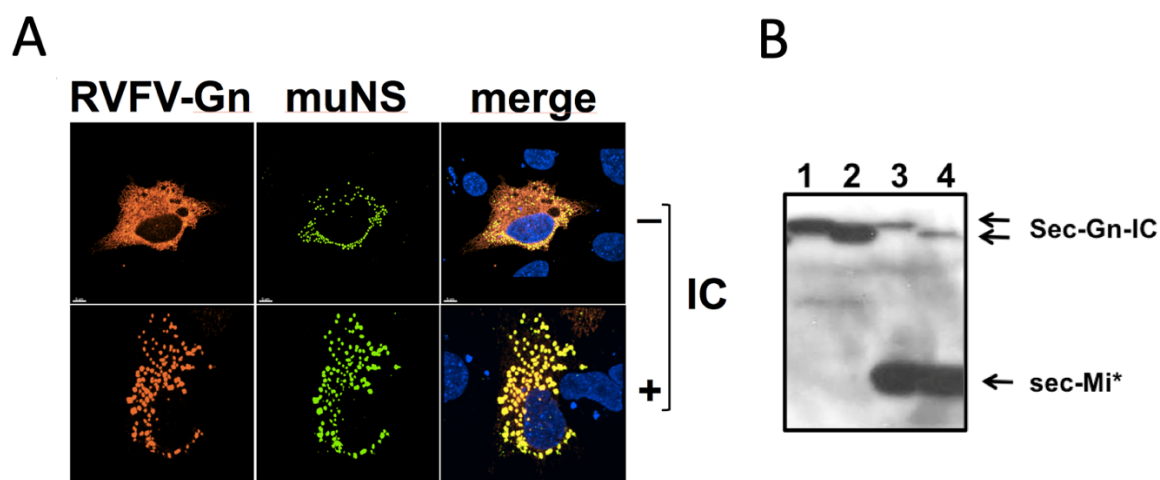


Figure 8. Characterization of the RVFV-Gn protein re-localization to sec-muNS-Mi MS inside the ER promoted by IC-tagging. Sec stands for “secretory” and are ER-expressed versions of the so-named proteins. **A.** Immunofluorescence analysis of DF-1 cells co-transfected either with the sec-muNS-Mi and either the sec-RVFV-Gn (upper row, non-IC-tagged) or sec-RVFV-Gn-IC (lower row, IC-tagged version). RVFV-Gn fluorescence is seen in red after detection with RVFV-Gn-specific antibodies, while sec-muNS-Mi is shown in green after detection with muNS-specific antibodies. Nuclei were stained blue with DAPI and shown in the merged images. The white bars represent a distance of 5 μ m. The pictures were taken with a confocal microscope. **B.** Western-blot analysis performed with a mix of antibodies against the RVFV-Gn epitope and muNS. The samples came from extracts from DF-1 cells transfected with expression plasmids for a RVFV-Gn (1 and 2) or co-transfected with sec-muNS-Mi (3 and 4) either before (1 and 3) or after (2 and 4) treatment with N-glycosidase. (Source: adapted from Barreiro-Piñeiro, Natalia, et al. "IC-Tagging methodology applied to the expression of viral glycoproteins and the difficult-to-express membrane-bound IGRP autoantigen." (2018)).

This methodology (Figure 9) presents a series of competitive advantages for immobilized protein production in relation to other techniques, such as synthetic nanoparticles, since the MS produced by this method are expressed, assembled and loaded with the protein of interest simultaneously in vivo. Thus, it is not necessary to generate and purify separately the components to subsequently carry out the coupling. In relation to the "virus like particles" (VLP), this system also has the advantage that it allows non-structural proteins to be loaded on these particles which, can also promote the activation of effective immune responses for some viruses (25).

Furthermore, the purification process is highly simple by mechanical methods, so there is no dependence on the use of columns or complex systems that tend to make the process expensive. This platform also presents a great competitive advantage in relation to classical subunit vaccines, since these require the use of adjuvants for inducing an immune response.

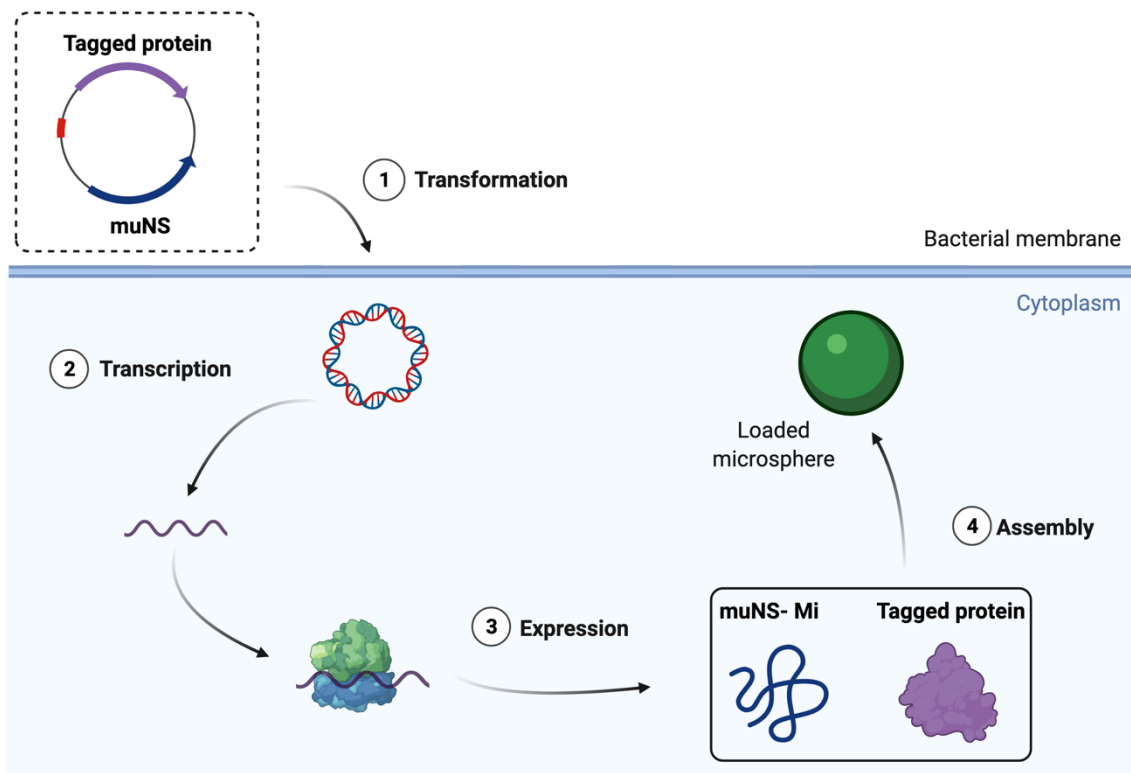


Figure 9. Representation of the process for the production of self-adjuvant epitope loaded microspheres (bacterial version).

2.2. 3D PRINTING

Three-dimensional (3D) printing, also known as additive manufacturing, is a rapid prototyping technique that was first invented over 30 years ago by Charles Hull (26). The term “stereolithography” (SLA) first appeared in his patent in 1986, defining it as a method and apparatus for creating solid objects by successively printing thin

layers of a curable material, e.g., by ultraviolet (UV) laser irradiation, one on top of the other (26). Later, he founded the company 3D Systems in California, making 3D printing commercially available (27). Nowadays, 3D printing is extensively used as a method for producing physical objects using a computer-aided design (CAD) software or an imaging technique. Since it fabricates in a layer-by-layer fashion, 3D printing has the potential to manufacture objects with novel and creative structures unattainable with conventional (subtractive) manufacturing, where complex geometries are achieved via material removal processes (28). It has applications in almost all areas of manufacturing (29, 30) and even the food industry (31). 3D printing has been considered a disruptive and transformative technology both in industry and healthcare, moving medical treatments towards personalized medicines (32), as it has the potential to fabricate small production batches of biological molecules on demand and in a cost-effective and simple setting (32).

A variety of innovative solutions using 3D printing have been reported, including efforts to develop biocatalytic materials that can be molded into controlled, predetermined structures with tunable permeability and surface area, such as the *Methylococcus capsulatus* pMMO in a PEGDA-based polymer hydrogel (33). Other efforts in the field of healthcare include orally disintegrating formulations (34), formulations with novel designs (35) and specific functions, multi-drug combinations (36), paediatric-friendly formulations (37), and various medical devices (38). By 2015, Spritam® (levetiracetam) for epilepsy treatment, the first 3D-printed medicine approved by the United States Food and Drug Administration (FDA), established a significant milestone for the use of 3D printing in manufacturing medicines (39). The American Society for Testing and Materials (ASTM) establish a classification of 3D printing technologies into seven major categories (40): binder jetting, powder bed fusion, material jetting, directed energy deposition, sheet lamination, material extrusion and vat polymerization, (41) (Figure 10)).

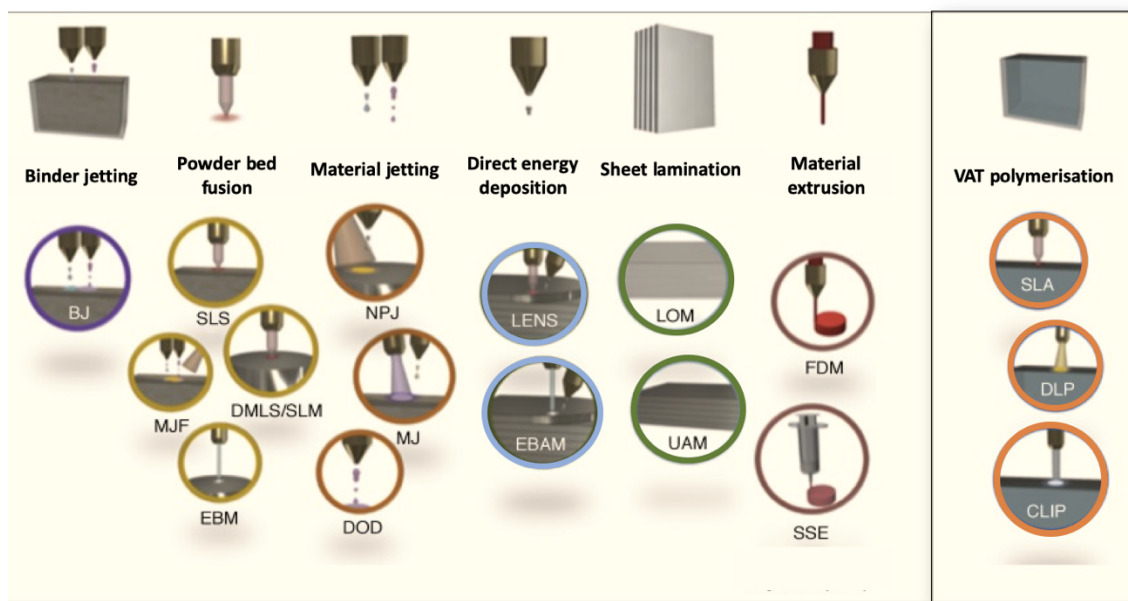


Figure 10. Graphical representation of the multiple 3D printing technologies. SLS, selective laser sintering; DMLS/SLM, direct metal laser sintering/selective laser melting; MJF, material jet fusion; EBM, electron beam melting; NPJ, nanoparticle jetting; MJ, material jetting; DOD, drop-on-demand; LENS, laser engineering net shape; EBAM, electron beam additive manufacturing; LOM, laminated object manufacturing; UAM, ultrasonic additive manufacturing; FDM, Fused deposition modelling; and SSE, semi-solid extrusion; SLA, stereolithography; DLP, direct light processing; CLIP, continuous liquid interface production; BJ, binder jetting. (Source: adapted from Awad, Atheer, et al. "Reshaping drug development using 3D printing." *Drug discovery today* 23.8 (2018)).

2.2.1. Binder jetting

Binder jetting was first invented by Sachs et al. at Massachusetts Institute of Technology in 1993 (42). Here, a layer of powder is spread on the building platform typically by a roller (43). Subsequently, a print head dispenses liquid binding agent onto the powder bed to form a 2D cross-section. Once a layer is solidified, the building platform descends to allow the next layer to be distributed on top of the previous one. Such steps are repeated layer-by-layer until the desired object is formed. The powder bed acts as a physical support for fabricating any overhanging geometries, eliminating the need for support design (44). A broad range of materials including polymers, ceramics, biomaterials, and metals have been processed in binder

jetting for diverse applications in the fields of casting, electronics, and tissue engineering to name a few (45-48). Since its invention, binder jetting has been widely researched in the pharmaceutical arena and the first article was published in 1996, demonstrating the feasibility of fabricating even drug delivery devices (49). Later, more formulations have been developed such as zero-order release tablets (50), erosion mechanism delayed-release tablets (51), and fast disintegrating tablets of the already mentioned Spritam® (Aprecia Pharmaceuticals) (52).

2.2.2. Powder bed fusion

Powder bed fusion refers to selective fusion of powder particles by a thermal source such as a laser into the desired 3D object in a layer-by-layer manner (53). During the printing process, the building platform is raised to its highest position whereupon the powder is homogeneously spread and flattened by a roller. The laser beam is then activated and directed to scan a cross-sectional pattern on the powder bed as dictated by the CAD data. Afterwards, the building platform is lowered while the reservoir platform ascends to allow a fresh layer of powder to be spread by the roller. The process repeats until completion and the printed object is recovered by removing excess unsintered powder with compressed air or by brushing. Currently, powder bed fusion has four subset technologies including selective laser sintering (SLS), selective laser melting (SLM), electron beam melting (EBM) and multijet fusion (MJF) where they differ by feedstock materials (e.g. thermoplastic polymers, metals, ceramics) and the type and amount of laser employed (54). To date, powder bed fusion has found applications in diverse fields including the aerospace, automotive, aviation, medical, dentistry, tissue engineering, and electronics (55-62). More recently, SLS has been exploited within the pharmaceutical sector to produce oral pharmaceutical dosage forms (63-66).



2.2.3. Material jetting

Material jetting is a process that resembles inkjet printing in which droplets of liquid materials selectively deposited through a nozzle onto a substrate (67, 68). During the printing process, water-soluble sacrificial materials such as wax are

automatically printed together to support overhanging structures. One of the main advantages offered by this technology is its multi-material capacity, for example, commercially available inkjet 3D printers such as Polyjet from Stratasys and MultiJet from 3D Systems are capable to dispense multiple photopolymers simultaneously which are immediately cured by the ultraviolet lamps to create multi-material structures. Material jetting has been widely adopted to produce customized anatomical models (69), soft robotics (70), microfluidics (71) as well as scaffolds for tissue engineering (72). Additionally, material jetting offers unique capacities for medical and pharmaceutical applications such as drug screening, compound synthesis, and genomics due to its miniature process, high resolution and lower manufacturing cost (73, 74).

2.2.4. Direct energy deposition

Direct energy deposition uses a focused energy source, typically a laser or electron beam, to melt the material which is simultaneously deposited by a nozzle in the form of wire or powder to build up the 3D object (75). Unlike other 3D printing technologies, the capability of multi-axial deposition enables direct energy deposition to fabricate objects with complex parts and not limited onto a flat substrate (76). This technology is often referred to the process as laser engineered net shaping (LENS), direct metal deposition (DMD), electron beam additive manufacturing (EBAM), and directed light fabrication (DLF). A wide selection of metals can be chosen for direct energy deposition 3D printing such as titanium, stainless steel, aluminium, copper, and nickel and combinations of materials are also allowed for the fabrication of components with composition gradients or hybrid structures (77). In addition, direct energy deposition is suitable for repairing and remanufacturing components including turbine blades, airfoils, and compressor seals in various industries (78, 79).



2.2.5. Sheet lamination

Sheet lamination, is a process that involves layer-by-layer cutting and lamination of materials for the fabrication of a designed object (80). First, a sheet of

adhesive-coated material (e.g. paper, plastic, metal) is supplied from the roller onto a build platform. Depending on the order in which the layers are cut and bonded together, the sheet lamination process can be divided into two different approaches (81). In the bond-then-form approach, the layers undergo a cutting process first by lasers or blades into the desired shape prior to bonding together whereas in the bond-then-form approach, the layers are bonded together to the substrate and are then cut according to the slice contour. The process of bonding and cutting is repeated until the final object is created. The form-then-bond technique such as laminated object manufacturing (LOM) facilitates the creation of parts with internal features and channels, enabling microfluidic structures which is challenging or impossible with the bond-then-form methodology. Ultrasonic additive manufacturing (UAM), a subcategory of sheet lamination, is a hybrid process combining ultrasonic metal seam welding and computer numerical control milling (82). Due to the fact that UAM is the only 3D printing technique where metals can be constructed at low temperatures, it offers the capability to allow the embedment of fibre optics, wires, and sensors into a metal matrix.

2.2.6. Material extrusion

Material extrusion is one of the most common 3D printing technologies, referring to a process in which the material is selectively dispensed through a nozzle onto the building platform. Based on the feeding materials and printing process, there are several variants of extrusion-based 3D printing techniques like fused deposition modelling (FDM) or semi-solid extrusion (SSE). FDM or fused filament fabrication (FFF) is a material extrusion process where a filament is fed through a heated nozzle under controlled temperature, molten and layer-by-layer deposited on a building platform to create solid geometries (83, 84). It is currently one of the most commonly used 3D printing technologies thanks to its low cost and ease of use. Typically, the feedstock filaments are made of thermoplastic polymers, for example, polylactic acid (PLA), polyvinyl alcohol (PVA), and acrylonitrile butadiene styrene (ABS). Recent advances in filament fabrication allows the preparation of composite filaments with hot melt extrusion (HME) by blending different materials such as wood (85), metallic

particles (86), conductive materials (87), and active pharmaceutical ingredients (88-90).

Apart from FDM, semi-solid extrusion (SSE), also residing under the material extrusion umbrella, is a process based on the deposition of gels or pastes on the building platform to create solid objects employing pressure-assisted microsyringes (83). Benefiting from the nature of the feedstock materials, printing at low temperature is allowed but post-processing steps, for instance, drying or cooling are required. This technology has been adapted for printing of biomaterials or even cell-embedded bioinks to fabricate and regenerate tissues and organs (91, 92). In terms of other applications, SSE has been utilized to prepare electronics (93-95), food (96, 97), and a range of pharmaceutical formulations such as chewable dosage forms for paediatric population (37, 98, 99), polypills (100, 101), and medical devices (102, 103).

2.2.7. Vat photopolymerisation

Vat photopolymerization is a generic term given to describe a range of 3D printing technologies that use computer-spatially-controlled photopolymerization to create solid objects from a vat of liquid resins under light irradiation (Figure 10 and 11). Conventionally, vat photopolymerization-based techniques such as SLA fabricate objects in a layer-by-layer fashion using a laser beam as the light source (104, 105). More recently, digital light processing (DLP) is gaining increasing interests where illumination of an entire layer can be achieved by a digital micromirror device or a liquid crystal display at once, significantly reducing the printing time. Using a similar concept as DLP, continuous liquid interface production (CLIP) emerged with the creation of a 'dead zone' in between the oxygen-permeable window and the cured part. This enables the printed 3D object to be continuously drawn out of the resin at production rates of hundreds of millimetres per hour (106, 107). Different from the aforementioned layer-based fabrication methods, tomographic volumetric additive manufacturing has been developed recently where the entire object can be solidified simultaneously from a volume of liquid photopolymer through photopolymerisation, allowing fast build speed and geometric versatility (108, 109). Compared with other 3D printing technologies, vat photopolymerisation-based techniques offer the

benefits of superior accuracy, smooth surface finish and printing resolution up to nano-scale region (100 nm), enabling the creation of complex microstructures (e.g. two-photon polymerisation (2PP)) (110, 111). By coupling with patient's clinical imaging data, they are also powerful tools for the fabrication of biomedical applications such as patient-specific medical devices and implants, tissue-engineered constructs for regeneration, diagnostic testing, surgical guide, and drug delivery (38, 39, 112-114).

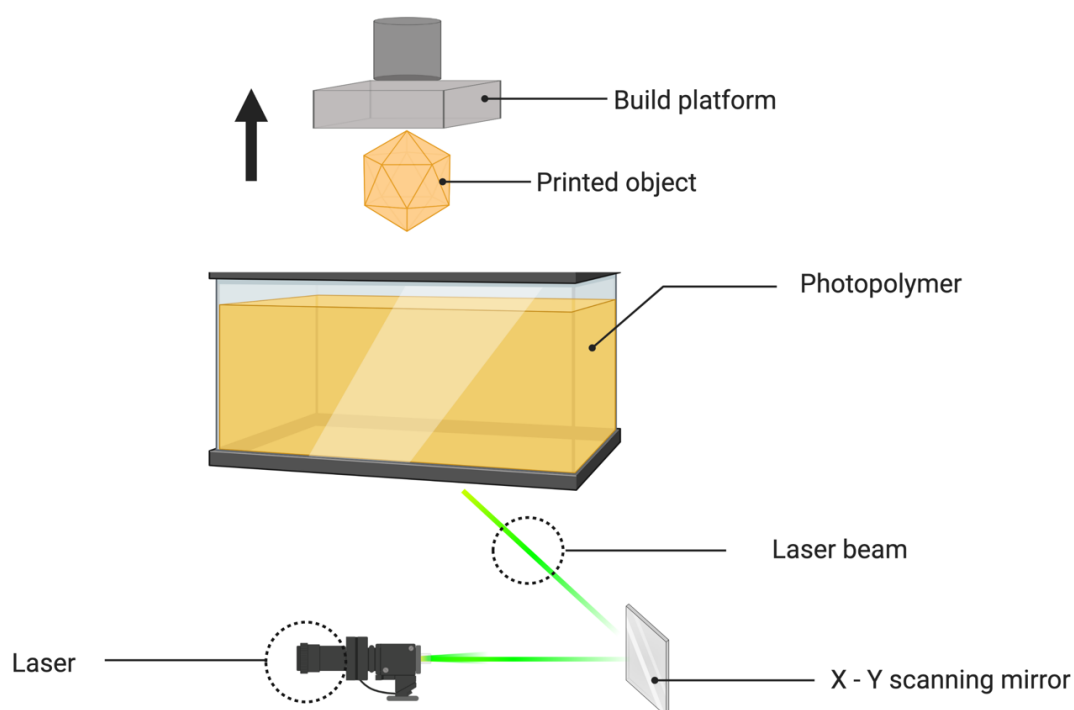


Figure 11. Vat photopolymerization 3D printing for the fabrication of 3D structures. The technology uses computer-spatially-controlled photopolymerization to create solid objects from a vat of liquid resins (photopolymers) under light irradiation.



In addition, vat photopolymerization is considered one of the most promising technologies (115), as it allows the fabrication of complex internal structures with intricate details. It also has a high production speed compared with other 3D printing

technologies (e.g., extrusion- or melting-based techniques), so more objects can be produced within a given timeframe [50]. Specifically, stereolithography (SLA) offers the possibility to fabricate crosslinked polymeric matrices via photopolymerization, with a superior resolution while avoiding the need of high temperatures.

Since its introduction, vat polymerization has rapidly grown as a promising manufacturing approach, expanding its boundless applications in a variety of fields, ranging from aerospace (116), electronics (117, 118), robotics (70), building and construction (119), food industry (120), as well as biomedical research such as personalized medicines (121-123), biosensors (124), and prosthesis (105). It even reached the fashion industry with 3D printed shoes and jewellery making (125). In the field of medicine, by combining vat polymerization with medical imaging techniques enables the production of patient-specific surgical tools, implants, and tissue engineering scaffolds. For all that, VAT polymerization is the technique chosen in this thesis to immobilize proteins with enzymatic activity.

OBJECTIVES

Considering all precedents and the current challenges in protein immobilization for multiple applications, this doctoral study aims at the design and testing of a new protein immobilization strategy offering enhanced performing capabilities than traditional technologies. The objectives of this thesis are:

1. Test the ability of the IC-tagging platform to produce enzymes for industrial use and whether this technology would improve the enzyme performance.
2. Immobilize via 3D printing of the Laccase from *Trametes Versicolor* for optimization purposes to address the potential of this technology for industrial purposes by checking the removal of pharmaceuticals and concerning micropollutants from aqueous environments.
3. Test the IC-Tagging platform as a possible self-adjuvant immobilization strategy in the field of cancer immunotherapy.

MATERIALS AND METHODS

1. MATERIALS

1.1. BIOLOGICAL MATERIAL

1.1.1. Eukaryotic cells

- B16-OVA cells: pseudo-metastasis model cell line expressing the OVA antigen, previously generated from the parent B16 cell line obtained by the Cancer Research UK Cell Service Laboratory.

- Peripheral blood mononuclear cells (PBMCs): contributed by the Joint United Kingdom Blood Transfusion and Tissue Transplantation Services Professional Advisory Committee (JPAC).

- Bone marrow derived dendritic cells (BMDCs): obtained from C57BL/6 mice, from which two derivatives were obtained, on one hand Flt3L-BMDCs derived by means of the Flt3L ligand, which has as receptor tyrosine kinase that regulates dendritic cell development. On the other hand, the GM-CSF-BMDC derived employing the granulocyte-macrophage colony stimulating factor or colony stimulating factor 2 (CSF2), a cytokine involved in the development and homeostasis of mononuclear phagocytes, which is widely used to generate CD11c + MHCII + cells.

- Splenocytes: obtained from immunized mice to carry out cytotoxic activity tests on T lymphocytes.

1.1.2. Prokaryotic cells

- XL1-Blue (Stratagene): *Escherichia coli* strain used for the growth and purification of plasmids. Genotype: recA1 endA1 gyrA96 thi-1 hsdR17 supE44 relA1 lac [F' proAB lacIqZΔM15 Tn10 (Tetr)].

- BL21 (DE3) Codon Plus-RP (Stratagene): *Escherichia coli* strain used for protein expression in bacteria through T7 polymerase. Genotype: B F- ompT hsdS (rB- mB-) dcm + Tetr gal λ (DE3) endA Hte [argU proLL Camr].

- Rosetta TM (DE3) Competent Cells - (Novagen): BL21 strain used for the expression of proteins in bacteria through T7 polymerase. Genotype: F-ompT hsdSB (rB- mB-) gal dcm (DE3) pRARE (CamR).

1.1.3. Plasmids

- pcDNA 3.1 (Invitrogen): vector for transient expression in eukaryotic cells. The cloned genes are under the control of the cytomegalovirus early promoter.

1.1.4. Antibodies

1.1.4.1. Primary antibodies

- Polyclonal antibodies against the muNS protein (Tourís-Otero et al., 2004b), generated in our laboratory by immunizing rabbits with the denatured muNS protein extracted from an SDS-PAGE gel. They were used in Western-blot at dilutions between 1: 5000 and 1: 10000 and in immunofluorescence at dilutions between 1: 1000 and 1: 5000.

1.1.4.2. Secondary antibodies

- Goat antibodies against rabbit and against mouse IgG conjugated with peroxidase for detection by Western-blot (Sigma-Aldrich, Madrid, Spain). Used at a 1:10,000 dilution.
- Goat antibodies against rabbit and against mouse IgG conjugated with various fluorochromes: Alexa Fluor 488, Alexa Fluor 594 (Invitrogen, Barcelona, Spain), for detection by fluorescence microscopy. All of them were used in dilutions that varied between 1:1000 and 1:20000.
- Biotin Rat Anti-Human IL-6 Clone MQ2-39C3 (RUO).
- IL-6 Monoclonal Antibody (MP5-32C11), Biotin, eBioscienceTM.
- IL-12/IL-23 p40 Monoclonal Antibody (C17.8), Biotin, eBioscienceTM.

- TNF alpha Monoclonal Antibody (MP6-XT3), Functional Grade, eBioscience™.
- Anti-Human IgG (H+L), HRP Conjugate (Promega).

1.1.4.3. Capture antibodies and standards for ELISA

Detected molecule	Coating reagent	Dilution	Source	Identifier	Detection antibody	Dilution	Source
Human IL-12p40	Mouse anti-human IL-12/p40	5µg/ml	BD	C8.3	Mouse anti-human IL-12, Biotin	2.5µg/ml	BD
Human IL-6	Rat anti-human IL-6	4µg/ml	BD	MQ2-13A5	Rat anti-human IL-6, Biotin	2.5µg/ml	BD
Mouse IL-12p40	Rat anti-mouse IL12/p40	5µg/ml	BD	C15.6	Rat anti-mouse IL-12/p40, Biotin	1µg/ml	BD
Mouse IL-6	Rat anti-mouse IL-6	4µg/ml	BD	MP5-20F3	Rat anti-mouse IL-6, Biotin	1.5µg/ml	BD
Mouse IFN α	Anti-mouse IFN α	1:100	Hycult Biotech	mAb F18	Mouse anti-rabbit biotin	1:1000	Jackson Immuno Research
Human TNF α	Anti-human TNF α	5µg/ml	BD	G281-2626	Mouse anti-human TNF α , Biotin	1µg/ml	BD

Table 1. List of antibodies and recombinant proteins used throughout the study for coating or detection in ELISA.

1.1.4.4. Standards

Standard	Starting concentration	Serial dilution	Source
Human IgG1, recombinant (RUO)	1 μ g/ml	1:2	BioLegend
Human IL-12, recombinant (RUO)	20ng/ml	1:3	BD
Human IL-6, recombinant (RUO)	5ng/ml	1:3	BD
Mouse IL-12, recombinant (RUO)	16.7 ng/ml	1:3	R&D
Mouse IL-6, recombinant (RUO)	50ng/ml	1:3	R&D
Mouse IFN α , recombinant (RUO)	10 000U/ml	1:3	Hycult Biotech HC
Human TNF α , recombinant (RUO)	20ng/ml	1:10	BD

Table 2.: List of standards used in ELISA (antibodies and recombinant proteins) used throughout the study.

1.1.5. Enzymes

- Laccase from *Trametes versicolor* (0.5 U/mg), Sigma-Aldrich (Dorset, UK).

1.2. NON-BIOLOGICAL MATERIAL

1.2.1. Culture media

- R10 medium containing RPMI 1640 medium, 10% heat-inactivated fetal bovine serum (Gibco), 100U/ml penicillin, 100mu/ml streptomycin (Sigma) and 50mM B-Mercaptoethanol were used to maintain the B16-OVA cell line.
- Luria-Bertani (LB) medium containing 0.2% glucose was used to culture the bacteria in suspension. To select transformed bacteria, 100µg/ml ampicillin, gentamicin (7µg/ml) (Sigma, Madrid, Spain), tetracycline (10µg/ml) (Sigma, Madrid, Spain) or kanamycin (50µg/ml) (Sigma, Madrid, Spain) were added to the medium, according to the selection method for each plasmid. For the culture in solid medium, the same medium was used with the same concentrations of antibiotics, supplemented with 1.5% bacto-agar (Sigma). The composition of these media is described in detail in the protocol manual of Sambrook et al. (1989).

1.2.2. Solutions and buffers

- DAPI: prepared at 100µg/ml in sterile water and sterilized through a 0.22µm filter.
- Mounting medium: 6g of glycerol; 2.4g of Mowiol 14-88; 6ml of H₂O and 12ml of 0.2 M Tris-HCl (pH 8.5).
- PBS-T-Milk: PBS-T with 4% skimmed milk powder.
- PBS-T: PBS with 0.05% Tween-20.
- PBS-EDTA: 137mM NaCl; 2,7 mM KCl; 8mM Na₂HPO₄; 1,5mM KH₂PO₄ and 5mM EDTA.

- PBS: 137mM NaCl; 2,7mM KCl; 8mM Na₂HPO₄ and 1,5mM KH₂PO₄.
- Transformation solution (TSS): 10% PEG 4000; 5% DMSO; 25mM MgCl₂; 10% glycerol in LB.
- Fekete solution: 70% EtOH, 3.7% PFA, 0,75M glacial acetic acid.
- DNA electrophoresis buffer (TAE): 40 mM Tris; 1,1%, acetic acid and 1mM EDTA, (pH 8.3).
- SDS-PAGE electrophoresis buffer (Tris-Glycine-SDS): 25mM Tris-HCl (pH 8.3); 192 mM glycine and 0,1% SDS.
- Sample buffer for 6x DNA: 15% Ficoll; 0,25% bromophenol blue and 0,25% xylene cyanol.
- Transfer buffer: 25mM Tris-HCl (pH 8.3); 192mM glycine and 20% methanol.
- Laemmli buffer (1x): 10% glycerol; 60mM Tris-HCl (pH 6.8); 5% β-mercaptoethanol; 0,05% bromophenol blue and 2% SDS.
- Bacterial lysis buffer: 20mM Tris-HCl (pH 7.5); 200mM NaCl; 1mM DTT; 2mM MgCl₂; 0,25% Tween 20; 1mg/ml lysozyme and 10mM protease inhibitor.
- TRB+ buffer: 10mM Hepes-KOH (pH 7.9); 10mM KCl and 5mM MgCl₂.
- TRB- buffer: 10mM Hepes-KOH (pH 7.9) and 10mM KCl.
- FACS buffer
- Citric acid monohydrate (Mw 210.15g/mol), Fisher Scientific (Loughborough, UK).
- Di-sodium hydrogen orthophosphate dodecahydrate (MW 358,137g/mol), Fisher Scientific (Loughborough, UK).
- Glutaraldehyde (70%), Sigma-Aldrich (Dorset, UK).
- 2,2'-azino-bis (3-ethylbenzothiazoline-6-sulfonic acid) (ABTS) (Sigma).
- NaCl, Sigma-Aldrich (Dorset, UK).
- ZnCl₂, Sigma-Aldrich (Dorset, UK).
- CaCl₂, Sigma-Aldrich (Dorset, UK).
- CuCl₂, Sigma-Aldrich (Dorset, UK).
- Dye reactive blue 19 (RB19).
- OPD (o-phenylenediamine dihydrochloride) (Thermo).
- Ligand AF660 (Promega).

- Polymyxin B sulfate salt, Sigma-Aldrich (Dorset, UK).
- CpG 1668 (Eurofin Genomics).
- PolyUs21 - (ThermoFisher Scientific).
- Organic solvents such as methanol, ethanol, acetone (Sigma-Aldrich, Dorset, UK).
- Collagenase/DNase: 25µl of the 40x stock of Collagenase D and 10µl of the 100x stock of DNase for each 1ml of R10 medium.
- Coating buffer: 0,1M NaHCO₃, pH 8.2 (except for mouse TNF ELISA: 0,1M Na₂HPO₄, pH 6.0)
- Washing buffer: PBS containing 0,05% Tween (0,5ml Tween-20 in 1000ml PBS).
- Flt3-ligand, recombinant, murine (Flt3L) (R&D Systems).
- GM-CSF, recombinant, murine (Peprotech).
- Blocking solution (ELISA buffer): PBS containing 2,5% FCS and 0,02% NaN₃.
- AP-Streptavidin, Sigma-Aldrich (Dorset, UK).
- RIPA buffer: 50mM Tris-HCl (pH 8.0); 150mM NaCl; 1% Nonidet P-40; 0,5% sodium deoxycholate and 0,1% SDS.
- TSS buffer: 10% PEG 4000; 5% DMSO; 25mM MgCl₂; 10% glycerol and 80% LB.
- Luciferase buffer: 220mM K₂HPO₄ and 30mM KH₂PO₄.
- Poly(ethylene glycol) diacrylate (PEGDA, average Mn 575), Sigma-Aldrich (Dorset, UK).
- Photoinitiator, lithium phenyl-2,4,6-trimethylbenzoylphosphinate (LAP, MW 294.21g/mol).

1.2.3. Pharmaceuticals

- Diclofenac sodium (Mw 318.13g/mol), Sigma-Aldrich (Dorset, UK).
- 17-Alpha-ethinyl estradiol (EE2), (Mw 296.40g/mol), Sigma-Aldrich (Dorset, UK).

1.2.4. Flow Cytometry Materials

- FACS tubes (BD).
- 96-well U-plates, sterile, non-TC treated (3788, Costar).
- LIVE/DEAD Fixable Violet Dead Cell Stain Kit (Thermo Fisher Scientific).
- Streck Cell Preservative (Alpha Laboratories).
- Paraformaldehyde (PFA) (VWR).
- FACS buffer: PBS, 1% heat-inactivated FCS, 5mM EDTA, 0,02% NaN₃.
- Intracellular buffer: FACS buffer supplemented with 0,1% saponin.
- OneComp eBeads™ Compensation Beads (eBioscience).
- FACS Canto II flow cytometer (BD).
- LSR Fortessa flow cytometer (BD).
- FACS Aria II (BD).
- FlowJo v10 software (FlowJo, LLC).

1.2.5. Enzyme-linked immunosorbent assay (ELISA) for detection of cytokines.

- Nunc Maxisorp Immunoplates, 96-well (Nunc 4-39454, Thermo Scientific).
- Flexiplates: Serocluster™ 96-well “U” bottom Plate, non-treated, vinyl (2797, Costar).
- Lid for flexible plate (BD).
- Coating buffer: 0,1M NaHCO₃, pH 8.2.
- PBS-Tween: PBS containing 0,05% Tween.
- Blocking buffer 1: PBS containing 2,5% FCS and 0,02% NaN₃
- ExtrAvidin®-AP: Steptavidin-Alkaline phosphatase (Sigma).
- ELISA substrate: SIGMAFAST™ p-Nitrophenyl phosphate tablets (Sigma).
- FreeStyle™ Expression Medium (Invitrogen).

- R10: RPMI 1640, 2mM glutamine, 10% FCS and 100U/ml penicillin, 100µg/ml streptomycin, 50µM 2-ME.
- PBS: 1x DPBS [-] CaCl₂, [-] MgCl₂ (Gibco).
- SpectraMax M5 96 well plate reader (Molecular Devices).

1.2.6. In vivo imaging Materials

- In Vivo Imaging System - IVIS Spectrum® (Perkin Elmer).
- Living Image® 4.7.2 (Caliper Life Sciences).
- XenoLight D-Luciferin, Potassium Salt (PerkinElmer).

2. METHODS

2.1. MANIPULATION OF CELL CULTURES

2.1.1. Handling conditions

The manipulation of the biological materials was carried out under sterile conditions inside a vertical laminar flow cabinet. The cell lines were kept inside a Napco incubator at 37°C, with a relative humidity of 95% and a partial pressure of CO₂ of 5%. The disposable material was sterilized in the autoclave before its final disposal.

2.1.2. Propagation and conservation of cell lines

In the freezing process, cells from confluent cultures were disaggregated and centrifuged for 5 min at 600xg. The pelleted cells were resuspended in 500µl of culture medium and 500µl of freezing medium (D-MEM or 199 supplemented with 40% FBS and 20% dimethyl sulfoxide as cryoprotective agent) were added. The cell suspensions were dispensed in 1ml aliquots, in sterile preservation cryotubes. The vials were kept

at 4°C for 5 min, later transferred to -80°C for at least 24 h, they were then stored in liquid nitrogen.

Thawing frozen cell stocks were performed by immersing the vials in a 37°C water bath to achieve rapid thawing. Subsequently, the contents of the vial were transferred to Falcon tubes containing complete culture medium previously heated to 37°C, and centrifuged for 5 min at 600xg to remove the freezing medium. The pelleted cells were then resuspended in culture medium, transferred to cell culture flasks with medium, and incubated at 37°C.

2.1.3. Obtaining bone marrow derived Flt3L dendritic cells (Flt3L -BMDCs)

Forceps and scissors were used to remove femurs and tibiae from the hind legs of the culled C57BL/6 mice. The bones are deposited in a Petri dish, where the ends are cut with the help of scissors, and the bone marrow is flushed out of the bone using a R10 RPMI medium loaded syringe with a 23G needle. The result is passed through a 70µm mesh and washed with R10 medium. Cells are counted and adjusted at a number of 1.5×10^6 cells/ml with R10 medium. The Flt3L ligand is then added to a final concentration of 50ng/ml and 5ml of the suspension is seeded per well in 6-well plates. On the fifth day, a partial exchange of the medium is made, removing 4.5 ml and adding 5 ml of fresh medium with a fresh concentration of 50ng/ml of Flt3L. On the eighth day the same procedure is repeated and on the tenth day, the cells are collected by pipetting and washing the non-adherent cells. Only non-adherent and loosely adherent cells are selected for the *in vitro* assays.

2.1.4. Obtaining GM-CSF dendritic cells derived from bone marrow (GM-CSF - BMDCs).

Forceps and scissors are used to remove femurs and tibiae from the hind legs of the culled C57BL/6 mice. The bones are deposited in a Petri dish, where the ends are cut with the help of scissors, and the bone marrow is flushed out of the bone using a R10 RPMI medium loaded syringe with a 23G needle and brought to a total volume of 4ml. This volume is transferred to a TC plate with 8ml of R10 medium and incubated for 30min in the 5% CO₂ incubator. Subsequently, non-adherent cells

are harvested and passed through a 70 μ m strainer, to be finally centrifuged 5min at 300xg, RT. Cells are then adjusted at 1.3x10⁶ cells/ml using 10cm TC dishes in 12ml of medium R10 RPMI supplemented with 20ng/ml GM-CSF, following previous work (126). The day the cells are cultured is deemed day 0. After two days, a partial exchange of the medium is made by replacing it with the same volume of fresh R10 medium containing 20ng/ml GM-CSF. On the third day, a total exchange of the medium is made and all non-adherent cells are discarded, taking special consideration in washing the adherent fibroblasts. On the fourth or fifth day, the non-adherent or partially adherent cells are collected by pipetting, thus discarding the adherent cells, these cells can be directly treated for activation tests.

2.1.5. Preparation of splenocytes for T-cell cytotoxic activity tests (CTL activity)

Splenocytes from C57BL/6 mice are obtained using aseptic techniques and sterile tools, mediated spleen digestion with 1mg/ml Collagenase D and 200 μ g/ml DNaseI. This enzymatic mixture is injected into the spleen and subsequently incubated for 30 minutes and 37°C. A subsequent trituration is performed through a 70 μ m mesh for cells in PBS-EDTA. The cells obtained are centrifuged at 300xg for 5 minutes and resuspended in 30ml of R10 medium, to be passed again through a 70 μ m cell mesh, centrifuged and aliquoted. Cells are then resuspended in 3ml of R10 containing 0 or 200nM of SIINFEKL (OVA class I-restricted peptide) for 60 to 90 minutes in a bath at 37°C. Over time, cells are washed twice using 10ml of PBS and resuspended in 2ml of PBS containing 5 μ M CFSE for the 0nM concentration antigen, and 0,5 μ M CFSE for 200nM concentration antigen by incubating cells for 10 minutes in a 37°C bath. The same amount of FCS is then added, and the cells are incubated for 1 minute at room temperature, after they are washed twice with PBS and the aliquots combined and passed through a 70 μ m mesh (BD), thus avoiding the presence of clots. These cells are stained for live/dead-cell discrimination and counted to be administered intravenously into the tail vein. The optimal injection time may vary depending on the frequency of the CTL precursor and its preparation.

2.1.6. Ex vivo Preparation and restimulation of splenocytes for flow cytometry

Spleens from sacrificed tumor-carrying animals are collected on ice, and 1ml of the Collagenase D/DNase solution is prepared per spleen. Each spleen is maintained with forceps over a 15ml Falcon tube, in order to inject 1ml of Collagenase D/Dnase into the spleen, a small amount will be retained in the spleen, as the swelling can be seen, but most effectively passes through, releasing the splenocytes and displaying a change in color. Once this is performed, the spleen is dropped into the Falcon tube with the Collagenase D/Dnase solution and incubated for 30min at 37°C. The cell suspension and spleen are then filtered through a 70µM cell mesh in a new 50ml Falcon tube. The spleen remaining on the mesh is washed once with PBS/EDTA and then ground with the plunger using for this the plunger of a 1ml syringe, followed by multiple washes with PBS/EDTA until the spleen tissue is completely bypassed inside the tube. Cells are centrifuged at 1500 rpm, 5 minutes and at 4°C and then resuspended in PBS/EDTA and passed again through the cell mesh and get rid of clots formed by dead cells. Cells are counted expecting approximately 10⁸ cells/spleen. Cells are resuspended in 2.5ml of FACS buffer and passed once more through the cell mesh, of the total 200µl is used for FACS analysis.

2.1.7. In vitro immune activation assay

The immune activation profile of both the TLR and non-TLR agonists used in this study (listed in Table 3), were evaluated *in vitro* using different strategies, such as human PBMCs, mouse GM-CSF derived BMDCs, mouse Flt3L-derived BMDCs. 1-5x10⁵ cells were used in 100µl complete R10 in TC-treated 96-well plates with flat bottom. For GM-CSF differentiated BMDCs, the R10 medium was also supplemented with 40ng/ml GM-CSF. In the same way, when Flt3L derived BMDCs were used *in vitro*, R10 medium was supplemented with 100ng/ml Flt3L. TLR agonists or controls were diluted to 100µl /replicate with R10 before adding to the wells. The final volume used in each well was always constant at 200µl. Each dilution of the agonist, control or testing nanospheres was performed in triplicate. The wells containing 100µl cells were completed with 75µl the medium R10 and 25µl of agonists

added per well. Plates were always placed in the incubator overnight at 37°C, 5% CO₂. The following day, plates were frozen at -20°C or -80°C to be used during the measurement. The read-out of the assay was cytokine production (typically IL-6 and IL-12p40) measured by ELISA, as described further.

Stimulus
Lipopolysaccharides (LPS)
Flagellin
Pam3CysSerLys4 (Pam3CSK4)
Resiquimod (R848)
Monophosphoryl Lipid A (MPLA)
Incomplete Freund's adjuvant (IFA)
Alhydrogel
AddaVax
QuilA
Polyinosinic:polycytidylic acid (poly I:C)
CpG oligodeoxynucleotides (CpG ODN)
Ovalbumin muNS (OVA muNS)
Luciferase muNS (luc muNS)
HaloTag muNS (Halo muNS)

Table 3. Adjuvants used during the study.

2.2. MANIPULATION OF NUCLEIC ACIDS.

2.2.1. Plasmid DNA purification.

Small-scale DNA purification for transformant analysis was performed using the NucleoSpin® Plasmid EasyPure system (Macherey-Nagel) from 3ml of bacterial culture. To obtain DNA on a larger scale, the plasmid was isolated from 50ml of bacterial culture using the PureYield™ Plasmid Midiprep System (Promega, Madrid, Spain), following the instructions of the commercial company.

2.2.2. Polymerase chain reaction

The standard reactions were carried out keeping the concentrations of the reagents and the amplification cycles constant, except for the hybridization temperature and the extension time, which varied depending on the oligonucleotides used and the size of the DNA used as template for start the reaction. Generally, the amplification program used was: 1 cycle (2 min at 94°C), 30 cycles (30 sec at 94°C, 30 sec between 55-65°C and between 30 sec –4 min at 72°C) and a final cycle of 10 min at 72°C. In all cases the amplification reaction contained 5 units of Pfu DNA polymerase (Thermo Scientific) and 2mM MgCl₂, 0.2mM dNTPs, 0.5μM of each primer and 1ng of plasmid.

2.2.3. Isolation and purification of DNA fragments

DNA fragments from PCR reactions or restriction enzyme digestions were separated by electrophoresis on 0.8-2% agarose gels in 1xTAE in the presence of 0.5μg/ml of ethidium bromide (127). The DNA band was cut from the gel with a blade, transferred to a microtube, and the DNA was purified using the commercial NucleoSpin® Gel and PCR Clean-up kit (Macherey-Nagel) following the supplier's instructions.

2.2.4. Cutting and joining of DNA fragments

Restriction enzyme digestions of DNA (Thermo Scientific) were carried out according to the supplier's instructions, in the supplied buffers and at the optimum temperature for each case. The ligation reactions were performed at room temperature with phage T4 DNA ligase (Thermo Scientific) with a molar ratio between vector and insert of 1:7.

2.2.5. Recombinant plasmids construction

- pcDNA IC-CotA

For this construction, the sequence of CotA was obtained by PCR amplification from the genomic DNA of *Bacillus Subtilis*. The forward primer was 5'-CGCTGCAGTATG ACACTTGAAAATTT-3' (PstI site is single underlined) and reverse primer was 5'-CGCGCGGCGC TTATTTATGGGGATCAGTT-3' (NotI site is single underlined and stop codon is double underlined). The PCR product was digested and cloned between the KpnI and XbaI targets into the plasmid pcDNA3.1Zeo-IC-Xa to generate the plasmid pcDNA-IC-Xa-CotA. This plasmid was previously made in our laboratory (data not shown) in which the IC had previously been cloned between the HindIII and KpnI restriction targets. In this way, we obtained the plasmid that expresses the protein called IC-CotA, with a molecular weight of 55.8 kDa).

- pcDNA OVA-IC

For this construction, the sequence of OVA was obtained by PCR amplification from the plasmid pcDNA3-OVA provided by Sandra Diebold from the NIBSC. The forward primer was 5'-GCGGAATTCACCATGGGCTCCATCGG-3' (EcoRI site is single underlined and ATG initiator is double underlined) and reverse primer was 5'-CGCTCTAGAAGGGGAAACACATCTGCC-3' (XbaI is single underlined). The PCR product was digested and cloned between the EcoRI and XbaI targets into the plasmid pcDNA3.1Zeo-Xa-IC to generate the plasmid pcDNA-Xa-

OVA-IC. In this way, we obtain the plasmid that expresses the protein called OVA-IC, with a molecular weight of 51kDa).

- pcDNA TRP2-IC

In this case, the sequence of TRP2 was obtained by PCR amplification from the plasmid pcDNA3-TRP2 provided by Sandra Diebold from the NIBSC. The forward primer was 5'-GCGGATATCACCATGGGCCTTGTGG -3' (EcoRV site is single underlined and ATG initiator is double underlined and reverse primer was 5'-CGCGCGGCCGCGGGGCTTCCTCCGTG -3' (NotI site is single underlined). The PCR product was digested and cloned between the EcoRV and NotI targets into the plasmid pcDNA3.1Zeo-Xa-IC to generate the plasmid pcDNA-Xa-TRP2-IC. In this way, we obtained the plasmid that expresses the protein called TRP2-IC, with a molecular weight of 67.2 kDa).

2.3. PROTEIN EXPRESSION AND MANIPULATION

2.3.1. Generation of dual plasmids for expression in bacteria

- pET Duet 1. muNS-Mi (24)
- pET Duet 1. muNS-Mi 2. IC-CotA

To express the IC-CotA protein at the same time as muNS-Mi.

- pET Duet IC-CotA (128)



To express the free IC-CotA protein as a control.

- muNS-Mi-OVA-IC-petDuet1

To express the OVA-IC protein at the same time as muNS-Mi, the recombinant plasmid pcDNA OVA-IC was subjected to amplification using the following primers: the forward primer was 5' – GCGAGATCTCACCATGGGCTCCATCGG -3' (BglII site is single underlined and ATG initiator is double underlined) and the reverse primer was 5'- GCGAAGCTTTTTACGCTTCCACACGGG -3' (XhoI site is single underlined and stop codon is double underlined). The PCR product was digested and cloned into the plasmid pET Duet 1. muNS-Mi to generate the plasmid pET Duet 1. muNS-Mi 2. OVA-IC.

- muNS-Mi-TRP2-IC-petDuet1.

To express the TRP2-IC protein at the same time as muNS-Mi, the recombinant plasmid pcDNA TRP2-IC was subjected to amplification using the following primers: the forward primer was 5' – GCGCATATGGGCCTTGTGGGATGG -3' (NdeI site is single underlined) and the reverse primer was 5'- CGCAGATCTTTTTACGCTTCCACACGGGGTTC -3' (BglII site is single underlined and stop codon is double underlined). The PCR product was digested and cloned into the plasmid pET Duet 1. muNS-Mi to generate the plasmid pET Duet 1. muNS-Mi 2. TRP2-IC.

- pET Duet 1. muNS-Mi 2. Luciferase-IC

To express the Luciferase-IC protein at the same time as muNS-Mi, the recombinant plasmid pFastBac Luciferase-IC was subjected to amplification using the following primers: the forward primer was 5' – GCGCATATGGGAAGACGCCAAAAAC-3' (NdeI site is single underlined) and the reverse primer was 5'- CGCAGATCTTTTTACGCTTCCACACGGGGTTC -3' (BglII site is underlined and stop codon is double underlined). The PCR product was digested and cloned into the plasmid pET Duet 1. muNS-Mi to generate the plasmid pET Duet 1. muNS-Mi 2. Luciferase-IC.

- pET Duet 1. muNS-Mi 2. Halotag-IC (24)

2.3.2. Protein expression in bacteria

For protein expression in bacteria, BL21 DE3 Codon plus-RP (Stratagene) or Rosetta™ (DE3) Competent Cells (Novagen) were transformed with the plasmid containing the sequences for the proteins of interest. Subsequently, a pre-culture of a colony from that plate is incubated at 37°C overnight. Then, it was diluted 25 times and incubated at 37°C until reaching an OD 600: 0.4-0.6. At this point, the bacteria were induced with 1mM IPTG and incubated at 37°C with shaking for 3h. The induced bacteria were centrifuged at 3200xg for 30 min at 4°C and washed twice with 1X PBS. Finally, the pellet was resuspended in lysis buffer and frozen for at least 24h before purification.

For the particular case of the expression of CotA in bacteria, Rosetta™ (DE3) Competent Cells (Novagen), and microaerobic conditions are required. The bacteria were transformed with the plasmid containing the sequences for the proteins of interest and a preculture is incubated at 37°C overnight. Then, bacteria were diluted 25 times with LB medium supplemented with 0.25mM CuCl₂ and incubated at 25°C with shaking at 100rpm for 5h. After that, shaking was stopped and the bacteria were further incubated overnight at 25°C. The induced bacteria were then centrifuged at 3200xg for 30min at 4°C and washed twice with PBS. Finally, the pellet was resuspended in lysis buffer and frozen for at least 24h before purification with protease inhibitor.

2.3.3. Purification of nanospheres from bacteria

The thawed pellet from bacteria is incubated for 30 minutes with 1mg/ml lysozyme at 37°C in the same lysis buffer that was used for the freezing process. Subsequently, the bacteria are lysed by passing the suspension three times through a French Press homogenizer. The homogenate was centrifuged at 2700x g for 5min at 4°C, washed three times using RB+T buffer, followed by three washes in RB+ buffer.

Finally, the pellet was resuspended in TRB+ and concentrated 10 times with respect to the initial volume of the lysis buffer for quantification. They were additionally visualized under the microscope at 1000x magnification. The incorporation of the desired epitope in the purified nanospheres is checked by SDS-PAGE, followed by Coomassie blue staining and/or Western-blot analysis. Protein quantification is performed by standard protein quantification techniques (Bio Rad protein assay) after NS disassemble.

2.3.4. Electrophoretic analysis by SDS-PAGE

SDS-polyacrylamide gel electrophoresis (SDS-PAGE) was carried out as previously described (Laemmli, 1970). The concentrations of polyacrylamide or ProtoGel (National Diagnostic, England) used for the separator gel were 12.5%, and for the concentrator gel 4%. Subsequently, the proteins were fixed and stained with 0.25% Coomassie blue in 33% methanol and 10% acetic acid, and they were stained in the same solution without dye.

2.3.5. Determination of luciferase activity in vitro

Levels of luciferase activity present in the purified Luciferase loaded NS were determined using a Luminoskan-Ascent luminometer (Thermo, Waltham, Massachusetts, USA). As a reaction mixture to measure luciferase activity, a solution was prepared containing 80% luciferase buffer (see solutions and buffers) and 10% 100mM ATP and 200mM MgCl₂. Subsequently, the luciferin substrate (20mM) (Biaffin, Kassel, Germany) was added to this solution so that it remained at a final concentration of (1mM). Each test was performed at least three times, obtaining very similar results.

2.3.6. Determination of Halo-tag activity in vitro

Levels of Halo-tag activity present in the purified Halo-tag loaded NS were determined using a Luminoskan-Ascent luminometer (Thermo, Waltham,

Massachusetts, USA). The Halotag expression was accomplished using the already generated pET Duet1. muNS-Mi 2. Halotag-IC (24). As a reaction mixture to measure the enzymatic activity, a solution was prepared containing the nanospheres incubated the Ligand AF660 in a final molar ratio of 1:2 (NS:ligand). After an incubation of 40 minutes at RT in the orbital, the sample was washed 3x and the measurement for fluorescent signal at 665nm with excitation at 690nm. Each test was performed at least three times, obtaining very similar results.

2.4. HANDLING OF CELL CULTURES

2.4.1. Propagation and preservation of cell lines

In the freezing process, the cells from the confluent cultures were disaggregated and centrifuged for 5min at 500 x g. The pelleted cells were resuspended in 500µl of culture medium and 500µl of freezing medium (DMEM supplemented with 40% FBS and 20% dimethyl sulfoxide (DMSO) as cryoprotective agent) was added. Cell suspensions were dispensed in 1ml aliquots into sterile storage cryotubes. The vials were kept at 4°C for 5min, subsequently transferred to -80°C and, after keeping them at that temperature for at least 24h, were stored in liquid nitrogen for long periods of conservation.

Cell thawing was performed by immersing the vials in a 37°C water bath to achieve rapid thawing. Subsequently, the contents of the vial were transferred to tubes containing complete culture medium preheated to 37°C and centrifuged for 5min at 500xg to remove the freezing medium. The pelleted cells were then resuspended in culture medium, transferred to cell culture flasks with medium, and incubated at 37°C. The medium was renewed before 24h to eliminate possible traces of cryoprotective agent and avoid a rise in pH.

2.5. IMMUNOLOGICAL TECHNIQUES

2.5.1. ELISA protocol for cytokine detection

First, the immunoplates were coated with the antibody of interest. This capture antibody was diluted to the indicated concentration in coating buffer (see table) (the TNF and the IL-10 ELISA require a different coating buffer), then 50 μ l of the antibody solution was added into each well of a 96-well flat-bottom ELISA plate using a multi-channel dispenser. Followed by an incubation of 6h to overnight at 4°C. The plate was washed two times with PBS-Tween using the ELISA washer and then blocked the non-specific binding sites by adding 150 μ l/well of blocking solution for 2h at RT. After the incubation, the plates are washed two times with PBS-Tween using the ELISA washer. Once washed, 50 μ l of relevant dilutions for the standards are added to the respective control wells, and the experimental supernatants are added in a final volume of 50 μ l R10 medium at an appropriate dilution. Starting concentrations for standards are shown in Table. An incubation for 4h at room temperature or, for higher sensitivity, overnight at 4°C is performed. Once the time is completed, the plates are washed four times with PBS-Tween using the ELISA washer, followed by the addition of 100 μ l detection antibody in blocking solution and an incubation of 1h RT. Once completed, the plates are washed 4 times with PBS-Tween using the ELISA washer. The next step is the addition of 100 μ l AP-Streptavidin (Sigma, 1:5000 in blocking buffer) and incubation for 1h at RT. For the preparation of the ELISA substrate stock solution, to make the stock: 1 buffer tablet plus 1 substrate tablet using the kit SIGMAFAST were diluted in 20ml H₂O. Wash four times with 300 μ l of PBS-Tween per well using the ELISA washer. To start the reaction, we add 100 μ l substrate, incubate 30min to overnight at room temperature, in a humid chamber and protected from the light (cover with foil or a flexible lid). The reaction can be stopped by adding 25 μ l/well of 3M NaOH if necessary. The reading is performed at 405nm using a plate reader. The OD A405 values from the standards are to obtain a standard curve. We used the linear part of the curve for accurate sample concentration determinations.

2.6. LIMULUS AMOEBOCYTE LYSATE (LAL) ASSAY

In order to test the presence of bacterial endotoxins in our MS preparations, the gel-clot method of the LAL assay was carried out employing Endosafe lysate from Charles River Laboratories in combination with the 3rd WHO International Standard (10/178). The semi-quantitative assay was carried out executing the protocol described as Method B in the European Pharmacopoeia Section 2.6.14. For that purpose, several stock samples were diluted to either 0.4mg/ml or 1:20 prior to testing. The LAL assays were carried out with the excellent assistance of Trusha Desai or Sophie Myhill at the NIBSC.

2.7. B16 HER2 PSEUDO-METASTASIS MOUSE MODEL

2.7.1. Mice

Seven to eight weeks old female C57BL/6 mice with weights of a minimum 18g were purchased from Envigo and were acclimated in the Mouse Facility at NIBSC for a minimum of 5 days before starting the experiments. All experiments were carried out following the Animal Scientific Procedures Act 1986 under the project license 70/8831, Novel Biologics for Tumour Immunotherapy. The Project Licence protocol is the protocol 3 “therapeutic tumour intervention”. The project licence holder (PLH) is Dr. Sandra Diebold and the Deputy is Dr. Sandrine Vessillier. It was established that this study, including its background, objectives, experimental design, species, genetic status and number of animals to be used, regulated procedures to be performed, nature of the test substance, humane endpoints and fate of animals on completion, it was authorized by the Project Licence specified above. The center where the studies took place is the National Institute for Biological Standards and Control in the United Kingdom. The animals were randomly assigned into the different study groups. The animal work was performed by the NIBSC personnel, and they were in charge during the administration of the treatment or tissue harvest.

2.7.2. Preparation of tumor cells

B16-derived tumor expressing the model antigen ovalbumin as a transgene cell line were seeded one day before the beginning of the *in vivo* experiments at $1.5-2 \times 10^6$ cells per 145cm^2 TC dishes using complete R10. The day after, PBS-EDTA is used in order to detach the cells and then centrifuged at $300 \times g$ for 5min and at 4°C . Subsequently, cells were resuspended employing ice-cold PBS, the number is calculated using Trypan Blue exclusion for the counting and adjusted to the concentration needed depending on the respective cell line and experiment, and finally injected intravenously (IV) in the mice within 40min from the harvesting.

2.7.3. Tumor growth profiles

Mice were administered on day 0 with intravenous injections (IV) in the tail vein containing $0.5-0.9 \times 10^5$ B16-derived tumor expressing the model antigen ovalbumin in $150\mu\text{l}$ PBS. The IV injections at NIBSC were performed by specifically trained personnel, in this case the procedure was performed by Alan Haynes. In order to determine the tumor burden, 15-18 days subsequently to the inoculation, mice were euthanized using $200\text{mg}/\text{kg}$ Pentobarbital by intraperitoneal (IP) route; in order to assess the tumor growth profile, the lungs were collected and washed in PBS. Then, the lungs were fixed by placing them in Fekete solution for at least 24 h. Afterwards, the lungs were weighed, and the number of pulmonary nodules were determined using an Olympus S2X10 microscope (DF PLAPO 1x-4 lens) and zoom magnification setting 0.63. Images of the lungs were taken using Olympus SC30 camera connected to an Olympus S2X10 microscope (DF PLAPO 1x-4 lens) using zoom magnification setting 0.63 and processed with CellSens Entry 1.5 software.



2.7.4. Treatment with NS and control

One-dose regimen

Mice were injected IV, on day 0, with $3-5 \times 10^6$ B14.3 cells in in 150 μ l PBS. Tumor-bearing mice were treated IP on day 7 with the different group, including the NS and the controls groups (table 4). Each treatment sample contained 270pmol of antibody per mouse for the positive control group and 50 μ g of NS preparation intraperitoneally in 200 μ l PBS. The target 1×10^7 CFSE-labelled, antigen-pulsed target cells (splenocytes) cells for the in vivo CTL assay were injected on day 12 or 7 post immunization and the mice were culled the next day when lungs and spleens were harvested and processed. For that purpose, lungs were fixed in Fekete solution for minimum 24h, then weighed and tumor nodules counted.

Day	Groups	Mice	Procedure	Material	Route/ Volume	Notes
Day 0	all groups	20	Tumor Inoculation	B14.3 in PBS ($3-5 \times 10^6$ cells)	I.V (150 μ l)	The tumour cells are quite big and sticky; to avoid embolism recommendation of $>100 \mu$ l for the I.V. injection.
Day 5	Group 1 Group 2 Group 3 Group 4	5 5 5 5	Immunization	397-OVA Ab OVA NS Ctrl NS Vehicle only	Footpad (50 μ l) I.P (200 μ l) I.P (200 μ l) I.P (200 μ l)	Group 1: pos. ctrl Group 4: neg. ctrl
Day 12 (7 days post immunisation)	all groups	20	Injection of target cells	CFSE-labelled, antigen-pulsed target cells (splenocytes)	I.V (100 μ l)	
Day 13 (one day post injection of target cells)	all groups	20	Cull	N/A	N/A	Harvesting of lungs & spleens.

Table 4. Procedure schedule and details for the treatment with NS and controls.

2.7.5. Statistical analysis

GraphPad Prism was used to depict data and for statistical analyses. Data are shown as mean \pm standard deviation (SD) or as mean \pm standard error of mean (SEM) in the case of tumor growth profiles. Luminescence intensity data from in vivo imaging experiments was analyzed using the CGGC test (Els0 et al. 2004) online platform at 10 000 permutations:

<http://bioinf.wehi.edu.au/software/compareCurves/>. The rest of data was analyzed in GraphPad Prism 8.1 (GraphPad; La Jolla, CA, USA), using appropriate statistical tests for each data set, as described separately for each figure. All t tests were two-tailed. Differences were considered significant when $p \leq 0.05$. Stars of significance are: * $p < 0.0001$.

2.8. IN VIVO IMAGING

2.8.1. Luciferase in vivo imaging

Mice were weighed and subsequently injected by NIBSC animal technicians IP (following the table 5). First with the luciferase-containing NS and then with 150mg/kg XenoLight D-Luciferin substrate and 1ml of 50mM ATP in a solution of DPBS which was corrected to a pH 6.2 with 1 M NaOH. This dose was equivalent to injecting a 30g mouse with 1mg of ATP per gram of body weight. After 10 min, mice were imaged under anaesthesia with 2% isoflurane using IVIS Spectrum® (Perkin Elmer) and the Living Image® 4.7.2 (Caliper Life Sciences) software. Acquisition was performed using a 22.5cm field of view (FOV) and excitation and emission filters open. A group of mice with expected high signal was imaged first to optimize additional acquisition settings (time, lens aperture (F), binning). Acquisition parameters were optimized for at the beginning of each imaging timepoint and kept constant among groups of mice. Regions of interest (ROI) of 2.647cm diameter were placed to measure luminescence signal in the thorax area. Data were expressed as luminescence intensity in the ROI area (photons/sec).

Day	Group	N° mice	Procedure	Material	Route	Notes
day 0	Group 1	12	nanosphere injection (dose: 50µg/mouse)	luc nanospheres	I.P. (100µl*)	divide up group 1 into 4x subgroups with 3x mice each (groups 1a, 1b, 1c & 1d)
	Group 2	2		ctrl nanospheres	I.P. 100µl	
	Group 3	2		untreated	I.P. 100µl	
day 0	Group 1a-c, Group 2 & Group 3	13	luciferin injection for imaging	Xeno-Light D-Luciferin (150mg/kg)	I.P.	Group 1a-c: imaging of 3x mice each at 30min, 1h & 2h Groups 2 & 3: imaging at 30min
day 1	all groups	16	Blood sampling (for serum)	N/A	N/A	This will be the only bleed performed (ideally am rather than pm)
day 1	Group 1d	3	luciferin injection for imaging	Xeno-Light D-Luciferin (150mg/kg)	I.P.	Group 1d: imaging of remaining 3x mice
day 2	Group 1a-b, Group 2 & Group 3	10	luciferin injection for imaging	Xeno-Light D-Luciferin (150mg/kg)	I.P.	Group 1a & 1b Groups 2 & 3
day 3	Group 1c-d	6	luciferin injection for imaging	Xeno-Light D-Luciferin (150mg/kg)	I.P.	Group 1c & 1d
day 4	Group 1a-b, Group 2 & Group 3	10	luciferin injection for imaging	Xeno-Light D-Luciferin (150mg/kg)	I.P.	This imaging session may not be necessary if NS have been cleared on day 1-3.

Table 5. Procedure schedule and details for the treatment with luciferase carrying NS and controls.

* The concentration of these nanosphere preparation is higher than for OVA nanospheres, so we can inject 0.1ml per mouse instead of 0.2ml.

** 10 µl of luciferin substrate will be injected per g of body weight per mouse.

2.8.2. HaloTag in vivo imaging

NS labelled at a 1:2 ratio with AlexaFluor 660 ligand were injected into mice at a dose of 50µg per mouse. The mice were kept under anaesthesia from 1h after NS injection for a total of 4h. During this time mice were using IVIS Spectrum® (Perkin

Elmer) at regular intervals using a variety of filter combinations and instrument settings. Acquisition was performed using a 22.5cm field of view (FOV) and excitation and emission filters open. A group of mice with expected high signal was imaged first to optimize additional acquisition settings (time, lens aperture (F), binning). Acquisition parameters were optimized for at the beginning of each imaging timepoint and kept constant among groups of mice. Regions of interest (ROI) of 2.647cm diameter were placed to measure luminescence signal in the thorax area. Data were expressed as luminescence intensity in the ROI area (photons/sec).

2.9. CotA ENZYMATIC ACTIVITY

2.9.1. Laccase standard activity assays

Kinetic studies were carried out in a reaction mixture containing 5mM ABTS in citrate-phosphate buffer at the pH and temperature that was indicated in each assay. The oxidation of ABTS was trailed by measurements of the absorbance at 420nm ($\epsilon_{420}=36000\text{M}^{-1}\text{cm}^{-1}$) at 25 °C employing a Tecan Infinite 200 Pro microplate reader. One unit (U) of activity was deemed as the quantity of enzyme forming 1 μmol of $\text{ABTS}^{+\bullet}$ radical per minute. The spectrophotometric measurements were developed using a Jasco V-770 UV-Visible/NIR Spectrophotometer. Laccase activity was indicated in U/l. All measurements were carried out in triplicate.

2.9.2. Optimum pH

The optimum was investigated using 50mM ABTS in a 0.1M citrate-phosphate buffers of pH ranging from 3 to 8. The relative activity was calculated as the ratio between the activity at each pH and the maximum attained, set as 100%. The effect of the pH on the enzyme stability was studied by incubating the enzyme in 0.1M citrate-phosphate buffer (pH 3-8) at room temperature ($24^{\circ}\pm 2^{\circ}\text{C}$) during 1, 3, 6 and 24h. Samples were transferred to standard reaction mixtures in order to determine the laccase activity under standard conditions. The residual activity was

calculated referred to the value of the initial activity at each pH. All measurements were performed in triplicate.

2.9.3. Optimum temperature and thermostability

We compared the heat stability of NS-CotA to a commercially available *Bacillus subtilis* CotA laccase. The effect of temperature (25–95°C) was determined by measuring activity at the corresponding temperature under standard conditions. The relative activity was calculated as the ratio between the activity at each temperature and the maximum attained. Thermal stability was determined by incubating the enzymes in 0.1M phosphate buffer (pH 7) at selected temperatures from 25° to 95°C over a period of 24h or the times indicated in each figure. Samples were then transferred to standard conditions to determine the activity.

2.9.4. Decolorization of RB19

The removal rate was determined by measuring the absorbance of the test samples by spectrophotometry at 593nm. The enzymatic transformation of RB19 was carried out over a period of 24h at pH 5 and pH 6 and 60°C in a final volume of 1ml reaction mixture containing 12mg/l of the dye and 100U/l of enzyme. Heat-inactivated laccase was used as negative control. After decolorization, the absorbance of the reaction mixtures was then measured at 593nm with a Tecan Infinite 200 Pro microplate reader.

2.9.5. Stability Against Inactivating Agents

100µl (10U) of enzyme were incubated in different solutions (50% (v/v) methanol, 50% (v/v) ethanol, 50% (v/v) acetone, 25mM NaCl, 25 mM CaCl₂ and 25mM ZnCl₂) in 5mM citrate-phosphate buffer, pH 7 at room temperature. The residual activity was measured 1h after, with ABTS under standard conditions.

2.9.6. Storage stability

It was investigated at 4°C and at room temperature (24±2°C). Enzyme samples were stored in a 0.1M citrate-phosphate buffer solution (pH 7). The residual activities were measured after 1, 2 and 3 months by measuring the remaining CotA activity with 50µM ABTS under standard conditions.

2.9.7. The reusability of the MS

It was evaluated in the operation of consecutive cycles using ABTS as substrate in standard conditions. The NS-CotA was collected by centrifugation and washed twice, one with RB+ and one with RB-. Thereafter, the procedure was repeated with a fresh aliquot of substrate. The reference value of 100% was the activity of the immobilized enzyme in the initial cycle.

2.10. 3D PRINTING PROCEDURE

2.10.1. 3D object design

Printzymes were digitally designed in four different shapes: cylinders (60 mm diameter, 3-4mm thickness) and toruses (60mm outer diameter, 50mm inner diameter, 3-4mm thickness) using 123D Design software (Autodesk Inc., USA). Thickness was varied to allow assessment of how surface area affected enzyme activity in the system. To allow designs to be read by the SLA printer, they were exported as stl. files.

2.10.2. Formulation and 3D printing of Printzyme

Photopolymer resins for SLA printing were composed of laccase, a photoinitiator (LAP), and a mixture of PEGDA and water at different mass ratios (Table 6). Laccase was added to the initial PEGDA/water mixture together with 0.5% w/w of LAP, followed by stirring at room temperature until complete dissolution. This enzyme-loaded resin was subsequently poured into a resin tank for printing.

Using a commercial Form 2 SLA 3D printer (Formlabs Inc., USA) equipped with a 405nm laser. All Printzymes were directly printed onto the printing platform. Printer settings were ‘Clear 04’ for material and 0.1mm for layer thickness. The total printing time was 1h 30min and more than 50 Printzymes can be fabricated at the same time. After printing, Printzymes were washed with isopropyl alcohol for 2min in a Form Wash (Formlabs Inc., USA), followed by post cure in a Form Cure (Formlabs Inc., USA) for 20min. This step was to remove the presence of any unreacted PEGDA monomers, LAP, or free laccase, on the device surface. All Printzymes were stored at 4 °C until further use.

Printzyme	Laccase from <i>Trametes versicolor</i> (% w/w)	PEGDA:Water ratio	PEGDA (% w/w)	Water (% w/w)
Printzyme 0.4-99	0.4	99.6:0	99.6%	0
Printzyme 0.4-20	0.4	20:80	19.82	79.28
Printzyme 0.4-50	0.4	50:50	49.55	49.55
Printzyme 4-20	4.0	20:80	19.10	76.40
Printzyme 4-50	4.0	50:50	47.75	47.75

Table 6. Composition of the printing resin.

*each resin includes 0.5% w/w LAP

2.10.3. Printlet mass and dimensions

The Printzymes weight and size were measured (width and height) using a digital caliper (0.150mm PRO-MAX, Fowler, mod S 235 PAT) for the weight and a digital caliber for the dimensions. The measurements were performed in triplicate.

2.10.4. Environmental scanning electron microscopy (ESEM)

Printzymes were sliced in half and subsequently attached to a self-adhesive carbon disc mounted on a 25mm aluminum stub with silver paint. An environmental scanning electron microscope (FEI Quanta 200 FEG, UK) in ESEM mode, at 200 Pa pressure, 20 kV accelerating voltage, and a large filled detector, was employed to obtain detailed images of the printed device.

2.10.5. 3D printed *Trametes versicolor* enzyme activity assay

The activities of free laccase and Printzymes were determined by a colorimetric assay. Here, 0.266mM ABTS was used as the laccase substrate, dissolved in citric phosphate buffer composed of 0.1M citric acid buffer and 0.2 M dibasic sodium phosphate buffer. When 3ml of this reaction medium was incubated with either free laccase (0.4% w/v aqueous solution) or one Printzyme of known weight, the enzymatic oxidation of ABTS was followed by measuring the incubation medium's change in absorbance at 420nm using a Jasco V-770 UV-visible/NIR spectrophotometer. Hence, the extent of ABTS oxidation was used as a measurement of laccase activity. Effective activity, in mU/mg, was that observed when using the Printzyme. All measurements were performed in triplicate. Immobilization yield was calculated as:

$$IY(\%) = \frac{A_P}{A_0} \cdot 100 \quad (1)$$

where A_0 is the theoretical loaded activity, and A_P represents the total laccase activity on the Printzyme. To determine A_P , the Printzyme was shredded into fine particles and the activity of the particles was measured. Five replicates were used to obtain this activity.

The effectiveness factor (dimensionless) is the ratio between enzymatic activity monitored in immobilized state compared to free solution:

$$\eta = \frac{\text{reaction rate Printzyme}}{\text{reaction rate free enzyme}} \quad (2)$$

2.10.6. Assessment of the enzymatic activity remaining within Printzyme

In order to test the final enzymatic activity after the printing process, Printzymes are pulverized, after that a determined amount in mg (which will depend on the enzyme percentage) of the powder is placed inside a 1ml with 3ml citrate phosphate buffer solution (pH 6.0) and using 0.266mM ABTS as an enzyme substrate. Enzyme activity is measured as in Section 3.7.5 using a Jasco V-770 UV-visible/NIR spectrophotometer. Laccase activity is given in U/l. All measurements were performed in triplicate.

2.10.7. Optimal pH and temperature for free *Trametes versicolor* laccase and Printzyme activities

To determine optimal pH of enzyme activity, free laccase and Printzymes were separately incubated in 3ml citric phosphate buffer plus 0.266mM ABTS, for 5min at 25°C. Enzyme activity of both free laccase and Printzymes were assessed as in Section 2.5. The pH of the citric phosphate buffer was varied from pH 3.0 to pH 6.0. The maximal reading for ABTS oxidation was considered as 100% enzyme activity, and relative activity was calculated as the ratio between the activity at a measured pH and the maximum activity. All measurements were performed in triplicate.

The optimal temperature for enzymatic activity was determined by incubating both free laccase and Printzymes at temperatures ranging from 30 to 80°C, for 5min in 3ml citric phosphate buffer plus 0.266mM ABTS at pH 3.0. Enzyme activity was assessed as in Section 2.5. The maximal reading for ABTS oxidation was considered as 100% enzyme activity, and relative activity was calculated as the ratio between the activity

at a measured temperature and the maximum activity. All measurements were performed in triplicate.

2.10.8. Effect of pH and temperature on free laccase and Printzyme stability

The 24-hour stability of both free laccase and Printzyme at selected pH readings (pH 3.0, pH 4.0, pH 6.0, pH 8.0) was determined with the enzyme activity assay outlined in Section 2.5. Free laccase and 60mg Printzyme 0.4-20 were incubated in 3ml citric phosphate buffer (or phosphate buffer for pH 8.0) plus ABTS for 24h at room temperature. Samples of the incubation medium were taken at defined timepoints (1, 3, 6 and 24h), and their enzymatic activity was measured immediately. The reading at time 0 was considered as 100% enzyme activity, and relative activity was calculated as the ratio between the activity for a specific reading and the maximum activity. All measurements were performed in triplicate.

The 24h stability of both free laccase and Printzyme at defined temperatures (25°C, 40°C, 50°C, 60°C) was determined with the enzyme activity assay outlined in Section 2.5. Free laccase and 60mg Printzyme 0.4-20 were incubated in 3ml citric phosphate buffer (pH 6.0) plus ABTS for 24h at room temperature. Samples of the incubation medium were taken at defined timepoints (1h, 3h, 6h, 24h), and their enzymatic activity was measured immediately. The reading at 0h was considered as 100 % enzyme activity, and relative activity was calculated as the ratio between the activity for a specific reading and the maximum activity. All measurements were performed in triplicate.

2.10.9. Reusability studies

Printzyme is intended as a reusable device. Thus, reusability was investigated by performing 18 isolated uses of one Printzyme lasting 5 minutes each. After each use, the Printzyme was filtered and washed with distilled water and subsequently used in the next iteration. Enzymatic activity was assessed after each use using the method outlined in Section 2.5. The activity of the enzyme in the initial cycle was considered as 100% and the relative activity was calculated as the ratio between the activity at each cycle and the initial activity [67]. All measurements were performed in triplicate.

2.10.10. Removal of pharmaceuticals by Printzyme

The ability of Printzyme 4-20 to remove drugs from water was tested using two model drugs, diclofenac and ethinylestradiol. Separate solutions of the two drugs were prepared in phosphate buffer (0.1M, pH 6.0) at concentrations of 2.5mg/l. 350mg Printzyme 4-20 was deposited into each drug solution (50ml) inside a 100ml flask, and continuously shaken at 100 rpm for 48h. Experiments with free laccase were carried out in the same conditions (≈ 340 U/l) as a comparison. These reaction mixtures were maintained at room temperature for the duration of the experiments, and samples were withdrawn at specific timepoints (2h, 4h, 8h, 24h, 48h). The concentration of drug in each withdrawn sample was determined using high performance liquid chromatography (HPLC) (Section 2.10). Control studies were run in parallel, whereby Printzyme formulations without laccase were used in place of active Printzymes. Measurements were performed in duplicate.

2.10.11. High-performance liquid chromatography (HPLC) analysis

A HPLC system (Hewlett Packard 1260 Series HPLC system, Agilent Technologies, Cheshire, UK) was used to measure the concentration of diclofenac or ethinylestradiol in samples exposed to Printzyme 4-20 for defined periods of time (Section 2.9). For both drugs, an Eclipse plus C18 column, 100 \times 4.6mm (Zorbax, Agilent technologies, Cheshire, UK) was used as the stationary phase. The mobile phase consisted of phosphate buffer (50mM, pH 4.5) with acetonitrile at isocratic conditions of 50:50 for diclofenac, and 40:60 for ethinylestradiol. For both drugs, sample injection volume was 100 μ l and mobile phase flow rate was 1.0ml/min. Diclofenac retention time was 6min and eluent absorbance was measured at 220nm. For ethinylestradiol, drug retention time was 10min, and an absorbance of 210nm was used for detection.

RESULTS

CHAPTER 1:
ENZYME IMMOBILIZATION AND
BIOCATALYSIS VIA THE IC - TAGGING
TECHNOLOGY

This chapter has been previously published in Scientific Reports (Sci Rep), with the title Chemical and thermal stabilization of CotA laccase via a novel one-step expression and immobilization in muNS-Mi nanospheres (see table below).

Title	Chemical and thermal stabilization of CotA laccase via a novel one-step expression and immobilization in muNS-Mi nanospheres.
Authors	Tomás Pose-Boirazian, Gemma Eibes, Natalia Barreiro-Piñeiro, Cristina Díaz-Jullien, Juan M. Lema & Jose Martínez-Costas.
Year	2021
ISSN	2045-2322
DOI	10.1038/s41598-021-82468-x
Journal	Scientific Reports (Sci Rep)
Volume, pages	vol. 11, no 1, p. 1-10.
Impact Factor	4.379
PhD student contribution	muNS-Mi nanospheres synthesis and characterization, activity and reusability experiments.

This is an open access article distributed under the terms of the Creative Commons CC BY license, which permits unrestricted use, distribution, and reproduction in any medium, provided the original work is properly cited. It is not required to obtain permission to reuse this article.

1. INTRODUCTION

Biocatalysts are critical tools for the production and degradation of pharmaceuticals and fine chemicals because of their high selectivity and specificity, mild reaction temperature, neutral or close to neutral pH activity. In addition, they provide lower pollution and hazardous outcomes and a lower energy consumption when compared to conventional catalysts processes. Biocatalysts also offer new opportunities for the synthesis of highly valuable compounds that could not be possible otherwise. The total number of biotransformation processes carried out on an industrial scale have been increasing continuously for the past decade (129). This is not a temporary trend, as it is expected to observe a dramatic growth on enzymatic applications of biocatalysts in large scale production of fine chemicals and bioremediation (130). Nonetheless, biocatalysts also present multiple limitations, for instance, if a reaction proceeds slowly under given temperature and an increase in temperature would lead to a better performance, this increase often leads to denaturation of enzyme involved in the process. Moreover, production of enzymes is expensive and they often need to be recovered and reused in order to make them cost-effective. For this purpose, soluble enzymes in aqueous media demand the use of tedious techniques for the separation from the reaction mixture.

However, these limitations can be tackled by enzyme immobilization. Immobilization of enzymes onto a solid support offers the most inexpensive way of recovering enzymes from reaction mixtures. Furthermore, it adds some special features to the biocatalysts such as operational improvement, an increase in thermal and pH stability, as well as protection against denaturation induced by solvent compounds. Major disadvantages upon immobilization are linked to the loss of activity, diffusional limitation and increased production costs. Despite those, immobilized enzymes are regularly used in pharmaceutical, food and chemical industries (131).

2. ENZYME IMMOBILIZATION

As stated, enzyme immobilization provides new opportunities for the practical application of biocatalysts in the pharmaceutical, chemical and food industry, but is

also key in other sectors such as medical diagnostics, therapy, and biomolecular detection (132). The main incentive for immobilizing enzymes is to extend their use by recovering and reusing them in several cycles, or even in continuous processes, providing a facile separation from the product. Furthermore, immobilization often improve long-term operational stability and shelf-storage life. These features result in higher catalyst productivities, which eventually determine the enzyme cost per kg of product. Hence, industrial bioprocesses will keep increasing in the future as far as stable, robust and preferably insoluble biocatalysts are developed (133). The common immobilization methods can be divided in three categories (Fig 12) (134): i) binding to a carrier support (carrier), ii) cross-linking of enzyme molecules and iii) entrapment in organic or inorganic polymer matrices.

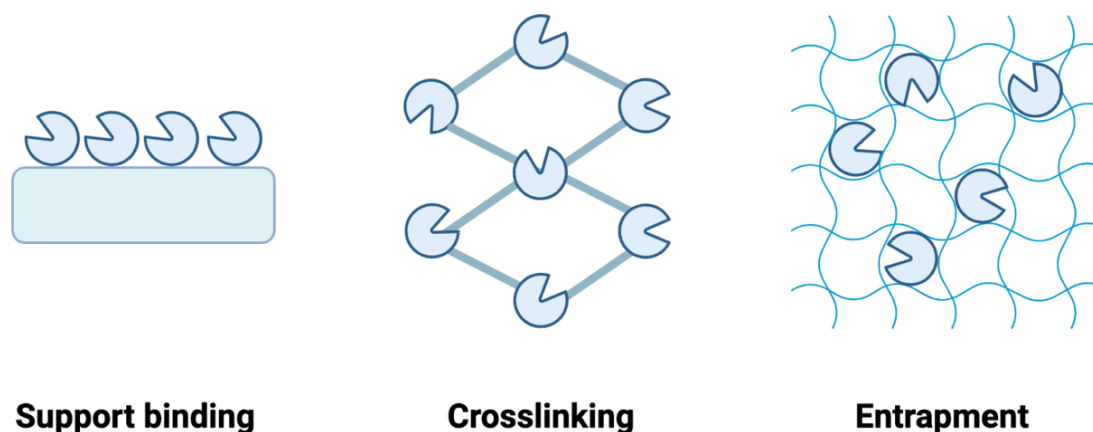


Figure 12. Different methods for enzyme immobilization.

Support binding can be physical, ionic or covalent and the carrier can be a synthetic organic polymer, a biopolymer or an inorganic polymer. Physical adsorption can lead to enzyme leaching, resulting in contamination of the product. On the other hand, covalent coupling methods would generally avoid leaching of the enzyme. However, covalent binding to a prefabricated carrier via epoxide bonds and/or

crosslinking reagents requires case-to-case optimization since a substantial loss of enzyme activity can be observed during the coupling procedure (135).

Cross-linking of enzyme aggregates (CLEAs) avoids the use of carriers, which are often expensive. During the preparation of CLEAs, enzymes are physically aggregated by nondenaturing precipitation followed by cross-linking with a bifunctional reagent. To avoid inactivation of the enzyme during the protocol, an individual optimization is commonly required, as described for the covalent binding methodology. Furthermore, the relatively small particle size of CLEAs (5-50 μ m) can be an issue in the operation of fixed-bed reactors (136).

Entrapment involves inclusion of an enzyme in a polymer network or a membrane device. In this immobilization method, the support is not prefabricated, but it is generally formed in the presence of the enzyme. Commonly the physical restraints are too weak, and therefore, covalent bonding is often required to avoid enzyme leakage and to enhance its reusability (134). Additionally, the catalytic efficiency is often hindered by diffusional limitations of the substrate entering into the particles. Despite these limitations, entrapment using polymeric gels, is a fast and simple immobilization method, applicable to a wide range of enzymes not requiring case-to-case optimization, and with little effect on the enzyme structure (135).

The entrapment is usually performed by mixing the monomers, a cross-linking agent, and the enzyme in a buffered solution and then adding the initiator of the polymerization process. Matrices used for enzyme immobilization are either natural polymeric materials, such as Ca-alginate, agarose, gelatin, κ -carrageenin, and collagen or synthetic ones, such as polyacrylamide and polyvinyl alcohol. Although the several advantages of the natural polymer gels (nontoxic, mild conditions, low loss of activity), the biggest limitation is the weak mechanical strength of the particles. In the past few years, increasing attention has been paid to acrylic polymers, probably because of the numerous options of varying the monomer used and thereby allowing a good control over the chemical physical properties of the polymer that is formed. Hydrogels can be formed by physical cross-linking (triggered by temperature, pH or ionic strength), chemical cross-linking (using cross-linking agents as glutaraldehyde) or radiation cross-linking (exposure to high energy source, such as gamma ray, x-ray or electron beam).

On this thesis, we will be focusing both on carrier bounding and physical entrapment. Regarding carrier bounding, while conventional methods focus on binding to a prefabricated support, we will combine in vivo generation and synthesis of both the carrier and the enzyme simultaneously with the immobilization process. Respecting the physical entrapment, conventional formative and subtractive manufacturing technologies typically require molds, tooling and machining, while the technology we will be focusing on which is 3D printing of hydrogels (Chapter 2), is a relatively new area of research much more flexible, precise in the elaboration of complex structures, less wasteful in materials and processes, and thus rapid and cost-effective (137).

3. EXPRESSION AND IMMOBILIZATION OF ENZYMES THROUGH THE IC-TAGGING SYSTEM.

3.1. Rationale

For the first approach, we decided to use the IC-tagging platform developed in our laboratory. Microparticles have been gathering increasingly attention over the years for their multiple applications in very different areas, going from industrial production to therapeutic treatment or diagnosis. On this approach, cost production as well as stability are the main challenges to overcome. With our method both the expression and the micro/nano-encapsulation are performed simultaneously by the cell avoiding the need for protein purification and coupling to a surface/particle. Also, no particular additives need to be incorporated to the normal growth media, and particle formation facilitates the encapsulated protein purification by mechanical means, overall reducing the cost of the entire production process. As our methodology allows the cost-effective production and purification of encapsulated proteins, we wanted to explore the ability of the MS and NS as enzyme carriers to promote both, enzyme reusability and stabilization of the integrated enzyme that might increase the applicability of the IC-tagging method for protein production.

As a model enzyme for this project we chose the laccase-like enzyme codified by the *Bacillus subtilis* CotA gene. Laccases (EC 1.10.3.2) are the largest subgroup of the protein superfamily of multi-copper oxidases (MCOs) and catalyze the one

electron oxidation of four substrate molecules using molecular oxygen as the final electron acceptor. Their broad substrate spectrum and their ease of use have generated a high interest, particularly within the wood, biofuel, paper, textile, fine chemicals and food industrial sectors (138). Different laccases from plant, fungal and bacterial origin have been identified and characterized. The remarkable characteristics of bacterial laccases from the industrial point of view, such as a broad range of temperature and pH with high stability against various inhibitory agents, have boosted their use and application in recent years (139). CotA laccase (Figure 13) is present in the coat of the *B. subtilis* endospore and has been previously characterized biochemically, showing a high stability against thermal denaturation.

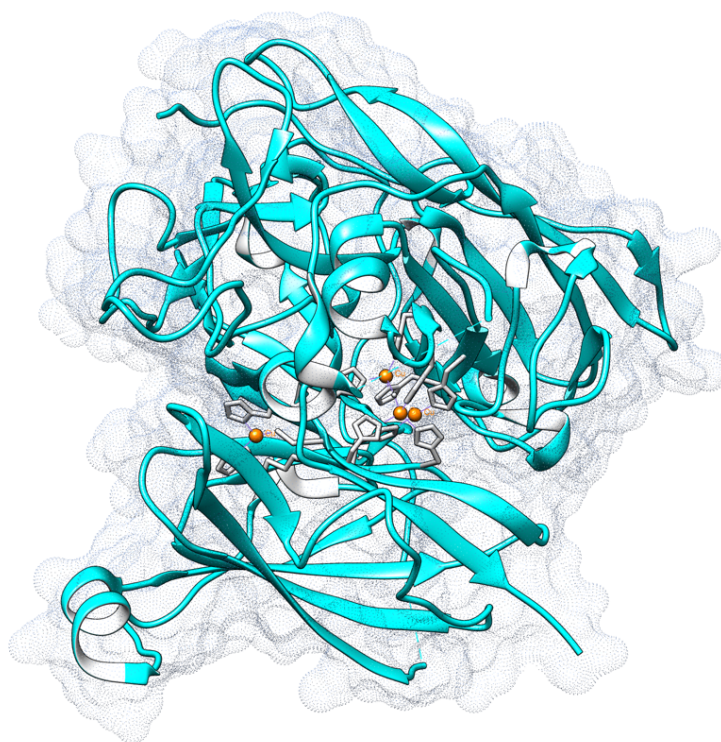


Figure 13. Representation of the CotA structure. We can appreciate a complex structure with a metallic center composed of 4 copper atoms, represented as orange spheres. Image generated with UCSF Chimera using PDB: 4q89.

We aimed to produce and purify NS loaded with CotA and characterize the activity of the nano-encapsulated enzyme according to the workflow showed in Figure 14.

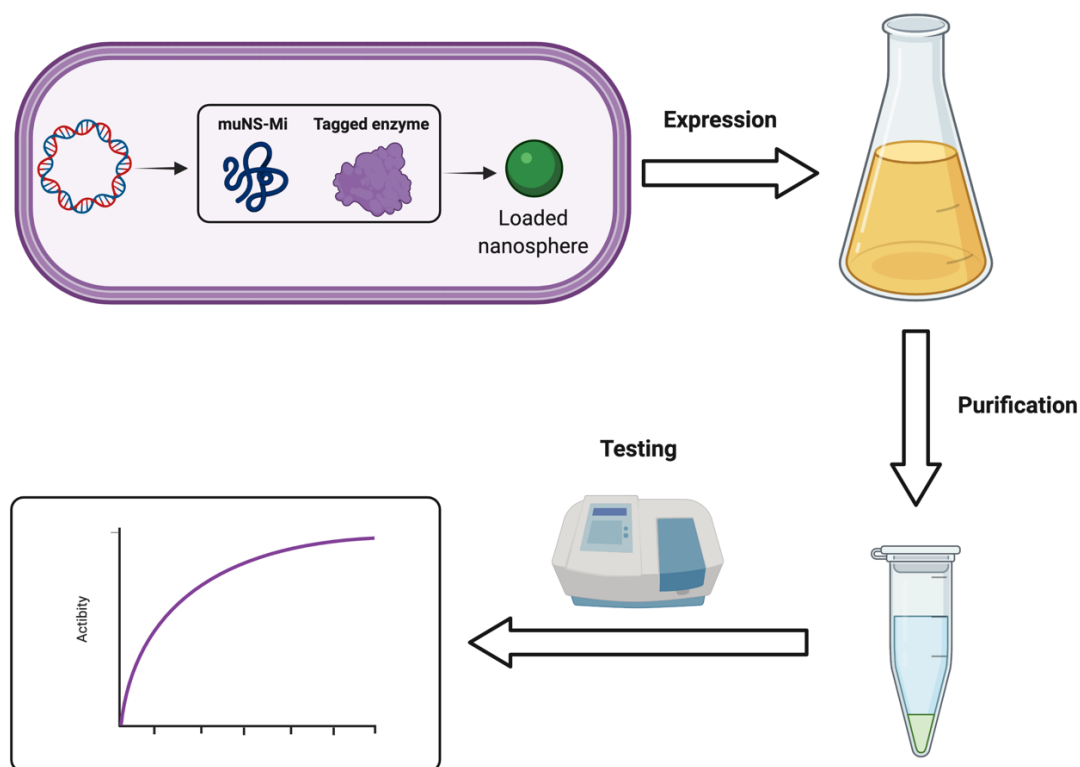


Figure 14. Workflow of the expression and reaction processes. The process begins with the transformation of competent bacteria with the dual-expression plasmid bearing both the muNS-Mi and the CotA laccase sequences. Upon expression of both proteins, the CotA laccase incorporates into the microsphere structure remaining active. Once purified, the activity can be assessed.

3.2. CotA gene construct tagged with the IC fragment

We first decided to clone the CotA gene into the second polylinker of the dual plasmid pET-Duet1-muNS-Mi, that already bears the sequence of muNS-Mi in the

first polylinker (24). Thus, upon IPTG induction, both proteins should be co-expressed inside the transformed bacteria. When we transformed BL21 bacteria with the recombinant plasmid and induced the expression with IPTG, we were able to spot the band corresponding to the muNS-Mi protein, but no band corresponding to the tagged CotA was evident in SDS-PAGE gels (not shown). Alternatively, we used the Rosetta strain of *E. coli* to try to overcome a possible difference in codon usage between *B. subtilis* and *E. coli*. After IPTG induction of the transformed Rosetta cells, total cell extracts were obtained and analyzed by SDS-PAGE, showing the presence of two prominent bands that were not present in extracts from uninduced cells (Figure 15A, compare lanes 1 and 2). The faster migrating band corresponds to muNS-Mi and is also present in extracts from Rosetta cells transformed with the muNS-Mi-pDuet plasmid (Figure 15A, lane 3), while the size of the bigger protein agrees with the size (64 kD) of the IC-tagged CotA laccase from *B. subtilis*. After detecting the presence of both proteins, the NS were purified as described previously (140). The presence and size of the NS were analyzed by microscopy and DLS, showing a monodisperse population of particles of around 400 nm in diameter (not shown). The protein content of the purified material was analyzed by SDS-PAGE and Coomassie staining, showing the co-purification of the CotA protein with muNS-Mi (Figure 15B, lane 1).

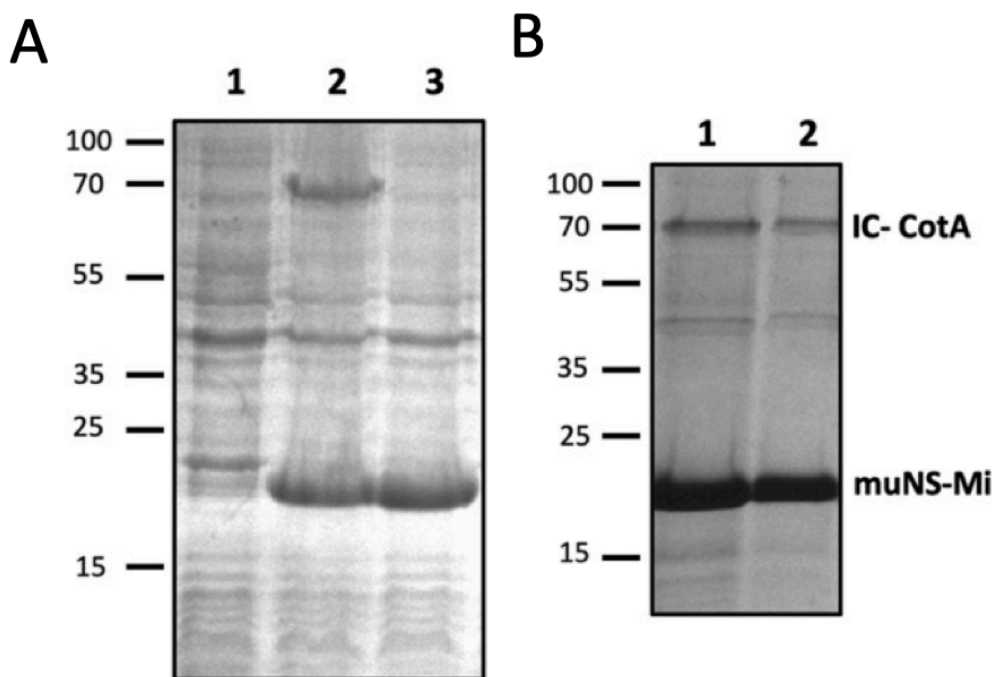


Figure 15. Expression and purification of NS-CotA. (A) Coomassie-blue stained, PAGE analysis of total extracts from non-induced (1), or IPTG-induced (2) *E. coli* transformed with dual expression plasmid muNS-Mi-CotA-pDuet1. Extracts from *E. coli* transformed with plasmid muNS-Mi-pDuet1 and induced with IPTG are shown in 3. (B) Protein content of the purified NS-CotA produced under standard (1) or microaerobic (2) conditions (see text), analyzed by SDS-PAGE and Coomassie staining.

3.3. Enzymatic activity of the encapsulated CotA

After NS purification, we wanted to test if the encapsulated protein kept its enzymatic activity by measuring the transformation of ABTS as substrate. Our initial attempts produced no detectable activity after incubation at the published CotA optimal pH. Those results were expected as it was previously published that incorporation of the essential copper atoms to the CotA active center is dependent on oxygen, and incubation in microaerobic conditions and addition of copper to the incubation medium (see Methods) are necessary for obtaining fully copper-loaded enzyme molecules (140, 141). However, laccase-containing MS produced in the baculovirus system showed some activity in the absence of any particular incubation conditions or additives (our unpublished results). Thus, the production of the

nanoencapsulated enzyme under standard conditions served first, to confirm that the predictable stabilization effect of the encapsulation makes no difference on the requirements for obtaining an active enzyme in bacteria, and second, as a control on the possible effect that the muNS-Mi protein might have on the transformation of the substrate ABTS used for the laccase activity determination. Next, a new batch was obtained under microaerobic conditions in LB medium containing 0.25mM CuCl₂. Similar results to those shown in Figure 15A were obtained in terms of IPTG-induction of protein expression. However, a decrease of 20% in total protein was obtained under microaerobic conditions that produced a similar decrease in total purified NS (Figure 15B, compare lane 1 with lane 2, quantified as indicated in Materials and Methods). However, estimation of bacterial growth by absorbance measurement (OD 600), showed a similar decrease in cell growth under microaerobic versus standard conditions, indicating that the observed difference in protein production is due to a difference in cell number, what in turn demonstrates that the presence of Cu and the microaerobic culture conditions have no detrimental effects on the expression of either muNS-Mi or CotA-IC. In addition, this Cu-loaded CotA did produce the appearance of a colored product after incubation with ABTS, indicating the presence of oxidase activity on the purified NS. The specific activity of NS-CotA measured at standard conditions was 39 mU/mg NS. Next, the activity of the encapsulated CotA was characterized and compared with a commercially available enzyme in its free soluble form.

3.4. Effect of pH on CotA activity and stability

We first compared the pH-activity profiles of the NS-contained CotA laccase to the free enzyme. The free CotA presented an optimum pH activity around pH 3.0 and 4.0 as previously reported (142), with a rapid decline of relative activity at pH 5 that became almost undetectable at pH 6 (Figure 16A, grey line). On the other hand, the NS-immobilized CotA presented a significative expansion of the optimum pH, covering a range between pH 3.0 and pH 5.0 (Figure 16A, blue line). In addition, NS-contained CotA maintained a 50% ABTS-oxidizing activity at pH 6.0 and 20% at pH 7.0 while the free enzyme was nearly inactive at those pH values.

As the incorporation into NS seems to stabilize the enzymatic activity of CotA, we decided to compare the resistance to incubation during 24 hours of free and NS-contained CotA at different pH values, ranging from 3 to 8. The results showed that at pH 3.0 and 4.0 both enzymes had a similar behavior (Figure 16B, compare the blue and orange bars from CotA vs NS-CotA). However, integration into NS improved CotA stability over the more neutral pH range. Thus, while free CotA laccase showed only 24% relative activity after 1 h incubation at pH 5.0 and decreased to 8% activity after 24h (Figure 16B, CotA, grey bar), the immobilized version did not experience a loss in activity during the first hour at the same pH, retained a 86% activity after 3 h and after 24 h still preserved a 28% activity (Figure 2B, NS/CotA, grey bar). An increased stability of NS-CotA over the free enzyme was also evident at pH 6 (Figure 16B, compare yellow bars from NS/CotA and CotA), while incubation at pH 7 (Figure 16B Blue bar) and 8 (Figure 16B Green bar) did not apparently decrease the activity of any of the two enzymes.

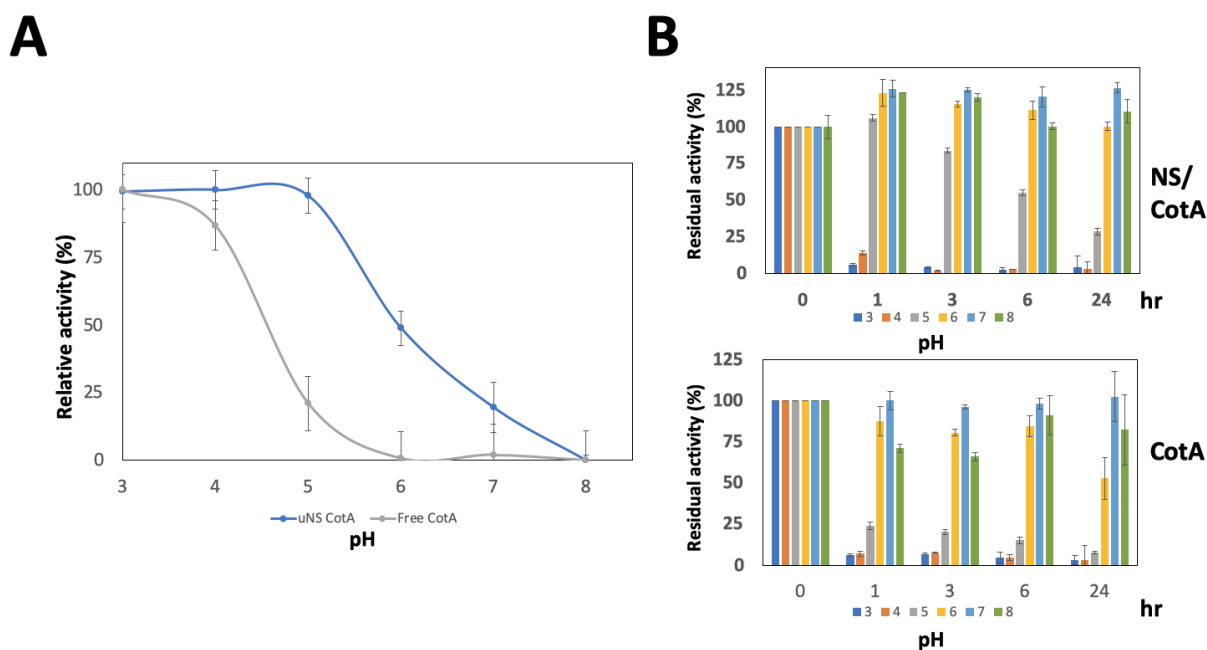


Figure 16- Comparison of pH activity and stability between free CotA and NS-CotA. (A) optimum pH. The graphic shows the ABTS-oxidizing activity of free (grey line) and NS-immobilized (blue line) CotA at pH ranging from 3 to 8. **(B)** pH stability. Residual activity (%) of free CotA and NS-CotA after incubation at different pH values (3 to 8). Data values represent mean \pm SD, which are not seen in some data points as they are smaller than the symbols.

3.5. Stability against inactivating agents

The next step was checking if the nanoencapsulation also confers stability against chemical inactivation. For that, free and NS-contained CotA were incubated for 1 hour at room temperature with the reagents shown in figure 17 and their activity was measured under standard conditions. The NS-CotA showed an extraordinarily tolerance to the presence of both organic solvents: 91% stability in 50% ethanol (v/v), a 95% stability in 50% methanol(v/v) and a 100% stability in 50% acetone (v/v) as well as for other chemical inactivators: a 100% stability against 25mM NaCl, a 94 % stability against 25mM ZnCl₂ and 100% stability in the presence of 25mM CaCl₂. In all the conditions tested, the nanoencapsulated protein (Figure 17 blue bars) outperformed the free enzyme (Figure 17 orange bars)

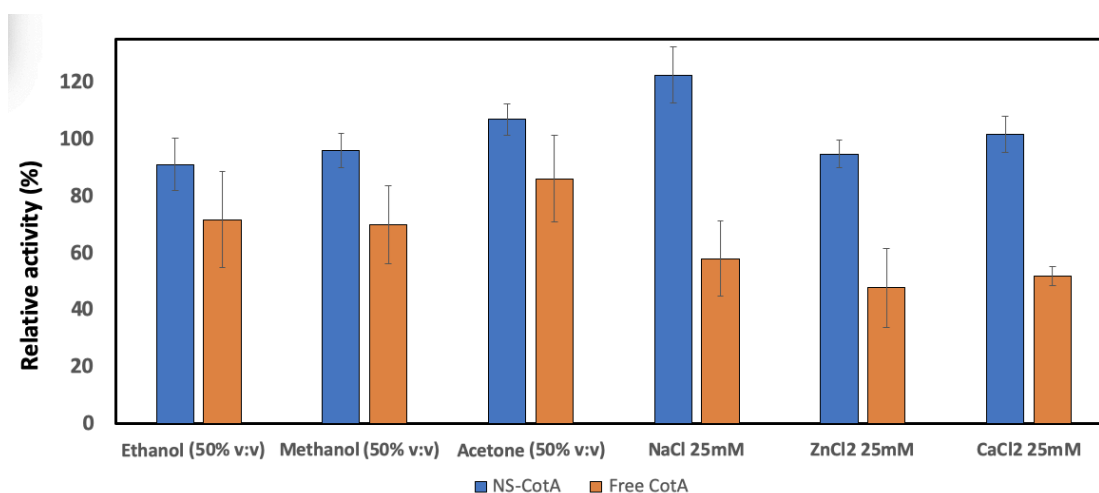


Figure 17. Residual activity (%) of free CotA (orange bars) and immobilized CotA (NS-CotA, blue bars) after 1h incubation with different inactivating agents shown in the figure at room temperature. Data values represent mean \pm SD, which are not seen in some data points as they are smaller than the symbols.

3.6. Optimum temperature and thermostability

To determine and compare the temperature range of action of both CotA versions, standard reactions were performed with both enzymes at different temperatures. The free CotA (Figure 18A, open circles, dashed line) was slightly more active at 70°C, but the nanoencapsulation increased the optimum temperature by 10°C to the 80°C (Figure 18A, filled circles, blue line). Furthermore, NS-CotA presented an increased relative activity in the entire range of temperatures from 25 to 95°C, being this increase more pronounced for the higher temperatures. Thus, for example, the free CotA became completely inactive at 90°C but NS-CotA still showed a 50% relative activity at that temperature. Furthermore, NS-CotA showed a similar relative activity at 25°C and at the striking temperature of 95°C, where the activity of the free enzyme was completely abolished.

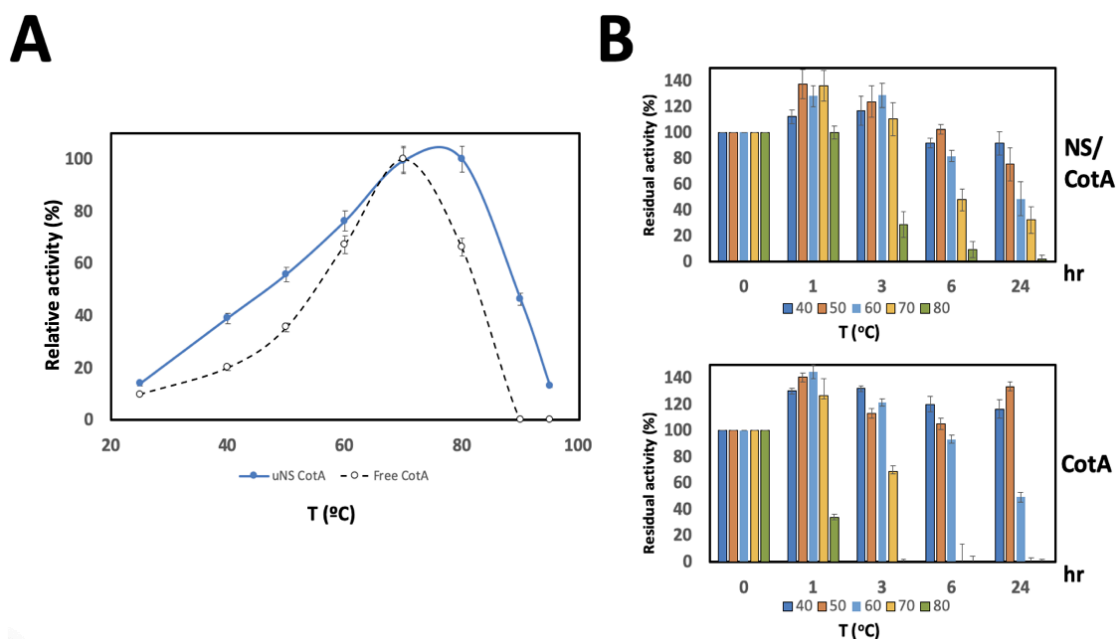


Figure 18. Influence of temperature on CotA activity. (A) Effect of temperature on ABTS-oxidizing activity of free (black line, open circles) and immobilized CotA (blue line, closed circles). Standard reactions were performed at the indicated temperatures. (B) Residual activity (%) of immobilized CotA (NS/CotA) and free CotA after incubation during the indicated times (hr) and different temperature values indicated by the color bars. Data values represent mean \pm SD, which are not seen in some data points as they are smaller than the symbols.

In view of those results we next decided to check the thermostability of both enzyme versions. For that, we incubated free and NS-contained CotA at pH 7 for different incubation times (Figure 18B) at selected temperatures ranging from 40 to 80 °C. NS-CotA (Figure 18B, upper panel) presented superior half-lives and lower inactivation rates when compared to the free enzyme (Figure 18B, lower panel), being more accentuated at the higher temperatures. After 1 h of incubation, both versions retained full activity from 40 to 70°C but at 80°C the free CotA showed only a 34% relative activity (Figure 18B, lower panel, green bar) while NS-CotA remained totally active (Figure 4b, lower panel, green bar). A similar behavior took place at 6 h where both versions remained totally active from 40 to 60°C. At the same incubation time and 70°C and 80°C (yellow and green bars), however, the free CotA was completely inactivated while the immobilized CotA retained almost 50% of the relative activity at 70°C and a 10% activity at 80°C.

With those results in mind, we decided to compare the behavior of both enzymes at even higher temperatures (90 and 95°C) for 30 minutes and checking the activity at different time points. We found that the stability at these temperatures is strikingly different (Figure 19). Thus, the free enzyme (Figure 19, yellow and green bars) is completely inactivated at 5 minutes at both temperatures, while NS-CotA activity (Figure 19, blue and orange bars) was not affected after 10 minutes of incubation at either temperature. At 90°C the activity of NS-CotA was also unaffected after 30 minutes of incubation and still retained 77% of its activity after 15 minutes of incubation at 95°C. Incubation at 95°C for 30 minutes were the only conditions found to eliminate the activity of the extremely heat-stable NS-contained enzyme.

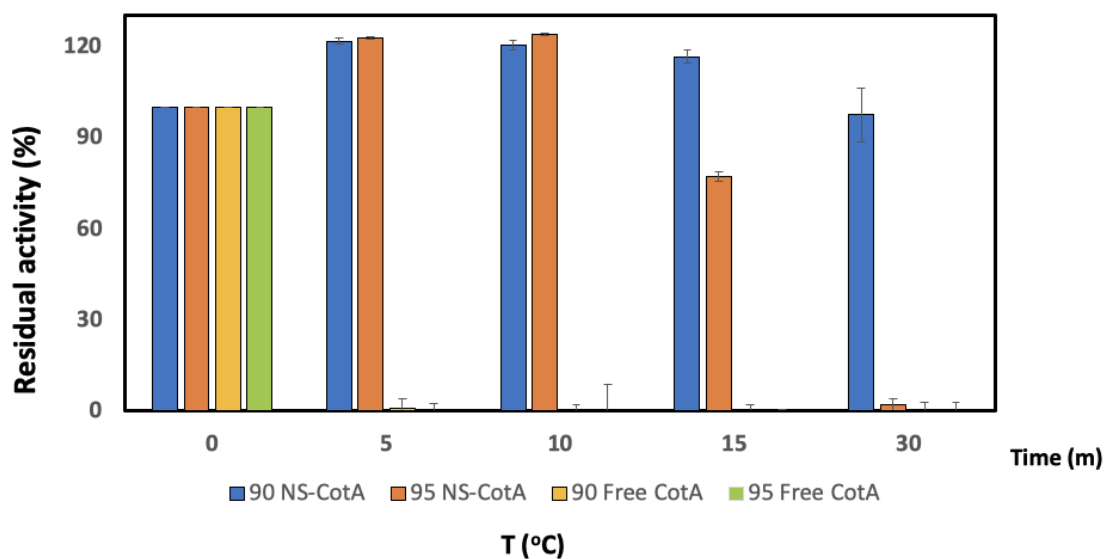


Figure 19. Stability of CotA activity at high temperatures. Residual activity (%) of free CotA (yellow and green bars) or NS-CotA (blue and orange bars) after incubation at the times indicated (min) and at 90 (blue and yellow bars) and 95°C (orange and green bars). Data values represent mean \pm SD, which are not seen in some data points as they are smaller than the symbols.

To discard the possibility that the IC tag itself is mediating the stabilization of the CotA, the IC-tagged CotA was expressed in the Rosetta strain in the absence of muNS-Mi using the same conditions as for the encapsulated version, and the laccase activity was determined using whole soluble bacterial extracts. Those extracts were then used to evaluate the temperature stability of the IC-tagged, soluble enzyme, at different temperatures using standard reaction conditions. For that, we incubated the IC-tagged CotA extracts at pH 7 for different incubation times (Figure 20) at selected temperatures ranging from 40 to 80 °C. As is evident from the figure, the non-encapsulated IC-tagged CotA presented an inferior half-lives and higher inactivation rates when compared both to the commercial free CotA evaluated previously, and the NS-CotA. This effect is more accentuated again at the higher temperatures. We can therefore discard the possibility that the IC tag itself is the responsible for the stabilization of the enzyme and reinforce the idea that the effect is attributable to the nanoencapsulation.

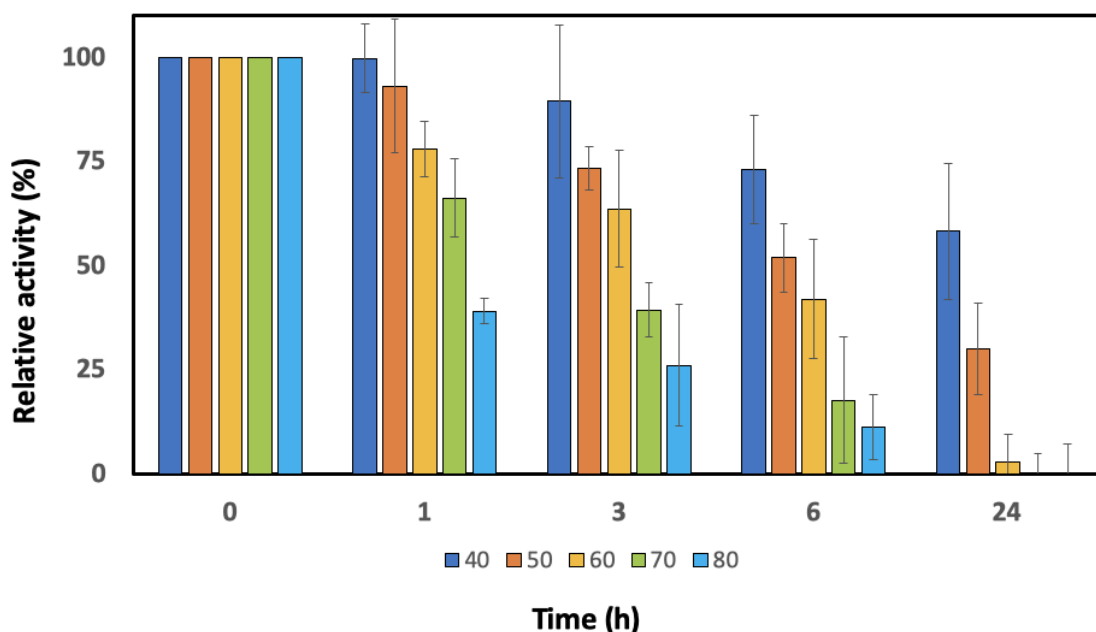


Figure 20. Residual activity (%) of IC-tagged free CotA after incubation during the indicated times (hr) and different temperature values indicated by different colour bars. Data values represent mean \pm SD, which are not seen in some data points as they are smaller than the symbols.

3.7. Reusability of NS-CotA and ability to decolorate organic dyes

The recalcitrant RB19 dye was used as a model compound to test the decolorization efficiency of the immobilized CotA at pH 5 and 60°C, in a final volume of 1ml reaction mixture containing 100U/1 of immobilized enzyme. A negative control with inactivated enzyme (not shown) did not show any significant RB19 decolorization, thus we can associate the enzymatic activity as the responsible for the removal of the dye. The reaction was monitored for periods of 1, 3, 6 and 24h to observe the progression (Figure 21A). The results showed that NS-CotA, in absence of any mediator, catalyzed 72.8% of the RB19 decolorization after 24h, showing a similar outcome to that of the free enzyme. The results also showed that most of the dye elimination took place during the first hours of reaction. Interestingly, the immobilized enzyme showed higher initial reaction rates compared to that of the free enzyme (53.2% and 37% decolorization after 5h for immobilized and free enzyme,

respectively). Future studies are needed to optimize dye removal, considering variables such as temperature, pH, enzyme dosage or addition of a mediator.

Having demonstrated the increased stability of the encapsulated enzyme, the next step was to proof if such encapsulation allowed its recovery and reuse in several reaction cycles, as this is one of the most critical aspects for potential industrial applications. For that, the activity of NS-CotA was measured as above and then the NS recovered by centrifugation. The pelleted NS were then resuspended again in reaction buffer containing ABTS and the activity measured. As can be seen in (Figure 21B), CotA activity was entirely conserved during 4 cycles, and after 6 cycles of use showed only a 20% loss of relative activity, a figure that matches exactly the percentage of protein lost after all the centrifugation steps used for the recovery.

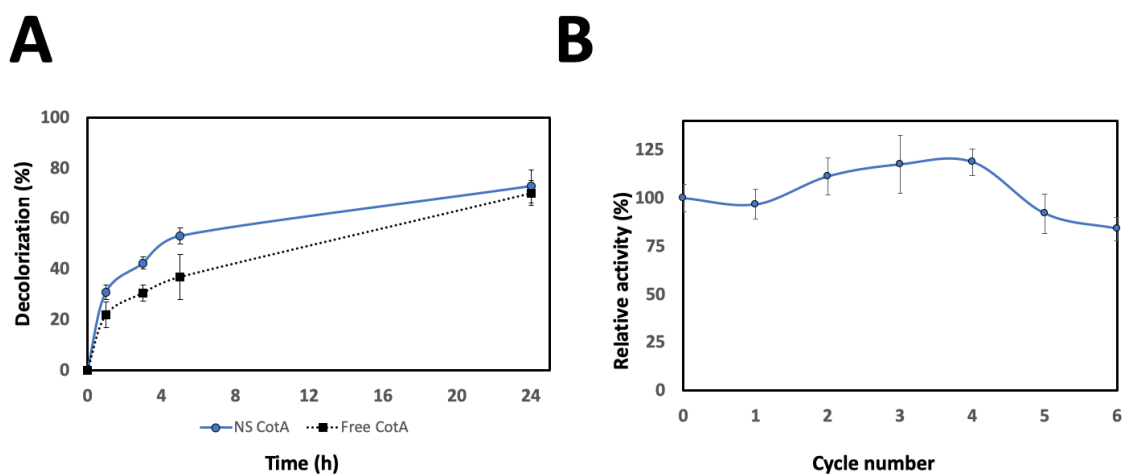


Figure 21. (A) Decolorization of RB19 by NS-CotA at 60°C and pH 5.0. (B) Recycling of NS-CotA. Residual activity (%) of NS-CotA during 6 cycles of 5mM ABTS oxidation and recovery. Data values represent mean \pm SD, which are not seen in some data points as they are smaller than the symbols.

3.8. Discussion

To test if our IC-Tagging methodology would result a good one-step enzyme immobilizing method we chose the *B. subtilis* laccase, first because of its multiple applications in different fields as industry or biotechnology, but also because its complex globular structure comprising an active center that should contain four coordinated copper atoms to be active. *Bacillus* laccase was produced at relevant concentrations by using the Rosetta strain of *E. coli*. The enzyme co-purified with muNS-Mi after lysis and centrifugation showing its integration into NS. Expression yields of 30–50 mg/l were observed under standard conditions, without performing any expression optimization studies. These are similar or even higher than values reported in previously works where optimization of CotA laccase production in *E. coli* was performed (143). However, in spite of the laccase content, no activity was present in the NS when the expression was performed under standard conditions, in keeping with the reported observation that only after supplementing the culture medium with copper and carrying out the expression under microaerobic conditions, the enzyme would get loaded with the necessary copper ions for carrying out its activity.

The copper-loaded enzyme was then produced at similar yields than the inactive version, and its activity was characterized by measuring its ability to oxidize ABTS. The immobilized activity was similar to the values reported for different laccases encapsulated by biomimetic silica mineralization (39U/g NS vs. 15.3–126.7 U/g (144). We found that the NS-contained enzyme presented an increased activity over a wider pH range when compared to the free enzyme, what agrees with a stabilizing effect of the nanoencapsulation on the enzyme. Furthermore, the stability of the enzymatic activity against incubation at different pH values also showed a remarkable increase upon nanoencapsulation.

Identical stabilization effects were observed on incubation with different inactivating agents such as organic solvents and salts. Concentrations of different reagents that produced a deleterious effect on the activity of the free enzyme had no effect on the NS-contained laccase. The increased stability in organic solvents is particularly interesting for the industrial application of enzymes. The use of organic

solvent systems instead of aqueous media for enzymatic reaction offers numerous advantages; however, organic solvents often inactivate enzymes (145). On the other hand, halides are known inhibitors of laccases, which may limit their application for bioremediation of industrial effluents with variable composition of inhibitors (146).

Synthetic dyes are extensively used in different industries, and 10–15% of dyes used during finishing and dyeing processes ends up in wastewater (147). Anthraquinone-based reactive dyes have attracted attention from the environmental and toxicological perspective, since they are extremely resistant to degradation and present acute toxicity of mutagenic effects (147). Conventional biological systems are not efficient for bioremediation and decolorization of dyes, and physico-chemical methods are associated to high operational cost, formation of undesirable by-products, etc. NS-CotA can be an eco-friendlier and practical choice for the bioremediation of dye polluted wastewater effluents. In this sense, the NS-contained enzyme was shown to decolorate the anthraquinonic dye RB19 quite efficiently compared to free enzyme. Although the RB19 decolorization rate was lower than that recently reported by using *Trametes versicolor* laccase in solution (148), it was remarkably higher than that achieved by an immobilized fungal laccase in absence of a mediator (149)(only 5% decolorization in 6 h). Furthermore, it should be highlighted that the transformation of the dye by NS-laccase could be optimized in terms of pH, enzyme dosage or temperature, for a more efficient transformation of the substrate.

Also, because of their particulate nature, the NS-contained enzyme can be recovered from the reaction and re-used for several times without a significant loss in activity. Furthermore, because their small size, some NS might have been lost during the repeated centrifugation steps and the small decay in activity can be explained by diminished protein content. An improved recovery method, involving filtration, NS-linking, or others, can be implemented to improve the recovery rates.

The most remarkable property that we have observed for this system is the thermal stabilization achieved. It is certain that the *B. subtilis* laccase is already intrinsically heat-stable. However, the NS-contained version surpasses extensively the abilities of the free enzyme. Although the encapsulated version outperforms the free one over all the temperature range, is at the highest values of 90 and 95 °C where the differences become remarkable. Thus, while the activity of the free enzyme is

completely abrogated after 5min incubation at 90°C, the NS-contained laccase resisted at least 30min of incubation at that temperature without any appreciable activity loss. The performance of the NS-laccase only started to decline to a 77% of the initial activity after 15min of incubation at 95°C. This extreme thermostability might be beneficial for transformations that might be accelerated by increasing the temperature, well laccase-mediated oxidations or multi-enzymatic complex reactions.

The IC-tagging methodology has been previously shown to produce micro and nano-encapsulated properly folded proteins. Here we have shown that this simple methodology can be also utilized for the production of active enzymes for industrial or other different uses, and that enzymes get stabilized while integrated into the NS and can be easily recovered and further reused. Between the IC-tagging characteristics are its simplicity, versatility, and the fact that it allows us to express and immobilize proteins and enzymes in one step, in either prokaryotic or eukaryotic cells. Once produced, the purification technique of these MS and NS is certainly straightforward, consisting in the use of cell lysis and centrifugation cycles bypassing the use of purification columns and other expensive methods, making this platform inexpensive and fewer time consuming. Also, we have previously demonstrated that several proteins can be simultaneously integrated into the same MS or NS, making them suitable for the easy creation of micro/nano reactors that integrate different immobilized enzymes for connected funneled multi-step transformations (150, 151). The stabilization observed can be particularly useful when performing complex reactions that require the use of different enzymatic activities requiring different co-factors that may not be fully compatible with all the participating enzymes.

CHAPTER 2:
ENZYME IMMOBILIZATION AND
BIOCATALYSIS VIA 3D PRINTING

1. INTRODUCTION

It is now common, and almost expected, that an individual will take dozens of medicines in their lifetime, especially with advancing age (152-154). As more medicines are consumed, more are consequentially excreted or disposed of, often permeating the world's water. Drugs and their metabolites are present in nearly all aquatic environments, from drinking water, to ground water, sea water, and waste water (155). The issue is global, with countries recording significant concentrations of pharmaceuticals in water across Europe, Africa, Asia, and the Americas. Presently, antibiotics, analgesics, lipid-lowering drugs, and estrogens are the most reported water-polluting drugs worldwide; however the true number and scale of drugs is likely larger than currently known, due to limitations and priorities in testing (156). This insidious infiltration of pollutants poses a significant risk to global health and ecological equilibrium. For example, diclofenac is known to be one of the most prolific drugs entering water, with a global average of 0.032 $\mu\text{g/L}$ present in all surface water compartments (156). The entrance of diclofenac into wild food chains is lethal for migratory birds, such as vultures. In fact, diclofenac has resulted in the population collapse of three vulture species in South Asia and poses a significant threat to several European species (157, 158). Elsewhere in the environment, the occurrence of estrogens in sewage effluents has led to feminization of male fish, dramatically impacting reproductive success (159-162). With regards to human health, the practice of irrigating crops with wastewater increases risk of consumer genotoxicity, due to the presence of solubilized antineoplastics (163). Moreover, antibiotics in water are thought to increase rates of bacterial antibiotic resistance, a currently critical challenge that threatens global health as whole (164-166). Even drugs of abuse are infiltrating water, as highlighted by studies in Madrid and Changzhou City, East China, which found cocaine, opioids, and methamphetamine in the cities' drinking supply and wastewater (167, 168).

In the face of this challenge, the World Health Organization (WHO) has launched a working group to address how pharmaceutical burden in water can be lessened. As such, several methods for removing drugs from water have been proposed, including sludge processes; biofiltration; reverse osmosis; ozonation;

chlorination; and nanofiltration. Unfortunately, many of these processes are variably efficient – with drug removal rates sometimes lower than 10% - and often require expertise with access to expensive and sizeable equipment (169). Thus, there is a global requirement for efficacious technologies that can remove drugs in water simply and cost-effectively. Ideally, methods should also work reliably in a range of different environments, regardless of pH, temperature, or physical space. As such, technologies that can be customized to fit into different physical spaces (such as pipes or machinery) are desirable.

3D printing is a key manufacturing method for customizable devices (170-172). In this study, we develop, manufacture, and validate a 3D printed biocatalytic device for the removal of drugs from water (termed Printzyme). The Printzyme has fully modifiable morphology, and utilizes the natural enzyme laccase, sourced from *Trametes versicolor*, as a drug oxidating agent (173). As mentioned, laccases are ubiquitously found in nature, and have been shown to effectively degrade a wide variety of pharmaceuticals, including several classes of antibiotics, paracetamol, diclofenac, naproxen, anti-depressants, and estrogens (174-176) (177) (178-180). Printzyme entraps laccase in a hydrogel via stereolithography (SLA) 3D printing. The novel process immobilizes the enzyme and simultaneously prints under mild conditions, representing an inexpensive and sustainable manufacturing process (figure 22).

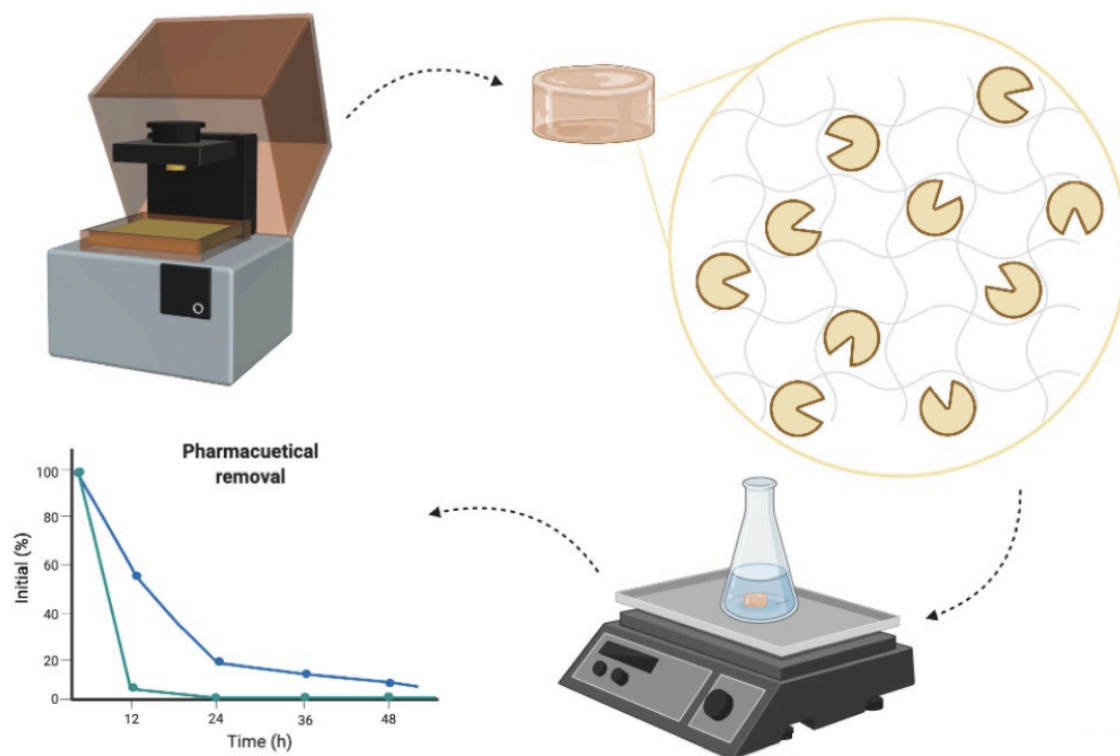


Figure 22. Workflow of the enzyme 3D printing process including final evaluation. The enzyme is first 3D printed using a commercial Form 2 SLA 3D printer, leading to the entrapment of the enzyme into the polymer matrix. The Printzyme is then evaluated for the activity determination.

We highlight Printzyme’s optimal conditions of use, stability at varying pH and temperature readings, and homogenous laccase immobilization. Crucially, we demonstrate Printzyme’s ability to remove diclofenac sodium and an oestrogen, ethinylestradiol, from water with excellent device reusability. Our results present a significantly effective, sustainable and potentially scalable approach to removal of pharmaceutical contaminants from aqueous systems and provide implications for the development of bioremediation (figure 23).

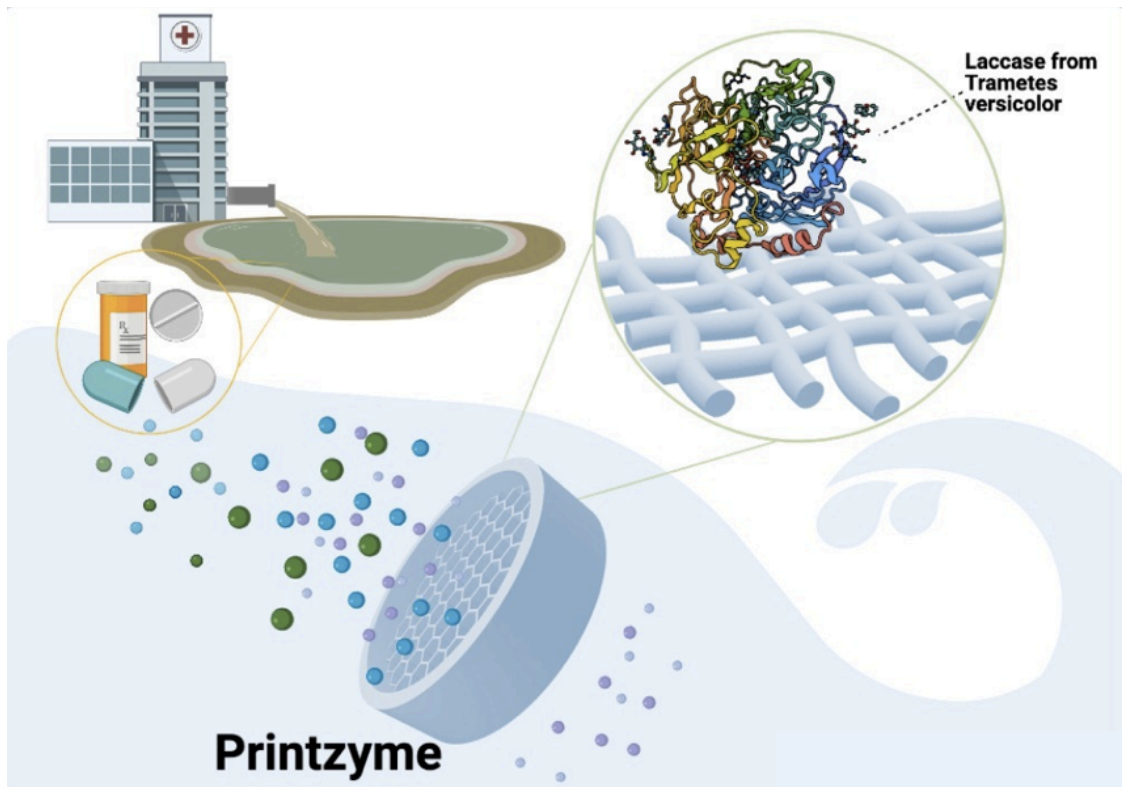


Figure 23. Graphical abstract of the Printzyme potential application in water bioremediation.

2. 3D DESIGNING OF THE PRINTZYME

The Printzymes were initially designed in two configurations; cylinder (60mm diameter, 4mm thickness) and torus (60mm outer diameter, 50mm inner diameter, 4mm thickness) using 123D Design software (Autodesk Inc., USA) and exported as an stl. files. (Figure 24). These two shapes were designed in order to evaluate the effect of surface area to volume ratio on activity.

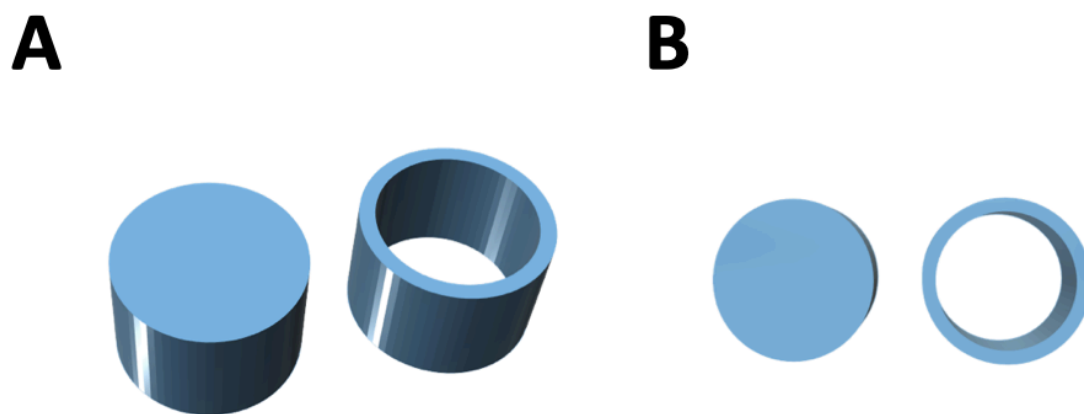


Figure 24. Images of the two shapes designed using the using 123D Design software for the study, seen from the side (A), and from the top (B).

3. FORMULATION AND 3D PRINTING OF PRINTZYME

Four formulations were initially investigated for the optimal Printzyme device (Table 6): Printzyme 0.4-20 (0.4% laccase, 20:80 PEGDA:water); Printzyme 0.4-50 (0.4% laccase, 50:50 PEGDA: water); Printzyme 4-20 (4.0% laccase, 20:80 PEGDA:water); and Printzyme 4-50 (4.0% laccase, 50:50 PEGDA:water). Poly(ethylene glycol) diacrylate PEGDA was selected as the formulation support due to its flexibility, biocompatibility, ease of crosslinking, and uniform pore size (181-183). LAP was chosen as the SLA photoinitiator due to its high water solubility and cytocompatibility (184).

Printzyme	Laccase from <i>Trametes versicolor</i> (% w/w)	PEGDA:Water ratio	PEGDA (% w/w)	Water (% w/w)
Printzyme 0.4-99	0.4	99.6:0	99.6%	0
Printzyme 0.4-20	0.4	20:80	19.82	79.28
Printzyme 0.4-50	0.4	50:50	49.55	49.55
Printzyme 4-20	4.0	20:80	19.10	76.40
Printzyme 4-50	4.0	50:50	47.75	47.75

Table 6. Composition of the photopolymer resin

*Each resin includes 0.5% w/w LAP

It was observed that the formulation intended as Printzyme 4-50 appeared as a suspension, meaning that the laccase was not fully dissolving in the PEGDA-water solution. This that would likely cause heterogenous distribution of the enzyme in the printed device and thus affect the reproducibility of enzyme activity in the final Printzyme. For this reason, the Printzyme 4-50 formulation was removed from the study. The remaining three formulations were observed to form solutions and were successfully printed into said two morphologies using SLA 3D printing, as shown in Figure 25.

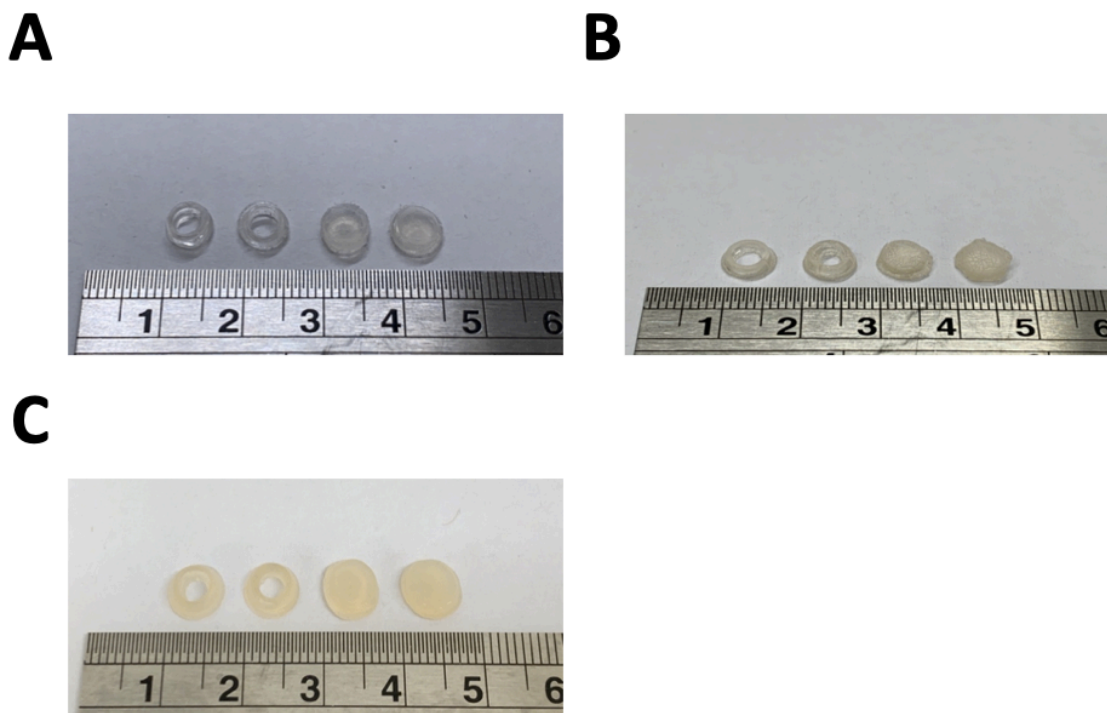


Figure 25. Pictures of two torus and two cylinders fabricated from (A) Printzyme 0.4-20, (B) Printzyme 0.4-50, and (C) Printzyme 4-20 via SLA 3D printing. The scale is in cm.

As seen in Figure 25, Printzyme 4-20 has an opaque appearance corresponding to its higher laccase content (4.0% w/w) compared to the more translucent Printzyme 0.4-20 and 0.4-50 formulations (containing 0.4% w/w laccase). A PEGDA to water ratio of 20:80 was found to produce Printzymes with adequate resolution and consistency in shape. Correspondingly, the Printzyme 0.4-50 formulation, with its higher PEGDA content, resulted in decreased resolution. Whilst the thickness of the designs was set to 3 or 4 mm, some shrinkage did occur after 3D printing, resulting in a loss of around 0.5 mm thickness.

ESEM allowed detailed inspection of the Printzyme surfaces (Figure 26). From the ESEM images, it is clear that the resolutions of Printzymes 0.4-20 and 4-20 are superior to Printzyme 0.4-50 (Figure 26B), that shows a fractured surface, most likely due to its lower water content. Previously, it has been reported that an increase in PEGDA concentration or decrease in water content in hydrogel formulations results in a reduction of the curing time required during SLA printing (185, 186). Optimal

SLA printing of Printzyme 0.4-50 likely requires a lower SLA curing time than Printzymes 0.4-20 and 4-20 (Figures 30A and 30C). For all Printzymes, ESEM shows the layers formed in the devices' internal structures, caused by the layer-by-layer curing method of the SLA printer (Figure 26).

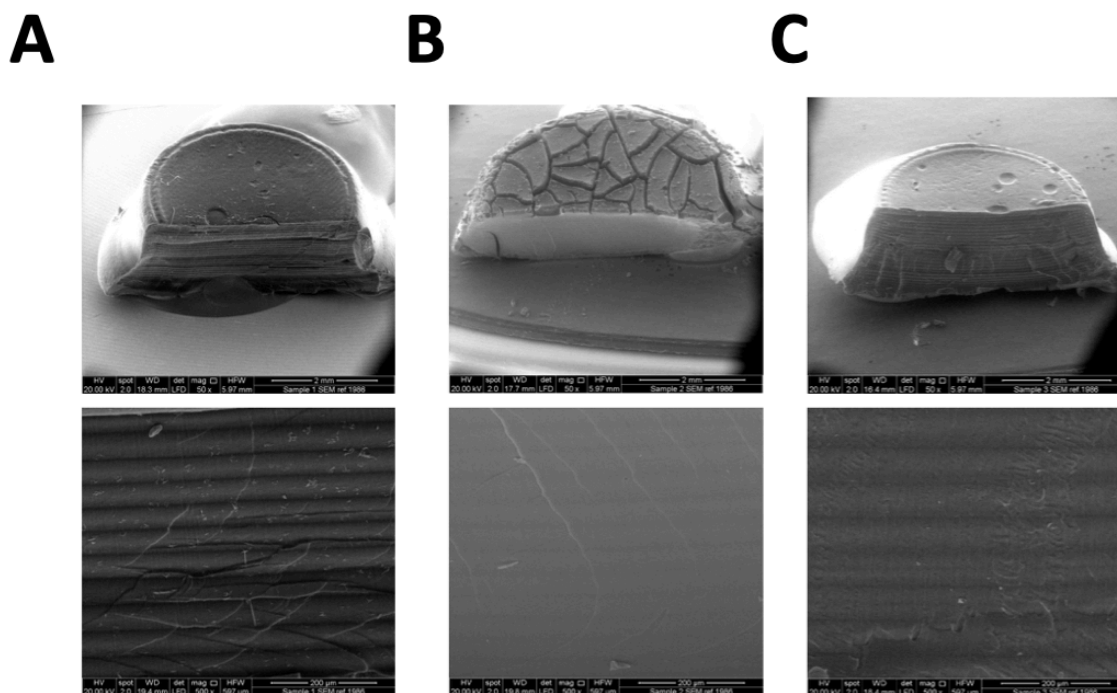


Figure 26. ESEM images of cylinder fabricated from (A) Printzyme 0.4-20, (B) Printzyme 0.4-50, and (C) Printzyme 4-20 via SLA 3D printing.

Although the minor cracks have no consequences on the integrity of Printzyme 0.4-50, it resulted in fluctuating measured activity as laccases are exposed differently to the substrate. As a result, Printzyme 0.4-50 was also removed from the study.

USC
UNIVERSIDADE
ESTADUAL DE SÃO CARLOS

4. INITIAL ENZYMATIC ACTIVITY ASSESSMENT OF PRINTZYMES

Printzyme 0.4-20 and 4-20 achieved reproducible levels of laccase activity (Table 7). The maximum specific activity of the devices was measured after shredding

the Printzymes into fine particles, in order to facilitate display of enzyme active sites. Table 7 shows that the process of SLA printing had a minor effect on enzyme activity, since the Printzyme constructs retained more than 75% of the activity of laccase incorporated in the formulation prior to printing. The immobilization yields (Eq. 1) attained here agree with previously reported works. For instance, laccase encapsulated in a silica sol-gel matrix demonstrated immobilisation yields of 83 to 59% (187).

Printzyme	Activity added ¹	Maximum activity ²	Immobilization yield ³ (%)	Shape	Apparent activity ⁴	
	(mU/mg)	(mU/mg)			(mU/mg)	(mU/mg)
					4 mm	3 mm
					thickness	thickness
Printzyme 0.4-20	6.60 ± 0.23	5.03 ± 0.54	76.2 ± 10.83	Cylinder	0.042 ± 0.013	0.240 ± 0.020
				Torus	0.109 ± 0.021	0.344 ± 0.017
Printzyme 4-20	66.0 ± 2.3	49.60 ± 6.90	75.2 ± 13.08	Cylinder	0.501 ± 0.027	1.377 ± 0.132
				Torus	1.022 ± 0.074	1.426 ± 0.068

Table 7. Immobilization yield and effective activity of the different Printzyme configurations.

¹ Theoretical initial activity, based on mg of enzyme added (1.65 U/mg enzyme).

² Printzyme was shredded into fine particles and the activity of the particles was measured.

³ Activity measured/activity added · 100

⁴ Apparent activities measured for each of the construct shapes.

The apparent activity of Printzymes with 4mm thickness was much lower than the maximum activity: the cylinder shapes showed a 99-120 fold reduction in apparent activity whereas torus shapes showed 46 to 48 fold reductions in apparent activity (Table 7). Hence, the effectiveness factor, which is the ratio between enzymatic activity monitored in the immobilised state compared to free solution (Eq. 2), was close to zero for the cylinder shape (0.008 and 0.01 for 0.4-20 and 4-20 cylinder shapes, respectively). This indicates that the substrate cannot penetrate through the device and thus the reaction rate is limited to the outer layer of the system (188). The apparent activities of the 3 mm thickness cylinder constructs were slightly higher than the 4mm counterparts, demonstrated by effectiveness factors of 0.03 - 0.07. However, reducing the thickness to 3mm affected the system's structural integrity, which was lost upon storage (data not shown). Hence, the 4mm thickness was selected for progression to further experimentation.

The torus designs of both Printzyme 0.4-20 and 4-20 at 4mm thickness had higher activities than their cylinder counterparts, due to an increased number of exposed laccase active sites arising from an increased surface area. The torus forms of Printzyme 0.4-20 and 4-20 had 159 % and 103 % higher relative activities than the cylinder designs. In practice, the geometry of Printzymes will be adapted to suit their application. For example, torus shapes may be best suited to line tubes or pipes, whereas more complex morphologies may be suited to other applications requiring bespoke designs. In any case, this data demonstrates that recognition of device surface area is a key design consideration with direct implications for Printzyme activity.

5. OPTIMAL PH AND TEMPERATURE FOR PRINTZYME ACTIVITY

Figure 27A shows how free laccase and Printzyme activity changed in conditions of varying pH (pH 3.0 to 6.0). For both, Printzyme formulations and free laccase, pH and enzyme activity showed an inverse correlation, i.e., with increasing pH, enzymatic activity decreased. Printzyme 0.4-20, Printzyme 4-20, and free laccase all demonstrated optimal activity at pH 3.0. This observation is in accordance with the literature, in which pH 3.0 has been shown as the optimal pH for free laccase and for laccase immobilised onto fumed silica nanoparticles (189, 190).

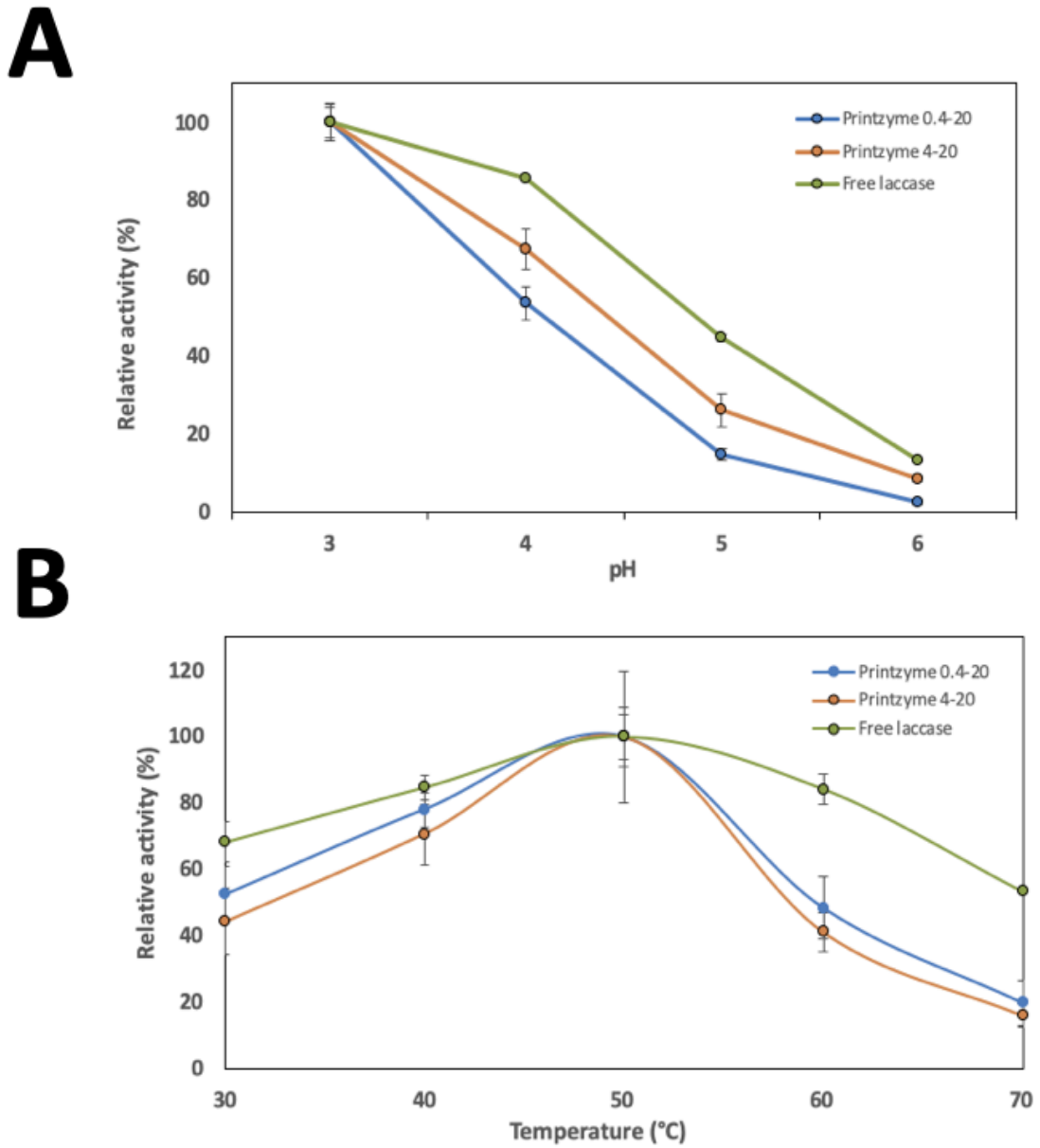


Figure 27. Effect of **(A)** pH and **(B)** temperature on the activity of free laccase (green), Printzyme 0.4-20 (blue) and Printzyme 4-20 (orange). Data values represent mean \pm SD, which are not seen in some data points as they are smaller than the symbols.

With regards to temperature, enzyme activity in both Printzyme formulations and free laccase demonstrated a bell-shaped curve, where enzyme activity peaked for all three at 50 °C (Figure 27B). These results concur with other studies, in which 50°C

was determined as the optimal temperature for laccase sourced from *T. versicolor* (190-192). The increase and subsequent decline in enzyme activity is unsurprising, as it follows the inherent behaviour of most biological enzymes. With increasing temperature, the energy in a system increases with the rate of enzyme catalysis, until an optimum temperature is reached; above which irreversible enzyme denaturation begins (193).

6. EFFECT OF PH AND TEMPERATURE ON PRINTZYME STABILITY

The results of the incubation of free laccase and Printzyme at different pH values and different times are shown in Figure 28. Interestingly, whilst free laccase and Printzyme activity is optimal at acidic pH (as shown in Figure 27A), enzyme activity suffers during extended exposure to acidic conditions. During the functional use of Printzyme it will likely be subjected to aqueous environments of varying pH and temperatures for extended periods. This data highlights that Printzyme should be stored around neutral pH, and only exposed to acidic media for short time periods, to retain maximal activity and reusability. Figure 28B demonstrates that immobilisation of laccase in Printzyme 0.4-20 protects it from inactivation, with minimal loss of enzyme activity after incubation from pH 4.0 to 8.0 over 24 hours. In comparison, free laccase is observed to lose activity in acidic environments (pH 3.0 and 4.0) when incubated for extended periods (Figure 28A). Such deactivation of free laccase has been noted in previous studies (194, 195). The protective effect of Printzyme could be attributed to the hydrogel matrix resulting in restricted conformational mobility of laccase (182, 187).

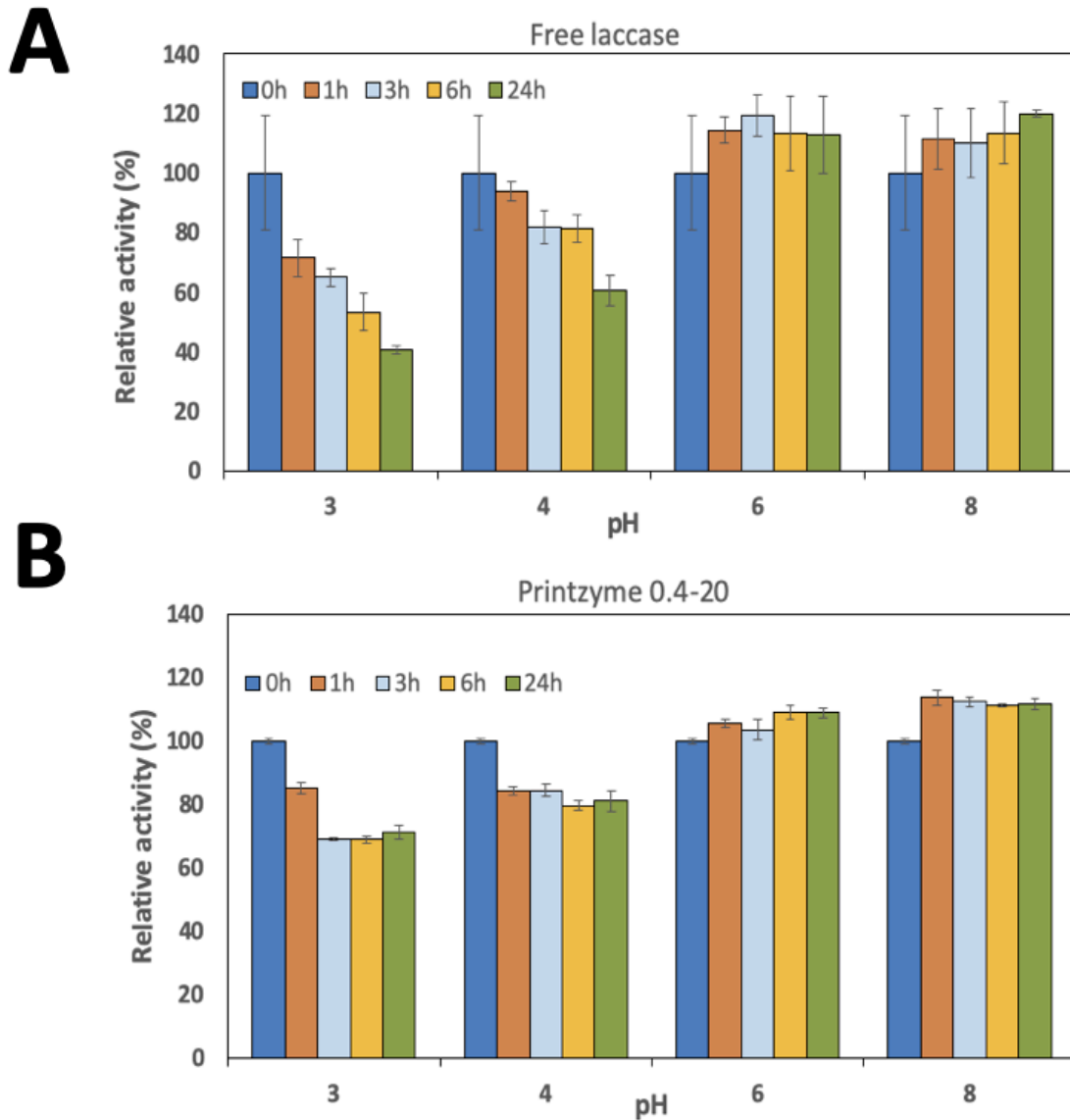


Figure 28. pH stability of **(A)** free laccase and **(B)** Printzyme 0.4-20 after incubation in buffers at the pH values indicated at the bottom of the diagram at room temperature at the times indicated by the color code. Data values represent mean \pm SD, which are not seen in some data points as they are smaller than the symbols.

The protective effect of Printzyme 0.4-20 was also observed in the thermostability study, where devices were incubated at 40°C for 24 hours (Figure 29). At 40°C, free laccase lost its activity from 6 hours onwards, whereas laccase in Printzyme did not experience substantial denaturation. This improved thermostability has also been observed with laccase-entrapped nanoparticles, though these systems

can be difficult to prepare compared to Printzyme's simultaneous print-and-immobilize manufacture (189). For both free laccase and Printzyme, biocatalytic activity decreased when maintained in aqueous conditions of 50 °C and over (however Printzyme did exert a protective effect for the first 3 hours). This progressive loss of enzyme activity is most likely due to thermal denaturation and loss of laccase tertiary structure, and indicates that Printzyme should not be stored at temperatures exceeding 40°C (194). The ability of Printzyme to protect laccase activity under conditions of varying pH and temperature may go some way to compensating towards its lower relative activities in certain conditions when compared to free laccase (Figure 29).

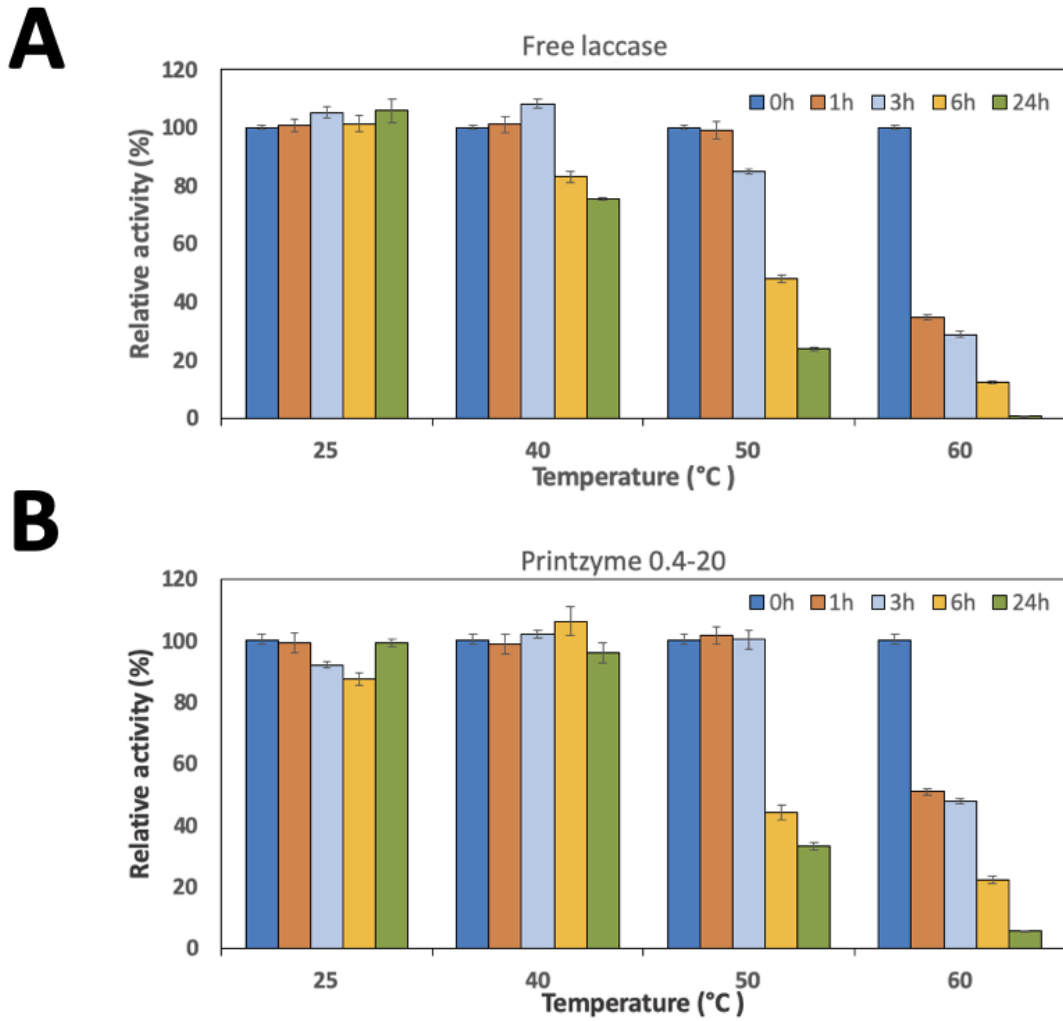


Figure 29. Thermal stability of (A) free laccase and (B) Printzyme 0.4-20 after 1h, 3h, 6h and 24h of incubation in citric-phosphate buffer (pH 6.0) at different temperature values (25°C, 40°C, 50°C and 60°C). Data values represent mean \pm SD, which are not seen in some data points as they are smaller than the symbols.

7. REUSABILITY OF PRINTZYMES

Figure 30 shows the activity of laccase over 18 consecutive uses of 5 minutes each, when immobilized in Printzyme 0.4-20 and 4-20. Clearly, both Printzyme formulations retained good activity despite multiple cycles of use, with Printzyme 4-20 demonstrating the best stability with its higher enzyme content. After 5 isolated uses, Printzymes 0.4-20 and 4-20 retained 85.4 ± 2.6 % and 87.0 ± 2.5 % of their initial activities, respectively. The enzymatic activity of both Printzymes remained

almost constant, achieving 83.0% and 107.0% relative activities, respectively, after 18 consecutive cycles.

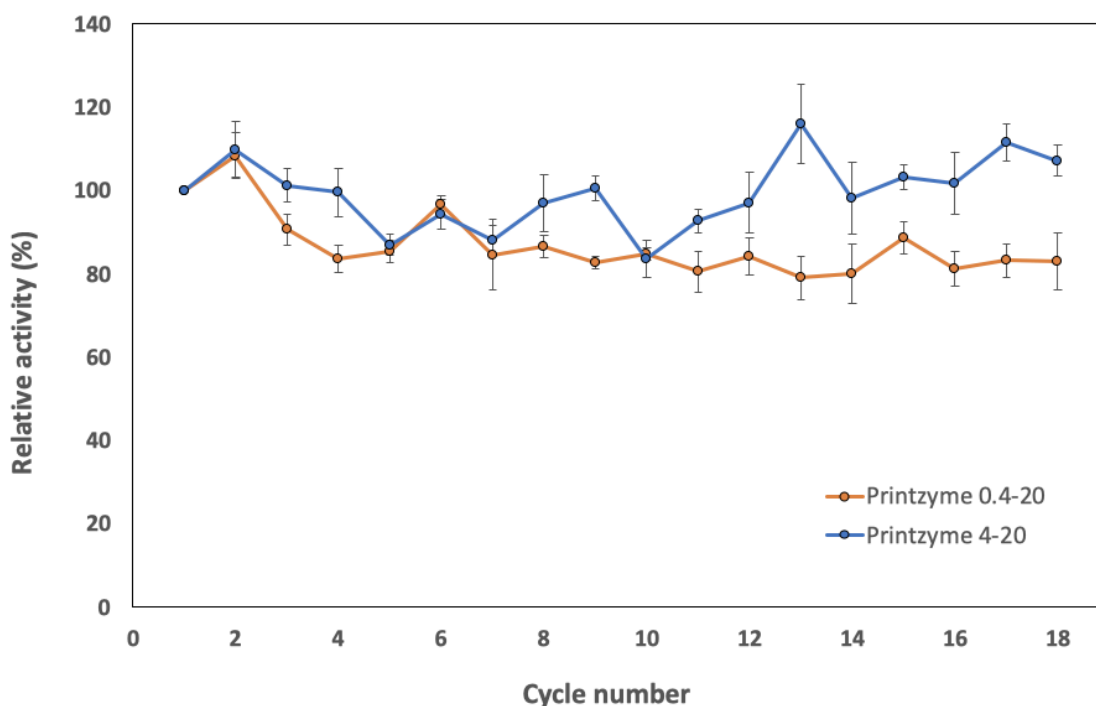


Figure 30. Reusability of Printzyme 0.4-20 and Printzyme 4-20, demonstrated by retention of laccase relative activity on consecutive reaction cycles. Data values represent mean \pm SD.

8. REMOVAL OF PHARMACEUTICALS USING PRINTZYME

Next, we decided to investigate the ability of our printed devices on the removal of pharmaceuticals commonly found in waste water. Figure 31 shows the degradation of diclofenac and ethinylestradiol over 48 hours, in the presence of Printzyme and free laccase. Clearly, both Printzyme shapes and free laccase achieved significant degradation of both drugs compared to controls from 2 hours onwards. Both drugs are common water pollutants on a global scale, and as such are present on the European watch list for environmental micropollutants (196). Printzyme 4-20

was selected for this investigation, due to its higher resolution, laccase content, and reusability compared to other formulations tested in the study. The fact that the formulation is 80 % water is an additional benefit, as this reduces the manufacture cost per device and decreases its carbon footprint (due to lower consumable PEGDA content).

Figure 31A shows that the torus form of Printzyme achieved faster and more complete removal of diclofenac compared to the cylinder, tablet-shaped, device. This is unsurprising, as Section 3.2 showed that laccase activity was enhanced by the torus' higher surface area. Using the torus Printzyme, 50 % of diclofenac was removed after 4 hours, and after 24 hours it had achieved near complete degradation of the anti-inflammatory. Regarding the cylinder, it achieved 50% degradation after 8 hours and after 48 hours the removal of diclofenac has been also nearly completed (>90 %).

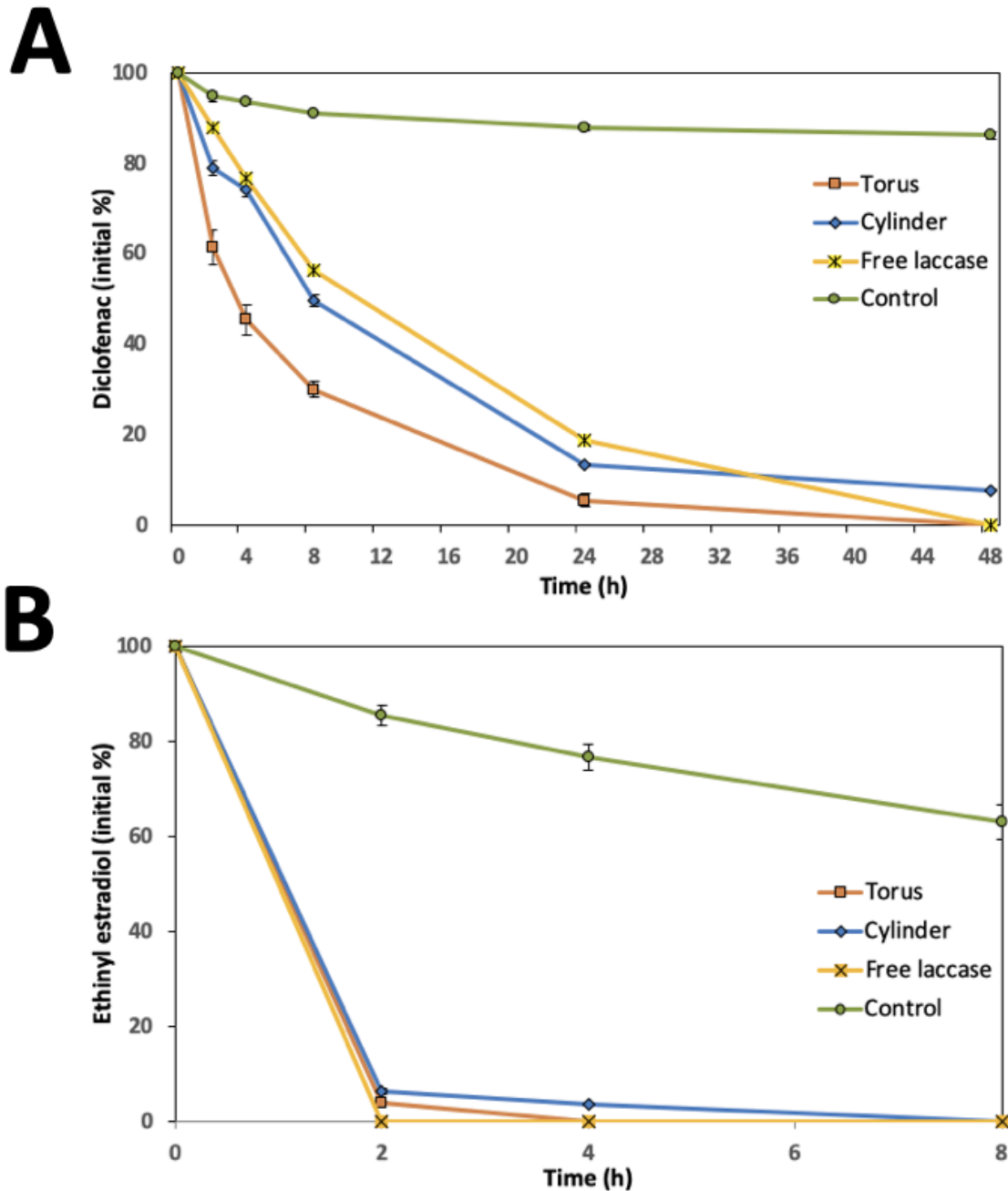


Figure 31 Effect of torus and cylinder Printzyme 4-20 on removal of **(A)** diclofenac and **(B)** ethinyl estradiol. Control uses Printzyme lacking laccase. Data values represent mean \pm SD, which are not seen in some data points as they are smaller than the symbols.

USC
 UNIVERSIDADE
 Figure 31B shows how both Printzyme designs also achieved near complete removal of soluble ethinylestradiol after just 2 hours. Similar results have been reported in previous studies in which more than 80 % of ethinyl estradiol has been removed following just 1 hour treatment of laccase from *T. versicolor* (178).

Noticeably, the control experiment containing laccase-free Printzyme, showed some removal of the oestrogen over the 48 hours. This is likely due to adsorption of the drug onto the Printzyme control. In fact, oestrogen recoveries of 81 % were obtained after extraction of the Printzyme with methanol (not shown), indicating that the drug was adsorbed onto the control Printzyme, demonstrating an additional mechanism of drug removal for the device (187, 197). Despite this, the data indicates that Printzyme's removal of ethinylestradiol was mainly due to the action of the immobilized laccase. The effectiveness factor (Eq. 2) for the estrogen removal was close to one in both cases (0.92 and 0.95 for cylinder and torus, respectively, at 2h), proving that mass transfer had a negligible effect on the overall reaction rate.

9. Discussion

In this study, we immobilized laccase sourced from *T. versicolor* for the first time in a PEGDA hydrogel via SLA printing, with the goal of developing a customisable, economic, and effective way of removing drugs from water: a key global issue. During formulation tests, it was determined that optimal SLA resins incorporated PEGDA and water in a 20:80 ratio. Successful design and 3D printing of devices produced Printzymes with homogeneously distributed 0.4% and 4% (w/w) laccase, in torus and cylinder shapes. Post-printing analysis of enzyme activity confirmed that higher resin laccase concentrations led to an increase in activity. By studying Printzyme activity at extremes of pH and temperature, it was confirmed that Printzymes function best in acidic solutions of around 50°C, however to retain maximal reusability they require storage at neutral pH and less than 40°C. Depending on the locations and types of water affected, drugs will require removal from aqueous systems of varying pH and temperatures. In the United States, rainfall can vary from lower than pH 4.3 to over pH 6.0 (198). Soil pH can vary widely from pH 2.0 - 9.0, depending on solubilised minerals, thus affecting the pH of groundwater (199). Wastewater pH will vary according to the processes and environments it has been exposed to. These data show that Printzyme performs best at acidic pH, which should be considered in its future applications.

Applications of Printzyme should consider this activity to temperature relationship, potentially avoiding use above 50 °C, as irreversible laccase denaturation will impact the reusability of devices.

In both the pH and temperature studies (Figures 28 and 29), free laccase demonstrated higher activity than when immobilised in Printzyme. This is likely because it is in solubilised form, all laccase active sites are freely accessible, whereas in Printzyme enzyme immobilization leads to a certain degree of steric inhibition. Whilst Printzymes do achieve lower activity in aqueous solutions compared to free laccase, they still retain substantial activity. Moreover, both Printzyme formulations demonstrated similar relationships to pH and temperature as free laccase, indicating that direct immobilization of laccase into PEGDA hydrogels does not alter the biocatalytic mechanism. In addition, immobilization affords benefits in storability and reusability that free enzyme in solution cannot accomplish (200). Enzyme entrapment within functional systems enhances sustainability and cost-effectiveness as expensive enzymes are not lost with every use. This is especially important for settings with limited storage, budgets, or access to deliveries (e.g., in remote locations).

With regards to reusability, Printzymes were shown to retain good laccase activity for at least 18 isolated uses; demonstrating their superiority over free laccase in solution. Both Printzymes achieved superior reusability compared with other immobilisation methods of laccase from *Trametes versicolor*, including iron oxide nanoparticles 33% (201), chitosan macrobeads (202), magnetic mesoporous silica spheres (203), poly(glycidyl methacrylate)-based microspheres (190), and agar-agar, polyacrylamide, and gelatin structures (204). As mentioned, a key benefit of Printzyme is its immobilisation of laccase, as this allows enzyme recovery and repeated use not possible with free enzyme in solution. These data highlight the concept's cost-effectiveness, sustainability, and fit for purpose. Further, Printzyme could successfully reduce the concentrations of two drugs, diclofenac and ethinylestradiol, in aqueous solution. The devices removed over 80 % of dissolved diclofenac within 24 hours, and 95 % of ethinylestradiol within just 2 hours, being more efficient the torus shape, because of the higher surface to volume ratio. The effectiveness factor for the estrogen removal was close to one (0.95 for torus Printzyme), demonstrating that

substrate diffusion across the Printzyme did not limit the transformation. Regarding diclofenac, the device provided higher initial removal rates than the free enzyme, with effectiveness factor of 1.55 (torus Printzyme), emphasizing the interest of using Printzyme for the transformation of substrates which can inhibit laccase. During the experiment, the degradative action of immobilized laccase within Printzyme was made visually clear, as the originally colourless solution of diclofenac gradually became dark yellow. This is likely due to the accumulation of a known diclofenac degradation product, 4-(2,6-dichlorophenylamino)-1,3-benzenedimethanol (175). Surprisingly, the initial removal rates with free laccase in solution were lower than those achieved with both Printzyme configurations. This implies that the effectiveness factor (Eq. 2) reached values higher than one (1.55 and 1.11 for torus and cylinder, respectively, calculated for the removal rates at 8 hours). Effectiveness factor generally lies between 0 and 1, but sometimes can be higher than one due to non-isothermal operation, because of the stabilisation of the encapsulated enzyme related to the free one or because of inhibitory effects (205). Here, the most plausible reason is the inhibition caused by high diclofenac concentrations, as reported by Lonappan et al. (206). These authors observed that at 5mg/l concentration, the kinetics of *T. versicolor* laccase shifted from first order to zero order, confirming substrate inhibition. In this work, Printzyme may have increased observed degradation rates by reducing the concentration of the substrate to non-inhibitory concentrations. Hence, Printzyme represents the more economic and sustainable option not only due to its reusability but also because it was more effective than the free enzyme in degrading diclofenac in the short term. Other pollutants reported as inhibitors of *T. versicolor* laccase include dyes (207) or phenolics from the olive oil industry (208).

Figure 31 demonstrates how Printzyme's removal capacity differed for the two investigated drugs. Laccase is a copper-containing oxidase that catalyses oxidation reactions through single electron transfer; it is known to show high activity against phenolic compounds (209, 210). Ethinylestradiol contains a phenolic moiety within its chemical structure whereas diclofenac does not, thus explaining why Printzyme removed ethinylestradiol faster than diclofenac. Phenol groups are common in medicinal chemistry, and are present in a wide variety of drugs, from the anti-

Parkinson's drug entacapone, to the antimuscarinic tolterodine, to ivacaftor for cystic fibrosis. This feature of laccase should be considered in Printzyme's applications. Particularly when the substrate can cause laccase inhibition, the use of Printzyme is highly recommendable, since shorter degradation times may be required compared to free enzyme. If fast removal (under 24 hours) of non-phenolic pharmaceuticals is required, then a mediator may be needed in the Printzyme formulation. Laccase mediators, including syringaldehyde, acetosyringone, vanillin, and p-coumaric acid have been previously shown to enhance the degradation of non-phenolic drugs (211). In general, Printzyme provides a reusable, customisable, cost-efficient, and sustainable way of effectively removing drugs from aqueous systems. It represents a flexible platform that can be used to immobilize a wide variety of enzymes for different specialist applications. Importantly, Printzyme technology has been shown to protect enzymes from deactivation at extremes of pH and temperature, making it a versatile tool for industrial processes including the removal of drugs from water.

This work highlights the potential of SLA 3D printing as a streamlined approach to entrap enzymes under mild conditions. Our results present a significantly effective and sustainable approach to removal of pharmaceutical contaminants from aqueous systems and provide implications for the development of bioremediation.

CHAPTER 3:
CANCER EPITOPES IMMOBILIZATION
VIA THE IC – TAGGING SYSTEM

1. INTRODUCTION

1.1. Cancer vaccines

The concept of mobilizing the human immune system against cancer dates back to at least the mid-nineteenth century when Rudolf Virchow, a German pathologist, observed immune infiltration in human tumors (212). Since 2011, owing to its potential for a large and sustained clinical benefit, immuno-oncology has become the fastest-growing area not only in oncology but in the entire pharmaceutical industry. Nevertheless, although some patients may achieve cure or long-term disease control with first- or second-generation treatments, the majority of patients are still in need of a beneficial next-generation treatment. Specifically, many patients are not responding to checkpoint inhibition or they respond and subsequently relapse. Innate immunity targets (for example, natural killer (NK) cell-targeting therapies) are gaining great interest, and novel approaches and drugs are emerging in this field. One of such approaches are vaccines which induce an immune response against unique tumor-specific antigens (neo-antigens). Thus, more individualized approaches based on new scientific insights into cancer vaccines are entering the immuno-oncology stage. Neoantigen-based vaccines (figure 32) should induce strong specific immune response and elicit stable therapeutic effects.

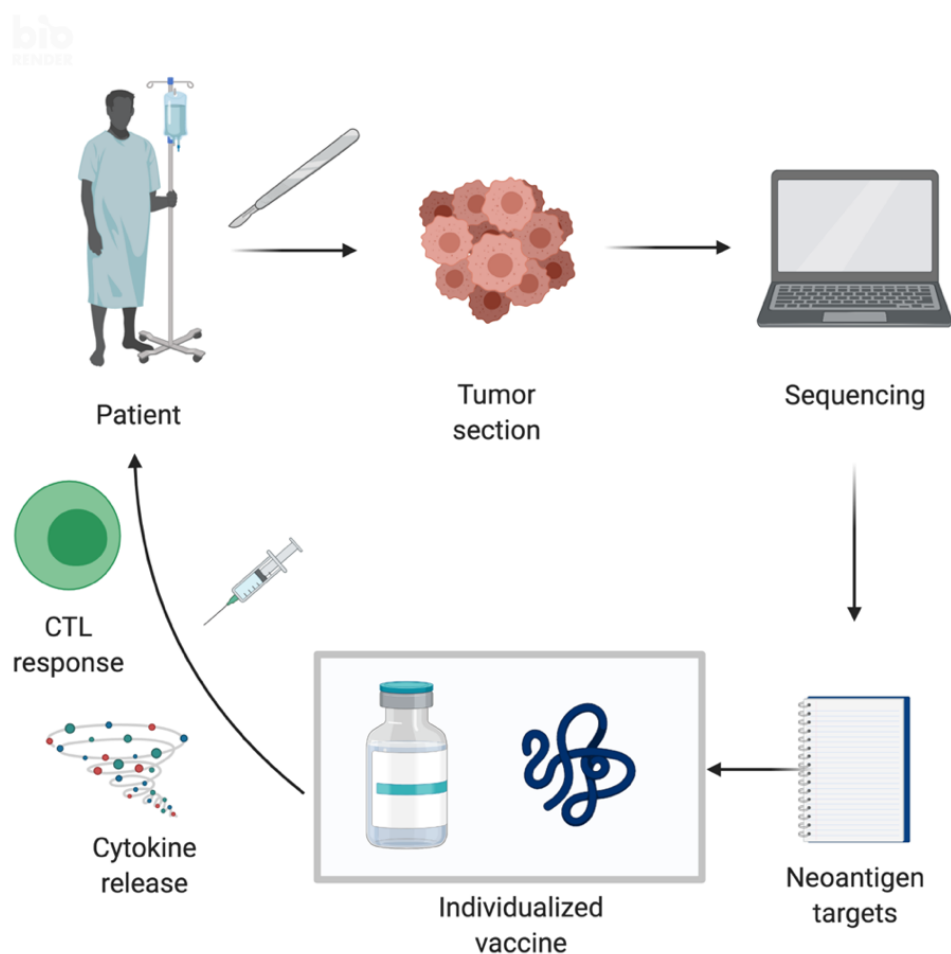


Figure 32: Schematic representation of neoantigen-based vaccines. The figure shows the theoretical workflow for individualized cancer vaccination. The cancer patient undergoes tumor resection surgery and biomaterial is collected. Using next generation sequencing and bioinformatics analysis of these biomaterials, tumor-specific neoantigens are identified and the selected peptides are synthesized following GMP guidance. The vaccine consists of synthesized peptides, peptide-loaded antigen-presenting vehicles, ex vivo expanded T cells or chimeric antigen receptor T cells and can be combined with adjuvants, immunogenic chemotherapeutics and/or immune checkpoint inhibitors to further enhance the potential to trigger an effective immune response. The patient will receive first vaccine shots ideally even before the chemotherapeutic intervention.



However, in the oncology field it is extremely complex to predict when and where tumor cells would occur (unless the patient suffers from specific rare syndromes) and which would be the antigenic signatures of those events and thus,

cancer vaccines are typically for therapeutic use. Hence, the term "vaccine" is referred to a formulation which usually include a strong adjuvant or it is adjuvant itself, and tumor proteins or peptides which prime the immune system (213).

1.2. Tumor antigen targets

The ideal target tumor antigen is expressed solely by malignant cells and features highly immunogenic mutations that produce neo-antigens; these proteins are defined as Tumor Specific Antigens (TSAs). Unfortunately, this is not a common scenario and most of the established tumor antigens which have been tested into the clinical settings are common with healthy cells. For instance, target epitopes such as HER-2, glycoprotein 100 (gp100), Telomerase or Tyrosinase Related Proteins (214) are present in normal tissues as well, hence they are defined as Tumor Associated Antigens (TAAs). Consequently, most of the responsive TAAs-reactive T-cells are eliminated during the thymic selection and maturation to avoid self-responses and cells who elude the selection are kept inactivated by the peripheral tolerance through the action of T-regulatory cells (215, 216). Despite these limitations, many studies displayed the potential of targeting TAAs. One example would be the efficacy of vaccination against gp100 demonstrated in different pre-clinical studies where mice pre-immunized with a fusion protein mimicking gp100 and the chemokine macrophage inflammatory protein 3 alpha (MIP3a) showed a reduced growth of B16F10 tumors (217). This fusion construct has been studied in therapeutic scenarios by Gordy and colleagues who found that therapeutic pre-clinical use of this fusion protein increased the survival of mice and reduced the size of their tumors (218). In addition, despite no clear differences in the number of infiltrating TILs, the number of gp100 reactive T cells was increased in the study group. Similarly, on a separate study the possibility of fusing the gp100 protein to the CD40L cytokine was explored in order to deliver the antigen specifically to DCs. Here, the therapeutic vaccination reduced the growth of B16F10 tumors and the effect was further increased by the addition of other cytokines such as IL-12 and GM-CSF to the preparation (219). Tumor-specific antigens (TSAs) are only expressed in malignant cells and they feature neo-epitopes, cancer testis antigens and embryonic antigens. However, this

expression can be oddly activated in tumors such as melanomas (220). One example are the melanoma associated antigens (MAGE) which are a cluster of genes on the chromosome Xq28 and their products have been identified on non-small cell lung cancer (NSCLC), sarcomas and head, bladder cancer, and neck cancer (220). All things considered, the previously mentioned potential targets highlight the complex scenario in which cancer vaccines operate. On one side, the efficacy of the therapy is in part determined by the strength to induce antigen-specific responses; on the other side, the induced antigen-specific T-cells after the vaccination, are usually inactivated by the suppressive component of the immune environment within tumors. These problems could be addressed by increasing the immunogenicity of the peptides included into the formulation, by using more immunogenic adjuvant platforms or by combining the vaccine with immune checkpoint inhibitors.

1.3. Adjuvant substances in cancer immunotherapy

It is a very common practice to introduce other substances in the vaccine formulation in order to increase the immune stimulatory activity of the candidate. Here, the ideal adjuvant should maximize the immunogenicity of the vaccine without compromising tolerability or safety. Unfortunately, adjuvant research has lagged behind other vaccine areas, with the consequence that only a very limited number of adjuvants based on aluminum salts, monophosphoryl lipid A, and oil emulsions are currently approved and/or have been used through history (figure 33). for human use.

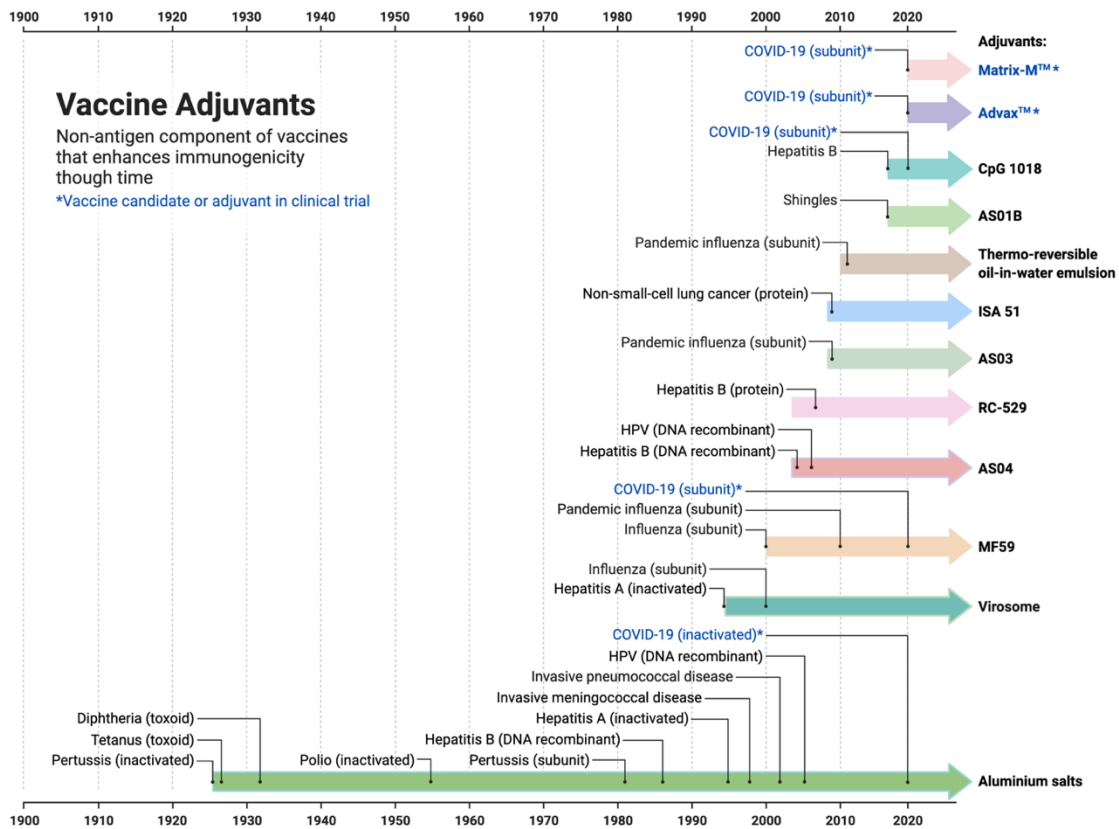



Figure 33: Vaccine adjuvants used in history. Adapted from: Iwasaki, A., & Omer, S. B. (2020). Why and how vaccines work. *Cell*, 183(2), 290-295.

Here, because of the specificity regarding the immunomodulatory profile, agonist targeting endosomal (Toll-like receptors) TLRs have been explored as adjuvant targets, also for this growing field of anti-tumor vaccines (221). Furthermore, endosomal TLR agonists have also been investigated as treatments with potential in cancer immunotherapy (222, 223).

1.4. Toll-like receptors (TLRs)

 Toll-like receptors (TLRs) are a protein family belonging to the pattern recognition receptors (PRRs) which is part of the innate immune system. These receptors recognize a variety of pathogen-associated molecular patterns (PAMPs) in order to initiate immune responses (224, 225). A common characteristic of TLRs is that all are membrane-bound proteins, and can be mainly divided in two categories

based on cellular localization, either on the plasma membrane (TLR1, TLR2, TLR4, TLR5, TLR6) or present in endosomal compartments (TLR3, TLR7, TLR8 and TLR9) (figure 34). The main difference is that in terms of PAMPs, cell surface TLRs recognize microbial membrane-bound ligands, such lipids, proteins or lipoprotein. While endosomal TLRs recognize nucleic acids (NA) of viruses and other endocytosed pathogens, for example TLR3 recognizes as double-stranded RNA (dsRNA), single-stranded RNA (ssRNA) by TLR7 and TLR8, and double-stranded DNA (dsDNA) by TLR9 (226, 227).

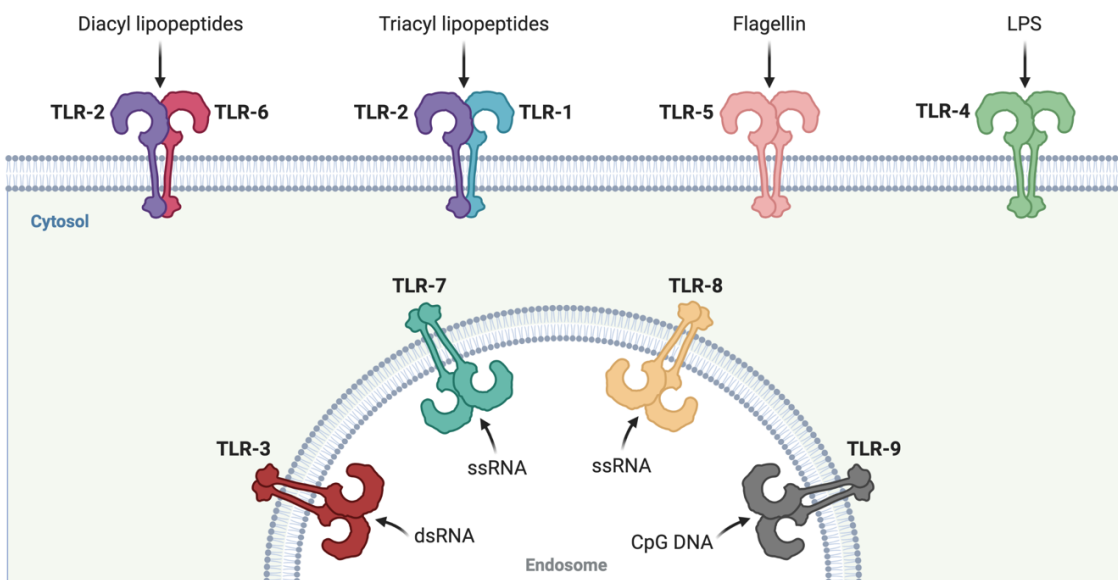



Figure 34. Detection of pathogen-associated molecular patterns PAMPs by Toll-Like Receptors (TLRs) distributed both on the plasma membrane and in endosomal compartments.

 TLRs are present in multiple immune cells such as monocytes, macrophages, dendritic cells (DCs) and B cells, but these receptors are also present in non-immune cells including fibroblasts (TLR3 and TLR4) and intestinal epithelial cells (TLR5) (225). In innate immune cells, when there is an activation, they respond by secreting

proinflammatory cytokines (228). In addition to the cytokine release, TLR stimulation triggers maturation of dendritic cells (DCs) which eventually results in antigen presentation, therefore, TLR signaling links the innate and the adaptive immunity (226). The activation profile of the adaptive immune response will depend on the type of PAMP and it can also be conditioned by components in the local environment as well (229, 230). More importantly, endosomal TLRs have evolved primarily to detect viral infections and therefore are specialized in inducing Th1 and cytotoxic T lymphocyte (CTL) responses, which are crucial for the eradication of virus-infected cells. These responses have the potential to be exploited for the clearance of tumor cells (230).

1.5. Endosomal TLR signaling

With regard to signaling, binding of the ligands to the endosomal leucine-rich-repeats domain of TLRs triggers a conformational switch in the cytoplasmic Toll-like/IL-1 receptor (TIR) domain, which then initiates the recruitment of adaptor molecules. TLR7, TLR8 and TLR9 use the adaptor MyD88 to start the signaling cascade ending in the activation of NF- κ B, IRF-1, and AP-1 transcription factors, which successively induce sequence transcription of cytokines with proinflammatory profile such as IL-12, TNF- α and IL-6 in the myeloid dendritic cells (mDCs) and macrophages. IRF-5 induces production of INF- α . Moreover, in plasmacytoid dendritic cells (pDCs), MyD88 induces IRF7 as well translating into higher levels of secreted type I interferons. On the other hand, the TLRs 7, 8 and 9, TLR3 recruits the adaptor TRIF and downstream signaling ultimately resulting in the activation of IRF3 and IFN- β production in mDCs and macrophages. TLR3 signaling can also include NF- κ B activation and production of proinflammatory cytokines (231, 232).

1.6. The IC-tagging technology for vaccine production

This technology has been tested for the development of vaccine candidates. The MS acted very effectively as a subunit vaccine in mouse animal models for two different viruses. One of them is the bluetongue virus (BTV), which belongs to the Orbivirus genus and infects both wild and domestic ruminants. This is a re-emerging

virus that cause serious economic losses in cattle. The experiments were carried out in collaboration with the group of Dr. Javier Ortego (CISA-CSIC, Valdeolmos, Madrid), who have developed a mouse model based on transgenic mice lacking the interferon alpha receptor (IFNAR(-/-)) for testing BTV vaccines. Current BTV vaccines consist in inactivated viruses that require the use of adjuvants, causing undesirable effects in animals, so their use can be problematic (233). In addition, these vaccines are serotype-specific and there are 29 knowns different BTV serotypes, determined by the reactivity of protein VP2. As a result, it would be necessary to use 29 different vaccines to reach complete protection. Based on previous studies by Dr. Ortego's group, the MS were loaded with two structural proteins, VP2 and VP7, and a non-structural protein, NS1. The purified MS were used to immunize IFNAR(-/-) mice, while two control groups, one injected with empty MS and another with the soluble epitopes, were also included in the study. No group received any adjuvant, and a second vaccine dose was administered 15 days after the first. All groups were allowed to develop immunity for 15 additional days, and then all mice were challenged with a lethal dose of the homologous BTV-4 (the same serotype included in the vaccine preparation). The group immunized with the MS containing the viral epitopes had a 100% survival, while both the group with the soluble epitopes and the group with the empty MS presented a 100% lethality 4-5 days post-infection. What is more, in the viremia analysis it could be seen how the surviving group maintained an undetectable viral titer throughout the process, while the animals from both controls presented high viral titers (Figure 35), (234).

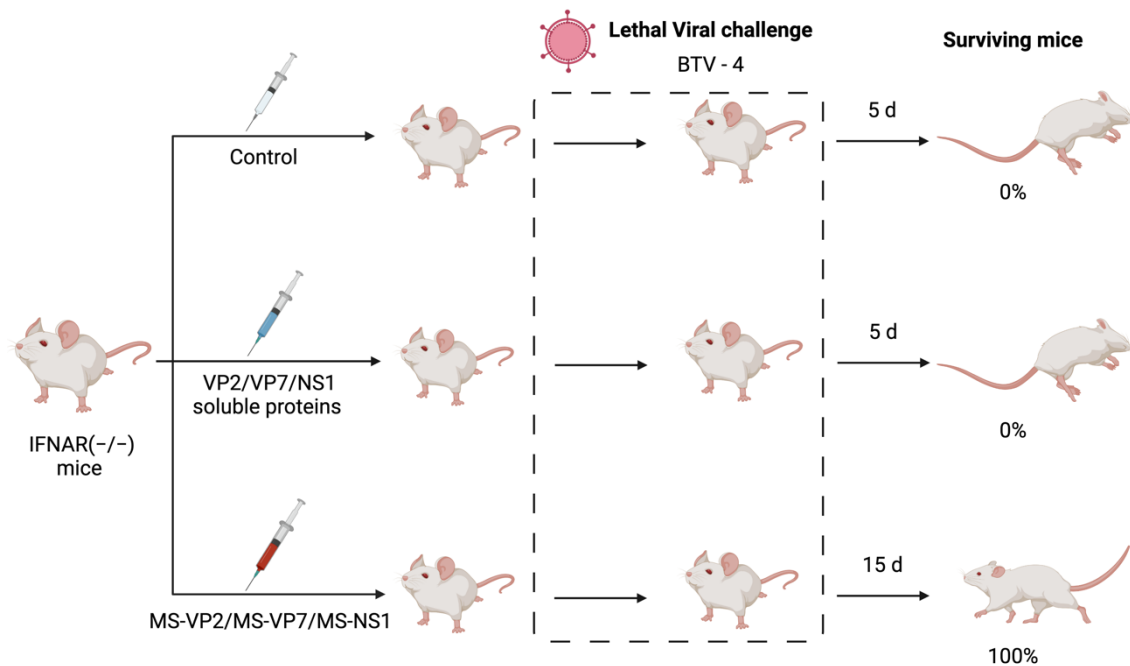


Figure 35. MS-based BTV vaccine. Protection of MS-VP2/MS-VP7/MS-NS1 vaccinated IFNAR(-/-) mice against a lethal challenge BTV-4 challenge. Mice were immunized twice by homologous prime boost vaccination with recombinant VP2/VP7/NS1 soluble proteins or MS-VP2/MS-VP7/MS-NS1. Two weeks after immunization all mice were subcutaneously inoculated with a lethal dose of BTV-4 and only MS-vaccinated survived (see text for details). (Source: adapted from Marín-López, Alejandro, et al. "VP2, VP7, and NS1 proteins of bluetongue virus targeted in avian reovirus muNS-Mi microspheres elicit a protective immune response in IFNAR (-/-) mice." *Antiviral research* 110 (2014): 42-51).

Interestingly, in the same study the MS loaded with the epitopes were able to confer partial (60%) cross-protection against a heterologous challenge using BTV serotype 1. This may be due to the presence of the non-protein structural NS1 that is fully conserved between serotypes (234). In a later study, a combination of MS with the viral vector, Modified Vaccinia Ankara (MVA) that expresses the same antigens loaded in the MS, resulted in 100% protection against homologous and heterologous challenges (25) (Figure 36). Again, blood tests showed that the animals vaccinated with the combination of both strategies maintained an undetectable blood viremia, which was not the case in the control groups.

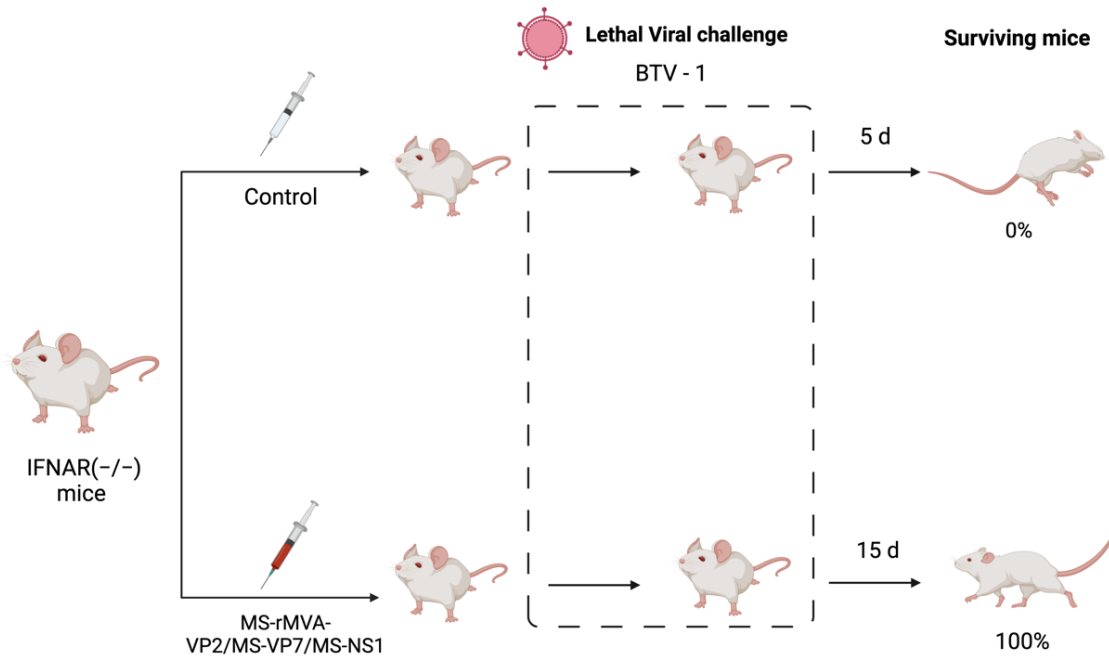


Figure 36. MS-MVA BTV vaccines. Protection of MS-rMVA-VP2/VP7/NS1 vaccinated IFNAR (-/-) mice against a lethal challenge with BTV-1. Mice were immunized with MS-VP2/VP7/NS1 and rMVA-VP2/VP7/NS1 boost administered 2/3 weeks apart. Non-immunized group was immunized with empty MS and boosted with rMVA as a control. Two weeks after the second immunization all mice were subcutaneously inoculated with lethal doses of BTV-1 and BTV-4. (See text for details). (Source: adapted from Marín-López, Alejandro, et al. "Microspheres-prime/rMVA-boost vaccination enhances humoral and cellular immune response in IFNAR (-/-) mice conferring protection against serotypes 1 and 4 of bluetongue virus." (2017)).

A similar result was obtained for a study against a different virus, the African Horse Sickness Virus (AHSV). This is also a member of the Orbivirus family and is endemic in areas such as sub-Saharan Africa, but has gained widespread in areas of Morocco, the Middle East, India and Pakistan. Some of the recent outbreaks place it in the Iberian Peninsula and Thailand, in addition there have been reports of its presence in the Americas, East Asia and Australia (235). It is transmitted through a high number of vectors, where the most important is *Culicoides imicola*, and its main hosts are equidae, with domestic horses from non-endemic countries being more susceptible to population where mortality reaches 90% (236). Similarly to BTV, the control of the disease is based on the use of attenuated virus vaccines, which involves

problems in relation to their degree of inactivation or residual virulence (237), in addition there are 9 known serotypes so that to vaccinate against all of them 9 different vaccines would be necessary. For this study, and again in collaboration with Dr. Ortego's group, only the nonstructural protein NS1 was included in the vaccine preparations (238). In this case, while the MS or MVA vaccines induced 80% of protection when used alone, they reached again 100% efficacy against the homologous and heterologous challenges (Figure 37).

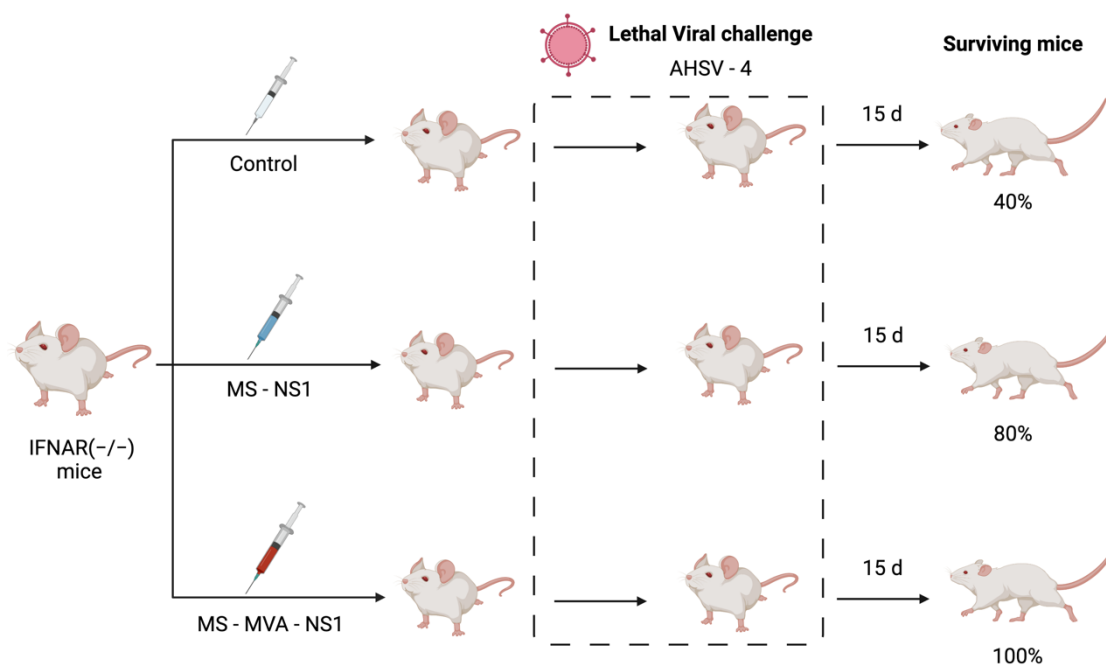


Figure 37. MS-MVA AHSV vaccine. NS1 heterologous prime boost vaccination provides immune protection against AHSV-4 challenge. IFNAR (-/-) mice were vaccinated three weeks apart by homologous (MS-NS1) or heterologous prime boost (MS-MVA-NS1) regimen. Control mice were not immunized. Two weeks post-boost animals were infected with AHSV-4. Survival rates after the challenge.

2. POSSIBLE APPLICATION OF THE IC-TAGGING SYSTEM IN THE FIELD OF CANCER IMMUNOTHERAPY

2.1. Rationale

The current landscape of clinical studies testing different TLR agonists for cancer immunotherapy elucidates the need for appropriate delivery and presentation methods to the tumor tissue. Intra-tumor immunotherapy is acquiring clinical momentum, since as presented, such approaches display promising results in triggering local tumor specific immunity, while avoiding potential off-target effects to healthy tissue, thus diminishing adverse effects (239-241).

Here, we aim to test if our innovative form of tunable multivalent antigen presentation methodology works also as a cancer vaccine when the MS or NS are loaded with cancer neoantigens, either individually or simultaneously in multivalent particles. For that we will use the B16-OVA pseudo-metastasis model which is an OVA-expressing melanoma cell line in a collaboration with Sandra Diebold at the NIBSC. In addition, we decided to include another antigen that is naturally expressed by B16 melanoma cells and can mediate anti-tumor immunity. This is tyrosinase-related protein 2 (TRP2) (214, 242). This antigen was described as a new tumor antigen recognized by CTL clones derived from tumor reactive TIL line. TRP-2 belong to the family of tyrosinase-related genes. Further experiments have led to the identification of the epitope peptide from the TRP-2 coding sequence that is recognized by T cell clones, indicating that T cells recognized a non-mutated self-peptide. In addition, similarly to other melanoma differentiation antigens, TRP-2 is only expressed in melanoma, melanocytes, and retina, but it is not present in other human tissues tested (214).

Bacteria transformed with dual-expression plasmids will produce NS containing the IC-tagged proteins upon induction of expression, suitable for vaccination (figure 38). By performing a thorough characterization of the innate immune and adaptive activation patterns regarding TLRs activation, we will be in position to design novel cancer vaccines based on our NS and/or MS.

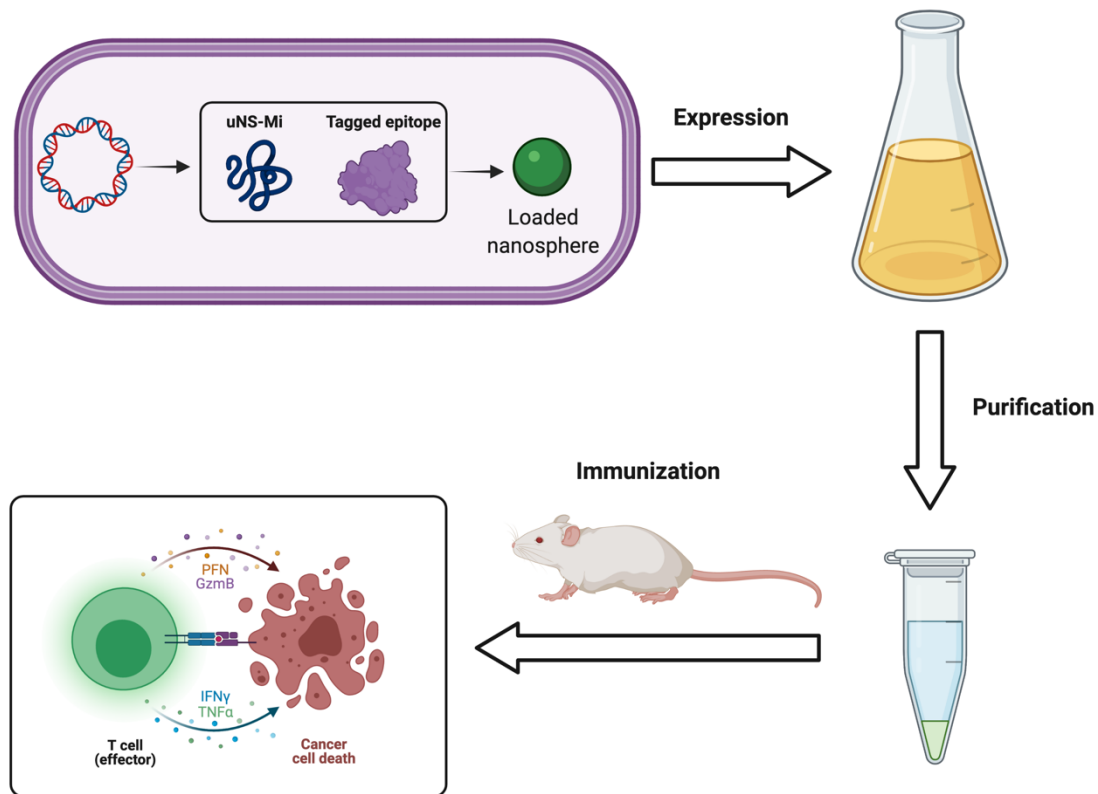


Figure 38. Workflow for the production of the tumor antigen-loaded nanospheres. First the antigen is immobilized via co-expression with the nanosphere-forming protein in bacteria. Subsequently, upon purification, the MS are ready to be further tested and characterized.

2.2. Construction of IC-tagged OVA and TRP2 for bacterial expression

For the production of vaccines against our tumor model, we focused on the production of NS containing OVA and TRP2 as neoantigen models. Thus, first we decided to tag both the OVA and the TRP2 proteins with IC on their C-terminus and introduce them individually in the second polylinker of plasmid muNS-Mi-petDuet1 to generate the constructs muNS-Mi-OVA-IC-petDuet1 and muNS-Mi-TRP2-IC-petDuet1.

Both constructs were used to transform BL21 bacteria, where expression was induced by IPTG. Induction of co-expression of muNS-Mi and OVA produced two

prominent Coomassie-stained bands with apparent molecular weights corresponding to both proteins (Figure 39A, compare lanes 1 and 2). SDS-PAGE analysis of the purified NS showed again the presence of both proteins in a correct amount and proportion (Figure 39A, lane 3), while DLS analysis showed a monodispersity around 400nm (not shown). On the other hand, initial attempts to express TRP were unsuccessful either in BL21 or in the Rossetta strain of *E. coli*. Removing the signal peptide present in the TRP2 sequence, the antigen could be expressed in BL21, as a band with an apparent molecular weight corresponding to the IC-tagged TRP2 (67.2 kDa) was apparent in extracts from IPTG-induced bacteria, together with the band corresponding to muNS-Mi (Figure 39B, compare lanes 1 and 2). These same bands showed up in the SDS-PAGE analysis of the purified NS from these extracts (Figure 39B, lane 3), although the proportion of TRP2 present in the NS is very low.

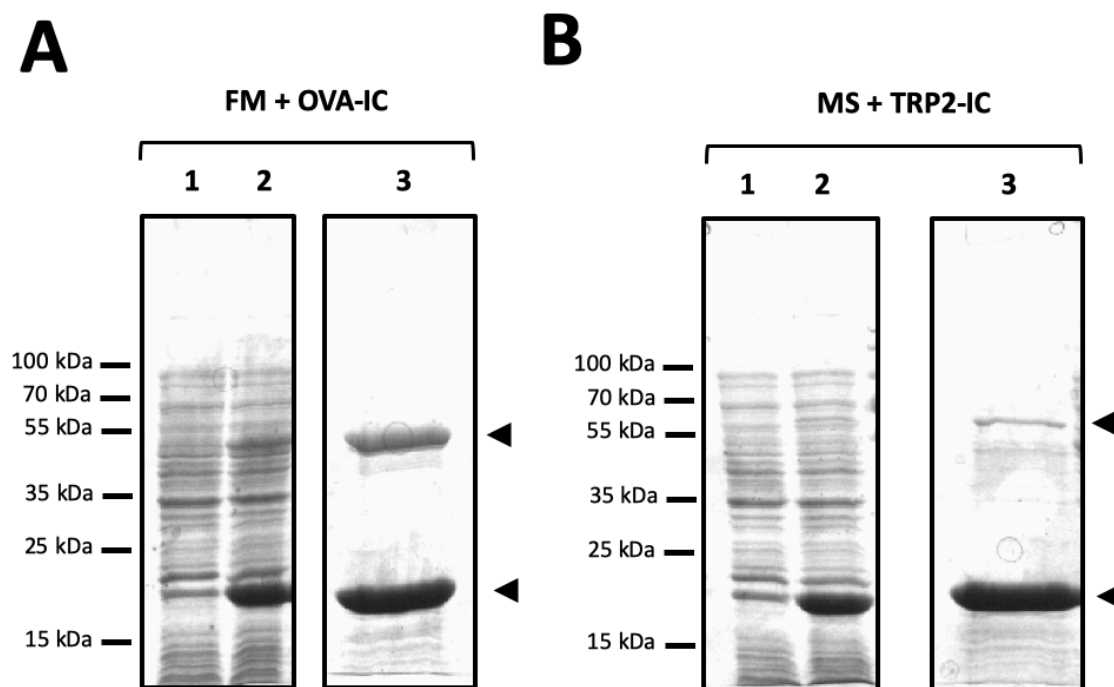


Figure 39. Expression and purification of NS-OVA and NS-TRP2. Coomassie-blue stained, SDS-PAGE analysis of extracts and final purification. **(A)** total extract from OVA-IC NS (1), lysate OVA-IC NS (2) and final purification OVA-IC NS (3). **(B)** Total extract from TRP2-IC NS (1), lysate TRP2-IC NS (2) and final purification TRP2-IC NS (3). Expression was carried out in *E. coli* BL21 transformed with dual expression plasmids for muNS-Mi-OVA-pDuet1 and muNS-Mi-TRP2-pDuet1.

2.3. Endotoxin levels in the preparations

At various time points of the process, the nanosphere preparations were analyzed using the Limulus Amebocyte Lysate (LAL) (Figure 40) test to determine the endotoxin levels (Table 8). The purpose of this process was to determine the content of LPS in our formulations, since they can influence the results as LPS is a potent adjuvant.

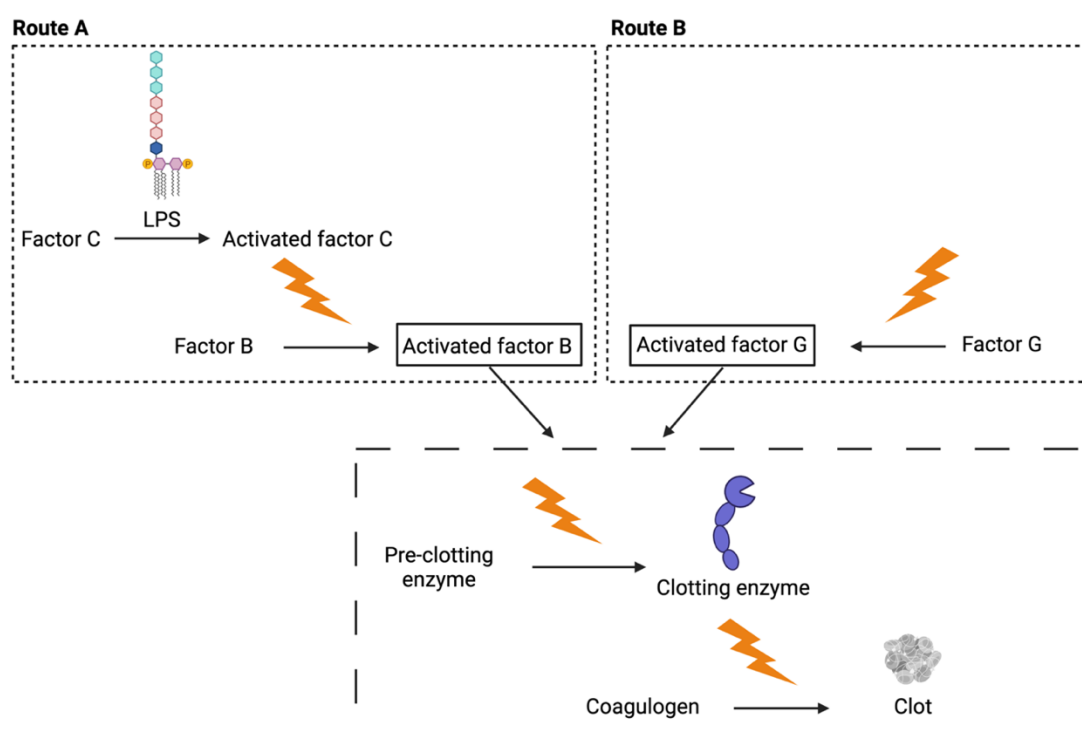


Figure 40. Basics of the LAL clotting test. A lysate reagent prepared from the amebocytes of horseshoe crab (*Limulus polyphemus*) is employed to detect bacterial endotoxins. As shown in the Figure, the cascade reactions begins by the presence of an endotoxin, thus Factor C, a serine protease precursor, is first activated. There follows the subsequential activation of Factor B, also a serine protease precursor and a proclotting enzyme, which hydrolyzes coagulogen into coagulin, forming an insoluble gel (clot).

When the values were high, further cleaning of the NS were performed with several washing steps using RB+ solution with Triton-X100 and the endotoxin level was evaluated again. Those formulations with high endotoxin levels were excluded from the study.

Preparation	Formulation	Endotoxin level	Used	Conc. Prep
OVA	FM +OVA 1	24000 IU/ml	not used	0.9 µg/µl
OVA	FM +OVA 2	30000 IU/ml	not used	1 µg/µl
OVA	FM +OVA 2 repurified	600 IU/ml	in vitro & in vivo	0.5 µg/µl
OVA	FM +OVA 4	600 IU/ml	in vitro & in vivo	0.36 µg/µl
Halo	Halo muNS	1200 IU/ml	in vitro & in vivo	1.82 µg/µl
Luc	Luc muNS	not tested	in vitro & in vivo	1.18 µg/µl
TRP2	FM + TRP2 1 repurified	1200 IU/ml	not used	0.36 µg/µl
TRP2	FM + TRP2 2	2400 IU/ml	not used	
TRP2	FM + TRP2 3	60000 IU/ml	not used	1 mg/ml

Table 8. Endotoxin levels in the different nanosphere solutions as determined in the LAL.



2.4. Comparison of the PBMC activation by NS by the in vitro Monocyte Activation Test (MAT).

To determine the ability to induce cytokine release, two groups of in vitro experiments were performed comparing the response of the NS with different commercial adjuvants.

In the first place, we decided to use the monocyte activation test (MAT) using peripheral blood mononuclear cells (PBMCs). These are any peripheral blood cell having a round nucleus: lymphocytes (T cells, B cells, NK cells) and monocytes (Figure 41), whereas erythrocytes and platelets are not, since those have no nuclei, and granulocytes (neutrophils, basophils, and eosinophils) have multi-lobed nuclei. In humans, lymphocytes make up the majority of the PBMC population, followed by monocytes, and only a small percentage of dendritic cells.

The in vitro monocyte activation test (MAT) is a replacement for the in vivo rabbit pyrogen test. It is used to quantify pro-inflammatory/pyrogenic contaminants of medicines and vaccines. The test is in accordance, where appropriate, with the current European Pharmacopoeia (EP) Method C (EP chapter 2.6.30). The PBMCs provided by the NIBSC were used after isolation, cryopreservation and determination of fitness for purpose of PBMCs from apheresis cones provided by the Oxford Blood Transfusion Centre.

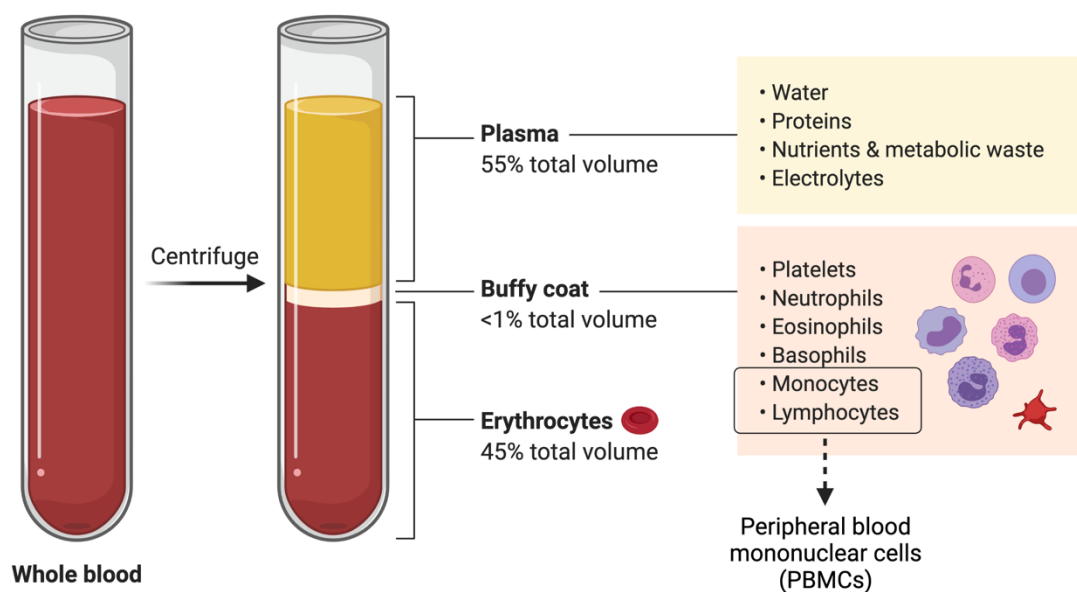


Figure 41. Representation of the cell populations used for the in vitro activation of PBMCs.

As controls, the endotoxin standard (0.1 IU/ml), untreated cells and a medium only were included on all tests. All samples were tested in quadruplicates at three different dilutions (Table 9).

The following TLR agonists were included as further reference points: Pam3CSK4 (TLR2), polyI:C (TLR3), LPS (TLR4), flagellin (TLR5), R848 (TLR7) and CpG ODN (TLR9). In addition, the following adjuvants were included for comparison: MPLA4, QuilA, AddaVax, Alhydrogel and IFA. All adjuvants were purchased from Invivogen.

Stimulus	Test 1	Test 2
LPS	100, 30, 10ng/ml	100, 30, 10ng/ml*
Flagellin	1000, 300, 100ng/ml	1000, 300, 100ng/ml
Pam3CSK4	100, 10, 1ng/ml	100, 10, 1ng/ml
R848	10, 3, 1µg/ml	10, 3, 1µg/ml
MPLA	300, 100, 30ng/ml	300, 100, 30ng/ml*
IFA	1:20, 1:60, 1:200	1:20, 1:60, 1:200
Alhydrogel	10, 3, 1µg/ml	10, 3, 1µg/ml
AddaVax	1:20, 1:60, 1:200	1:20, 1:60, 1:200
QuilA	10, 3, 1µg/ml	10, 3, 1µg/ml
polyI:C	100, 30, 10µg/ml	100, 30, 10µg/ml
CpG ODN	10, 3, 1µg/ml	10, 3, 1µg/ml
OVA NS**	20, 6.65, 2µg/ml	20, 6.65, 2µg/ml*
luc NS**	40, 13.3, 4µg/ml	40, 13.3, 4µg/ml*
Halo NS**	40, 13.3, 4µg/ml	40, 13.3, 4µg/ml*

Table 9. Overview of the concentrations or dilutions of the different stimuli tested in the different MAT assays.

(*) Samples were measured +/-polymyxin (50µg/ml) in MAT TEST 2.

(**) Lower concentrations required

The concentrations of stimuli used in the 1st and 2nd MAT (Test 1 and Test 2) were identical. Supernatants were harvested and frozen at -20°C after overnight culture. The IL-6 concentration in the supernatant was determined by sandwich ELISA.

The overall pattern of cytokine release for the different stimuli was similar for all four donors, however, the absolute levels of cytokine release varied widely between donors (Figure 42). When the results from all four donors are compared in one graph,

it becomes even more apparent that the overall cytokine induction pattern is similar for all donors, but the actual levels of cytokines that are produced can vary between them (Figure 43).

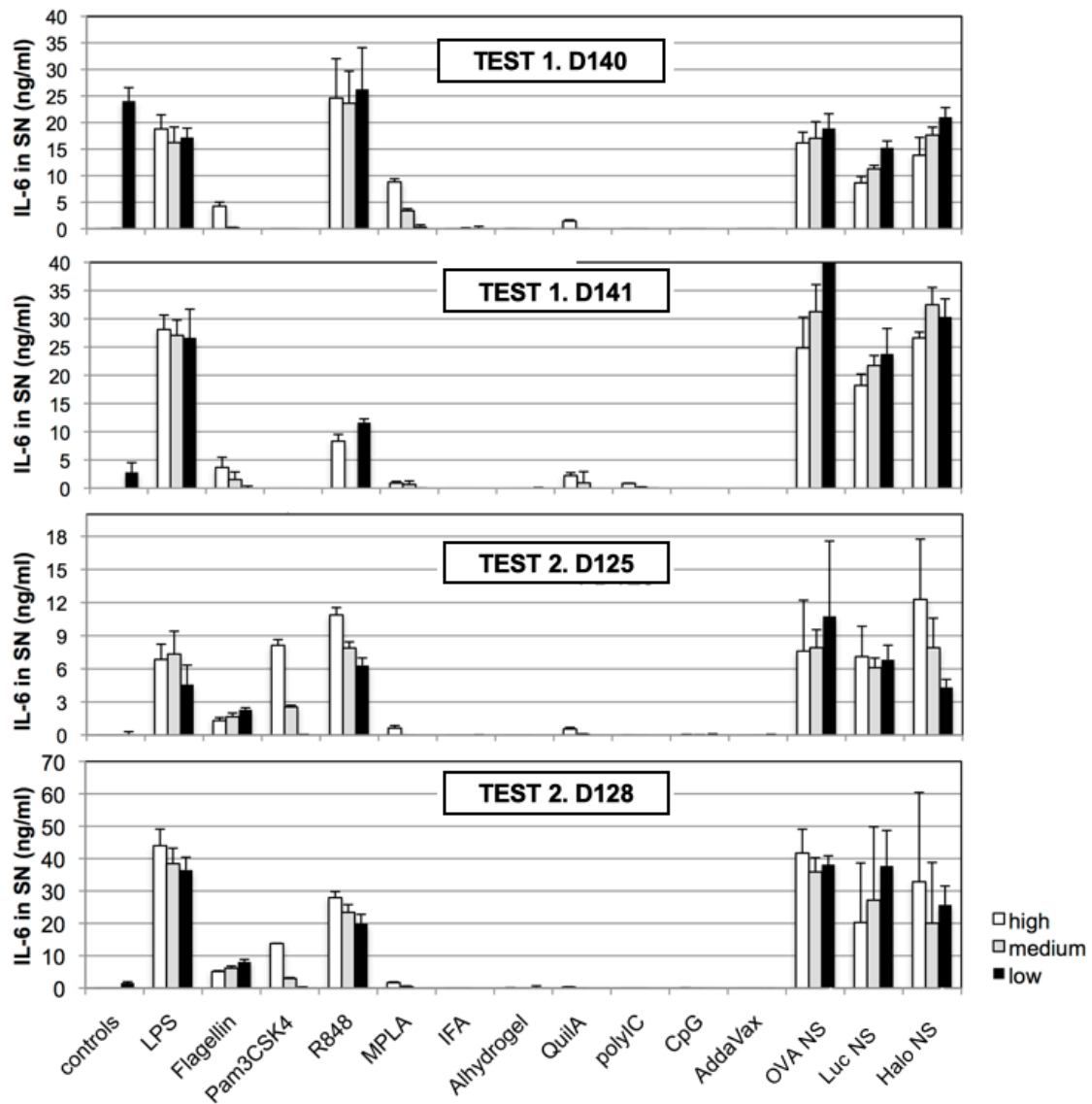


Figure 42. IL-6 values for individual donors for MAT Test 1 & MAT Test 2 using 4 different donors (D140, D141, D125 and D128). The values were corrected for MAT Test 1 (outliers were removed). Supernatants were measured at different dilutions and all data points were in range. (Note: For the lowest dilution of OVA nanospheres for donor D141, two of the values were high and two low resulting in a high standard deviation. The value in the graph is cut-off to align the graph with the other values. The actual value was 59.3 +/-37.7ng/ml IL-6.)

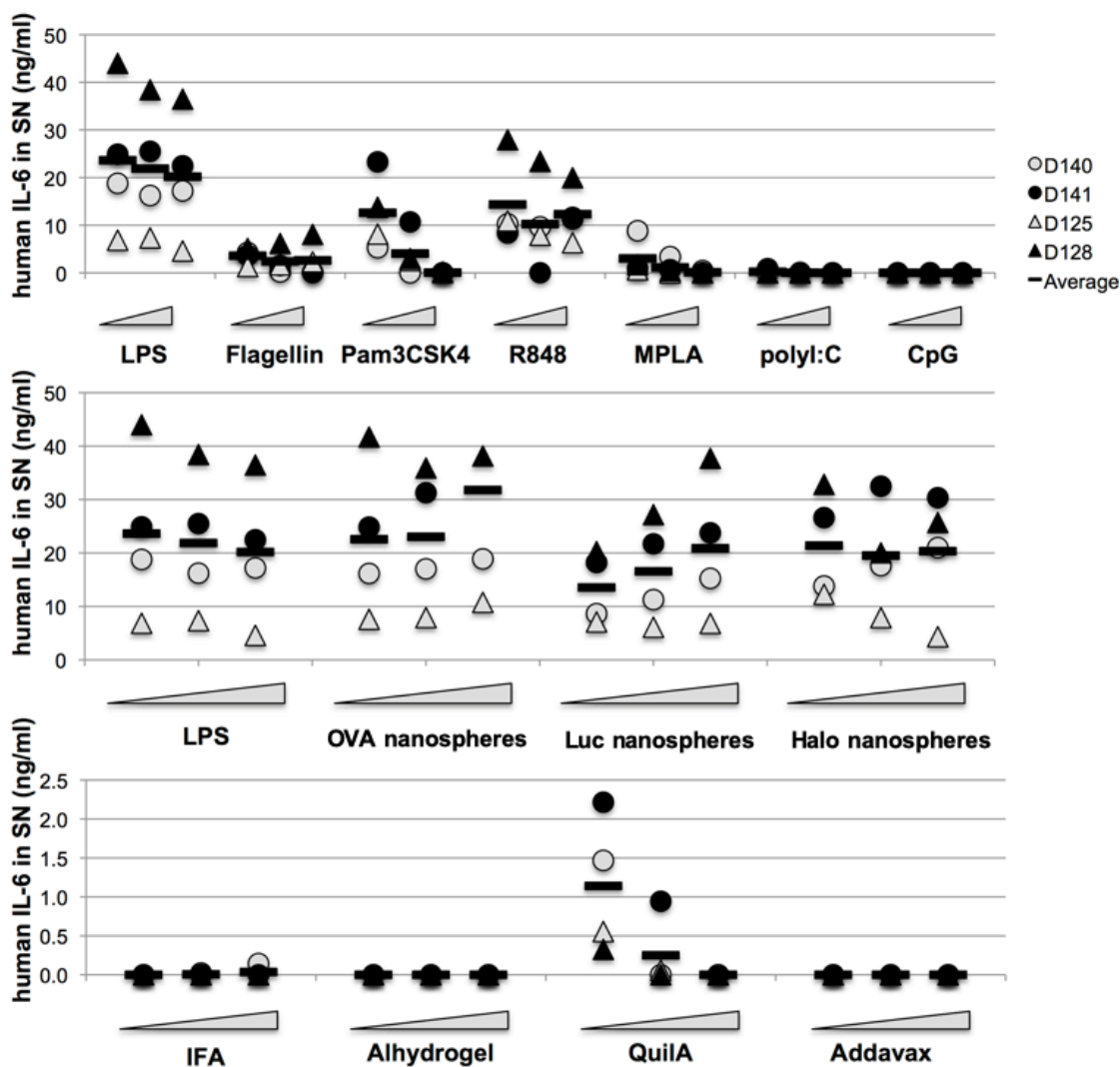


Figure 43. Direct comparison of IL-6 values for individual donors for MAT Test 1 & MAT Test 2. Values are shown for TLR agonists (top panel), nanospheres (NS) versus LPS (middle panel) and adjuvants (bottom panel).

In order to determine whether the cytokine release observed in response to the NS preparations was entirely or in part attributable to the presence of endotoxin, polymyxin b (Figure 44) was added to the nanospheres, LPS and MLPA at a concentration of 50µg/ml, and consequently added to the cells for stimulation in the second MAT assay (Test 2). At this concentration, IL-6 cytokine release in response to LPS was entirely blocked (Figure 45). Interestingly, cytokine release in response to NS preparations was altered, but while the IL-6 levels for donor 125 were decreased

in the presence of polymyxin, for donor 128 IL-6 levels were increased in the presence of polymyxin (Figure 45).

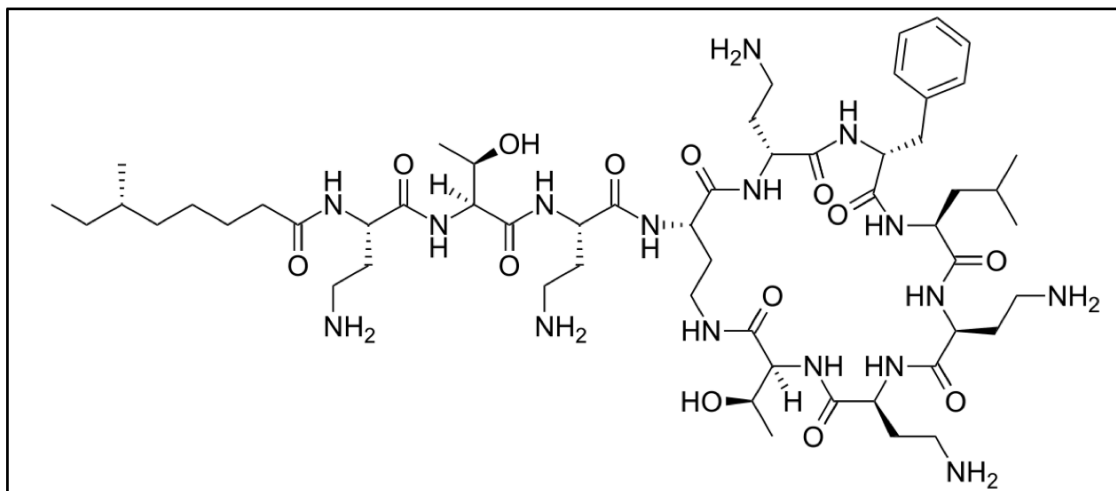


Figure 44. Structure of Polymyxin B added to the formulations.

From the polymyxin results in the MAT, we concluded at this stage that NS do trigger a pattern recognition receptor other than TLR4. However, this requires further confirmation.

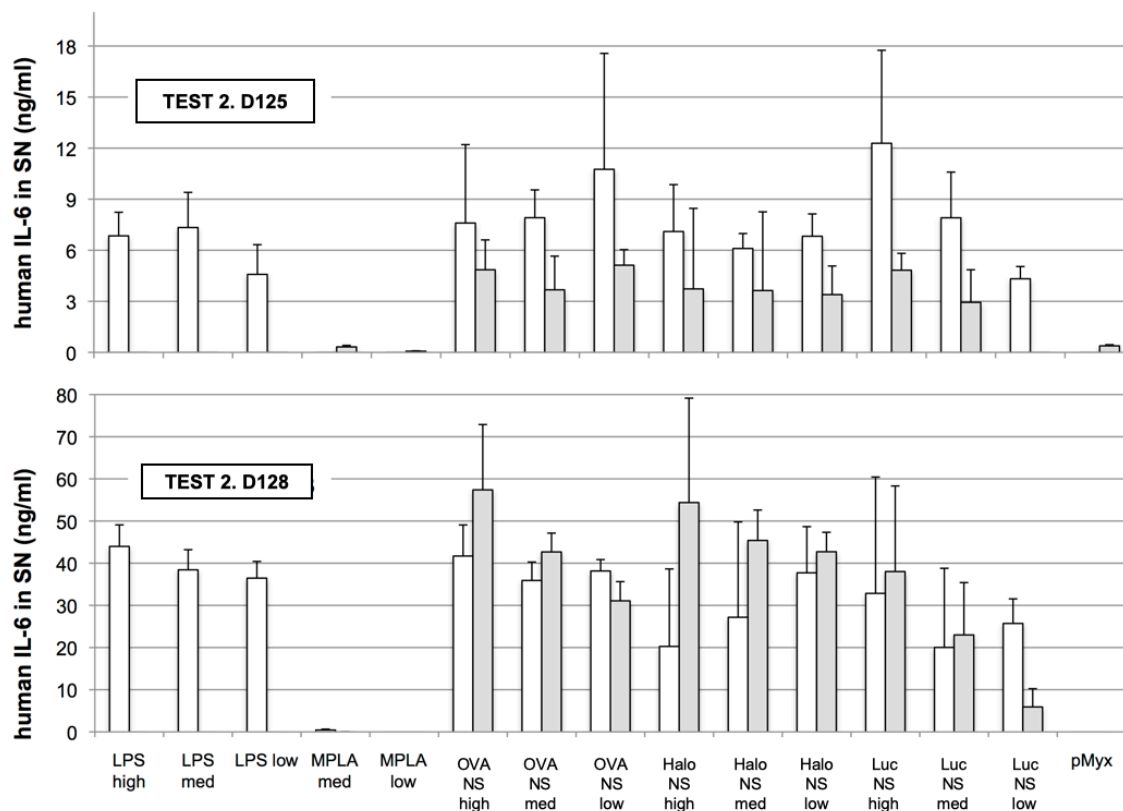


Figure 45. IL-6 values for individual donors 125 and 128 of MAT Test 2 in the presence (grey bars) and absence (white bars) of 50 µg/ml polymyxin.

In order to identify whether the pattern of IL-6 release matched the pattern of release of other cytokines, we determined the concentrations of TNF alpha and Subunit beta of interleukin 12 (IL-12 p40) in the cell supernatant by sandwich ELISA. Interestingly, the NS induced approximately 10-fold higher levels of TNF alpha than LPS or R848 (Figure 46). The reasons for stronger induction of TNF alpha over IL-6 by nanospheres will have to be confirmed using alternative strategies. However, if the high induction levels of TNF alpha by NS compared to LPS and R848 are confirmed, this could be an indication that NS induce cytokine release via a non-TLR pattern recognition receptor either exclusively or in combination with a TLR.

For IL-12 p40 induction, supernatants were measured diluted 1:2, except for supernatants from samples treated with LPS or NS, which were diluted 1:25 and supernatants from Pam3CSK4 treated samples, which were not included in the assay. The ELISA results were largely negative, except for the R848-treated samples (Figure

47). This indicates that the 1:25 dilution for LPS- and NS-treated samples may have been too high to allow for detection of the rather low levels of IL-12 p40 that were induced. The IL-12 p40 ELISA will have to be repeated for the LPS and the NS samples at a dilution of 1:2.

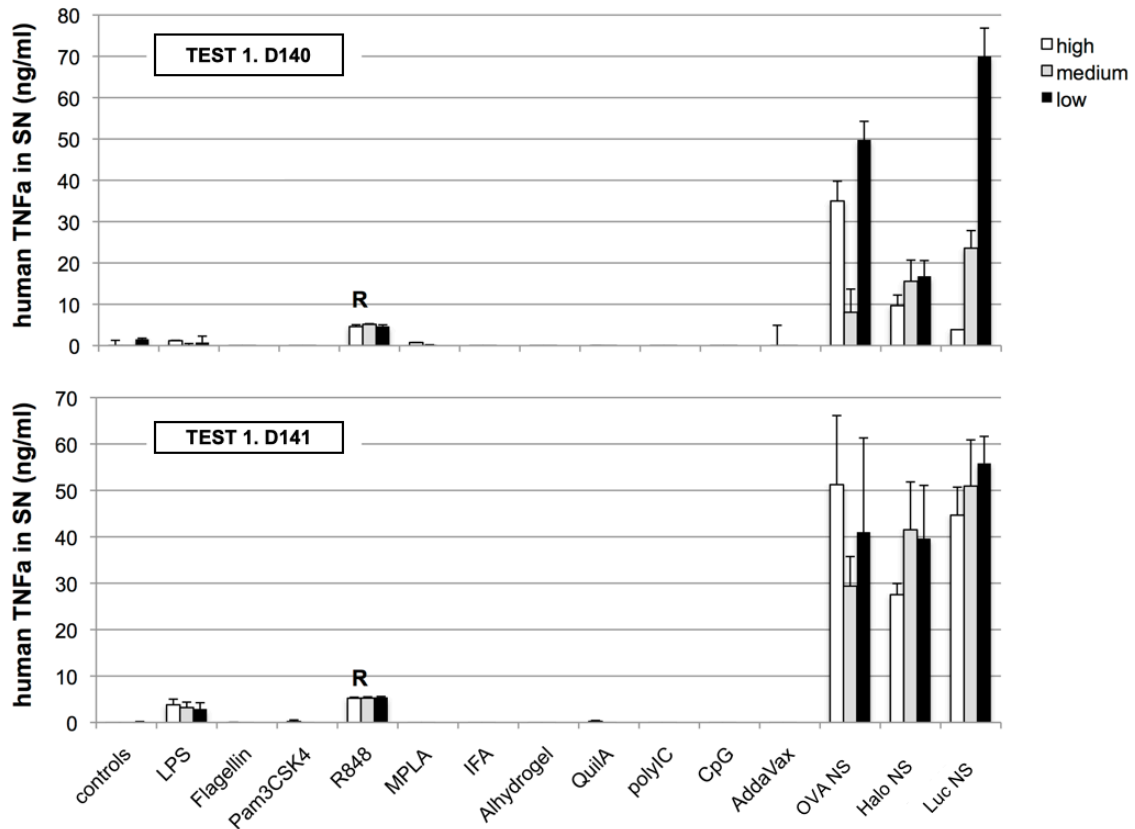


Figure 46. TNF alpha values for individual donors for MAT Test 1. The values were corrected (outliers were removed). Supernatants were measured at different dilutions and except for R848 all data points were in range.

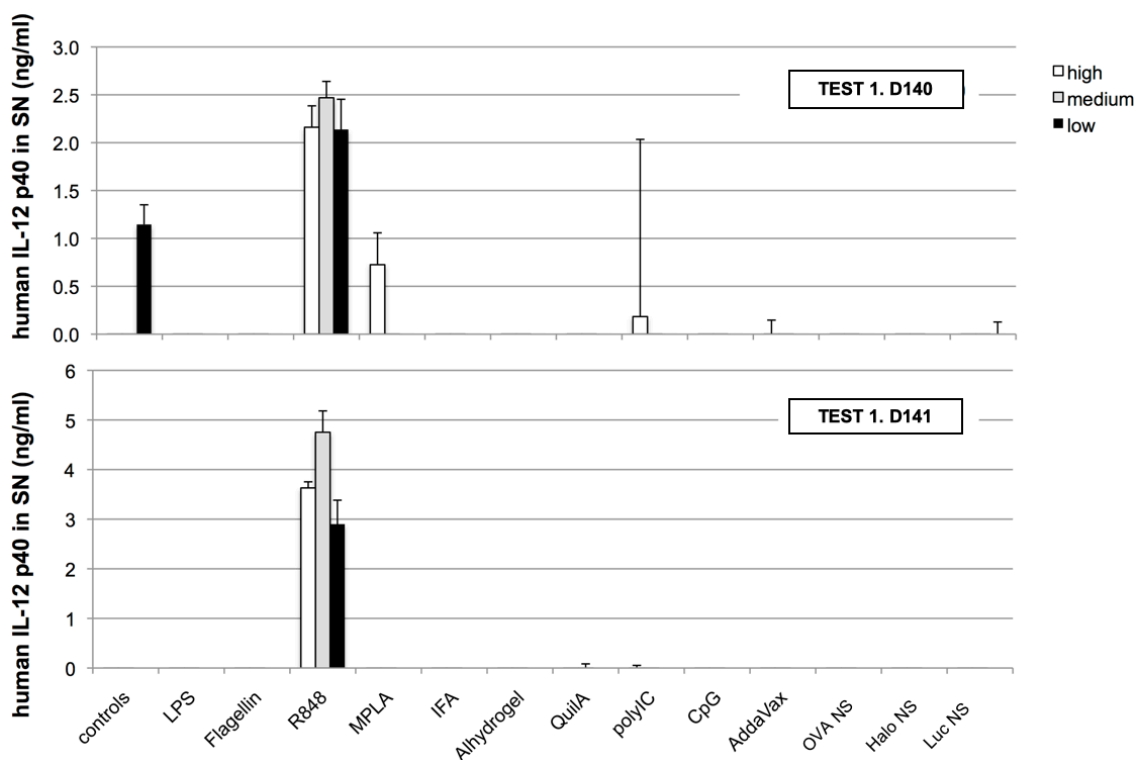


Figure 47. IL-12 p40 values for individual donors for MAT Test 1. Supernatants were measured at a dilution of 1:2 except for LPS and NS samples, which were measured at a dilution of 1:25. The latter samples will have to be measured again at a lower dilution.

The IL-6 sandwich ELISA as performed in the SD lab and the Pyrogen lab differs regarding the antibodies used, the general SOP and the substrate used for assay development. Both protocols were compared side-by-side for samples from MAT 20-01 in order to ensure that the results obtained agree in terms of the overall cytokine release pattern and to confirm that the absolute values obtained do not differ widely. The overall values agreed rather well with the highest IL-6 values in the SD lab IL-6 ELISA reaching 25 and 30ng/ml for each of the donors, respectively while the Pyrogen lab IL-6 ELISA reached values of 20ng/ml for both donors (Figure 48 and Figure 49).



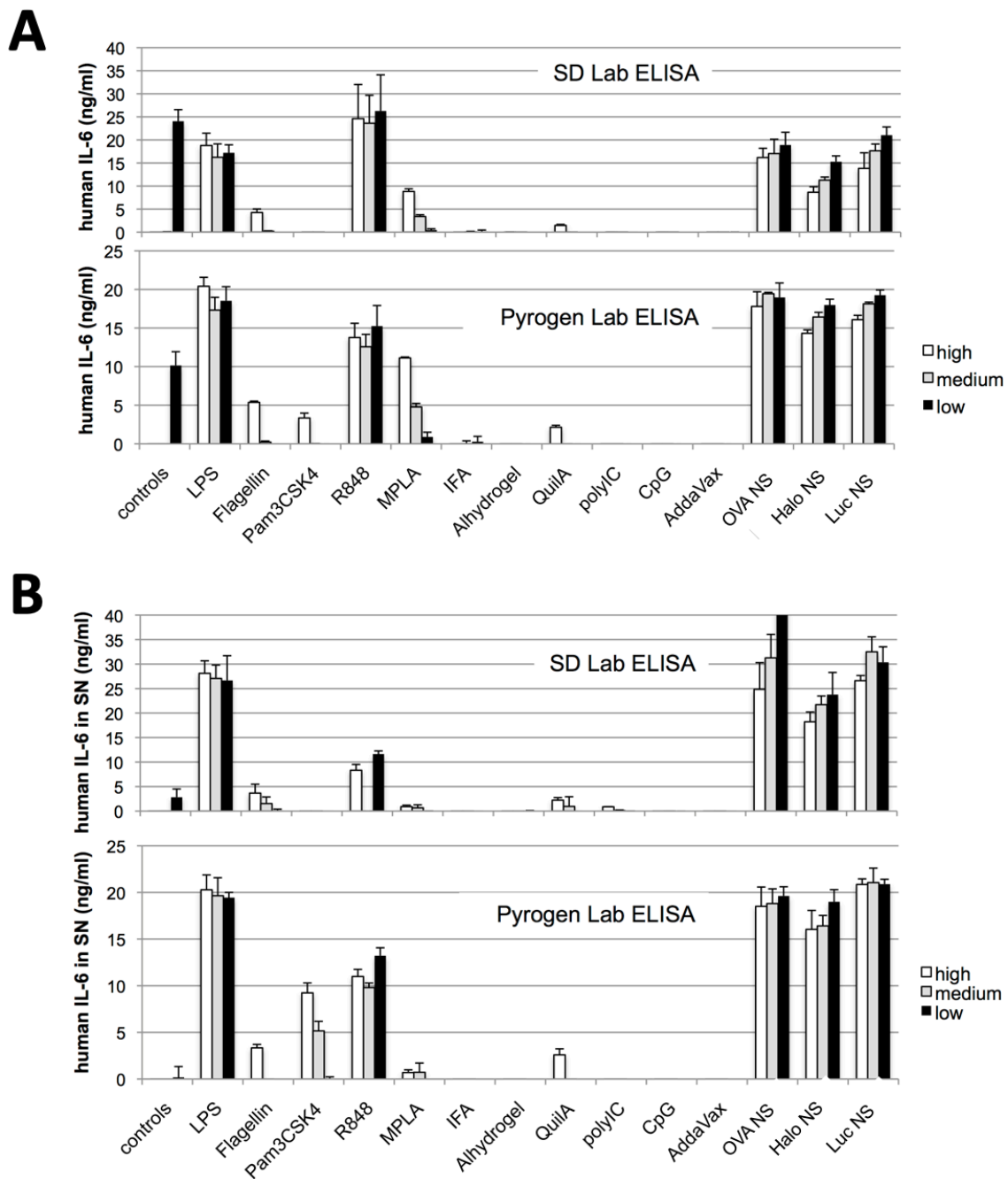


Figure 48. IL-6 values for individual donors for MAT Test 1 as measured by the SD lab versus the Pyrogen lab IL-6 ELISA. Comparison of donor 140 is shown in panel A whereas the comparison of values for donor 141 is shown in panel B.



In a separate ELISA, the standard curves used in the two different IL-6 sandwich ELISA protocols were compared directly using the SD lab protocol. This comparison was designed to ensure that the standard curves used do not differ widely

in the absolute IL-6 values that they produce. Overall, the international IL-6 standard gave higher values and the two standard curves were not parallel. However, for the performed assay, the highest value (5ng/ml) could not be included in the linear regression for the international IL-6 standard, since the fit was suboptimal. It would be good to confirm this result in a separate IL-6 ELISA assay and to include the 1:4 dilution in addition to the 1:3 dilution.

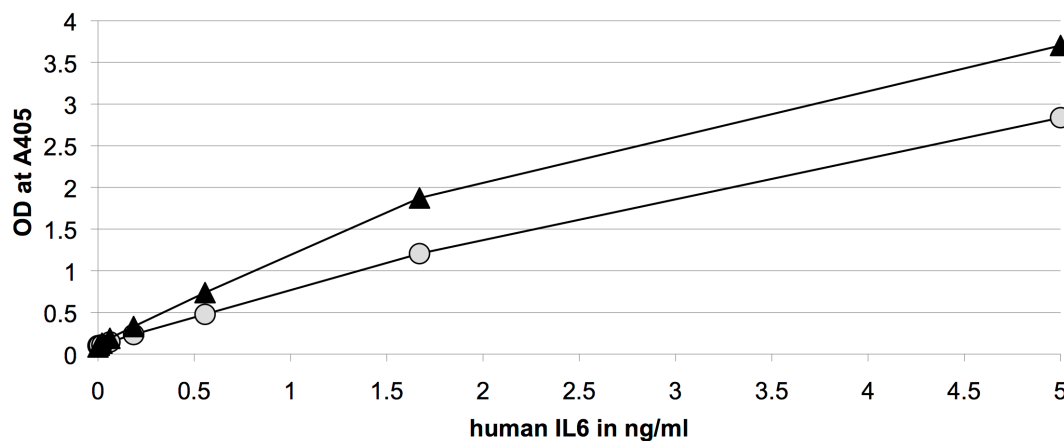


Figure 49. Direct comparison of the IL-6 standards in the SD lab sandwich ELISA. For the assay both standards were used at the same dilutions as used in the SD lab protocol (1:3 serial dilution starting from 5ng/ml). However, the Pyrogen lab ELISA SOP usually uses the international IL-6 standard (black triangles) at 4, 1, 0.25 and 0.0625ng/ml IL-6 (1:4 serial dilution) instead of the 1:3 dilutions used here. The SD lab ELISA uses IL-6 purchased from BD Biosciences (#550071) at concentrations of 5, 1.667, 0.555, 0.185, 0.0617, 0.0206 and 0.0069ng/ml (grey circles).

Last but not least, the IL-6 induction for the control stimulus (endotoxin standard) was plotted to estimate differences in the endotoxin response between donors. As expected, the absolute levels of IL-6 induced in response to endotoxin (0.1 IU/ml) varied widely between donors from 0.06 - 24.04 ng/ml IL-6 in the cell supernatant (Figure 50). It could be possible that the dose of endotoxin used as a reference point should be increased at least to 1 IU/ml.

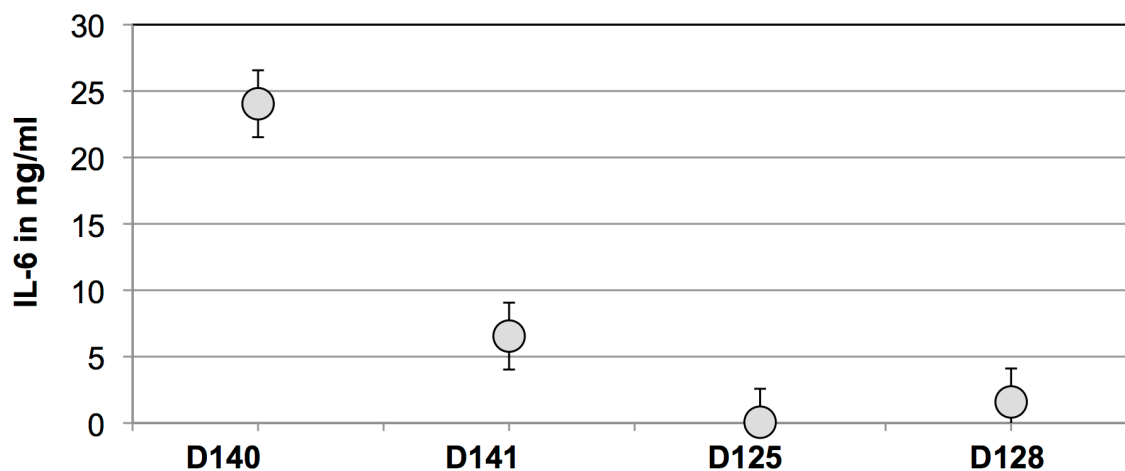


Figure 50. IL-6 induction in response to endotoxin control (0.1 IU/ml) by individual donors.

2.5. Comparison of the in vitro DCs activation test by the NS formulation and by different commercial adjuvants.

The same stimuli and dilutions as used in the MAT were used in DC activation assay with Granulocyte-macrophage colony-stimulating factor (GM-CSF) and FMS-like tyrosine kinase 3 ligand (Flt3L) BMDC cultures. As for the MAT, the cell supernatants were harvested after overnight culture and the cytokine levels in the supernatants were measured by sandwich ELISA. We performed two assays with GM-CSF BMDC and two assays with Flt3L BMDC. However, for some of the stimuli the dilutions were changed for the second sets of assays (Table 10).

Stimulus	GM DC TEST 1	GM DC TEST 2	Flt3L DC TEST 1	Flt3L DC TEST 2
LPS	100, 30, 10ng/ml	100, xx*, 10ng/ml*	100, 30, 10ng/ml	100, 30, 10ng/ml*
Flagellin	1000,300,100ng/ml	1000,300,100ng/ml	1000,300,100ng/ml	1000,300,100ng/ml
Pam3CSK4	100, 10, 1ng/ml	1000, 100, 10ng/ml	100, 10, 1ng/ml	1000, 100, 10ng/ml
R848	10, 3, 1µg/ml	10, 3, 1µg/ml	10, 3, 1µg/ml	10, 3, 1µg/ml
MPLA	300, 100, 30ng/ml	3000, 300, 30ng/ml	300, 100, 30ng/ml	3000,300,30ng/ml
IFA	1:20, 1:60, 1:200	1:20, 1:60, 1:200	1:20, 1:60, 1:200	1:20, 1:60, 1:200
Alhydrogel	10, 3, 1µg/ml	100, 10, 1µg/ml	10, 3, 1µg/ml	100, 10, 1µg/ml
AddaVax	1:20, 1:60, 1:200	1:20, 1:60, 1:200	1:20, 1:60, 1:200	1:20, 1:60, 1:200
QuilA	10, 3, 1 µg/ml	100, 10, 1 µg/ml	10, 3, 1 µg/ml	100, 10, 1 µg/ml
polyI:C	100, 30, 10µg/ml	100, 30, 10µg/ml	100, 30, 10µg/ml	100, 30, 10µg/ml
CpG ODN	10, 3, 1µg/ml	10, 3, 1µg/ml	10, 3, 1µg/ml	10, 3, 1µg/ml
OVA NS	20, 6.65, 2µg/ml	13.3, 4, 1.33µg/ml*	20, 6.65, 2µg/ml	13.3, 4, 1.33µg/ml*
luc NS	40, 13.3, 4µg/ml	13.3, 4, 1.33µg/ml*	40, 13.3, 4µg/ml	13.3, 4, 1.33µg/ml*
Halo NS	40, 13.3, 4µg/ml	13.3, 4, 1.33µg/ml*	40, 13.3, 4µg/ml	13.3, 4, 1.33µg/ml*

Table 10. Overview of the concentrations or dilutions of the different stimuli tested in the different DC activation assays. Stimuli for which the concentrations were changed in the second set of experiments are highlighted in light yellow.

(*) Samples were measured +/-polymyxin (100µg/ml).

As expected, the overall IL-6 induction pattern was different between the mouse DC and the human PBMC used in the MAT (Figure 51). Also, there were obvious differences in the response to particular stimuli between the GM-CSF and the Flt3L BMDC, which are most likely also due to differences in the expression profile of pattern recognition receptors such as Toll-like receptors (TLR). Mouse DC

responded poorly to the endotoxin control and in future DC activation the concentration of endotoxin should be increased by a factor of 100 or even 1000 (Figure 51). Interestingly, mouse DC responded better to Flagellin and Pam3CSK4 than PBMC and also showed a good response to CpG ODN unlike human PBMC (Figure 51). The IL-6 induction levels in response to R848, MPLA and the NS was comparable although absolute IL-6 levels were rather low for the Flt3L BMDC in comparison to the GM-CSF BMDC. Obvious differences between the GM-CSF and Flt3L BMDC cultures, was the absence of IL-6 production in response to LPS in the Flt3L BMDC whereas the GM-CSF BMDC induced robust levels of up to 80ng/ml. IL-6 levels in response to the NS were comparable to IL-6 levels in response to LPS for the MAT and for the GM-CSF BMDC, respectively. In contrast, Flt3L BMDC did show no response to LPS at the dilutions tested and had a low response to the nanospheres. Overall, the supernatant of Flt3L BMDC should be re-measured at lower dilutions to confirm the negative to low results for IL-6 in response to LPS and nanospheres in particular.

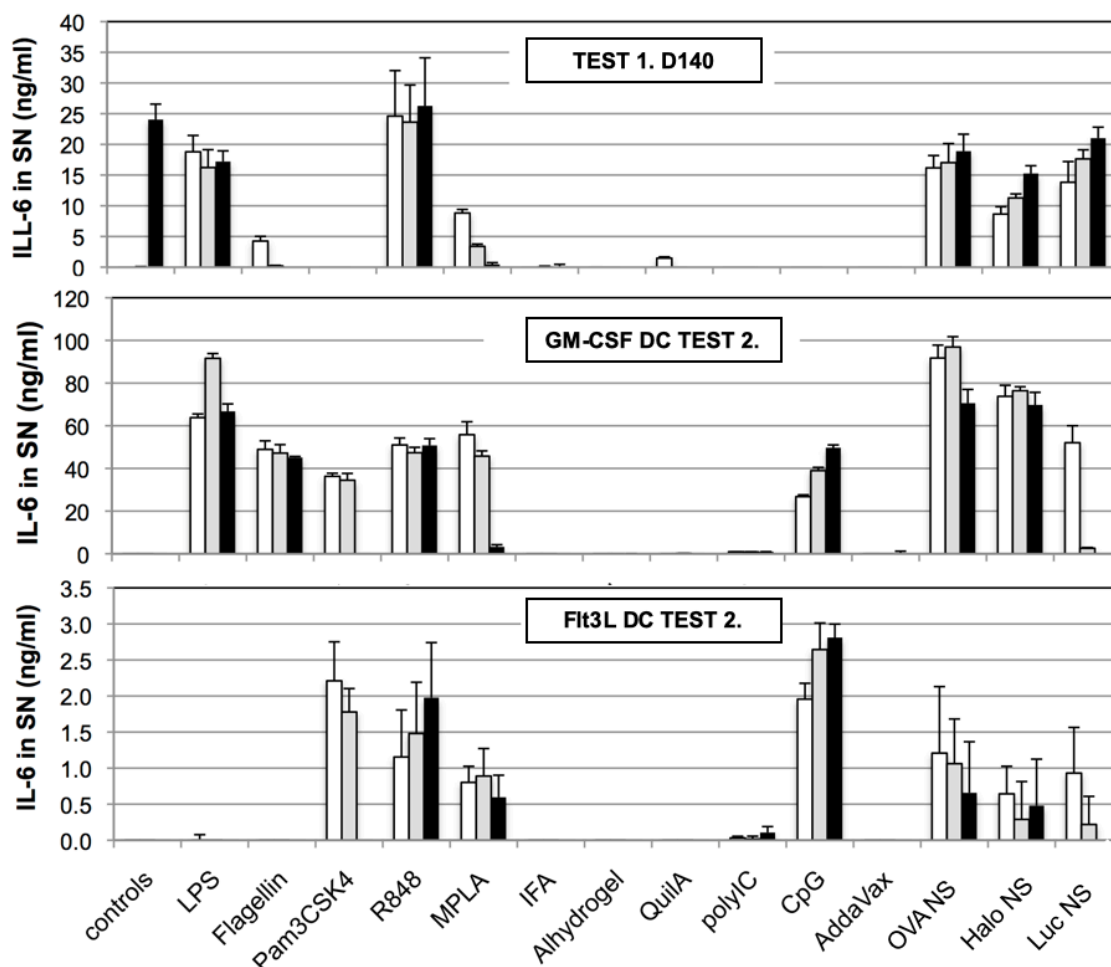


Figure 51. Representative IL-6 induction levels for human PBMC (TEST 1) as compared to DC activation assays using GM-CSF (GM DC TEST 2) and Flt3L BMDC (Flt3L DC TEST 2).

Comparisons of the two repeats of the activation assay for the GM-CSF BMDC and the Flt3L BMDC are depicted in Figures 52 and 53, respectively. However, the concentrations for some of the stimuli were altered between the two repeats as outlined in Table 3 and the results are therefore not directly comparable for all stimuli. Interestingly, in the activation assay for the Flt3L BMDC TEST 1, cells produced much higher levels of IL-6 in response to CpG ODN than to any of the other stimuli. This was not observed for the repeat (Flt3L DC TEST 2) even though the same concentration of CpG ODN was employed. For clarification of some of the

observed characteristics, it is necessary to repeat the assay with comparable concentrations of the respective stimuli.

As tested in the MAT, addition of polymyxin was employed in the second set of activation assays to sequester and inhibit endotoxin present in the NS preparations. For GM-CSF BMDC, which unlike Flt3L BMDC produced robust levels of IL-6 in response to LPS, there was a total block in IL-6 induction in the presence of 100 µg/ml polymyxin in the cultures (Figure 54). Interestingly, there was a clear reduction in the IL-6 induction levels in response to NS for GM-CSF BMDC and at lower levels there was a total or near total block in IL-6 production. This result makes it even more important to identify how many international units (IU) of endotoxin are neutralized in the assay at a concentration of 50 or 100 µg/ml polymyxin. It also raises the question, how much of the induced cytokine response is mediated by the endotoxin contamination present in the NS preparations and whether NS are detected by a yet unidentified PRR in human PBMC that is absent in mouse GM-CSF BMDC. These are crucial questions that need to be addressed prior to publication of the study.

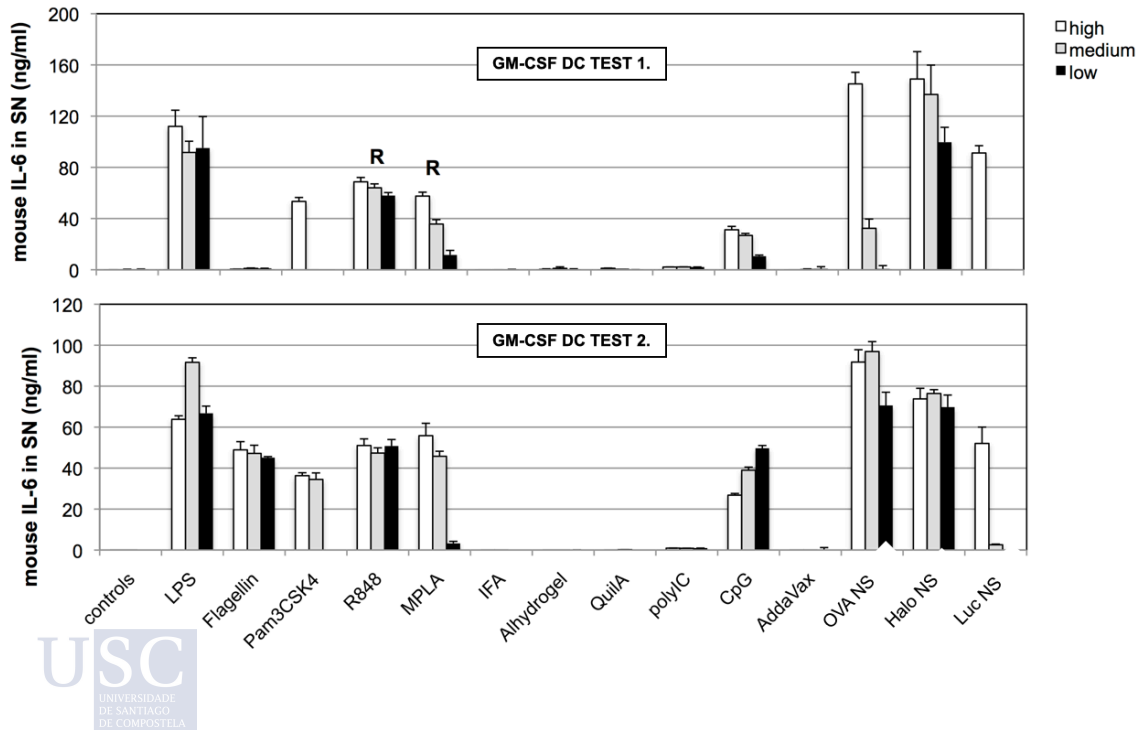


Figure 52. IL-6 induction levels for the two repeats of the DC activation assays using GM-CSF BMDC (GM-CSF DC TEST 1 & GM-CSF DC TEST 2). For the following stimuli, the concentrations used were higher for the second repeat: Pam3CSK4, MPLA, Alhydrogel and QuilA. In contrast the concentrations used for the nanospheres were lower for the second repeat.

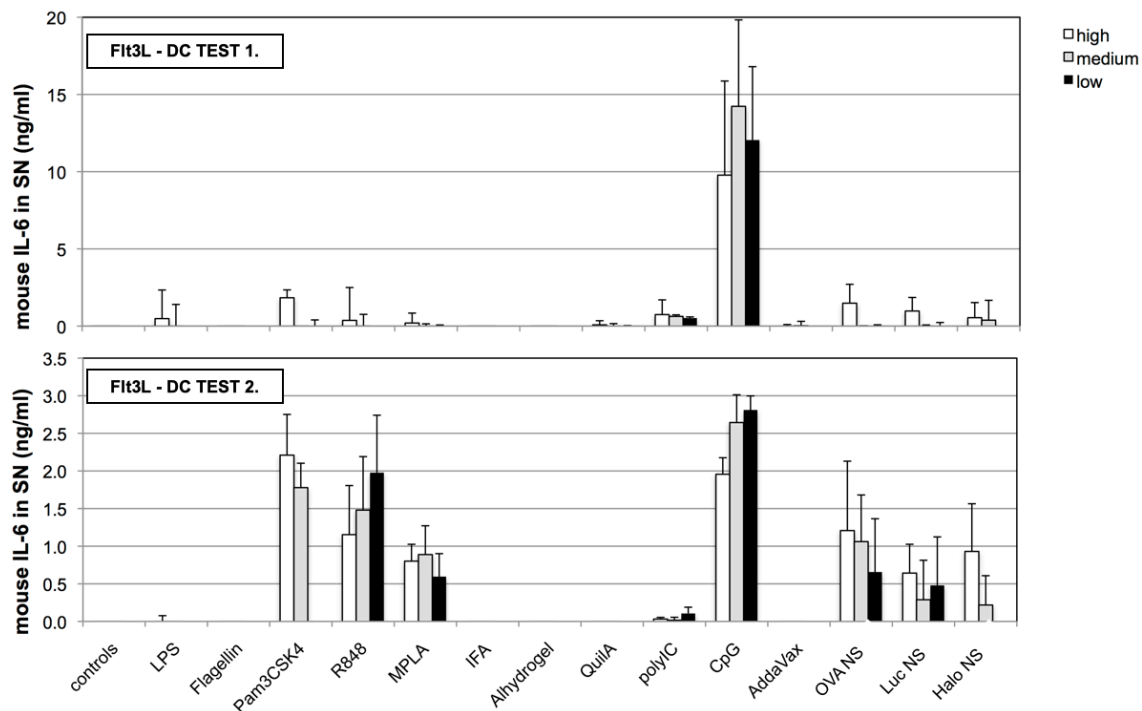


Figure 53. IL-6 induction levels for the two repeats of the DC activation assays using Flt3L BMDC (Flt3L - DC TEST 1 & Flt3L - DC TEST 2). For the following stimuli, the concentrations used were higher for the second repeat: Pam3CSK4, MPLA, Alhydrogel and QuilA. In contrast the concentrations used for the nanospheres were lower for the second repeat.

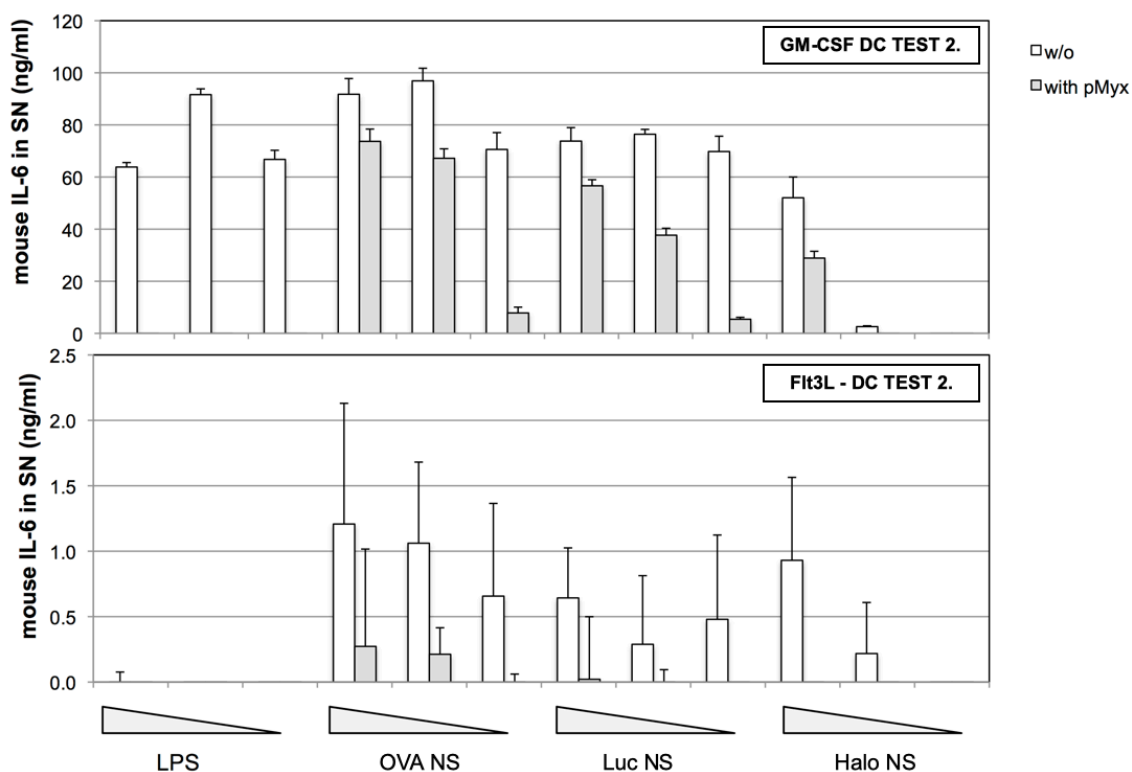


Figure 54. IL-6 induction in response to LPS and NS preparations in the presence (grey bars) and absence (white bars) of 100 μ g/ml polymyxin for the GM-CSF and the Flt3L BMDC activation assay.

In the GM-CSF BMDC activation assay, polymyxin seems to induce some low level of IL-6 in a dose-dependent manner (Figure 55). While this was not observed for Flt3L BMDC, low levels of IL-6 in response to polymyxin were observed in the MAT (MAT 20-04; data not shown). However, it is important to note that these levels of IL-6 are much lower than the levels observed in response to LPS or NS (factor of 50 difference).

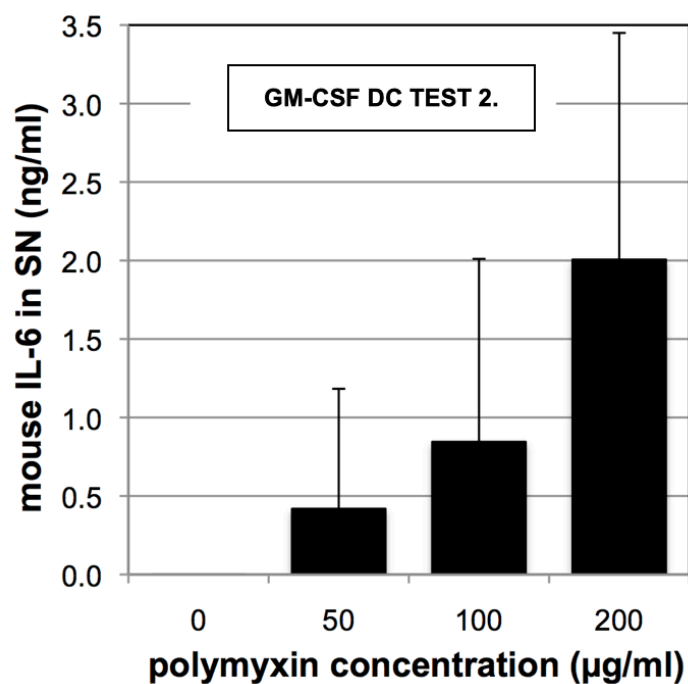


Figure 55. IL-6 induction in response to increasing doses of polymyxin in the GM-CSF BMDC activation assay (GM-CSF DC TEST 2).

For the DC activation assay with GM-CSF BMDC (GM-CSF DC TEST 1), the induction of IL12 p40 was investigated in parallel to the induction of IL-6. From our experience, these two cytokines show the same induction pattern for all TLR agonists that signal via the adaptor molecule MyD88. Upon comparison of IL-6 and Il-12 p40 levels, this phenomenon was confirmed for the TLR agonists used for this project and was also observed for the NS preparations (Figure 56).

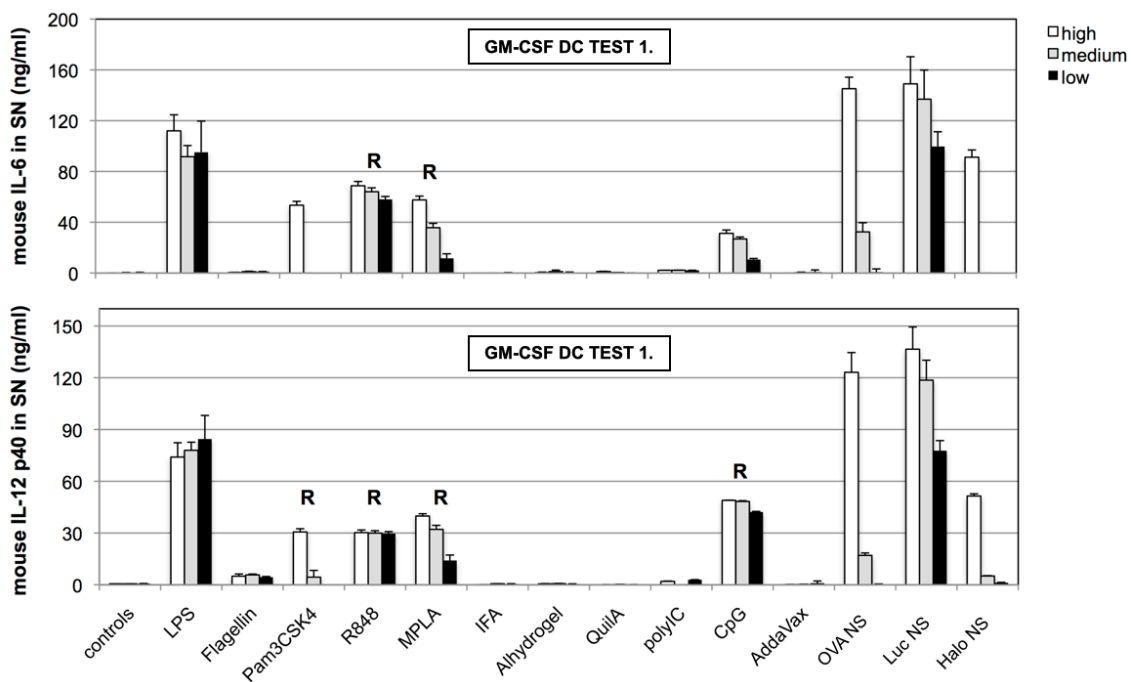


Figure 56. Comparison of the IL-6 and the IL-12 p40 induction pattern in the GM-CSF BMDC activation assay (GM-CSF DC TEST 1).

2.6. Induction of anti-tumor immunity by NS

In order to test the in-vivo anti-tumor immune response, both the tumor recession and the induced CTL-activity were assessed (Figure 57).

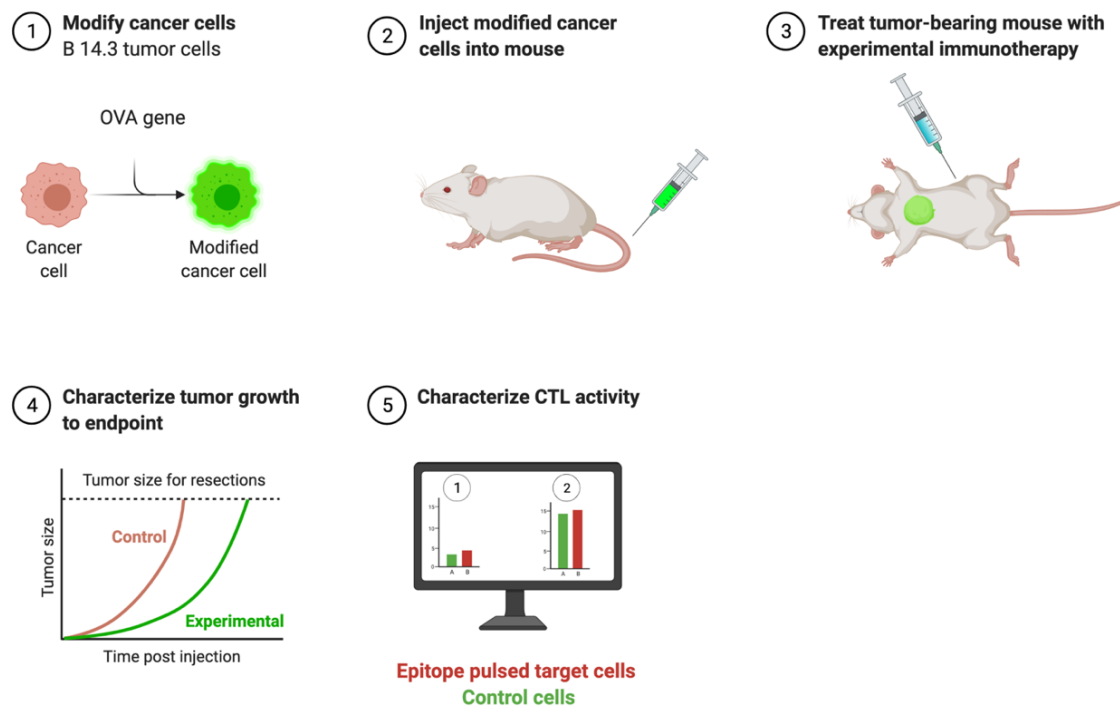


Figure 57. Representation of the tumor recession and the induced CTL-activity assessment.
1) A modified line of melanoma cells was developed expressing the model antigen OVA. **2)** The cells are injected in the mice where the development of a tumor will take place. **3)** The tumor-bearing mouse is treated with the immunotherapy candidate in order to induce a recession on the tumor. **4)** and **5)** The recession of the tumor is followed as well as the in vivo CTL activity.

For the first in vivo experiment (IN VIVO 1), we decided to vaccinate mice with 50µg of NS intraperitoneally as previously described for inducing anti-viral immunity (25). Due to time constraints within the experiment, mice were vaccinated with a single dose of NS and not twice in three-week intervals as described for the previous study involving vaccination with MS. As positive control, a group of mice was vaccinated with anti-Dec205/OVA fusion antibody in combination with CpG ODN by footpad injection as described in a previous study to be effective in inducing anti-tumor immunity (243). B16 tumor cells expressing the model antigen ovalbumin as a transgene (B14.3 cells) were injected intravenously into the mice at the start of the experiment. Vaccination took place at day 7 post tumor inoculation. The target cells for the in vivo CTL assay were injected on day 7 post immunization and the

mice were culled the next day when lungs and spleens were harvested and processed (Figure 58).

All experiments were carried out following the Animal Scientific Procedures Act 1986 under the project license 70/8831, Novel Biologics for Tumour Immunotherapy. The Project Licence protocol is the protocol 3 “therapeutic tumour intervention”. The project licence holder (PLH) is Dr. Sandra Diebold and the Deputy is Dr. Sandrine Vessillier. It was established that this study, including its background, objectives, experimental design, species, genetic status and number of animals to be used, regulated procedures to be performed, nature of the test substance, humane endpoints and fate of animals on completion, it was authorized by the Project Licence specified above. The center where the studies took place is the National Institute for Biological Standards and Control in the United Kingdom. The animals were randomly assigned into the different study groups. The animal work was performed by the NIBSC personnel, and they were in charge during the administration of the treatment or tissue harvest.

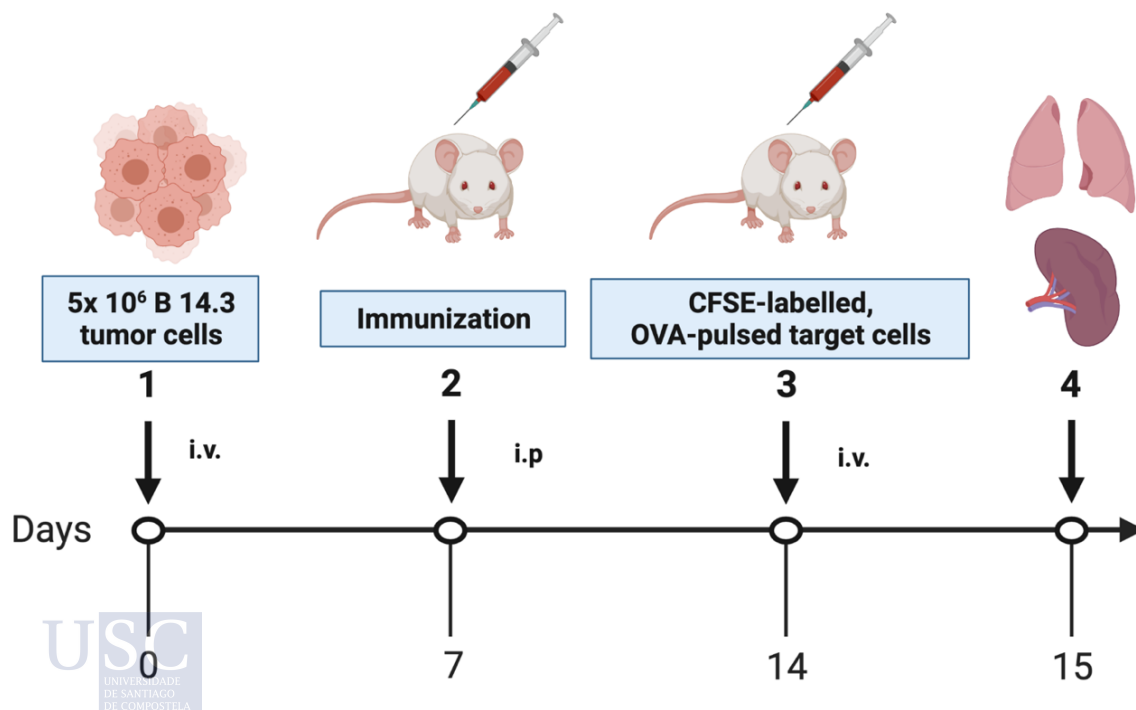


Figure 58. Schematic overview over the experimental plan of the *in vivo* experiment evaluating anti-tumor immunity induction.

When antigen-specific killing of target cells was analyzed by flow cytometry in the *in vivo* CTL assay, it became obvious that the dose of DC-targeting antibody and CpG ODN had been too low to induce an OVA-specific CTL response (Figure 59). However, mice injected with 50 μ g of OVA NS (OVA muNS) showed an OVA-specific CTL response with 50% of the target cells being killed on average. In contrast, the control nanospheres (Halo muNS) only achieved background levels of killing of approx. 10% on average, similar to what was observed for PBS injected mice and only slightly higher of what was observed with the ineffective DC-targeting Ab control. From this we concluded that OVA nanospheres have the capacity to induce antigen-specific CTL responses that are effective in killing tumor cells.

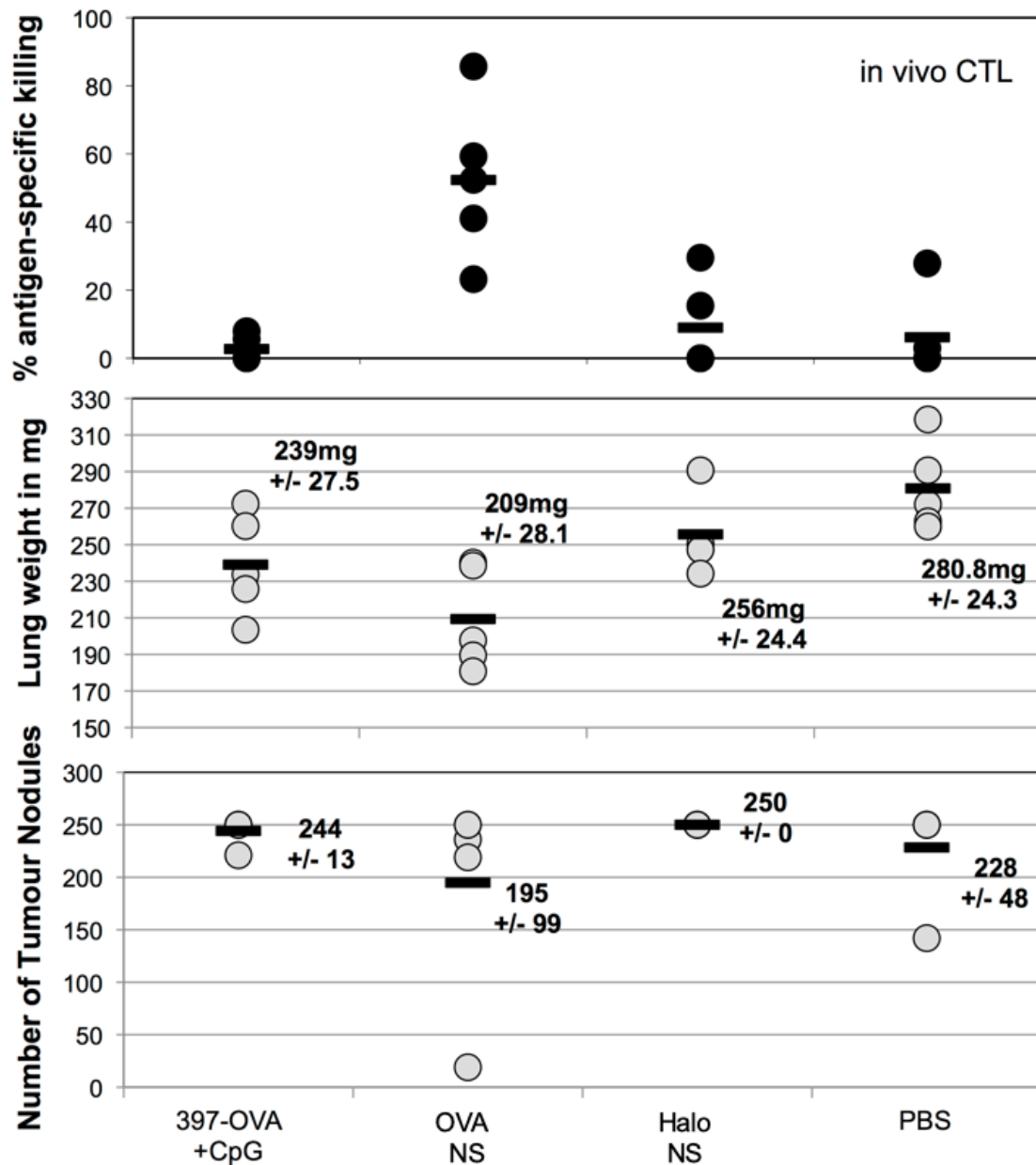


Figure 59. Data from first in vivo experiment (IN VIVO 1). Mice were injected with 50µg OVA or Halo NS intraperitoneally while control mice were injected with anti-Dec205/OVA fusion antibody in combination with CpG into the footpad (n=5). Negative control mice were injected with PBS intraperitoneally. Seven days post-treatment mice were injected intravenously with OVA-pulsed target cells and mice were sacrificed the next day. Splenocyte preparations were analyzed by flow cytometry to determine the percentage of antigen-specific killing (in vivo CTL assay), while the lungs were weighted prior to fixation and lung nodules were counted after fixation for evaluation of the tumor burden.

In addition to analyzing the antigen specific killing of target cells in the individual mice, we also determined the number of tumor nodules in the lungs and weighted the lungs in order to quantify the tumor burden. While the weight of lungs correlated with the level of antigen-specific immune response that was observed for individual mice, the number of tumor nodules was relatively high for all mice reaching the maximum number of nodules that can be counted per lung (250) with only two mice having a tumour burden below 200 (Figure 59, lower panel). From this we concluded that the enumeration of tumor nodules is not a good marker for evaluating tumor burden in this experimental setup whereas the weight of the lungs is. This was also observed in previous experiments when studying the efficacy of DC-targeting fusion antibodies (243). The number of tumor nodules may already be established by the time treatment commences. The treatment may reduce or block tumor growth once the anti-tumor immune response has been initiated, but there may not be enough time to eradicate all existing tumor cells within the experimental set-up. Mice could be kept until day 18 as specified on the project license for this model, however seven days post vaccination is the optimal time point to inject target cells for the in vivo CTL assay.

In a second in vivo experiment (IN VIVO 2), mice underwent the same experimental procedure, however, the mice were vaccinated at day 4 instead of day 7 post tumor inoculation. The in vivo CTL was performed seven days post vaccination and the mice were culled on day 12 instead of day 15. The positive control with the DC-targeting fusion antibody was omitted, instead OVA NS were injected at a dose of 50µg per mouse plus and minus polymyxin, and at an increased dose of 75µg per mouse plus polymyxin (Figure 60). As negative control Halo NS were used and an additional group of five mice was vaccinated with TRP2 NS, both in the presence of polymyxin. PBS injected mice were used as negative controls.

Unfortunately, the tumor burden of the mice was significantly lower than expected even for day 12 post tumor inoculation. Hence, the tumor burden did not yield any useful insight into the anti-tumor immune response levels induced in the mice in this experiment (data not shown). In contrast, the in vivo CLT assay performed well. Background levels were low ranging from 2% for the PBS group to 12% for the TRP2 group and up to 26% of antigen-specific killing for the Halo

nanospheres injected mice (Figure 60). In contrast, all mice injected with OVA nanospheres yielded levels of OVA-specific killing above 37%. The best killing was observed for mice vaccinated with the higher dose of OVA nanospheres in the presence of polymyxin which achieved 66% of antigen-specific killing compared to the lower dose of OVA nanospheres in the presence of polymyxin which yielded 36% of antigen-specific killing on average. The lower dose of OVA nanospheres in the absence of polymyxin achieved 43% of antigen-specific killing on average. The slightly higher level of antigen-specific killing in the absence of polymyxin may be attributable to the adjuvant effect of the endotoxin present within the nanospheres. However, the difference is not statistically significant, and this point would need further confirmation.

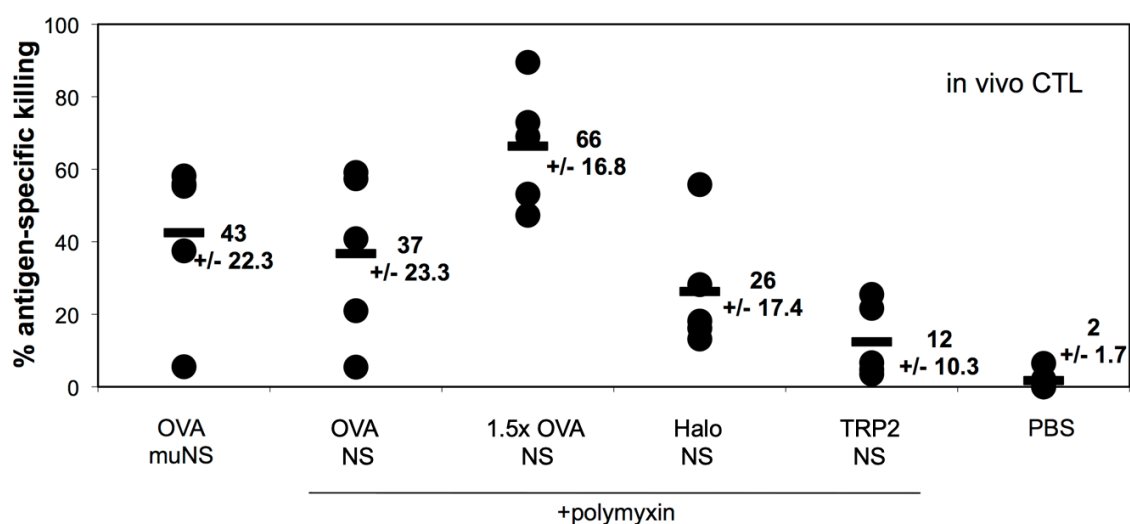


Figure 60. Data from second in vivo experiment (IN VIVO 2). Mice were injected with 50µg OVA or Halo NS intraperitoneally in the presence and absence of 50µg of polymyxin as indicated (n=5). Two additional groups of mice were injected with a 75µg of OVA NS plus polymyxin or 50µg of TRP2 NS plus polymyxin. Negative control mice were injected with PBS intraperitoneally. Seven days post treatment mice were injected intravenously with OVA-pulsed target cells and mice were sacrificed the next day. Splenocyte preparations were analysed by flow cytometry to determine the percentage of antigen-specific killing (in vivo CTL assay).

The question whether the TRP2 NS are effective in inducing an anti-tumor immune response will have to be addressed in a subsequent experiment using target cells that are pulsed with a TRP2-specific peptide antigen. Unfortunately, this technical aspect had been overlooked in the second in vivo experiment.

2.7. Monitoring the bio-distribution of NS by in vivo imaging

In addition to the in vivo experiments for evaluating the anti-tumor immunity induction in response to NS, we also performed in vivo imaging experiments to explore whether the bio-distribution of nanospheres could be assessed by whole body imaging of mice upon the injection of luciferase-tagged (Luc Imaging) or Halo-tagged (Halo Imaging) NS (Figure 61).

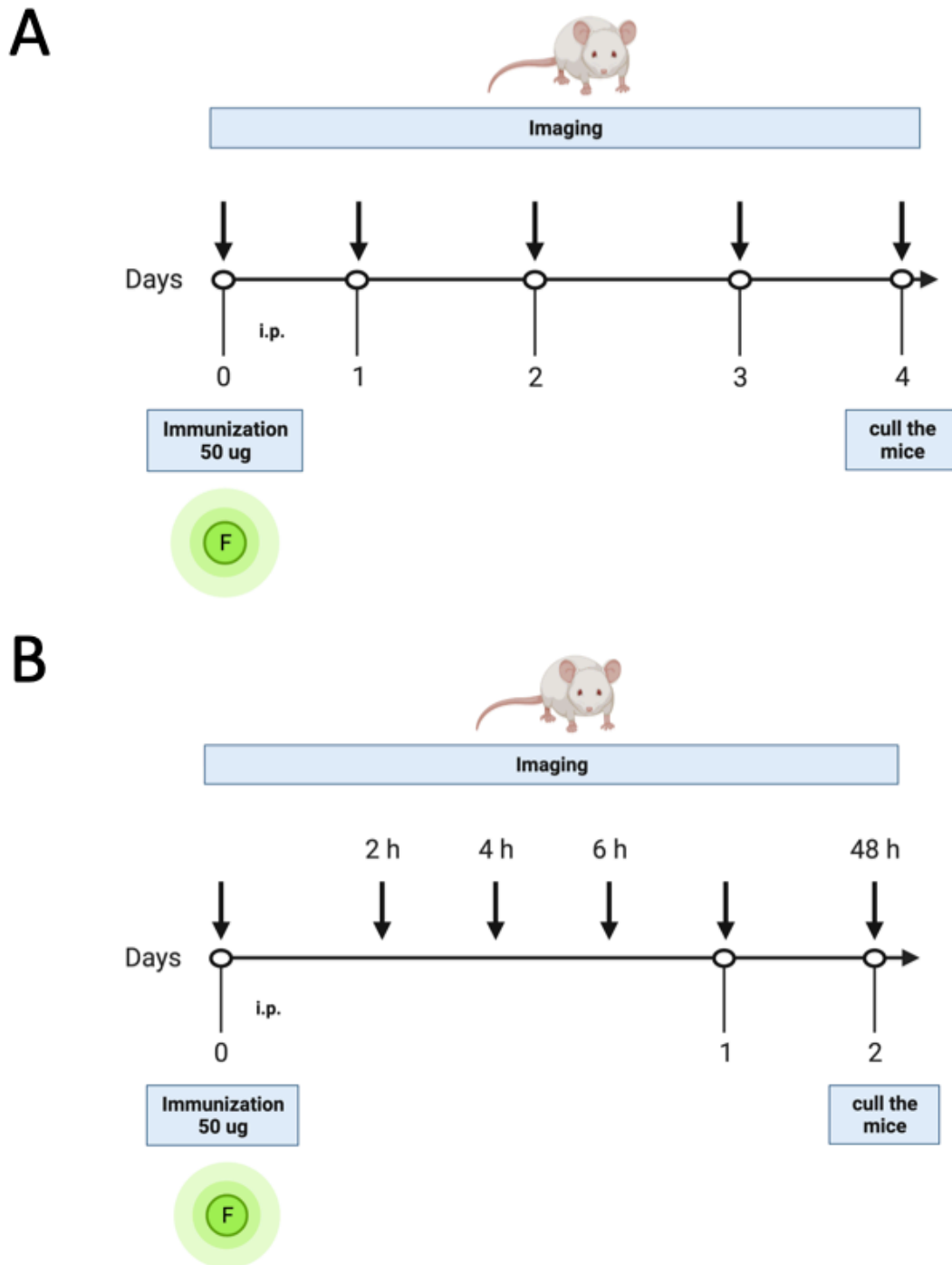


Figure 61. Schematic overview over the experimental plan of the *in vivo* imaging experiment for evaluation of the bio-distribution of NS upon intraperitoneal injection. For the luciferase-tagged NS (Luc Imaging) two mice per group of 4 were imaged every two days **(A)** whereas for the Halo-tagged NS (Halo Imaging) the mice which were imaged on day 1 were kept under anaesthesia for several hours and imaged repeatedly while another set of mice was imaged on day 2 **(B)**.

Before performing the *in vivo* experiment, the luciferase activity associated with luciferase-tagged NS was quantified *in vitro*. Addition of luciferin alone was not sufficient to initiate the enzymatic response and ATP had to be provided in addition to the luciferin. The samples were analyzed in the β -microcounter and in the ELISA reader in parallel and both instruments yielded comparable relative results (Figure 62). The luciferase-tagged NS were compared side by side to luciferase expressing B14.3 cells. At the respective densities of cells and NS chosen for this assay, both yielded similar levels of luciferase activity in the assay whereas the negative controls produced no result as expected.

When testing the NS the next day *in vitro* upon addition of luciferin and ATP in the *in vivo* imaging machine under similar conditions, the cells showed a stronger signal in the IVIS machine than the NS (data not shown). Upon injection of luciferase NS alone or in combination with ATP into mice, the IVIS machine was not able to pick up a bioluminescent signal in the mice (data not shown). At this stage it is unclear whether the inability to detect a bioluminescent signal is a direct consequence of the weak signal emitted by the nanospheres or whether the co-injection of ATP into the mice is not suitable to support the enzymatic reaction of the NS-associated luciferase with its substrate *in vivo*. It is important to note that one mouse co-injected with ATP and NS showed a mild adverse response (hunched posture, inattentive). We therefore refrained from co-injecting the other mice with ATP.

Irrespective of the reason for the inability to detect a signal, luciferase-tagged nanospheres seem unsuited for monitoring the bio-distribution of NS by *in vivo* imaging.

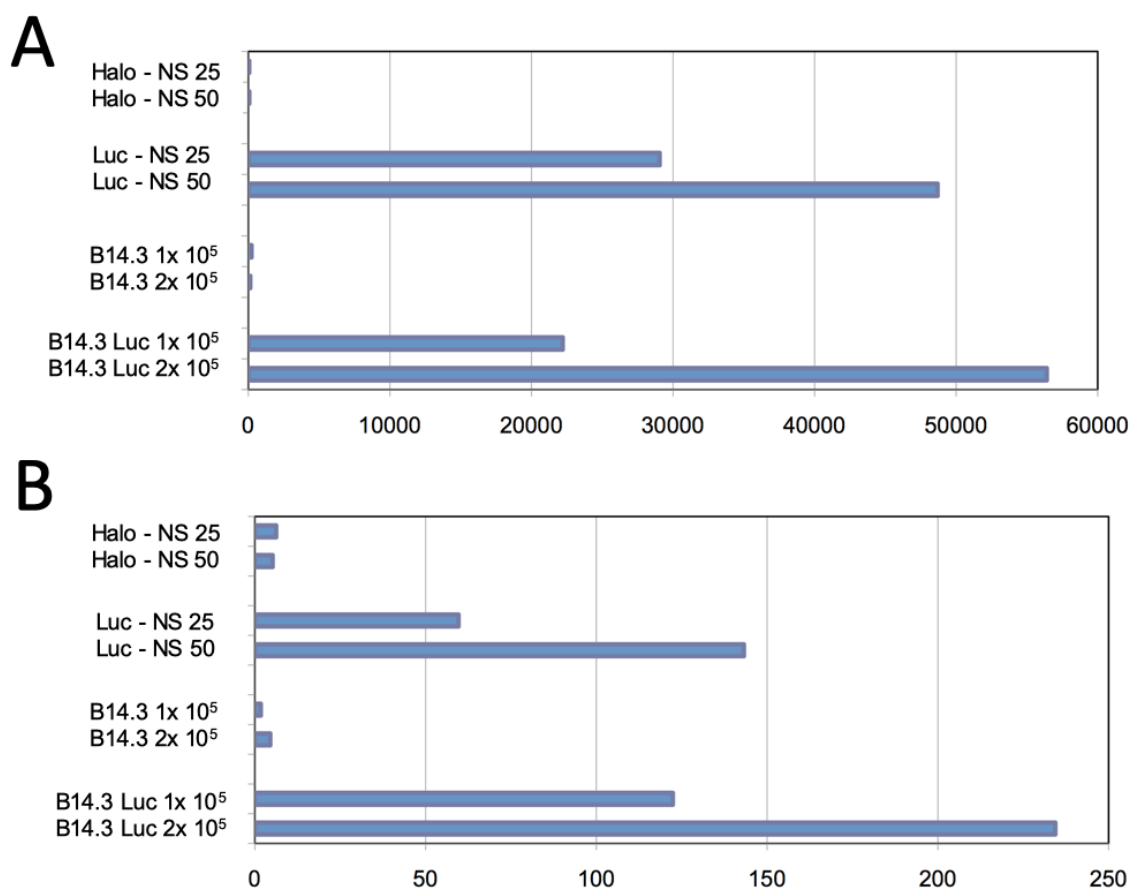


Figure 62. In vitro luciferase assay for comparison of luciferase-tagged NS with luciferase expressing B14.3 melanoma cells. Luciferase activity was quantified using the β -micro counter **(A)** and the ELISA reader **(B)**.

In a second attempt to investigate the bio-distribution of the NS by in vivo imaging, we explored the use of HaloTag-loaded NS. For this purpose, we labelled the HaloTag-NS in vitro with AlexaFluor 660 ligand, adjusting the molecular ratio of NS to ligand to approximately 1:2 and 1:4 for the labelling. When analyzed, the NS labelled with fluorescent ligand at a 1:2 ratio was clearly above the background levels and the nanospheres labelled at a ratio of 1:4 with ligand showed stronger signal (Figure 63).

Next, labelled NS were injected into mice at a dose of 50 μ g per mouse. The mice were kept under anaesthesia from 1h after injection for a total of 4h. During this time mice were imaged in the IVIS machine at regular intervals using a variety of filter

combinations and instrument settings. However, at none of the settings tested could we detect a fluorescent signal over the background (Figure 64).

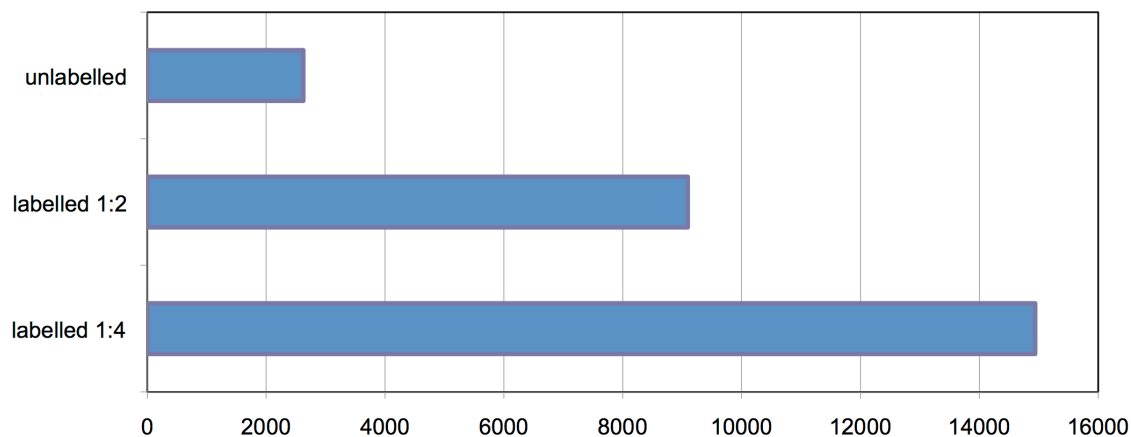


Figure 63. Fluorescent emission for fluorescently labelled HaloTag-NS as measured in the ELISA reader (excitation: 690nm; detection: 665nm). HaloTag-NS were labelled with fluorescent ligand at a nanosphere: ligand ration of 1:2 or 1:4 or left unlabelled.

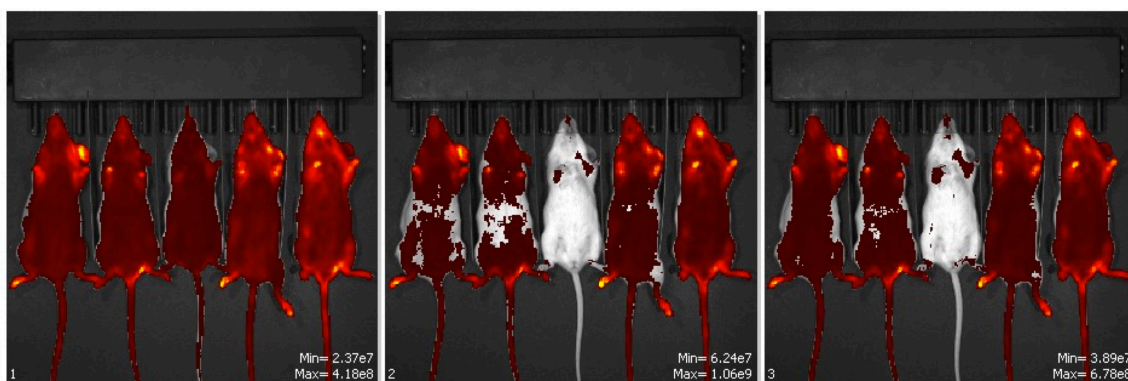


Figure 64. Representative in vivo images of mice injected with labelled or unlabelled HaloTag-NS for detection of Fluorescence at 660nm in the IVIS instrument. The same five mice were scanned using three different instrument settings. The two mice on the right were injected with labelled HaloTag-NS, while the three mice on the left were injected with unlabelled NS 24h prior to the acquisition of the image.

3. DISCUSSION

In summary, we have introduced a new approach in selective cancer immunotherapy through the use of the IC-tagging system. As part of this project, first with the LAL evaluation, we observed that the endotoxin levels of NS generated in the *E. coli* expression system vary widely and should always be determined prior to use. In addition, washing the NS with Triton X-100 solution was an effective method to reduce the endotoxin content in the NS preparations as seen for TRP2 and OVA NS preparations (FM +OVA 2 repurified and FM + TRP2 1 repurified). To address this matter, we have now expressed the antigens using a genetically modified bacterial strain lacking the LPS component, but it hasn't been tested yet due to the Covid-19 situation that interrupted this work.

Secondly, with the help of the MAT using PBMCs, we demonstrated that the NS induce high levels of IL-6 and other cytokines. The immunogenicity of the NS is still present when endotoxin is blocked using polymyxin. However, we have to show that the amount of polymyxin used is sufficient to neutralize all the endotoxin present in the NS preparations. Furthermore, TNF alpha seems to be induced at proportionally higher levels in response to NS when compared to LPS. In addition, the results from the SD lab and the Pyrogen lab IL-6 ELISA are comparable and it was deemed acceptable to use the SD lab protocol throughout the study as not to deplete the batch release resources. Regarding the IL-6 standards, the international IL-6 standard gave higher values in the assay. However, this should be confirmed in a separate assay. Third, using the DCs activation test, we were able to see that the NS induce high levels of IL-6 and IL-12 p40 in the DC activation assay. GM-CSF BMDC are more responsive to the stimulatory activity of LPS and NS and seems to be more suitable for studying the innate immune activation pattern of NS than Flt3L BMDC. This is most likely a consequence of the different pattern recognition receptor expression profile of these different DC cultures. Taking in account this discrepancy between donors in combination with the high variability within the quadruplicates for

each donor, it is currently unclear to what extent the endotoxin contamination influences the cytokine response. To clarify this point, further tests will have to be performed. Also, increasing doses of endotoxin standard in the presence and absence of polymyxin should be included to clarify how much endotoxin IU can be neutralized with the given dose of polymyxin.

Regarding the *in vivo* induction of anti-tumor response in mice (which is likely the most important result), we were able to see that the NS induce an antigen-specific CTL response *in vivo* in mice. In addition, the first experiment indicated the induction of an effective anti-tumor immune response in the *in mouse* pseudo-metastasis model. Further experiments are required to evaluate the anti-tumor immune response and to investigate whether targeting the *bona fide* tumor-associated antigen TRP2 is also effective in inducing anti-tumor immunity.

Finally, we weren't able to accomplish the *in vivo* monitoring of the NS bio-distribution. The reason is that the luciferase-tagged NS don't seem suitable for monitoring the bio-distribution of nanospheres by *in vivo* imaging. Luciferase expressing cells provide the required ATP for the enzymatic reaction to take place in the presence of the substrate luciferin, however, it is unclear in what form ATP could be provided *in vivo* to enable the enzymatic reaction in case of luciferase-tagged NS. And the IVIS machine doesn't seem to be sensitive enough to pick up the fluorescent signal emitted from the labelled Halo-tagged nanospheres. It is also possible that labelling the NS at a higher NS:ligand ratio could overcome this issue. Another option is using NS loaded with an ATP-Independent Bioluminescent Reporter, for example the *Renilla* Luciferase (RLuc) from the sea pansy *Renilla reniformis*.

GENERAL CONCLUSIONS

- 1- IC-Tagging derived nanospheres (NS) are suitable as enzyme carriers to promote both, enzyme reusability and stabilization of the integrated enzyme, increasing the applicability of this platform for enzyme immobilization.
- 2- NS encapsulation increases enzyme activity over a wider pH range when compared to the free enzyme.
- 3- NS encapsulated CotA are stabilized against incubation at different pH values and incubation with different inactivating agents such as organic solvents and salts.
- 4- Nanoencapsulated CotA laccase become extremely resistant to thermal denaturation.
- 5- Stereolithography (SLA) 3D printing is a streamlined approach to entrap enzymes under mild conditions, providing a useful solution for bioremediation.
- 6- The 3D printing methodology immobilizes the enzyme and simultaneously produces 3D-tunable devices, representing an inexpensive and sustainable manufacturing process.
- 7- NS induce the release of high levels of IL-6, TNF alpha and other cytokines *in vitro*.
- 8- NS induce an antigen-specific CTL anti-tumor response in mice pseudo-metastasis model that produce a tumor weight regression.

SUMMARY

Protein immobilization on solid supports offers a wide range of opportunities in the biotech industry. Its many possible applications in diverse fields cover from enzyme immobilization promoting an enhancement in the physicochemical properties, to vaccine candidate generation, reducing the associated production costs and improving the immunogenic performance of the vaccine candidate. The immobilization process implicates profound science in both substrate surface and proteins. Proteins are composed of amino acids polymerized jointly through the formation of peptide bonds. One or more polypeptide chains fold into a 3-dimensional (3-D) bioactive protein, with many exposed functional groups such as carboxyl, amine, hydroxyl, and sulfhydryl. Regarding the immobilization strategy, the conformation of the immobilized protein needs to be seriously considered. In the enzyme field, the active site is usually a groove or pocket where the target or substrate molecules bind and experience a chemical reaction. In order to function properly, this active site needs to be in specific and appropriate conformation and accessible to the target. This is why protein immobilization in random orientation on a solid support can result in unexpected denaturation and blocking of the active site followed by the natural loss of activity. On the other field discussed in this thesis, protein-based vaccine generation strategies, immobilization strategies have been also demonstrated to deliver quality results. This is because immune responses to a particular antigen are considerably improved if the antigen is presented and coupled to some sort of virus-sized particle in an ordered, repetitive array. In this field, the correct protein folding is also critical for the generation of the optimal immune response against the chosen epitope/protein as the generation of antibodies or the triggering of a cellular response is very dependent of the antigen conformation.

The present study explores two fundamentally different methods for protein immobilization: the IC-Tagging methodology using a modified viral protein, and 3D printing through the use of Stereolithography (SLA). We investigate the feasibility of these strategies and its efficiency in generating properly folded immobilized proteins for different applications in the field of biocatalysts and cancer immunotherapy.

Chapter 1. Enzyme immobilization and biocatalysis via the IC - Tagging technology.

Biocatalysts are critical tools for the production and degradation of pharmaceuticals and fine chemicals because of their high selectivity and specificity, mild reaction temperature and neutral or close to neutral pH activity. In addition, catalysts provide lower pollution and hazardous outcomes and a lower energy consumption when compared to conventional catalysts processes. Biocatalysts also offer new opportunities for the synthesis of highly valuable compounds that could not be possible otherwise. The total number of biotransformation processes carried out on an industrial scale have been increasing continuously for the past decade. Nonetheless, biocatalysts also present multiple limitations, for instance, if a reaction proceeds slowly under given temperature and an increase in temperature would lead to a better performance, this increase often leads to denaturation of enzyme involved in the process. Moreover, production of enzymes is expensive, and they often need to be recovered and reused in order to make them cost-effective. For this purpose, soluble enzymes in aqueous media demand the use of tedious techniques for the separation from the reaction mixture. However, these limitations can be tackled by enzyme immobilization. Immobilization of enzymes onto a solid support offers the most inexpensive way of recovering enzymes from reaction mixtures. Furthermore, it adds some special features to the biocatalysts such as operational improvement, an increase in thermal and pH stability, as well as protection against denaturation induced by solvent compounds. Major disadvantages upon immobilization are linked to the loss of activity, diffusional limitation and increased production costs. Despite those, immobilized enzymes are regularly used in pharmaceutical, food and chemical industries.

In this field, we decided to test the IC-tagging platform developed in our laboratory. The rationale behind our approach is that microparticles have been gathering increasingly attention over the years for their multiple applications in very different areas, going from industrial production to therapeutic treatment or diagnosis. On this implementation, cost production as well as stability are the main

challenges to overcome. With our method both the expression and the micro/nano-encapsulation are performed simultaneously by the cell avoiding the need for protein purification and coupling to a particle. The reason is that this protein is capable to self-assemble into spherical structures inside living eukaryotic and prokaryotic cells, forming microspheres (MS) and nanospheres (NS) that can be easily purified. Moreover, the tagging of any protein with the so-called IC-tag causes the re-location of the selected protein/enzyme to the forming MS or NS, ending with the micro or nano-encapsulation of the tagged protein inside MS or NS. In this process, no additives need to be incorporated to the normal growth media, and particle formation facilitates the encapsulated protein purification by mechanical means, overall reducing the cost of the entire production process. As our methodology allows the cost-effective production and purification of encapsulated proteins, we wanted to explore the ability of NS as enzyme carriers to promote both, enzyme reusability and stabilization of the integrated enzyme that might increase the applicability of the IC-tagging method for protein production.

As a model enzyme for this project, we chose the laccase-like enzyme codified by the *Bacillus subtilis* CotA gene. Laccases (EC 1.10.3.2) are the largest subgroup of the protein superfamily of multi-copper oxidases (MCOs) and catalyze the one electron oxidation of four substrate molecules using molecular oxygen as the final electron acceptor. Their broad substrate spectrum and their ease of use have generated a high interest, particularly within the wood, biofuel, paper, textile, fine chemicals and food industrial sectors. Using this strategy, we accomplished the generation of a fully functional enzymatic reactor within the NS. After the immobilization, we performed enzymatic activity and stability characterization resulting in better stability and reusability features and demonstrating also to be viable against the model recalcitrant agent Reactive Blue 19 (RB19).

Expression yields of 30–50 mg/l were observed under standard conditions, without performing any expression optimization studies. These are similar or even higher than values reported in previously works where optimization of CotA laccase production in *E. coli* was performed. We found that the NS-contained enzyme presented an increased activity over a wider pH range when compared to the free enzyme, what agrees with a stabilizing effect of the nanoencapsulation on the enzyme.

Furthermore, the stability of the enzymatic activity against incubation at different pH values also showed a remarkable increase upon nanoencapsulation.

Identical stabilization effects were observed on incubation with different inactivating agents such as organic solvents and salts. Concentrations of different reagents that produced a deleterious effect on the activity of the free enzyme had no effect on the NS-contained laccase. The increased stability in organic solvents is particularly interesting for the industrial application of enzymes. The use of organic solvent systems instead of aqueous media for enzymatic reaction offers numerous advantages; however, organic solvents often inactivate enzymes. On the other hand, halides are known inhibitors of laccases, which may limit their application for bioremediation of industrial effluents with variable composition of inhibitors.

Regarding the recalcitrant agent model, synthetic dyes are extensively used in different industries, and 10–15% of dyes used during finishing and dyeing processes ends up in wastewater. Anthraquinone-based reactive dyes have attracted attention from the environmental and toxicological perspective, since they are extremely resistant to degradation and present acute toxicity of mutagenic effects. Conventional biological systems are not efficient for bioremediation and decolorization of dyes, and physico-chemical methods are associated to high operational cost, formation of undesirable by-products, etc. NS-CotA can be an eco-friendlier and practical choice for the bioremediation of dye polluted wastewater effluents. In this sense, the NS-contained enzyme was shown to decolorate the anthraquinonic dye RB19 quite efficiently compared to free enzyme. Although the RB19 decolorization rate was lower than that recently reported by using *Trametes versicolor* laccase in solution, it was remarkably higher than that achieved by an immobilized fungal laccase in absence of a mediator (only 5% decolorization in 6 h). Furthermore, it should be highlighted that the transformation of the dye by NS-laccase could be optimized in terms of pH, enzyme dosage or temperature, for a more efficient transformation of the substrate.

Also, because of their particulate nature, the NS-contained enzyme can be recovered from the reaction and re-used for several times without a significant loss in activity. Furthermore, because their small size, some NS might have been lost during the repeated centrifugation steps and the small decay in activity can be explained by

diminished protein content. An improved recovery method, involving filtration, NS-linking, or others, can be implemented to improve the recovery rates.

The most remarkable property that we have observed for this system is the thermal stabilization achieved. It is certain that the *B. subtilis* laccase is already intrinsically heat-stable. However, the NS-contained version surpasses extensively the abilities of the free enzyme. Although the encapsulated version outperforms the free one over all the temperature range, is at the highest values of 90 and 95 °C where the differences become remarkable. Thus, while the activity of the free enzyme is completely abrogated after 5min incubation at 90°C, the NS-contained laccase resisted at least 30min of incubation at that temperature without any appreciable activity loss. The performance of the NS-laccase only started to decline to a 77% of the initial activity after 15min of incubation at 95°C. This extreme thermostability might be beneficial for transformations that might be accelerated by increasing the temperature, well laccase-mediated oxidations or multi-enzymatic complex reactions.

Chapter 2. Enzyme immobilization and biocatalysis via 3D printing

It is now common, and almost expected, that an individual will take dozens of medicines in their lifetime, especially with advancing age. As more medicines are consumed, more are consequentially excreted or disposed of, often permeating the world's water. Drugs and their metabolites are present in nearly all aquatic environments, from drinking water, to ground water, sea water, and wastewater. The issue is global, with countries recording significant concentrations of pharmaceuticals in water across Europe, Africa, Asia, and the Americas. Presently, antibiotics, analgesics, lipid-lowering drugs, and estrogens are the most reported water-polluting drugs worldwide; however, the true number and scale of drugs is likely larger than currently known, due to limitations and priorities in testing. This insidious infiltration of pollutants poses a significant risk to global health and ecological equilibrium. For example, diclofenac is known to be one of the most prolific drugs entering water, with a global average of 0.032 µg/L present in all surface water compartments. The

entrance of diclofenac into wild food chains is lethal for migratory birds, such as vultures. In fact, diclofenac has resulted in the population collapse of three vulture species in South Asia and poses a significant threat to several European species. Elsewhere in the environment, the occurrence of estrogens in sewage effluents has led to feminization of male fish, dramatically impacting reproductive success. With regards to human health, the practice of irrigating crops with wastewater increases risk of consumer genotoxicity, due to the presence of solubilized antineoplastic. Moreover, antibiotics in water are thought to increase rates of bacterial antibiotic resistance, a currently critical challenge that threatens global health as whole. Even drugs of abuse are infiltrating water, as highlighted by studies in Madrid and Changzhou City, East China, which found cocaine, opioids, and methamphetamine in the cities' drinking supply and wastewater.

In the face of this challenge, the World Health Organization (WHO) has launched a working group to address how pharmaceutical burden in water can be lessened. As such, several methods for removing drugs from water have been proposed, including sludge processes; biofiltration; reverse osmosis; ozonation; chlorination; and nanofiltration. Unfortunately, many of these processes are variably efficient – with drug removal rates sometimes lower than 10% - and often require expertise with access to expensive and sizeable equipment. Thus, there is a global requirement for efficacious technologies that can remove drugs in water simply and cost-effectively. Ideally, methods should also work reliably in a range of different environments, regardless of pH, temperature, or physical space. As such, technologies that can be customized to fit into different physical spaces (such as pipes or machinery) are desirable.

To address this issue, we propose the use of 3D printing a key manufacturing method for customizable devices. In this study, we develop, manufacture, and validate a 3D printed biocatalytic device for the removal of drugs from water (we decided to term as Printzyme). The Printzyme has fully modifiable morphology, and utilizes the natural enzyme laccase, sourced from *Trametes versicolor*, as a drug oxidizing agent. As mentioned, laccases are ubiquitously found in nature, and have been shown to effectively degrade a wide variety of pharmaceuticals, including several classes of antibiotics, paracetamol, diclofenac, naproxen, anti-depressants, and estrogen.

Printzyme entraps laccase in a hydrogel via stereolithography (SLA) 3D printing. The novel process immobilizes the enzyme and simultaneously prints under mild conditions, representing an inexpensive and sustainable manufacturing process.

This study is part of a collaboration with Dr. Alvaro Goyanes and Prof. Abdul Bassit at the University College of London (UCL), and with Dr. Gemma Eibes from the CRETUS at the University of Santiago (USC). The basis behind the initiative is lies on this technology's ability to support the building of objects by consecutively placing layers of material based on a computer design. Therefore, providing the means to manufacture personalized objects on demand to be used in different areas including healthcare and industry. Specifically, stereolithography (SLA) offers the possibility to fabricate crosslinked polymeric matrices via photopolymerization, with a superior resolution while avoiding the need of high temperatures. For this reason, SLA was used to produce enzyme-loaded hydrogels containing variable water content. SLA was successful in producing hydrogels maintaining the enzyme activity and improving features such as stability and reusability. Modification of enzyme performance was also possible by varying the enzyme content and geometry of the prints, proving to be suitable for the fabrication of enzymatic reactors on a flexible and straightforward manner.

When studying both the pH and temperature requirements for enzyme activity, free laccase demonstrated higher activity than when immobilised in Printzyme. This is likely because since it is in solubilised form, all laccase active sites are freely accessible, whereas in Printzyme enzyme immobilization leads to a certain degree of steric inhibition. Whilst Printzymes do achieve lower activity in aqueous solutions compared to free laccase, they still retain substantial activity. Moreover, the Printzyme formulations demonstrated similar relationships to pH and temperature as free laccase, indicating that direct immobilisation of laccase into PEGDA hydrogels does not alter the biocatalytic mechanism. In addition, immobilization affords benefits in storability and reusability that free enzyme in solution can not accomplish. Enzyme entrapment within functional systems enhances sustainability and cost-effectiveness as expensive enzymes are not lost with every use. This is especially important for settings with limited storage, budgets, or access to deliveries (e.g., in remote locations).

With regards to reusability, Printzymes displayed good laccase activity for at least 18 isolated uses; demonstrating their superiority over free laccase in solution. Both Printzymes designs achieved superior reusability compared with other immobilisation methods of laccase from *Trametes versicolor*, including iron oxide nanoparticles 33%, chitosan microbeads, magnetic mesoporous silica spheres, poly (glycidyl methacrylate)-based microspheres, and agar-agar, polyacrylamide, and gelatine structures. As mentioned, a key benefit of Printzyme is its immobilization of laccase, as this allows enzyme recovery and repeated use not possible with free enzyme in solution. These data highlight the concept's cost-effectiveness, sustainability, and fit for purpose. Further, Printzyme could successfully reduce the concentrations of two drugs, diclofenac and ethinylestradiol, in aqueous solution. The devices removed over 80 % of dissolved diclofenac within 24 hours, and 95 % of ethinylestradiol within just 2 hours, being more efficient the torus shape, because of the higher surface to volume ratio. The effectiveness factor for the estrogen removal was close to one (0.95 for torus Printzyme), demonstrating that substrate diffusion across the Printzyme did not limit the transformation. Regarding diclofenac, the device provided higher initial removal rates than the free enzyme, with effectiveness factor of 1.55 (torus Printzyme), emphasizing the interest of using Printzyme for the transformation of substrates which can inhibit laccase. This implies that the effectiveness factor reached values higher than one. Effectiveness factor generally lies between 0 and 1, but sometimes can be higher than one due to non-isothermal operation, because of the stabilisation of the encapsulated enzyme related to the free one or because of inhibitory effects, being the most plausible explanation here the possible inhibition caused by high diclofenac concentrations on the free enzyme. Printzyme may have increased degradation rates by reducing the concentration of the substrate to non-inhibitory concentrations. Hence, Printzyme represents the more economic and sustainable option not only due to its reusability but also because it was more effective than the free enzyme in degrading diclofenac in the short term.

This work highlights the potential of SLA 3D printing as a streamlined approach to entrap enzymes under mild conditions. Our results present a significantly effective and sustainable approach to removal of pharmaceutical contaminants from

aqueous systems and provide implications for the development of bioremediation solutions.

Chapter 3. Cancer epitopes immobilization via the IC - Tagging technology

The concept of mobilizing the human immune system against cancer dates back to at least the mid-nineteenth century when Rudolf Virchow, a German pathologist, observed immune infiltration in human tumors. Since 2011, owing to its potential for a large and sustained clinical benefit, immuno-oncology has become the fastest-growing area not only in oncology but in the entire pharmaceutical industry. Nevertheless, although some patients may achieve cure or long-term disease control with first- or second-generation treatments, the majority of patients are still in need of a beneficial next-generation treatment. Specifically, many patients are not responding to checkpoint inhibition, or they respond and subsequently relapse. Innate immunity targets (for example, natural killer (NK) cell-targeting therapies) are gaining great interest, and novel approaches and drugs are emerging in this field. One of such approaches are vaccines which induce an immune response against unique tumor-specific antigens (neo-antigens). Thus, more-individualized approaches based on new scientific insights into cancer vaccines are entering the immuno-oncology stage. Neoantigen-based vaccines should induce strong specific immune response and elicit stable therapeutic effects. However, in the oncology field it is extremely complex to predict when and where tumor cells would occur (unless the patient suffers from specific rare syndromes) and which would be the antigenic signatures of those events and thus, cancer vaccines are typically for therapeutic use. Hence, the term "vaccine" is referred to a formulation which usually include a strong adjuvant, or it is adjuvant itself, and tumor proteins or peptides which prime the immune system.

The current landscape of clinical studies testing different activation routes for cancer immunotherapy elucidates the need for appropriate delivery and presentation methods to the tumor tissue. Tumor immunotherapy is acquiring clinical momentum, since as presented, such approaches display promising results in triggering local tumor

specific immunity, while avoiding potential off-target effects to healthy tissue, thus diminishing adverse effects.

Here, we aim to test if the prior mentioned IC-tagging platform in the form of tunable multivalent antigen presentation methodology works on a cancer immunotherapy setup when NS are loaded with cancer neoantigens, either individually or simultaneously in multivalent particles. This study was performed at The National Institute for Biological Standards and Control (NIBSC) with the collaboration of Dr. Sandra Diebold. The Cellular Immunology Section at NIBSC has expertise in investigating antibody-adjuvant conjugates for tumor immunotherapy, including an established mouse tumor model and various *in vitro* activation and cytokine release assays, as well as *in vivo* cytotoxic T lymphocyte (CTL) assays. For this purpose, we decided to use the B16-OVA pseudo-metastasis model which is an OVA-expressing melanoma cell line. In addition, we decided to include another antigen that is naturally expressed by B16 melanoma cells and can mediate anti-tumor immunity known as TRP2.

For this work, bacteria transformed with modified plasmids produced NS containing the IC-tagged proteins upon induction of expression, suitable for vaccination. By performing a thorough characterization of the innate immune and adaptive activation patterns both *in vivo* and *in vitro*, we are in position to identify the strengths in designing novel cancer vaccines based on our NS and/or MS.


First for the *in vitro* experimentation, with the help of the monocyte activation test (MAT) using peripheral blood mononuclear cells (PBMCs) and the use of bone marrow dendritic cells (BMDC) we demonstrated that the NS induce high levels of IL-6 and other cytokines. Furthermore, TNF alpha seems to be induced at proportionally higher levels in response to NS when compared to LPS.

Secondly, regarding the *in vivo* induction of anti-tumor response in mice (which is likely the most important result), we were able to see that the NS induce an antigen-specific CTL response *in vivo* in mice. In addition, we were able to identify the induction of an effective anti-tumor immune response in the in mouse pseudo-metastasis model. Further experiments are required to evaluate the anti-tumor immune response and to investigate whether targeting the bona fide tumor-associated antigen TRP2 is also effective in inducing anti-tumor immunity

Finally, we weren't able to accomplish the *in vivo* monitoring of the NS bio-distribution. The reason is that the luciferase-tagged NS don't seem suitable for monitoring the bio-distribution of nanospheres by *in vivo* imaging. Luciferase expressing cells provide the required ATP for the enzymatic reaction to take place in the presence of the substrate luciferin, however, it is unclear in what form ATP could be provided *in vivo* to enable the enzymatic reaction in case of luciferase-tagged NS. And the IVIS machine doesn't seem to be sensitive enough to pick up the fluorescent signal emitted from the labelled Halo-tagged nanospheres. It is also possible that labelling the NS at a higher NS:ligand ratio could overcome this issue.

RESUMO

A inmovilización de proteínas en soportes sólidos ofrece unha ampla gama de oportunidades na industria da biotecnoloxía. As súas moitas posibles aplicacións en diversos campos abranguen desde a inmovilización enzimática que promove un aumento das propiedades fisicoquímicas, ata a xeración de vacinas candidatas, reducindo os custos de produción asociados e mellorando o rendemento inmunogênico da vacina candidata. O proceso de inmovilización implica unha ciencia profunda tanto na superficie do substrato como nas proteínas. As proteínas están compostas por aminoácidos polimerizados conxuntamente a través da formación de enlaces peptídicos. Unha ou máis cadeas polipeptídicas pregáranse nunha proteína bioactiva tridimensional (3-D), con moitos grupos funcionais expostos como carboxilo, amina, hidroxilo e sulfhidriilo. En canto á estratexia de inmovilización, hai que considerar seriamente a conformación da proteína inmovilizada. No campo dos encimas, o sitio activo adoita ser unha ranura ou peto onde as moléculas diana ou substrato únense e experimentan unha reacción química. Para funcionar correctamente, este sitio activo debe estar conformado de xeito específico e adecuado e ser accesible ao destino. É por iso que a inmovilización de proteínas en orientación aleatoria sobre un soporte sólido pode producir desnaturalización inesperada e bloqueo do sitio activo seguido da perda natural de actividade. No outro campo discutido nesta tese, as estratexias de xeración de vacinas baseadas en proteínas, tamén se demostraron que as estratexias de inmovilización producen resultados de calidade. Isto débese a que as respostas inmunes a un antíxeno particular mellóranse considerablemente se o antíxeno se presenta e se une a algún tipo de partícula do tamaño dun virus nunha matriz ordenada e repetitiva. Neste campo, o pregamento correcto das proteínas tamén é fundamental para a xeración da resposta inmune óptima fronte ao epítopo / proteína elixido xa que a xeración de anticorpos ou o desencadeamento dunha resposta celular depende moito da conformación do antíxeno.

 O presente estudo explora dous métodos fundamentalmente diferentes para a inmovilización de proteínas: a metodoloxía IC-Tagging usando unha proteína viral modificada e a impresión 3D pensou no uso da estereolitografía (SLA). Investigamos a viabilidade destas estratexias e a súa eficiencia na xeración de proteínas

inmovilizadas correctamente dobradas para diferentes aplicacións no campo dos biocatalizadores e a inmunoterapia contra o cancro.

Capítulo 1. Inmovilización de enzimas e biocatalise mediante a tecnoloxía IC - Tagging.

Os biocatalizadores son ferramentas críticas para a produción e degradación de produtos farmacéuticos e produtos químicos finos debido á súa alta selectividade e especificidade, temperatura de reacción suave e actividade de pH neutra ou próxima a neutra. Ademais, os catalizadores proporcionan menos contaminación e resultados perigosos e un menor consumo de enerxía en comparación cos procesos convencionais de catalizadores. Os biocatalizadores tamén ofrecen novas oportunidades para a síntese de compostos de gran valor que doutro xeito non serían posibles. O número total de procesos de biotransformación realizados a escala industrial aumentou continuamente durante a última década. Non obstante, os biocatalizadores tamén presentan múltiples limitacións, por exemplo, se unha reacción se produce lentamente baixo a temperatura dada e un aumento da temperatura conduciría a un mellor rendemento, este aumento a miúdo leva á desnaturalización do encima implicado no proceso. Ademais, a produción de encimas é cara e adoitan ser necesarios para recuperalos e reutilizalos para que sexan rendibles. Para este propósito, os encimas solubles en medios acuosos requiren o uso de técnicas tediosas para a separación da mestura de reacción. Non obstante, estas limitacións poden abordarse mediante a inmovilización de encimas. A inmovilización de encimas nun soporte sólido ofrece o xeito máis barato de recuperar os encimas a partir de mesturas de reacción. Ademais, engade algunhas características especiais aos biocatalizadores como a mellora operativa, un aumento da estabilidade térmica e do pH, así como protección contra a desnaturalización inducida polos compostos solventes. As maiores desvantaxes da inmovilización están relacionadas coa perda de actividade, a limitación difusiva e o aumento dos custos de produción. A pesar diso, os encimas inmovilizados úsanse regularmente nas industrias farmacéutica, alimentaria e química.

Neste campo, decidimos probar a plataforma de etiquetaxe IC desenvolvida no noso laboratorio. O razoamento detrás do noso enfoque é que as micropartículas foron chamando cada vez máis a atención ao longo dos anos polas súas múltiples aplicacións en áreas moi diferentes, desde a produción industrial ata o tratamento terapéutico ou o diagnóstico. Nesta implementación, a produción de custos e a estabilidade son os principais retos a superar. Co noso método tanto a expresión como a micro / nano-encapsulación realízanse simultaneamente pola célula evitando a necesidade de purificación de proteínas e acoplamento a unha partícula. A razón é que esta proteína é capaz de auto-ensamblarse en estruturas esféricas dentro de células eucariotas e procariotas vivas, formando microesferas (MS) e nanosferas (NS) que se poden purificar facilmente. Ademais, o marcado de calquera proteína coa chamada etiqueta IC provoca a reubicación da proteína / encima seleccionada para formar MS ou NS, terminando coa micro ou nano encapsulación da proteína marcada dentro de MS ou NS. Neste proceso, non hai que incorporar aditivos particulares aos medios de crecemento normais e a formación de partículas facilita a purificación de proteínas encapsuladas por medios mecánicos, reducindo en xeral o custo de todo o proceso de produción. Como a nosa metodoloxía permite a produción e purificación de custos efectivos de proteínas encapsuladas, quixemos explorar a capacidade de NS como portadores de encimas para promover tanto a reutilización de encimas como a estabilización do encima integrado que podería aumentar a aplicabilidade do método de marcado IC para produción de proteínas.

Como encima modelo para este proxecto, escollemos o encima tipo lacasa codificado polo xene CotA de *Bacillus subtilis*. As lacasas (EC 1.10.3.2) son o subgrupo máis grande da superfamilia de proteínas de oxidasas multi-cobre (MCO) e catalizan a oxidación por un electrón de catro moléculas de substrato usando o osíxeno molecular como aceptor final de electróns. O seu amplo espectro de substratos e a súa facilidade de uso xeraron un gran interese, especialmente nos sectores da madeira, biocombustibles, papel, téxtil, produtos químicos finos e alimentarios. Usando esta estratexia, conseguimos a xeración dun reactor enzimático totalmente funcional dentro do NS. Despois da inmovilización, realizamos unha actividade enzimática e caracterización de estabilidade dando lugar a mellores

características de estabilidade e reutilización e demostrando que tamén é viable contra o modelo de axente recalcitrante Reactive Blue 19 (RB19).

Os rendementos de expresión de 30-50 mg / l observáronse en condicións estándar, sen realizar ningún estudo de optimización da expresión. Estes son similares ou incluso superiores aos valores relatados en traballos anteriores onde se realizou a optimización da produción de lacA de CotA en *E. coli*. Descubrimos que o encima contido en NS presentaba unha actividade aumentada nun rango de pH máis amplo en comparación co encima libre, o que concorda cun efecto estabilizador da nanoencapsulación sobre o encima. Ademais, a estabilidade da actividade enzimática fronte á incubación a diferentes valores de pH tamén mostrou un notable aumento na nanoencapsulación.


Observáronse idénticos efectos de estabilización na incubación con diferentes axentes inactivantes como disolventes orgánicos e sales. As concentracións de diferentes reactivos que produciron un efecto nocivo sobre a actividade do encima libre non tiveron ningún efecto sobre a lacasa contida en NS. A maior estabilidade en disolventes orgánicos é particularmente interesante para a aplicación industrial de encimas. O uso de sistemas de disolventes orgánicos en lugar de medios acuosos para a reacción enzimática ofrece numerosas vantaxes; con todo, os disolventes orgánicos a miúdo inactivan os encimas. Por outra banda, os haluros son inhibidores coñecidos das lacasas, o que pode limitar a súa aplicación para a bioremediación de efluentes industriais con composición variable de inhibidores.

En canto ao modelo de axente recalcitrante, os colorantes sintéticos úsanse extensamente en diferentes industrias e o 10-15% dos colorantes empregados durante os procesos de acabado e tingimento acaban nas augas residuais. Os colorantes reactivos baseados en antraquinonas chamaron a atención desde a perspectiva ambiental e toxicolóxica, xa que son extremadamente resistentes á degradación e presentan toxicidade aguda de efectos mutaxénicos. Os sistemas biolóxicos convencionais non son eficientes para a bioremediación e descoloración de colorantes e os métodos físico-químicos están asociados a un alto custo operativo, á formación de subprodutos indesexables, etc. tinguir efluentes de augas residuais contaminadas. Neste sentido, demostrouse que o encima contido en NS decolora o colorante antracínico RB19 con bastante eficiencia en comparación co encima libre. Aínda

que a taxa de descoloración RB19 foi inferior á que se informou recentemente usando *Trametes versicolor* lacasa en solución, foi notablemente superior á alcanzada por unha lacasa fúngica inmovilizada en ausencia dun mediador (só un 5% de decoloración en 6 h). Ademais, cómpre resaltar que a transformación do colorante por NS-lacase podería optimizarse en termos de pH, dosificación de encimas ou temperatura, para unha transformación máis eficiente do substrato.

Ademais, debido á súa natureza particulada, o encima contido en NS pódese recuperar da reacción e volver utilizalo varias veces sen unha perda significativa de actividade. Ademais, debido ao seu pequeno tamaño, algúns NS poderían perderse durante os repetidos pasos de centrifugación e a pequena desintegración da actividade pode explicarse polo contido proteico diminuído. Pódese implementar un método de recuperación mellorado, que inclúa filtración, conexión NS ou outros, para mellorar as taxas de recuperación.

A propiedade máis notable que observamos para este sistema é a estabilización térmica conseguida. É certo que a *B. subtilis* laccase xa é intrínsecamente estable á calor. Non obstante, a versión contida en NS supera amplamente as habilidades do encima libre. Aínda que a versión encapsulada supera a libre en todo o rango de temperatura, está nos valores máis altos de 90 e 95 ° C onde as diferenzas fanse notables. Así, mentres a actividade do encima libre está completamente abrogada despois de 5 min de incubación a 90 ° C, a lacasa contida en NS resistiu polo menos 30 minutos de incubación a esa temperatura sen ningunha perda de actividade apreciable. O rendemento da NS-lacasa só comezou a diminuír ata o 77% da actividade inicial despois de 15 minutos de incubación a 95 ° C. Esta termoestabilidade extrema pode ser beneficiosa para transformacións que se poden acelerar aumentando a temperatura, oxidacións ben mediadas pola lacasa ou reaccións complexas multiencimáticas.



Capítulo 2. Inmovilización de encimas e biocatalise mediante impresión 3D

Agora é común, e case se espera, que un individuo tome dúcias de medicamentos na súa vida, especialmente coa idade avanzada. A medida que se consumen máis medicamentos, consecuentemente excrétanse ou elimínanse, a miúdo impregnan a auga do mundo. As drogas e os seus metabolitos están presentes en case todos os ambientes acuáticos, desde a auga potable ata a auga subterránea, a de mar e as augas residuais. A cuestión é mundial, con países que rexistran importantes concentracións de produtos farmacéuticos na auga en Europa, África, Asia e América. Actualmente, os antibióticos, os analxésicos, os fármacos para baixar os lípidos e os estróxenos son os medicamentos máis contaminados pola auga en todo o mundo; con todo, é probable que o número e a escala reais de drogas sexa maior do que se coñece actualmente, debido ás limitacións e prioridades nas probas. Esta insidia infiltración de contaminantes representa un risco significativo para a saúde global e o equilibrio ecolóxico. Por exemplo, o diclofenaco é un dos medicamentos máis prolíficos que entran na auga, cunha media global de 0,032 µg / L presente en todos os compartimentos de auga superficial. A entrada do diclofenaco nas cadeas alimentarias salvaxes é letal para as aves migratorias, como os voitres. De feito, o diclofenaco provocou o colapso da poboación de tres especies de voitres no sur de Asia e supón unha ameaza significativa para varias especies europeas. Noutros lugares do ambiente, a aparición de estróxenos nos efluentes de augas residuais provocou a feminización dos peixes machos, repercutindo drasticamente no éxito reprodutivo. En canto á saúde humana, a práctica de regar cultivos con augas residuais aumenta o risco de xenotoxicidade dos consumidores, debido á presenza de antineoplásicos solubilizados. Ademais, crese que os antibióticos na auga aumentan as taxas de resistencia a antibióticos bacterianos, un desafío crítico actualmente que ameaza a saúde global no seu conxunto. Incluso as drogas de abuso infiltranse na auga, como destacaron estudos realizados en Madrid e a cidade de Changzhou, China oriental, que atoparon cocaína, opioides e metanfetamina no abastecemento de auga potable e residuais das cidades.

Ante este desafío, a Organización Mundial da Saúde (OMS) puxo en marcha un grupo de traballo para tratar como se pode reducir a carga farmacéutica na auga. Como tal, propuxéronse varios métodos para eliminar drogas da auga, incluídos os procesos de lodos; biofiltración; osmose inversa; ozonización; cloración; e

nanofiltración. Desafortunadamente, moitos destes procesos son variablemente eficientes (con taxas de eliminación de medicamentos ás veces inferiores ao 10%) e, a miúdo, requiren coñecementos técnicos para acceder a equipos caros e de gran tamaño. Así, hai un requisito global de tecnoloxías eficaces que poidan eliminar os medicamentos na auga de forma sinxela e rendible. Idealmente, os métodos tamén deberían funcionar de forma fiable nun rango de ambientes diferentes, independentemente do pH, temperatura ou espazo físico. Polo tanto, son desexables tecnoloxías que se poden personalizar para encaixar en diferentes espazos físicos (como tubos ou maquinaria).

Para solucionar este problema, propoñemos o uso da impresión 3D como método clave de fabricación para dispositivos personalizables. Neste estudo, desenvolvemos, fabricamos e validamos un dispositivo biocatalítico impreso en 3D para a eliminación de medicamentos da auga (decidimos denominalo Printzyme). O Printzyme ten unha morfoloxía totalmente modificable e utiliza o encima lacasa natural, procedente de *Trametes versicolor*, como axente oxidante de fármacos. Como se mencionou, as lacasas atópanse de xeito omnipresente na natureza e demostrouse que degradan efectivamente unha gran variedade de produtos farmacéuticos, incluíndo varias clases de antibióticos, paracetamol, diclofenaco, naproxeno, antidepressivos e estrógenos. Printzyme atrapa a lacasa nun hidrogel mediante impresión 3D por estereolitografía (SLA). O novo proceso inmoviliza o encima e imprime simultaneamente en condicións suaves, o que representa un proceso de fabricación barato e sostible.

Ante este desafío, a Organización Mundial da Saúde (OMS) puxo en marcha un grupo de traballo para tratar como se pode reducir a carga farmacéutica na auga. Como tal, propuxéronse varios métodos para eliminar drogas da auga, incluídos os procesos de lodos; biofiltración; osmose inversa; ozonización; cloración; e nanofiltración. Desafortunadamente, moitos destes procesos son variablemente eficientes (con taxas de eliminación de medicamentos ás veces inferiores ao 10%) e, a miúdo, requiren coñecementos técnicos para acceder a equipos caros e de gran tamaño. Así, hai un requisito global de tecnoloxías eficaces que poidan eliminar os medicamentos na auga de forma sinxela e rendible. Idealmente, os métodos tamén deberían funcionar de forma fiable nun rango de ambientes diferentes,

independentemente do pH, temperatura ou espazo físico. Polo tanto, son desexables tecnoloxías que se poden personalizar para encaixar en diferentes espazos físicos (como tubos ou maquinaria).

Para solucionar este problema, propoñemos o uso da impresión 3D como método clave de fabricación para dispositivos personalizables. Neste estudo, desenvolvemos, fabricamos e validamos un dispositivo biocatalítico impreso en 3D para a eliminación de medicamentos da auga (decidimos denominalo Printzyme). O Printzyme ten unha morfoloxía totalmente modificable e utiliza o encima lacasa natural, procedente de *Trametes versicolor*, como axente oxidante de fármacos. Como se mencionou, as lacasas atópanse de xeito omnipresente na natureza e demostrouse que degradan efectivamente unha gran variedade de produtos farmacéuticos, incluíndo varias clases de antibióticos, paracetamol, diclofenaco, naproxeno, antidepressivos e estrógenos. Printzyme atrapa a lacasa nun hidrogel mediante impresión 3D por estereolitografía (SLA). O novo proceso inmoviliza o encima e imprime simultaneamente en condicións suaves, o que representa un proceso de fabricación barato e sostible.

Este estudo forma parte dunha colaboración co doutor Alvaro Goyanes e o profe Abdul Bassit no University College de Londres (UCL) e coa doutora Gemma Eibes do CRETUS da Universidade de Santiago (USC). A base detrás da iniciativa reside na capacidade desta tecnoloxía para soportar a construción de obxectos colocando consecutivamente capas de material baseadas nun deseño de ordenador. Polo tanto, proporcionar os medios para fabricar obxectos personalizados baixo demanda que se usarán en diferentes áreas, incluíndo a saúde e a industria. En concreto, a estereolitografía (SLA) ofrece a posibilidade de fabricar matrices poliméricas reticuladas mediante fotopolimerización, cunha resolución superior evitando a necesidade de altas temperaturas. Por esta razón, o SLA empregouse para producir hidroxelos cargados de encimas que contiñan un contido variable en auga. O SLA tivo éxito na produción de hidroxelos mantendo a actividade enzimática e mellorando características como a estabilidade e a reutilización. A modificación do rendemento dos encimas tamén foi posible variando o contido enzimático e a xeometría das impresións, demostrando ser adecuado para a fabricación de reactores encimáticos de forma flexible e directa.

Ao estudar os requirimentos de pH e temperatura para a actividade enzimática, a lacasa libre demostrou unha actividade maior que a inmovilizada en Printzyme. Isto é probable porque dado que está en forma solubilizada, todos os sitios activos de lacasa son de libre acceso, mentres que en Printzyme a inmovilización do encima leva a un certo grao de inhibición estérica. Aínda que Printzymes conseguen unha actividade máis baixa en solucións acuosas en comparación coa lacasa libre, aínda conservan unha actividade substancial. Ademais, as formulacións Printzyme demostraron relacións similares ao pH e á temperatura como a lacasa libre, o que indica que a inmovilización directa da lacasa en hidroxelos PEGDA non altera o mecanismo biocatalítico. Ademais, a inmovilización proporciona beneficios para almacenar e reutilizar que o encima libre en solución non pode conseguir. O atrapamento de encimas dentro de sistemas funcionais mellora a sostibilidade e a relación custo-efectividade xa que non se perden encimas caros con cada uso. Isto é especialmente importante para axustes con almacenamento limitado, orzamentos ou acceso a entregas (por exemplo, en lugares remotos).

En canto á reutilización, Printzymes mostrou unha boa actividade lacasa durante polo menos 18 usos illados; demostrando a súa superioridade sobre a lacasa libre en solución. Ambos os dous deseños Printzymes lograron unha reutilización superior en comparación con outros métodos de inmovilización da lacasa de *Trametes versicolor*, incluíndo nanopartículas de óxido de ferro ao 33%, microconxuntos de quitosano, esferas magnéticas de sílice mesoporosas, microesferas baseadas en poli (glicidil metacrilato) e agar-agar, poliacrilamida e xelatina estruturas. Como se mencionou, un dos principais beneficios de Printzyme é a súa inmovilización da lacasa, xa que isto permite a recuperación do encima e o uso repetido non é posible co encima libre en solución. Estes datos destacan a relación custo-efectividade, a sustentabilidade e o axuste ao propósito. Ademais, Printzyme podería reducir con éxito as concentracións de dous fármacos, o diclofenaco e o etinilestradiol, en solución acuosa. Os dispositivos eliminaron máis do 80% de diclofenaco disolto en 24 horas e o 95% de etinilestradiol en só 2 horas, sendo a forma do toro máis eficiente debido á maior relación superficie / volume. O factor de eficacia para a eliminación de estróxenos foi próximo a un (0,95 para o toro Printzyme), demostrando que a difusión do substrato a través do Printzyme non

limitou a transformación. En canto ao diclofenaco, o dispositivo proporcionou maiores taxas de eliminación inicial que o encima libre, cun factor de efectividade de 1,55 (toro Printzyme), facendo fincapé no interese de usar Printzyme para a transformación de substratos que poden inhibir a lacasa. Isto implica que o factor de efectividade alcanzou valores superiores a un. O factor de eficacia xeralmente atópase entre 0 e 1, pero ás veces pode ser superior a un debido a un funcionamento non isotérmico, debido á estabilización do encima encapsulado relacionado co libre ou por efectos inhibitorios, sendo a explicación máis plausible aquí o posible inhibición causada por altas concentracións de diclofenaco no encima libre. O printzima pode ter taxas de degradación aumentadas ao reducir a concentración do substrato a concentracións non inhibitorias. Polo tanto, Printzyme representa a opción máis económica e sostible non só pola súa reutilización senón tamén porque foi máis eficaz que o encima libre na degradación do diclofenaco a curto prazo.

Este traballo destaca o potencial da impresión 3D SLA como un enfoque simplificado para atrapar encimas en condicións suaves. Os nosos resultados presentan un enfoque significativamente eficaz e sostible para a eliminación de contaminantes farmacéuticos de sistemas acuosos e proporcionan implicacións para o desenvolvemento de solucións de biorremediación.

Capítulo 3. Inmobilización de epítomos do cancro a través da tecnoloxía IC - Tagging

O concepto de mobilizar o sistema inmunitario humano contra o cancro remóntase polo menos a mediados do século XIX cando Rudolf Virchow, un patólogo alemán, observou infiltración inmune en tumores humanos. Desde 2011, debido ao seu potencial para obter un gran beneficio clínico sostido, a inmunoncología converteuse na área de maior crecemento non só en oncoloxía, senón en toda a industria farmacéutica. Non obstante, aínda que algúns pacientes poden lograr a curación ou o control da enfermidade a longo prazo con tratamentos de primeira ou segunda xeración, a maioría dos pacientes aínda necesitan un tratamento beneficioso de próxima xeración. En concreto, moitos pacientes non responden á

inhibición do punto de control ou responden e posteriormente recaen. Os obxectivos de inmunidade innata (por exemplo, as terapias de orientación celular por asasinos naturais (NK)) están a gañar moito interese e neste campo están xurdindo novos enfoques e medicamentos. Un destes enfoques son as vacinas que inducen unha resposta inmune contra antígenos únicos específicos do tumor (neoantígenos). Así, enfoques máis individualizados baseados en novas ideas científicas sobre as vacinas contra o cancro están entrando na etapa de inmuno-oncoloxía. As vacinas baseadas en neoantígenos deberían inducir unha forte resposta inmune específica e provocar efectos terapéuticos estables. Non obstante, no campo da oncoloxía é moi complexo predicir cando e onde se producirían as células tumorais (a non ser que o paciente sufra de síndromes raros específicos) e cales serían as sinaturas antixénicas deses eventos e, polo tanto, as vacinas contra o cancro adoitan ser de uso terapéutico. Por iso, o termo "vacina" refírese a unha formulación que normalmente inclúe un adxuvante forte ou é adxuvante en si, e proteínas ou péptidos tumorais que ceban o sistema inmunitario.

O mencionado panorama actual de estudos clínicos que proban diferentes rutas de activación da inmunoterapia contra o cancro elucida a necesidade de entrega e métodos de presentación adecuados ao tecido tumoral. A inmunoterapia tumoral está a adquirir impulso clínico, xa que, tal e como se presentou, tales enfoques mostran resultados prometedores ao desencadear a inmunidade específica do tumor local, evitando ao mesmo tempo os potenciais efectos fóra do obxectivo para o tecido saudable, diminuíndo así os efectos adversos.

Aquí, pretendemos probar se a anterior plataforma de etiquetaxe IC mencionada en forma de metodoloxía de presentación de antígenos sintonizables multivalentes funciona nunha configuración de inmunoterapia contra o cancro cando os NS están cargados de neoantígenos cancerixenos, individualmente ou simultaneamente en partículas multivalentes. Este estudo realizouse no Instituto Nacional de Estándares e Control Biolóxicos (NIBSC) coa colaboración da doutora Sandra Diebold. A Sección de Inmunoloxía Celular de NIBSC ten experiencia na investigación de conxugados anticorpo-adxuvante para a inmunoterapia tumoral, incluído un modelo de tumor de rato establecido e varios ensaios de activación in vitro e liberación de citocinas, así como ensaios de linfocitos T citotóxicos (CTL) in

vivo. Para este propósito, decidimos empregar o modelo de pseudo-metástase B16-OVA que é unha liña celular de melanoma que expresa OVA. Ademais, decidimos incluír outro antígeno que se expresa naturalmente polas células do melanoma B16 e pode mediar a inmunidade antitumoral coñecida como TRP2.

Para este traballo, as bacterias transformadas con plásmidos modificados produciron NS que conteñen as proteínas marcadas con IC á indución da expresión, adecuadas para a vacinación. Ao realizar unha caracterización completa dos patróns innatos de activación inmune e adaptativa tanto in vivo como in vitro, estamos en condicións de identificar os puntos fortes no deseño de novas vacinas contra o cancro baseadas na nosa NS e / ou EM.

Primeiro para a experimentación in vitro, coa axuda da proba de activación de monocitos (MAT) usando células mononucleares de sangue periférico (PBMCs) e o uso de células dendríticas da medula ósea (BMDC) demostramos que as NS inducen altos niveis de IL-6 e outras citocinas. Ademais, o TNF alfa parece estar inducido en niveis proporcionalmente máis altos en resposta ao NS cando se compara co LPS.

En segundo lugar, con respecto á indución in vivo da resposta antitumoral en ratos (que é probablemente o resultado máis importante), puidemos ver que o NS induce unha resposta CTL específica ao antígeno in vivo en ratos. Ademais, puidemos identificar a indución dunha resposta inmune antitumoral efectiva no modelo de pseudo-metástase do rato. Requírense máis experimentos para avaliar a resposta inmune antitumoral e investigar se dirixirse ao antígeno asociado ao tumor de boa fe TRP2 tamén é eficaz para inducir a inmunidade antitumoral.

Finalmente, non fomos capaces de realizar o seguimento in vivo da biodistribución NS. A razón é que o NS marcado con luciferase non parece adecuado para controlar a bio-distribución de nanosferas mediante imaxes in vivo. As células que expresan luciferase proporcionan o ATP necesario para que a reacción enzimática teña lugar en presenza do substrato luciferina, con todo, non está claro en que forma se podería proporcionar ATP in vivo para permitir a reacción enzimática en caso de NS marcado con luciferase. E a máquina IVIS non parece ser o suficientemente sensible como para captar o sinal fluorescente emitido desde as nanosferas etiquetadas con Halo. Tamén é posible que etiquetar o NS cunha relación NS: ligando máis alta poida superar este problema.

Declaration of conflict of interest

I declare that I have no conflict of interest in relation to the doctoral thesis with title: Novel protein immobilization approaches for the development of vaccine candidates and enzymatic reactors.

Declaration of authorship of figures

I declare that all figures are made by me unless those indicated at the figure footer.



Tomas Pose Boirazian

References

1. Bachmann MF, Jennings GT. Vaccine delivery: a matter of size, geometry, kinetics and molecular patterns. *Nature Reviews Immunology*. 2010;10(11):787-96.
2. Morrison TG. Protein conformation in a vaccine matters. *Oncotarget*. 2015;6(26):21781.
3. Oh SJ, Hong BJ, Choi KY, Park JW. Surface modification for DNA and protein microarrays. *OMICS: A journal of Integrative Biology*. 2006;10(3):327-43.
4. Rusmini F, Zhong Z, Feijen J. Protein immobilization strategies for protein biochips. *Biomacromolecules*. 2007;8(6):1775-89.
5. Barbosa O, Torres R, Ortiz C, Berenguer-Murcia An, Rodrigues RC, Fernandez-Lafuente R. Heterofunctional supports in enzyme immobilization: from traditional immobilization protocols to opportunities in tuning enzyme properties. *Biomacromolecules*. 2013;14(8):2433-62.
6. Samanta D, Sarkar A. Immobilization of bio-macromolecules on self-assembled monolayers: methods and sensor applications. *Chemical Society Reviews*. 2011;40(5):2567-92.
7. Rhim JS, Jordan LE, Mayor HD. Cytochemical, fluorescent-antibody and electron microscopic studies on the growth of reovirus (ECHO 10) in tissue culture. *Virology*. 1962;17(2):342-55.
8. Dryden KA, Wang G, Yeager M, Nibert ML, Coombs KM, Furlong DB, et al. Early steps in reovirus infection are associated with dramatic changes in supramolecular structure and protein conformation: analysis of virions and subviral particles by cryoelectron microscopy and image reconstruction. *The Journal of cell biology*. 1993;122(5):1023-41.
9. Benavente J, Martínez-Costas J. Avian reovirus: structure and biology. *Virus research*. 2007;123(2):105-19.
10. Rosenberger J, Sterner F, Botts S, Lee K, Margolin A. In vitro and in vivo characterization of avian reoviruses. I. Pathogenicity and antigenic relatedness of several avian reovirus isolates. *Avian diseases*. 1989:535-44.
11. Grande A, Rodriguez E, Costas C, Everitt E, Benavente J. Oligomerization and Cell-Binding Properties of the Avian Reovirus Cell-Attachment Protein ζ C. *Virology*. 2000;274(2):367-77.
12. Shapouri MR, Arella M, Silim A. Evidence for the multimeric nature and cell binding ability of avian reovirus σ 3 protein. *Journal of General Virology*. 1996;77(6):1203-10.
13. Duncan R, Chen Z, Walsh S, Wu S. Avian reovirus-induced syncytium formation is independent of infectious progeny virus production and enhances the rate, but is not essential, for virus-induced cytopathology and virus egress. *Virology*. 1996;224(2):453-64.
14. Labrada L, Bodelón G, Viñuela J, Benavente J. Avian reoviruses cause apoptosis in cultured cells: viral uncoating, but not viral gene expression, is required for apoptosis induction. *Journal of Virology*. 2002;76(16):7932-41.
15. Martínez-Costas J, Varela R, Benavente J. Endogenous enzymatic activities of the avian reovirus S1133: identification of the viral capping enzyme. *Virology*. 1995;206(2):1017-26.
16. Silverstein SC, Schur PH. Immunofluorescent localization of double-stranded RNA in reovirus-infected cells. *Virology*. 1970;41(3):564-6.
17. Tourís-Otero F, Cortez-San Martín M, Martínez-Costas J, Benavente J. Avian reovirus morphogenesis occurs within viral factories and begins with the selective recruitment of sigmaNS and lambdaA to microNS inclusions. *Journal of molecular biology*. 2004;341(2):361.
18. Bodelón G, Labrada La, Martínez-Costas J, Benavente J. Modification of Late Membrane Permeability in Avian Reovirus-infected Cells VIROPORIN ACTIVITY OF

THE S1-ENCODED NONSTRUCTURAL p10 PROTEIN. *Journal of Biological Chemistry*. 2002;277(20):17789-96.

19. Rodríguez-Grille J, Busch LK, Martínez-Costas J, Benavente J. Avian reovirus-triggered apoptosis enhances both virus spread and the processing of the viral nonstructural muNS protein. *Virology*. 2014;462:49-59.
20. Touris-Otero F, Martínez-Costas J, Vakharia VN, Benavente J. Avian reovirus nonstructural protein μ NS forms viroplasm-like inclusions and recruits protein σ NS to these structures. *Virology*. 2004;319(1):94-106.
21. Brandariz-Nuñez A, Menaya-Vargas R, Benavente J, Martínez-Costas J. A versatile molecular tagging method for targeting proteins to avian reovirus muNS inclusions. Use in protein immobilization and purification. *PLoS One*. 2010;5(11):e13961.
22. Yarbrough D, Wachter RM, Kallio K, Matz MV, Remington SJ. Refined crystal structure of DsRed, a red fluorescent protein from coral, at 2.0-Å resolution. *Proceedings of the National Academy of Sciences*. 2001;98(2):462-7.
23. Brandariz-Nuñez A, Otero-Romero I, Benavente J, Martínez-Costas JM. IC-tagged proteins are able to interact with each other and perform complex reactions when integrated into muNS-derived inclusions. *Journal of biotechnology*. 2011;155(3):284-6.
24. Barreiro-Piñero N, Lostalé-Seijo I, Varela-Calviño R, Benavente J, Martínez-Costas JM. IC-Tagging methodology applied to the expression of viral glycoproteins and the difficult-to-express membrane-bound IGRP autoantigen. *Scientific reports*. 2018;8(1):1-12.
25. Marín-López A, Calvo-Pinilla E, Barriales D, Lorenzo G, Benavente J, Brun A, et al. Microspheres-prime/rMVA-boost vaccination enhances humoral and cellular immune response in IFNAR (-/-) mice conferring protection against serotypes 1 and 4 of bluetongue virus. *Antiviral research*. 2017;142:55-62.
26. Hull CW. Apparatus for production of three-dimensional objects by stereolithography. United States Patent, Appl, No 638905, Filed. 1984.
27. Ligon SC, Liska R, Stampfl J, Gurr M, Mulhaupt R. Polymers for 3D printing and customized additive manufacturing. *Chemical reviews*. 2017;117(15):10212-90.
28. Huang SH, Liu P, Mokasdar A, Hou L. Additive manufacturing and its societal impact: a literature review. *The International Journal of Advanced Manufacturing Technology*. 2013;67(5):1191-203.
29. Touri M, Kabirian F, Saadati M, Ramakrishna S, Mozafari M. Additive manufacturing of biomaterials— the evolution of rapid prototyping. *Advanced Engineering Materials*. 2019;21(2):1800511.
30. Bose S, Ke D, Sahasrabudhe H, Bandyopadhyay A. Additive manufacturing of biomaterials. *Progress in materials science*. 2018;93:45-111.
31. Liu Z, Zhang M, Bhandari B, Wang Y. 3D printing: Printing precision and application in food sector. *Trends in Food Science & Technology*. 2017;69:83-94.
32. Trenfield SJ, Awad A, Goyanes A, Gaisford S, Basit AW. 3D printing pharmaceuticals: drug development to frontline care. *Trends in pharmacological sciences*. 2018;39(5):440-51.
33. Blanchette CD, Knipe JM, Stolaroff JK, DeOtte JR, Oakdale JS, Maiti A, et al. Printable enzyme-embedded materials for methane to methanol conversion. *Nature communications*. 2016;7(1):1-9.
34. Fina F, Goyanes A, Rowland M, Gaisford S, W Basit A. 3D Printing of Tunable Zero-Order Release Printlets. *Polymers*. 2020;12(8):1769.
35. Sadia M, Arafat B, Ahmed W, Forbes RT, Alhnan MA. Channelled tablets: An innovative approach to accelerating drug release from 3D printed tablets. *Journal of Controlled Release*. 2018;269:355-63.
36. Pereira BC, Isreb A, Isreb M, Forbes RT, Oga EF, Alhnan MA. Additive manufacturing of a Point-of-Care “Polypill.” Fabrication of concept capsules of complex

geometry with bespoke release against cardiovascular disease. *Advanced Healthcare Materials*. 2020;9(13):2000236.

37. Rycerz K, Stepien KA, Czapiewska M, Arafat BT, Habashy R, Isreb A, et al. Embedded 3D printing of novel bespoke soft dosage form concept for pediatrics. *Pharmaceutics*. 2019;11(12):630.

38. Goyanes A, Det-Amornrat U, Wang J, Basit AW, Gaisford S. 3D scanning and 3D printing as innovative technologies for fabricating personalized topical drug delivery systems. *Journal of controlled release*. 2016;234:41-8.

39. Xu X, Awad A, Martinez PR, Gaisford S, Goyanes A, Basit AW. Vat photopolymerization 3D printing for advanced drug delivery and medical device applications. *Journal of Controlled Release*. 2020.

40. Williams H, Butler-Jones E. Additive manufacturing standards for space resource utilization. *Additive Manufacturing*. 2019;28:676-81.

41. Trenfield SJ, Awad A, Madla CM, Hatton GB, Firth J, Goyanes A, et al. Shaping the future: recent advances of 3D printing in drug delivery and healthcare. *Expert opinion on drug delivery*. 2019;16(10):1081-94.

42. Sachs EM, Haggerty JS, Cima MJ, Williams PA. Three-dimensional printing techniques. *Google Patents*; 1993.

43. Ziaee M, Crane NB. Binder jetting: A review of process, materials, and methods. *Additive Manufacturing*. 2019;28:781-801.

44. Mirzababaei S, Pasebani S. A review on binder jet additive manufacturing of 316L stainless steel. *Journal of Manufacturing and Materials Processing*. 2019;3(3):82.

45. Shirazi SFS, Gharekhani S, Mehrali M, Yarmand H, Metselaar HSC, Kadri NA, et al. A review on powder-based additive manufacturing for tissue engineering: selective laser sintering and inkjet 3D printing. *Science and technology of advanced materials*. 2015.

46. Le Néel TA, Mognol P, Hascoët J-Y. A review on additive manufacturing of sand molds by binder jetting and selective laser sintering. *Rapid Prototyping Journal*. 2018.

47. Rojas-Nastrucci EA, Nussbaum JT, Crane NB, Weller TM. Ka-band characterization of binder jetting for 3-D printing of metallic rectangular waveguide circuits and antennas. *IEEE Transactions on Microwave Theory and Techniques*. 2017;65(9):3099-108.

48. Inzana JA, Olvera D, Fuller SM, Kelly JP, Graeve OA, Schwarz EM, et al. 3D printing of composite calcium phosphate and collagen scaffolds for bone regeneration. *Biomaterials*. 2014;35(13):4026-34.

49. Wu BM, Borland SW, Giordano RA, Cima LG, Sachs EM, Cima MJ. Solid free-form fabrication of drug delivery devices. *J Control Release*. 1996;40(1-2):77-87.

50. Wang C-C, Tejwani MR, Roach WJ, Kay JL, Yoo J, Surprenant HL, et al. Development of near zero-order release dosage forms using three-dimensional printing (3-DPT™) technology. *Drug development and industrial pharmacy*. 2006;32(3):367-76.

51. Katstra W, Palazzolo R, Rowe C, Giritlioglu B, Teung P, Cima M. Oral dosage forms fabricated by Three Dimensional Printing™. *J Control Release*. 2000;66(1):1-9.

52. Apprecia Pharmaceuticals. FDA Approves the First 3D Printed Drug Product 2015 [Available from: <https://www.aprecia.com/news/fda-approves-the-first-3d-printed-drug-product>].

53. Fina F, Gaisford S, Basit AW. Powder bed fusion: The working process, current applications and opportunities. *3D printing of pharmaceuticals*: Springer; 2018. p. 81-105.

54. Awad A, Fina F, Goyanes A, Gaisford S, Basit AW. 3D printing: Principles and pharmaceutical applications of selective laser sintering. *Int J Pharm*. 2020;586:119594.

55. Novakov T, Jackson M, Robinson G, Ahmed W, Phoenix D. Laser sintering of metallic medical materials—a review. *The International Journal of Advanced Manufacturing Technology*. 2017;93(5):2723-52.

56. George M, Aroom KR, Hawes HG, Gill BS, Love J. 3D printed surgical instruments: the design and fabrication process. *World journal of surgery*. 2017;41(1):314-9.
57. Tan K, Chua C, Leong K, Cheah C, Cheang P, Bakar MA, et al. Scaffold development using selective laser sintering of polyetheretherketone–hydroxyapatite biocomposite blends. *Biomaterials*. 2003;24(18):3115-23.
58. Chua C, Leong K, Tan K, Wiria F, Cheah C. Development of tissue scaffolds using selective laser sintering of polyvinyl alcohol/hydroxyapatite biocomposite for craniofacial and joint defects. *Journal of Materials Science: Materials in Medicine*. 2004;15(10):1113-21.
59. Revilla-León M, Özcan M. Additive manufacturing technologies used for 3D metal printing in dentistry. *Current Oral Health Reports*. 2017;4(3):201-8.
60. Hettesheimer T, Hirzel S, Roß HB. Energy savings through additive manufacturing: An analysis of selective laser sintering for automotive and aircraft components. *Energy Efficiency*. 2018;11(5):1227-45.
61. Williams J, Revington P. Novel use of an aerospace selective laser sintering machine for rapid prototyping of an orbital blowout fracture. *International journal of oral and maxillofacial surgery*. 2010;39(2):182-4.
62. Theodorakos I, Zacharatos F, Geremia R, Karnakis D, Zergioti I. Selective laser sintering of Ag nanoparticles ink for applications in flexible electronics. *Applied surface science*. 2015;336:157-62.
63. Fina F, Goyanes A, Gaisford S, Basit AW. Selective laser sintering (SLS) 3D printing of medicines. *Int J Pharm*. 2017;529(1-2):285-93.
64. Fina F, Madla CM, Goyanes A, Zhang J, Gaisford S, Basit AW. Fabricating 3D printed orally disintegrating printlets using selective laser sintering. *International journal of pharmaceutics*. 2018;541(1-2):101-7.
65. Awad A, Fina F, Trenfield SJ, Patel P, Goyanes A, Gaisford S, et al. 3D Printed Pellets (Miniprintlets): A Novel, Multi-Drug, Controlled Release Platform Technology. *Pharmaceutics*. 2019;11(4).
66. Awad A, Yao A, Trenfield SJ, Goyanes A, Gaisford S, Basit AW. 3D Printed Tablets (Printlets) with Braille and Moon Patterns for Visually Impaired Patients. *Pharmaceutics*. 2020;12(2):172.
67. Yap YL, Wang C, Sing SL, Dikshit V, Yeong WY, Wei J. Material jetting additive manufacturing: An experimental study using designed metrological benchmarks. *Precision engineering*. 2017;50:275-85.
68. Awad A, Trenfield SJ, Goyanes A, Gaisford S, Basit AW. Reshaping drug development using 3D printing. *Drug Discov Today*. 2018;23(8):1547-55.
69. Yap YL, Tan YSE, Tan HKJ, Peh ZK, Low XY, Yeong WY, et al. 3D printed bio-models for medical applications. *Rapid prototyping journal*. 2017.
70. Wallin T, Pikul J, Shepherd R. 3D printing of soft robotic systems. *Nature Reviews Materials*. 2018;3(6):84-100.
71. Bhattacharjee N, Urrios A, Kang S, Folch A. The upcoming 3D-printing revolution in microfluidics. *Lab Chip*. 2016;16(10):1720-42.
72. Nikolova MP, Chavali MS. Recent advances in biomaterials for 3D scaffolds: A review. *Bioactive materials*. 2019;4:271-92.
73. Scoutaris N, Ross S, Douroumis D. Current trends on medical and pharmaceutical applications of inkjet printing technology. *Pharm Res*. 2016;33(8):1799-816.
74. Buanz AB, Saunders MH, Basit AW, Gaisford S. Preparation of personalized-dose salbutamol sulphate oral films with thermal ink-jet printing. *Pharm Res*. 2011;28(10):2386-92.
75. Ian Gibson IG. *Additive Manufacturing Technologies 3D Printing, Rapid Prototyping, and Direct Digital Manufacturing*. Springer; 2015.

76. Najmon JC, Raeisi S, Tovar A. Review of additive manufacturing technologies and applications in the aerospace industry. *Additive manufacturing for the aerospace industry*. 2019;7-31.
77. Saboori A, Aversa A, Marchese G, Biamino S, Lombardi M, Fino P. Application of directed energy deposition-based additive manufacturing in repair. *Applied Sciences*. 2019;9(16):3316.
78. Portolés L, Jordá O, Jordá L, Uriondo A, Esperon-Miguez M, Perinpanayagam S. A qualification procedure to manufacture and repair aerospace parts with electron beam melting. *Journal of Manufacturing Systems*. 2016;41:65-75.
79. Mudge RP, Wald NR. Laser engineered net shaping advances additive manufacturing and repair. *Welding Journal-New York-*. 2007;86(1):44.
80. Ambrosi A, Pumera M. 3D-printing technologies for electrochemical applications. *Chemical Society Reviews*. 2016;45(10):2740-55.
81. Gibson I, Rosen DW, Stucker B. Sheet lamination processes. *Additive Manufacturing Technologies*: Springer; 2010. p. 223-52.
82. Bournias-Varotsis A, Friel RJ, Harris RA, Engstrøm DS. Ultrasonic Additive Manufacturing as a form-then-bond process for embedding electronic circuitry into a metal matrix. *Journal of Manufacturing Processes*. 2018;32:664-75.
83. Azad MA, Olawuni D, Kimbell G, Badruddoza AZM, Hossain M, Sultana T. Polymers for extrusion-based 3D printing of pharmaceuticals: A holistic materials–process perspective. *Pharmaceutics*. 2020;12(2):124.
84. Awad A, Gaisford S, Basit AW. Fused Deposition Modelling: Advances in Engineering and Medicine. In: Basit AW, Gaisford S, editors. *3D Printing of Pharmaceuticals*. Cham: Springer International Publishing; 2018. p. 107-32.
85. Tao Y, Wang H, Li Z, Li P, Shi SQ. Development and application of wood flour-filled polylactic acid composite filament for 3D printing. *Materials*. 2017;10(4):339.
86. Palmero EM, Casaleiz D, de Vicente J, Hernández-Vicen J, López-Vidal S, Ramiro E, et al. Composites based on metallic particles and tuned filling factor for 3D-printing by Fused Deposition Modeling. *Composites Part A: Applied Science and Manufacturing*. 2019;124:105497.
87. Gnanasekaran K, Heijmans T, Van Bennekom S, Woldhuis H, Wijnia S, de With G, et al. 3D printing of CNT-and graphene-based conductive polymer nanocomposites by fused deposition modeling. *Applied materials today*. 2017;9:21-8.
88. Tan DK, Maniruzzaman M, Nokhodchi A. Advanced pharmaceutical applications of hot-melt extrusion coupled with fused deposition modelling (FDM) 3D printing for personalised drug delivery. *Pharmaceutics*. 2018;10(4):203.
89. Melocchi A, Uboldi M, Cerea M, Foppoli A, Maroni A, Moutaharrik S, et al. A graphical review on the escalation of fused deposition modeling (FDM) 3D printing in the pharmaceutical field. *J Pharm Sci*. 2020;109(10):2943-57.
90. Goyanes A, Fina F, Martorana A, Sedough D, Gaisford S, Basit AW. Development of modified release 3D printed tablets (printlets) with pharmaceutical excipients using additive manufacturing. *Int J Pharm*. 2017;527(1-2):21-30.
91. Jiang T, Munguia-Lopez JG, Flores-Torres S, Kort-Mascort J, Kinsella JM. Extrusion bioprinting of soft materials: An emerging technique for biological model fabrication. *Applied Physics Reviews*. 2019;6(1):011310.
92. Placone JK, Engler AJ. Recent advances in extrusion-based 3D printing for biomedical applications. *Advanced healthcare materials*. 2018;7(8):1701161.
93. Muth JT, Vogt DM, Truby RL, Mengüç Y, Kolesky DB, Wood RJ, et al. Embedded 3D printing of strain sensors within highly stretchable elastomers. *Adv Mater*. 2014;26(36):6307-12.

94. Yuk H, Lu B, Lin S, Qu K, Xu J, Luo J, et al. 3D printing of conducting polymers. *Nature communications*. 2020;11(1):1-8.
95. Agarwala S, Lee JM, Ng WL, Layani M, Yeong WY, Magdassi S. A novel 3D bioprinted flexible and biocompatible hydrogel bioelectronic platform. *Biosensors and Bioelectronics*. 2018;102:365-71.
96. Karyappa R, Hashimoto M. Chocolate-based ink three-dimensional printing (Ci3DP). *Scientific reports*. 2019;9(1):1-11.
97. Yang F, Zhang M, Prakash S, Liu Y. Physical properties of 3D printed baking dough as affected by different compositions. *Innovative food science & emerging technologies*. 2018;49:202-10.
98. Goyanes A, Madla CM, Umerji A, Piñeiro GD, Montero JMG, Diaz MJL, et al. Automated therapy preparation of isoleucine formulations using 3D printing for the treatment of MSUD: First single-centre, prospective, crossover study in patients. *Int J Pharm*. 2019;567:118497.
99. Karavasili C, Gkaragkounis A, Moschakis T, Ritzoulis C, Fatouros DG. Paediatric-friendly chocolate-based dosage forms for the oral administration of both hydrophilic and lipophilic drugs fabricated with extrusion-based 3D printing. *Eur J Pharm Sci*. 2020:105291.
100. Khaled SA, Burley JC, Alexander MR, Yang J, Roberts CJ. 3D printing of five-in-one dose combination polypill with defined immediate and sustained release profiles. *J Control Release*. 2015;217:308-14.
101. Rowe C, Katstra W, Palazzolo R, Giritlioglu B, Teung P, Cima M. Multimechanism oral dosage forms fabricated by three dimensional printing™. *J Control Release*. 2000;66(1):11-7.
102. Seoane-Viaño I, Ong JJ, Luzardo-Álvarez A, González-Barcia M, Basit AW, Otero-Espinar FJ, et al. 3D printed tacrolimus suppositories for the treatment of ulcerative colitis. *Asian Journal of Pharmaceutical Sciences*. 2020.
103. Naseri E, Cartmell C, Saab M, Kerr RG, Ahmadi A. Development of 3D printed drug-eluting scaffolds for preventing piercing infection. *Pharmaceutics*. 2020;12(9):901.
104. Li W, Mille LS, Robledo JA, Uribe T, Huerta V, Zhang YS. Recent Advances in Formulating and Processing Biomaterial Inks for Vat Polymerization-Based 3D Printing. *Advanced Healthcare Materials*. 2020:2000156.
105. Ghosh U, Ning S, Wang Y, Kong YL. Addressing unmet clinical needs with 3D printing technologies. *Advanced healthcare materials*. 2018;7(17):1800417.
106. Johnson AR, Caudill CL, Tumbleston JR, Bloomquist CJ, Moga KA, Ermoshkin A, et al. Single-Step Fabrication of Computationally Designed Microneedles by Continuous Liquid Interface Production. *PLOS ONE*. 2016;11(9):e0162518.
107. Tumbleston JR, Shirvanyants D, Ermoshkin N, Januszewicz R, Johnson AR, Kelly D, et al. Continuous liquid interface production of 3D objects. *Science*. 2015;347(6228):1349-52.
108. Loterie D, Delrot P, Moser C. High-resolution tomographic volumetric additive manufacturing. *Nature communications*. 2020;11(1):1-6.
109. Kelly BE, Bhattacharya I, Heidari H, Shusteff M, Spadaccini CM, Taylor HK. Volumetric additive manufacturing via tomographic reconstruction. *Science*. 2019;363(6431):1075-9.
110. Kawata S, Sun H-B, Tanaka T, Takada K. Finer features for functional microdevices. *Nature*. 2001;412(6848):697-8.
111. Ng WL, Lee JM, Zhou M, Chen Y-W, Lee K-XA, Yeong WY, et al. Vat polymerization-based bioprinting—process, materials, applications and regulatory challenges. *Biofabrication*. 2020;12(2):022001.

112. Vivero-Lopez M, Xu X, Muras A, Otero A, Concheiro A, Gaisford S, et al. Antibiofilm multi drug-loaded 3D printed hearing aids. *Materials Science and Engineering: C*. 2020;111606.
113. Bagheri A, Jin J. Photopolymerization in 3D Printing. *ACS Applied Polymer Materials*. 2019;1(4):593-611.
114. Wang MO, Vorwald CE, Dreher ML, Mott EJ, Cheng MH, Cinar A, et al. Evaluating 3D-Printed biomaterials as scaffolds for vascularized bone tissue engineering. *Adv Mater*. 2015;27(1):138-44.
115. Gardan J. Additive manufacturing technologies: state of the art and trends. *International Journal of Production Research*. 2016;54(10):3118-32.
116. Joshi SC, Sheikh AA. 3D printing in aerospace and its long-term sustainability. *Virtual and Physical Prototyping*. 2015;10(4):175-85.
117. Valentine AD, Busbee TA, Boley JW, Raney JR, Chortos A, Kotikian A, et al. Hybrid 3D printing of soft electronics. *Adv Mater*. 2017;29(40):1703817.
118. Lewis JA, Ahn BY. Three-dimensional printed electronics. *Nature*. 2015;518(7537):42-3.
119. Tay YWD, Panda B, Paul SC, Noor Mohamed NA, Tan MJ, Leong KF. 3D printing trends in building and construction industry: a review. *Virtual and Physical Prototyping*. 2017;12(3):261-76.
120. Yang F, Zhang M, Bhandari B. Recent development in 3D food printing. *Critical reviews in food science and nutrition*. 2017;57(14):3145-53.
121. Prendergast ME, Burdick JA. Recent advances in enabling technologies in 3D printing for precision medicine. *Adv Mater*. 2020;32(13):1902516.
122. Trenfield SJ, Awad A, Madla CM, Hatton GB, Firth J, Goyanes A, et al. Shaping the future: recent advances of 3D printing in drug delivery and healthcare. *Expert opinion on drug delivery*. 2019:1081-94.
123. Awad A, Trenfield SJ, Gaisford S, Basit AW. 3D printed medicines: A new branch of digital healthcare. *Int J Pharm*. 2018;548(1):586-96.
124. Elbadawi M, Ong JJ, Pollard TD, Gaisford S, Basit AW. Additive Manufacturable Materials for Electrochemical Biosensor Electrodes. *Advanced Functional Materials*. 2020:2006407.
125. Wannarumon S, Bohez EL. Rapid prototyping and tooling technology in jewelry CAD. *Computer-Aided Design and Applications*. 2004;1(1-4):569-75.
126. Inaba K, Inaba M, Romani N, Aya H, Deguchi M, Ikehara S, et al. Generation of large numbers of dendritic cells from mouse bone marrow cultures supplemented with granulocyte/macrophage colony-stimulating factor. *The Journal of experimental medicine*. 1992;176(6):1693-702.
127. Sambrook H. *Molecular cloning: a laboratory manual*. Cold Spring Harbor, NY. 1989.
128. Pose-Boirazian T, Eibes G, Barreiro-Piñeiro N, Díaz-Jullien C, Lema JM, Martínez-Costas J. Chemical and thermal stabilization of CotA laccase via a novel one-step expression and immobilization in muNS-Mi nanospheres. *Scientific reports*. 2021;11(1):1-10.
129. Straathof AJ, Panke S, Schmid A. The production of fine chemicals by biotransformations. *Current opinion in biotechnology*. 2002;13(6):548-56.
130. Tabañag IDF, Chu I, Wei Y-H, Tsai S-L. The role of yeast-surface-display techniques in creating biocatalysts for consolidated bioprocessing. *Catalysts*. 2018;8(3):94.
131. Katchalski-Katzir E, Kraemer DM. Eupergit® C, a carrier for immobilization of enzymes of industrial potential. *Journal of molecular catalysis B: enzymatic*. 2000;10(1-3):157-76.
132. Homaei AA, Sariri R, Vianello F, Stevanato R. Enzyme immobilization: an update. *Journal of chemical biology*. 2013;6(4):185-205.

133. Polizzi KM, Bommarius AS, Broering JM, Chaparro-Riggers JF. Stability of biocatalysts. *Current opinion in chemical biology*. 2007;11(2):220-5.
134. Zdarta J, Meyer AS, Jesionowski T, Pinelo M. A general overview of support materials for enzyme immobilization: characteristics, properties, practical utility. *Catalysts*. 2018;8(2):92.
135. Kazenwadel F, Wagner H, Rapp B, Franzreb M. Optimization of enzyme immobilization on magnetic microparticles using 1-ethyl-3-(3-dimethylaminopropyl) carbodiimide (EDC) as a crosslinking agent. *Analytical Methods*. 2015;7(24):10291-8.
136. Sheldon RA, van Pelt S. Enzyme immobilisation in biocatalysis: why, what and how. *Chemical Society Reviews*. 2013;42(15):6223-35.
137. Li J, Wu C, Chu PK, Gelinsky M. 3D printing of hydrogels: Rational design strategies and emerging biomedical applications. *Materials Science and Engineering: R: Reports*. 2020;140:100543.
138. Couto SR, Herrera JLT. Industrial and biotechnological applications of laccases: a review. *Biotechnology advances*. 2006;24(5):500-13.
139. Arregui L, Ayala M, Gómez-Gil X, Gutiérrez-Soto G, Hernández-Luna CE, de los Santos MH, et al. Laccases: structure, function, and potential application in water bioremediation. *Microbial cell factories*. 2019;18(1):200.
140. Durao P, Chen Z, Fernandes AT, Hildebrandt P, Murgida DH, Todorovic S, et al. Copper incorporation into recombinant CotA laccase from *Bacillus subtilis*: characterization of fully copper loaded enzymes. *JBIC Journal of Biological Inorganic Chemistry*. 2008;13(2):183-93.
141. Mohammadian M, Fathi-Roudsari M, Mollania N, Badoei-Dalfard A, Khajeh K. Enhanced expression of a recombinant bacterial laccase at low temperature and microaerobic conditions: purification and biochemical characterization. *Journal of Industrial Microbiology and Biotechnology*. 2010;37(8):863-9.
142. Cho E-A, Seo J, Lee D-W, Pan J-G. Decolorization of indigo carmine by laccase displayed on *Bacillus subtilis* spores. *Enzyme and microbial technology*. 2011;49(1):100-4.
143. Wang T-N, Zhao M. A simple strategy for extracellular production of CotA laccase in *Escherichia coli* and decolorization of simulated textile effluent by recombinant laccase. *Applied microbiology and biotechnology*. 2017;101(2):685-96.
144. Pistone L, Ottolina G, De S, Romero AA, Martins LO, Luque R. Encapsulated Laccases for the Room-Temperature Oxidation of Aromatics: Towards Synthetic Low-Molecular-Weight Lignins. *ChemSusChem*. 2016;9(7):756-62.
145. Stepankova V, Bidmanova S, Koudelakova T, Prokop Z, Chaloupkova R, Damborsky J. Strategies for stabilization of enzymes in organic solvents. *ACS Catalysis*. 2013;3(12):2823-36.
146. Enaud E, Trovaslet M, Naveau F, Decristoforo A, Bizet S, Vanhulle S, et al. Laccase chloride inhibition reduction by an anthraquinonic substrate. *Enzyme and microbial technology*. 2011;49(6-7):517-25.
147. Bilal M, Rasheed T, Iqbal HM, Li C, Wang H, Hu H, et al. Photocatalytic degradation, toxicological assessment and degradation pathway of CI Reactive Blue 19 dye. *Chemical Engineering Research and Design*. 2018;129:384-90.
148. Dauda MY, Erkurt EA. Investigation of reactive Blue 19 biodegradation and byproducts toxicity assessment using crude laccase extract from *Trametes versicolor*. *Journal of hazardous materials*. 2020;393:121555.
149. Yuan H, Chen L, Cao Z, Hong FF. Enhanced decolourization efficiency of textile dye Reactive Blue 19 in a horizontal rotating reactor using strips of BNC-immobilized laccase: Optimization of conditions and comparison of decolourization efficiency. *Biochemical Engineering Journal*. 2020;156:107501.

150. Kang W, Ma T, Liu M, Qu J, Liu Z, Zhang H, et al. Modular enzyme assembly for enhanced cascade biocatalysis and metabolic flux. *Nature communications*. 2019;10(1):1-11.
151. Pogodaev AA, Fernández Regueiro CL, Jakštaitė M, Hollander MJ, Huck WT. Modular design of small enzymatic reaction networks based on reversible and cleavable inhibitors. *Angewandte Chemie*. 2019;131(41):14681-5.
152. Mieirol L, Beuscart JB, Knol W, Van Riet-Nales D, Orlu M. Achieving appropriate medication for older adults: A multidimensional perspective. *Maturitas*. 2019;124:43-7.
153. National Center for Health Statistics. Health, United States. United States; 2019.
154. Age UK. Age UK calls for a more considered approach to prescribing medicines for older people 2019. Available from: <https://www.ageuk.org.uk/latest-press/articles/2019/august/age-uk-calls-for-a-more-considered-approach-to-prescribing-medicines-for-older-people/>.
155. Patel M, Kumar R, Kishor K, Mlsna T, Pittman Jr CU, Mohan D. Pharmaceuticals of emerging concern in aquatic systems: chemistry, occurrence, effects, and removal methods. *Chemical reviews*. 2019;119(6):3510-673.
156. aus der Beek T, Weber F-A, Bergmann A, Hickmann S, Ebert I, Hein A, et al. Pharmaceuticals in the environment—Global occurrences and perspectives. *Environmental Toxicology and Chemistry*. 2016;35(4):823-35.
157. Margalida A, Oliva-Vidal P. The shadow of diclofenac hangs over European vultures. *Nature Ecology & Evolution*. 2017;1(8):1050-.
158. Swan G, Naidoo V, Cuthbert R, Green RE, Pain DJ, Swarup D, et al. Removing the threat of diclofenac to critically endangered Asian vultures. *PLoS Biol*. 2006;4(3):e66.
159. Gross-Sorokin MY, Roast SD, Brighty GC. Assessment of feminization of male fish in English rivers by the Environment Agency of England and Wales. *Environmental health perspectives*. 2006;114(Suppl 1):147-51.
160. Mills MR, Arias-Salazar K, Baynes A, Shen LQ, Churchley J, Beresford N, et al. Removal of ecotoxicity of 17 α -ethinylestradiol using TAML/peroxide water treatment. *Scientific reports*. 2015;5:10511.
161. Auriol M, Filali-Meknassi Y, Tyagi RD, Adams CD, Surampalli RY. Endocrine disrupting compounds removal from wastewater, a new challenge. *Process biochemistry*. 2006;41(3):525-39.
162. Pérez-Coyotl I, Galar-Martínez M, García-Medina S, Gómez-Oliván LM, Gasca-Pérez E, Martínez-Galero E, et al. Polluted water from an urban reservoir (Madín dam, México) induces toxicity and oxidative stress in *Cyprinus carpio* embryos. *Environmental Pollution*. 2019;251:510-21.
163. Russo C, Graziani V, Lavorgna M, D'Abrosca B, Piscitelli C, Fiorentino A, et al. Lymphocytes exposed to vegetables grown in waters contaminated by anticancer drugs: metabolome alterations and genotoxic risks for human health. *Mutation Research - Genetic Toxicology and Environmental Mutagenesis*. 2019;842:125-31.
164. Mishra M, Arukha AP, Patel AK, Behera N, Mohanta TK, Yadav D. Multi-drug resistant coliform: Water sanitary standards and health hazards. *Frontiers in Pharmacology*. 2018;9(JUN).
165. World Health Organization W. Lack of new antibiotics threatens global efforts to contain drug-resistant infections Geneva2020 [Available from: <https://www.who.int/news-room/detail/17-01-2020-lack-of-new-antibiotics-threatens-global-efforts-to-contain-drug-resistant-infections>].
166. Singh AK, Das S, Kumar S, Gajamer VR, Najar IN, Lepcha YD, et al. Distribution of Antibiotic-Resistant Enterobacteriaceae Pathogens in Potable Spring Water of Eastern Indian Himalayas: Emphasis on Virulence Gene and Antibiotic Resistance Genes in *Escherichia coli*. *Frontiers in Microbiology*. 2020;11.

167. Mendoza A, Zonja B, Mastroianni N, Negreira N, López de Alda M, Pérez S, et al. Drugs of abuse, cytostatic drugs and iodinated contrast media in tap water from the Madrid region (central Spain): A case study to analyse their occurrence and human health risk characterization. *Environment International*. 2016;86:107-18.
168. Deng Y, Guo C, Zhang H, Yin X, Chen L, Wu D, et al. Occurrence and removal of illicit drugs in different wastewater treatment plants with different treatment techniques. *Environmental Sciences Europe*. 2020;32(1):28.
169. World Health Organization W. *Pharmaceuticals in Drinking-water*. Geneva, Switzerland; 2011. Contract No.: WHO/HSE/WSH/11.05.
170. Vivero-Lopez M, Xu X, Muras A, Otero A, Concheiro A, Gaisford S, et al. Antibiofilm multi drug-loaded 3D printed hearing aids. *Materials Science and Engineering C*. 2021;119.
171. Awad A, Yao A, Trenfield SJ, Goyanes A, Gaisford S, Basit AW. 3D printed tablets (Printlets) with braille and moon patterns for visually impaired patients. *Pharmaceutics*. 2020;12(2).
172. Elbadawi M, Ong JJ, Pollard TD, Gaisford S, Basit AW. Additive Manufacturable Materials for Electrochemical Biosensor Electrodes. *Advanced Functional Materials*. 2020;n/a(n/a):2006407.
173. Yang J, Li W, Ng TB, Deng X, Lin J, Ye X. Laccases: production, expression regulation, and applications in pharmaceutical biodegradation. *Frontiers in microbiology*. 2017;8:832.
174. Lloret L, Eibes G, Lú-Chau T, Moreira M, Feijoo G, Lema J. Laccase-catalyzed degradation of anti-inflammatories and estrogens. *Biochemical Engineering Journal*. 2010;51(3):124-31.
175. Marco-Urrea E, Pérez-Trujillo M, Cruz-Morató C, Caminal G, Vicent T. Degradation of the drug sodium diclofenac by *Trametes versicolor* pellets and identification of some intermediates by NMR. *Journal of Hazardous Materials*. 2010;176(1-3):836-42.
176. Ba S, Haroune L, Cruz-Morató C, Jacquet C, Touahar IE, Bellenger J-P, et al. Synthesis and characterization of combined cross-linked laccase and tyrosinase aggregates transforming acetaminophen as a model phenolic compound in wastewaters. *Science of the total environment*. 2014;487:748-55.
177. Tahmasbi H, Khoshayand MR, Bozorgi-Koushalshahi M, Heidary M, Ghazi-Khansari M, Faramarzi MA. Biocatalytic conversion and detoxification of imipramine by the laccase-mediated system. *International Biodeterioration & Biodegradation*. 2016;108:1-8.
178. Auriol M, Filali-Meknassi Y, Adams CD, Tyagi RD, Noguero T-N, Pina B. Removal of estrogenic activity of natural and synthetic hormones from a municipal wastewater: efficiency of horseradish peroxidase and laccase from *Trametes versicolor*. *Chemosphere*. 2008;70(3):445-52.
179. Becker D, Rodriguez-Mozaz S, Insa S, Schoevaart R, Barceló D, de Cazes M, et al. Removal of endocrine disrupting chemicals in wastewater by enzymatic treatment with fungal laccases. *Organic Process Research & Development*. 2017;21(4):480-91.
180. Tamagawa Y, Yamaki R, Hirai H, Kawai S, Nishida T. Removal of estrogenic activity of natural steroidal hormone estrone by ligninolytic enzymes from white rot fungi. *Chemosphere*. 2006;65(1):97-101.
181. Blanchette CD, Knipe JM, Stolaroff JK, DeOtte JR, Oakdale JS, Maiti A, et al. Printable enzyme-embedded materials for methane to methanol conversion. *Nature communications*. 2016;7:11900.
182. Li XY, Yu SY, Park HJ, Zhao M. Polyethyleneglycol diacrylate microspheres: a novel carrier for laccase immobilisation. *Journal of microencapsulation*. 2015;32(1):22-8.

183. Steier A, Schmiegl B, Irtel von Brenndorff Y, Meier M, Nirschl H, Franzreb M, et al. Enzyme Scaffolds with Hierarchically Defined Properties via 3D Jet Writing. *Macromolecular bioscience*. 2020;20(9):2000154.
184. Fairbanks BD, Schwartz MP, Bowman CN, Anseth KS. Photoinitiated polymerization of PEG-diacrylate with lithium phenyl-2, 4, 6-trimethylbenzoylphosphinate: polymerization rate and cytocompatibility. *Biomaterials*. 2009;30(35):6702-7.
185. HuangáGoh W, HoseináSakhaei A. Highly stretchable hydrogels for UV curing based high-resolution multimaterial 3D printing. *Journal of Materials Chemistry B*. 2018;6(20):3246-53.
186. Madzarevic M, Medarevic D, Vulovic A, Sustersic T, Djuris J, Filipovic N, et al. Optimization and prediction of ibuprofen release from 3D DLP printlets using artificial neural networks. *Pharmaceutics*. 2019;11(10):544.
187. Lloret L, Eibes G, Feijoo G, Moreira M, Lema J, Hollmann F. Immobilization of laccase by encapsulation in a sol-gel matrix and its characterization and use for the removal of estrogens. *Biotechnology progress*. 2011;27(6):1570-9.
188. Doran P. *Bioprocess Engineering Principles*. Press A, editor. Amsterdam, Netherlands: Elsevier; 2012.
189. Arca-Ramos A, Ammann E, Gasser C, Nastold P, Eibes G, Feijoo G, et al. Assessing the use of nanoimmobilized laccases to remove micropollutants from wastewater. *Environmental Science and Pollution Research*. 2016;23(4):3217-28.
190. Vera M, Rivas BL. Immobilization of *T rametes versicolor* laccase on different PGMA-based polymeric microspheres using response surface methodology: Optimization of conditions. *Journal of Applied Polymer Science*. 2017;134(36):45249.
191. Litwińska K, Bischoff F, Matthes F, Bode R, Rutten T, Kunze G. Characterization of recombinant laccase from *Trametes versicolor* synthesized by *Arxula adenivorans* and its application in the degradation of pharmaceuticals. *AMB Express*. 2019;9(1):102.
192. Šnajdr J, Baldrian P. Temperature affects the production, activity and stability of ligninolytic enzymes in *Pleurotus ostreatus* and *Trametes versicolor*. *Folia Microbiologica*. 2007;52(5):498-502.
193. Peterson ME, Daniel RM, Danson MJ, Eisenthal R. The dependence of enzyme activity on temperature: determination and validation of parameters. *Biochem J*. 2007;402(2):331-7.
194. Kurniawati S, Nicell JA. Characterization of *Trametes versicolor* laccase for the transformation of aqueous phenol. *Bioresource technology*. 2008;99(16):7825-34.
195. Rancano G, Lorenzo M, Molares N, Couto SRg, Sanromán MÁ. Production of laccase by *Trametes versicolor* in an airlift fermentor. *Process Biochemistry*. 2003;39(4):467-73.
196. Barbosa MO, Moreira NFF, Ribeiro AR, Pereira MFR, Silva AMT. Occurrence and removal of organic micropollutants: An overview of the watch list of EU Decision 2015/495. *Water Res*. 2016;94:257-79.
197. Lloret L, Hollmann F, Eibes G, Feijoo G, Moreira M, Lema J. Immobilisation of laccase on Eupergit supports and its application for the removal of endocrine disrupting chemicals in a packed-bed reactor. *Biodegradation*. 2012;23(3):373-86.
198. National Trends Network. pH of rainfall in the USA, 2002 United States: United States Geological Survey; 2002 [Available from: <https://www.usgs.gov/media/images/ph-rainfall-usa-2002>].
199. Thomas GW. Soil pH and Soil Acidity. *Methods of Soil Analysis* 1996. p. 475-90.
200. Fernandez-Fernandez M, Sanromán MÁ, Moldes D. Recent developments and applications of immobilized laccase. *Biotechnology Advances*. 2013;31(8):1808-25.

201. Iriarte-Mesa C, Díaz-Castañón S, Abradelo DG. Facile immobilization of *Trametes versicolor* laccase on highly monodisperse superparamagnetic iron oxide nanoparticles. *Colloids and Surfaces B: Biointerfaces*. 2019;181:470-9.
202. Apriceno A, Bucci R, Girelli AM. Immobilization of laccase from *Trametes versicolor* on chitosan macrobeads for anthracene degradation. *Analytical Letters*. 2017;50(14):2308-22.
203. Zhu Y, Kaskel S, Shi J, Wage T, van Pée K-H. Immobilization of *Trametes versicolor* laccase on magnetically separable mesoporous silica spheres. *Chemistry of Materials*. 2007;19(26):6408-13.
204. Asgher M, Noreen S, Bilal M. Enhancement of catalytic, reusability, and long-term stability features of *Trametes versicolor* IBL-04 laccase immobilized on different polymers. *International journal of biological macromolecules*. 2017;95:54-62.
205. Chaplin MF, Bucke C. *Enzyme Technology*: Cambridge University Press; 1990.
206. Lonappan L, Rouissi T, Laadila MA, Brar SK, Hernandez Galan L, Verma M, et al. Agro-industrial-Produced Laccase for Degradation of Diclofenac and Identification of Transformation Products. *ACS Sustainable Chemistry & Engineering*. 2017;5(7):5772-81.
207. Stoilova I, Krastanov A, Stanchev V. Properties of crude laccase from *Trametes versicolor* produced by solid-substrate fermentation. *Advances in Bioscience and Biotechnology*. 2010;Vol.01No.03:4.
208. Canfora L, Iamarino G, Rao MA, Gianfreda L. Oxidative Transformation of Natural and Synthetic Phenolic Mixtures by *Trametes versicolor* Laccase. *Journal of Agricultural and Food Chemistry*. 2008;56(4):1398-407.
209. Rodríguez-Delgado MM, Alemán-Nava GS, Rodríguez-Delgado JM, Dieck-Assad G, Martínez-Chapa SO, Barceló D, et al. Laccase-based biosensors for detection of phenolic compounds. *TrAC Trends in Analytical Chemistry*. 2015;74:21-45.
210. Jeon J-R, Baldrian P, Murugesan K, Chang Y-S. Laccase-catalysed oxidations of naturally occurring phenols: from in vivo biosynthetic pathways to green synthetic applications. *Microb Biotechnol*. 2012;5(3):318-32.
211. Becker D, Varela Della Giustina S, Rodriguez-Mozaz S, Schoevaart R, Barcelo D, de Cazes M, et al. Removal of antibiotics in wastewater by enzymatic treatment with fungal laccase - Degradation of compounds does not always eliminate toxicity. *Bioresour Technol*. 2016;219:500-9.
212. Hoos A. Development of immuno-oncology drugs—from CTLA4 to PD1 to the next generations. *Nature reviews Drug discovery*. 2016;15(4):235-47.
213. Ye Z, Qian Q, Jin H, Qian Q. Cancer vaccine: learning lessons from immune checkpoint inhibitors. *Journal of Cancer*. 2018;9(2):263.
214. Wang R-F, Appella E, Kawakami Y, Kang X, Rosenberg SA. Identification of TRP-2 as a human tumor antigen recognized by cytotoxic T lymphocytes. *The Journal of experimental medicine*. 1996;184(6):2207-16.
215. Ju J-M, Jung MH, Nam G, Kim W, Oh S, Kim HD, et al. Escape from thymic deletion and anti-leukemic effects of T cells specific for hematopoietic cell-restricted antigen. *Nature communications*. 2018;9(1):1-15.
216. Dash B, Shapiro MJ, Chung JY, Arocha SR, Shapiro VS. Treg-specific deletion of NKAP results in severe, systemic autoimmunity due to peripheral loss of Tregs. *Journal of autoimmunity*. 2018;89:139-48.
217. Schiavo R, Baatar D, Olkhanud P, Indig FE, Restifo N, Taub D, et al. Chemokine receptor targeting efficiently directs antigens to MHC class I pathways and elicits antigen-specific CD8+ T-cell responses. *Blood*. 2006;107(12):4597-605.
218. Gordy JT, Luo K, Zhang H, Biragyn A, Markham RB. Fusion of the dendritic cell-targeting chemokine MIP3 α to melanoma antigen Gp100 in a therapeutic DNA vaccine

significantly enhances immunogenicity and survival in a mouse melanoma model. *Journal for immunotherapy of cancer*. 2016;4(1):1-11.

219. Gupta S, Termini JM, Rivas Y, Otero M, Raffa FN, Bhat V, et al. A multi-trimeric fusion of CD40L and gp100 tumor antigen activates dendritic cells and enhances survival in a B16-F10 melanoma DNA vaccine model. *Vaccine*. 2015;33(38):4798-806.

220. Babatunde KA, Najafi A, Salehipour P, Modarressi MH, Mobasher MB. Cancer/Testis genes in relation to sperm biology and function. *Iranian journal of basic medical sciences*. 2017;20(9):967.

221. Duthie MS, Windish HP, Fox CB, Reed SG. Use of defined TLR ligands as adjuvants within human vaccines. *Immunological reviews*. 2011;239(1):178-96.

222. Sluijter BJ, van den Hout MF, Koster BD, van Leeuwen PA, Schneiders FL, van de Ven R, et al. Arming the melanoma sentinel lymph node through local administration of CpG-B and GM-CSF: recruitment and activation of BDCA3/CD141+ dendritic cells and enhanced cross-presentation. *Cancer immunology research*. 2015;3(5):495-505.

223. Iribarren K, Bloy N, Buqué A, Cremer I, Eggermont A, Fridman WH, et al. Trial Watch: Immunostimulation with Toll-like receptor agonists in cancer therapy. *Oncoimmunology*. 2016;5(3):e1088631.

224. Medzhitov R. Toll-like receptors and innate immunity. *Nature Reviews Immunology*. 2001;1(2):135-45.

225. Takeda K, Akira S. Toll-like receptors in innate immunity. *International immunology*. 2005;17(1):1-14.

226. Iwasaki A, Medzhitov R. Toll-like receptor control of the adaptive immune responses. *Nature immunology*. 2004;5(10):987-95.

227. O'Neill LA, Golenbock D, Bowie AG. The history of Toll-like receptors—redefining innate immunity. *Nature Reviews Immunology*. 2013;13(6):453-60.

228. Medzhitov R. Recognition of microorganisms and activation of the immune response. *Nature*. 2007;449(7164):819-26.

229. Diebold SS. Activation of dendritic cells by toll-like receptors and C-type lectins. *Dendritic Cells*. 2009:3-30.

230. Iwasaki A, Medzhitov R. Control of adaptive immunity by the innate immune system. *Nature immunology*. 2015;16(4):343-53.

231. Blasius AL, Beutler B. Intracellular toll-like receptors. *Immunity*. 2010;32(3):305-15.

232. O'Neill LA, Bowie AG. The family of five: TIR-domain-containing adaptors in Toll-like receptor signalling. *Nature Reviews Immunology*. 2007;7(5):353-64.

233. Tomljenovic L, A Shaw C. Aluminum vaccine adjuvants: are they safe? *Current Medicinal Chemistry*. 2011;18(17):2630-7.

234. Marín-López A, Otero-Romero I, de la Poza F, Menaya-Vargas R, Calvo-Pinilla E, Benavente J, et al. VP2, VP7, and NS1 proteins of bluetongue virus targeted in avian reovirus muNS-Mi microspheres elicit a protective immune response in IFNAR (-/-) mice. *Antiviral research*. 2014;110:42-51.

235. Costard S, Mur L, Lubroth J, Sanchez-Vizcaino J, Pfeiffer DU. Epidemiology of African swine fever virus. *Virus research*. 2013;173(1):191-7.

236. Penrith M-L, Vosloo W. Review of African swine fever: transmission, spread and control. *Journal of the South African Veterinary Association*. 2009;80(2):58-62.

237. Rock D. Challenges for African swine fever vaccine development—"... perhaps the end of the beginning." *Veterinary microbiology*. 2017;206:52-8.

238. Marín-López A, Barreiro-Piñero N, Utrilla-Trigo S, Barriales D, Benavente J, Nogales A, et al. Cross-protective immune responses against African horse sickness virus after vaccination with protein NS1 delivered by avian reovirus muNS microspheres and modified vaccinia virus Ankara. *Vaccine*. 2020;38(4):882-9.

239. Marabelle A, Kohrt H, Caux C, Levy R. Intratumoral immunization: a new paradigm for cancer therapy. *Clinical Cancer Research*. 2014;20(7):1747-56.
240. Murthy V, Minehart J, Sterman DH. Local immunotherapy of cancer: innovative approaches to harnessing tumor-specific immune responses. *JNCI: Journal of the National Cancer Institute*. 2017;109(12):dix097.
241. Hamid O, Ismail R, Puzanov I. Intratumoral immunotherapy—update 2019. *The oncologist*. 2020;25(3):e423.
242. Sancho D, Mourão-Sá D, Joffre OP, Schulz O, Rogers NC, Pennington DJ, et al. Tumor therapy in mice via antigen targeting to a novel, DC-restricted C-type lectin. *The Journal of clinical investigation*. 2008;118(6):2098-110.
243. Kreutz M, Giquel B, Hu Q, Abuknesha R, Uematsu S, Akira S, et al. Antibody-antigen-adjuvant conjugates enable co-delivery of antigen and adjuvant to dendritic cells in cis but only have partial targeting specificity. *PLoS One*. 2012;7(7):e40208.